Understanding the transport mechanisms of BSEP to improve the prediction of DILI compounds

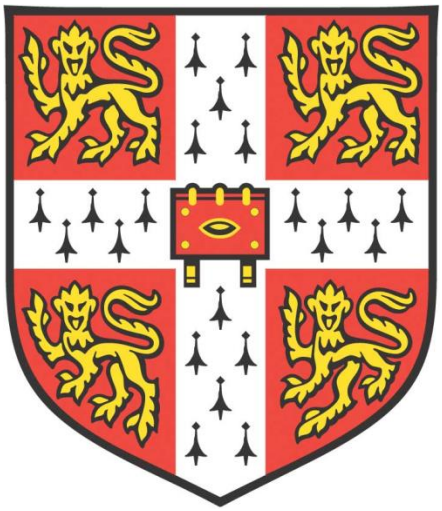

Robbin de Kruijf

Darwin College

Department of Pharmacology

University of Cambridge

This thesis is submitted for the degree of Doctor of Philosophy

September 2019

Ik wijd mijn thesis toe aan mijn mama en papa en aan mijn oma en opa.

Zij zijn de oorsprong van mijn nieuwsgierigheid,

De reden voor mijn stoerheid.

Declaration

This thesis is the result of my own work and includes nothing which is the outcome of work done in collaboration except as declared in the Preface and specified in the text. It is not substantially the same as any that I have submitted, or, is being concurrently submitted for a degree or diploma or other qualification at the University of Cambridge or any other University or similar institution except as declared in the Preface and specified in the text. I further state that no substantial part of my thesis has already been submitted, or, is being concurrently submitted for any such degree, diploma or other qualification at the University of Cambridge or any other University or similar institution except as declared in the Preface and specified in the text. It does not exceed the prescribed word limit for the relevant Degree Committee.

Abstract

Understanding the transport mechanisms of BSEP to improve the prediction of DILI compounds

Robbin de Kruijf

At present, Drug-Induced Liver Injury (DILI) is the most frequent cause of acute liver injury, with an incidence ranging from 0.023-1.5‰ in developed countries. DILI can be separated into two different types. Whereas intrinsic DILI concerns predictable dose-dependent hepatoxicity, idiosyncratic DILI refers to unpredictable adverse drug reactions for which there is no existing pharmacological explanation. Many prescription and over-the-counter drugs causing DILI do so in an undiscovered and idiosyncratic pattern. It is the latter that causes DILI to be the most frequent cause of safety-related drug withdrawals. This causes delays in the availability of treatments and is responsible for 20% to 40% of liver transplants and hepatic failures. While several mechanisms might be responsible for idiosyncratic DILI, a broad industry-wide consensus was reached in 2016 on the importance of the liver bile salt export pump (BSEP) and the need to test for BSEP inhibition at an early stage of drug development.

An assay for BSEP-mediated bile acid transport was established to study the biochemical mechanisms of inhibition of BSEP activity by organic compounds. The four selected compounds showed competitive inhibition of taurocholate transport in Lineweaver-Burk plots but also other types of inhibition in Eadie-Hofstee plots. These results indicate that these inhibitors might compete with taurocholate for binding in the substrate-binding pocket and possibly, that the inhibitors are transported by BSEP. Interestingly, this work shows a strong inhibitory effect of excess Mg^{2+} on the ability of BSEP to transport glycocholic acid; the transport of taurocholic acid was not inhibited by Mg^{2+}. To get more insight in structure-function relationships in BSEP, a condense and accurate database of all known BSEP point mutations from published literature was compiled. This database shows a total of 264 known mutations associated with several pathogenic and non-pathogenic phenotypes. To date, there is still little known about the effects of many of these mutations on BSEP activity. Only 82 of the 264 mutations have currently been investigated for their impact on function and expression level of BSEP.

2D and 3D primary cultured hepatocytes were used to establish the effect of DILI-inducing drugs on the synthesis of bile acids and their distribution across the cell and the media. Multivariate analyses of the data demonstrate that drugs can change the bile acid composition in hepatocytes and their environment. This might occur by regulating bile acid synthesis pathways and/or by modulating the selectivity of BSEP itself. Interestingly, some of the detected changes in bile acid concentrations might be early indicators of cell stress and cell death. The experiments also suggest that drugs can cause a change in BSEP expression in the plasma membrane, through changes in the trafficking of protein to and from the plasma membrane. These changes could explain the existence of non-pathogenic BSEP inhibitors. These findings increase our understanding of the influence of compounds on bile acid production and BSEP distribution and their potential roles in idiosyncratic DILI.

Acknowledgements

I wish to thank everyone who has accompanied me on this journey.

I would like to express my deep gratitude to Rik, for his valuable and constructive suggestions during the planning, development and execution of the project, for his guidance and enthusiastic encouragement during the years here at Cambridge.

Next, I would like to say thank you to my lab mates Lisa, Himansha, David, and Charlotte for not only being my lab mates but for also being my friends and confidantes and ear when things went wrong and were not working, and for providing feedback and for all the memories. In short for making the workplace so much better and making it a joy to come to the lab every day. With a special shout out to Lisa and Himansha, for pulling me out when I went under and for putting me right when I was simply wrong.

A special thank you goes to the DMS team at AstraZeneca, under the guidance of Dominic, Alison, Katie, Sophie and Helen. I am incredibly grateful to them for teaching me new techniques providing me with constructive feedback and having me present so often (those were invaluable for the writing process of this thesis). I am grateful for AstraZeneca's financial support during my PhD. Because of you I was able to experience the best of pharmaceutical industry.

I would also like to express my gratitude to the MRC Toxicology Unit in Leicester for awarding the Integrative-Toxicology Training Partnership (ITTP) PhD studentship. I thoroughly enjoyed the yearly ITTP training weeks.

Thank you to all the friends I made in Darwin, to Elaine, Meltem and Brenda. For adopting me to have a social life, for the emotional support, for helping me with statistical questions. To the rest of Darwin that taught me that I was not the only one anxious and suffering from imposter syndrome, that I was not alone with my problems.

Mijn vrienden van de basisschool en van de middelbare, jullie zijn fantastisch.

To all my friends and family away from home, I'd like to say please look up "vriend" by Toon Hermans. His poem describes much better what I feel about you all. You all make me realise how blessed I really am.

Schließlich meine Familie, meine Brüder die immer meine Brüder gewesen sind. Ab und zu seid ihr Idioten und Clowns aber die meiste Zeit weiß ich das ich immer auf euch zählen kann. Ob es mitten in der Nacht ist oder auf der anderen Seite der Welt.

Uiteindelijk zou ik graag mijn tante willen bedanken. Woorden zijn hier niet genoeg, maar ik hoop dat zij weet hoeveel haar liefde, haar ondersteuning, haar optimisme, haar hardnekkigheid en haar pragmatisme voor mij betekenen. Zij is een grote inspiratie voor mij, en zonder haar zou ik nooit, maar dan ook echt nooit, zover gekomen zou zijn. Ik noem haar misschien niet mama, maar mama is alleen een word, alle gevoelens die erbij horen zijn voor mij geassocieerd met "Agnes".

There are so many people I'd like to thank, so many memories I treasure and initially I wanted to put a picture collage of all my memories in here but thought the better of it. Still I made a collage for myself with all the pictures I gathered and put it in my own copy.

Thank You,

Thank you so much

List of Abbreviations and Acronyms

2D	2 dimensional (sandwich culture)
3D	3 dimensional (spheroid culture)
ABC transporter	ATP binding cassette transporter
ABCB1	ATP binding cassette subfamily B member 1
ABCB11	ATP binding cassette subfamily B member 11
AKR1C4	aldo-keto reductase family 1 member C4
AKR1D1	aldo-keto reductase family 1 member D1
AKT	AKT serine/threonine Kinase
AMACR	alpha-methylacyl-CoA racemase
aMCA	alpha-muricholic acid
AMP	adenosine monophosphate
ASBT	apical sodium-dependent bile acid transporter
ATP	adenosine triphosphate
AZ	Astrazeneca
BAAT	bile acid-CoA:amino acid N-acyltransferase
BCOX	acyl-CoA oxidase 2
bMCA	beta-muricholic acid
BRIC2	benign recurrent intrahepatic cholestasis type 2
BS	bosentan treatment
BSA	bovine serum albumin
BSEP	bile salt export pump
CA	cholic acid
cAMP	cyclic adenosine monophosphate
CDCA	chenodeoxycholic acid
CH	cyclohexamide treatment
CP	clobetasol propionate treatment
CVB	covalent binding burden
Cyp27A1	cytochrome P450 family 27 subfamily A member 1
DCA	deoxycholic acid
DILI	Drug-induced liver injury
DM	DMSO treatment
DMSO	dimethyl sulfo-oxide
DNA	deoxyribonucleic acid
DPBS	dulbecco's phosphate buffered saline
E.Coli	*Escherichia coli*
EDTA	ethylenediaminetetraacetic acid
EGTA	ethylene glycol-bis(β-aminoethyl ether)-N,N,N’,N’-tetraacetic acid
EMA	European Medicines Agency
ES	estradiol treatment
FCS/FBS	fetal calf serum/fetal bovine serum
FDA	U.S. Food and Drug Administration
FXR	farnesoid X nuclear receptor
GCA	glycocholic acid

GCDCA	glycochenodeoxycholic acid
GDCA	glycodeoxycholic acid
GUDCA	glycoursodeoxycholic acid
hBSEP	human bile salt export pump
IC_{50}	Half-maximal inhibitory concentration
ICH	International Council for Harmonisation of Technical Requirements for Pharmaceuticals for Human Use
iDILI	idiosyncratic drug-induced liver injury
IHC	intrahepatic cholestasis
IL1a	interleukin 1 alpha
IL6	interleukin 6
ISOV	inside out membrane vesicle
Km	Michealis constant
LCA	lithocholic acid
MDs	membrane domains
MRP2	multidrug resistance-associated protein 2
MS	mass spectrometry
NBDs	Nucleotide-binding domains
NTCP	Na^+/taurocholate co-transporting polypeptide
OATP2	sodium-independent organic anion-transporting polypeptide 2
PBS	phosphate buffered saline
PCA-X	principal component analysis type x
PFIC2	progressive familiar intrahepatic cholestasis type 2
PHH	primary human hepatocytes
PI3K	phosphatidylinositol-4,5-bisphosphate 3-kinase catalytic subunit
PKC	protein kinase C
PNK	polynucleotide kinase
PSI	pounds per square inch
RXR	retinoid X receptor
Sf21	*Spodoptera frugiperda* insect cells
sPGP	sister of P-glycoprotein
TCA	taurocholic acid
TCDCA	taurochenodeoxycholic acid
TDCA	taurodeoxycholic acid
THDCA	taurohyodeoxycholic acid
THLE	transformed human liver epithelial cells
TMHs	transmembrane helix
TNFa	tumour necrosis factor alpha
TUDCA	tauroursedeoxycholic acid
UDCA	ursodeoxycholic acid
V.C.	viable cells
Vmax	maximum velocity
WT	wild type

Table of contents

1. Introduction

Background

To maintain their viability, all cells continually need to import nutrients and export toxic waste. For this purpose, cells express a wide range of membrane transporters that are embedded in the plasma membrane and mediate the movement of their substrates across this permeability barrier. One important superfamily of transport proteins in prokaryotic, eukaryotic and plant cells, involved in this process, is that of the ATP binding cassette (ABC) transporters [1]. These transporters comprise two nucleotide-binding domains (NBDs) and two membrane domains (MDs) and sometimes contain additional domains. ABC transporters are able to transport a broad range of compounds from simple ions, through polar, amphipathic and hydrophobic organic molecules to peptides, complex lipids and even small proteins. [2]. Since the discovery of the first known mammalian multidrug ABC transporter P-glycoprotein (also referred to as ABCB1) in 1974 [3], 47 other members of the superfamily have been identified in mammals [4]. These transporters have a standardized nomenclature consisting of subfamily and specified gene name based on their sequence and common architecture.

This thesis will focus on the mammalian ABC transporter *ABCB11*, also referred to as the bile salt export pump (BSEP). BSEP is specifically expressed in the liver and is predominantly present in the apical membrane of hepatocytes where it is one of the most abundant canalicular efflux transporters [5]. Bile acids are produced in the liver and released as bile into the intestines, after which 95% bile acids are reabsorbed in the terminal ileum and recycled back to the liver [6]. This efficient enterohepatic circulation of bile acids plays an important role in liver function, metabolic regulation and liver physiology. Bile contains an intricate mixture of endogenous bile salts, bilirubin, phospholipids, cholesterol, amino acids, steroids, enzymes, porphyrins, vitamins and heavy metals as well as exogenous, xenobiotics and environmental toxins. Bile functions as a powerful detergent that facilitates lipid and nutrition absorption as well as cholesterol and toxic metabolite excretion [7]. Due to the hydrophobic characteristics of bile acids, their accumulation in the hepatocytes would cause cell membrane damage, impair liver function and lead to cholestasis and cirrhosis. The accumulation of bile acids often leads to drug induced liver injury (DILI). In 10% of cases, DILI is associated with acute hepatitis, which is the most frequently cited reason for safety-related drug withdrawals [8,9]. DILI does not only cause the suffering of individual patients and

increased health care costs but is also a major economic challenge to the pharmaceutical industry. Many prescription and over-the-counter drugs causing DILI do so with an undiscovered and idiosyncratic pattern. The annual incidence of DILI is between 10 and 15 per 10,000 to 100,000 patients using prescribed medicines [7,10–12]. Due to this low frequency, compounds causing severe DILI are challenging to identify in clinical trials and often remain unidentified until post-marketing monitoring when the drug has become available to a larger population. Initial cell stress in the liver can be caused by a wide range of mechanisms including inhibition of hepatocellular function, e.g. canalicular bile salt secretion, through inhibition of the BSEP activity [13]. Understanding the working mechanisms of BSEP and its interactions with therapeutic drugs will help to avoid DILI and is also relevant in the development of new screening assays and treatments methods for Progressive familial intrahepatic cholestasis type 2 (PFIC2). However, current knowledge about BSEP is very sparse and more research into the molecular mechanisms of this pump is therefore necessary.

This introduction will:

- provide a summary of current standards in pharmacovigilance (Section 1.1),
- highlight the current understanding of bile acid production and functions (Section 1.2),
- summarize current insights in the regulation and activity of BSEP (Section 1.3),
- give an overview of the research chapters and objectives (Section 1.4).

1.1 Pharmacovigilance

Pharmacovigilance is defined by the World Health Organisation as: “the process and science of monitoring the safety of medicines and taking action to reduce the risks and increase the benefits of medicines”. The time for developing a new drug from idea to market launch can take between 12-15 years and costs over $1 billion [14]. The international council for harmonisation of technical requirements for pharmaceuticals for human use (ICH) has set a series of guidelines regarding quality, safety, efficacy and multidisciplinary science regarding drug safety (https://www.ich.org/products/guidelines.html). Most pharmaceutical and drug regulatory agencies like the USA Food and Drug Administration (FDA) and the European Medicines Agency (EMA) adhere to these pre-set guidelines. In recent years, research has streamlined the selection procedure of compounds before entering the clinical testing stages, containing several compound safety checks along the way. Drug development can be summarised into the following four steps and consists of drug discovery, pre-clinical development, clinical development and regulatory approval (see Figure 1). Each step contains a subset of tests that needs to be passed before the compound can advance to the next stage. While pre-clinical assays are relatively cheap, starting from the *in-vivo* stage, the money spent on testing and advancing compounds increases steadily. The pharmaceutical industry, therefore, attempts to discriminate drugs with a high propensity to cause idiosyncratic adverse drug reactions from those with a low propensity to cause such reactions, by profiling their adverse biological effects *in vitro* [13].

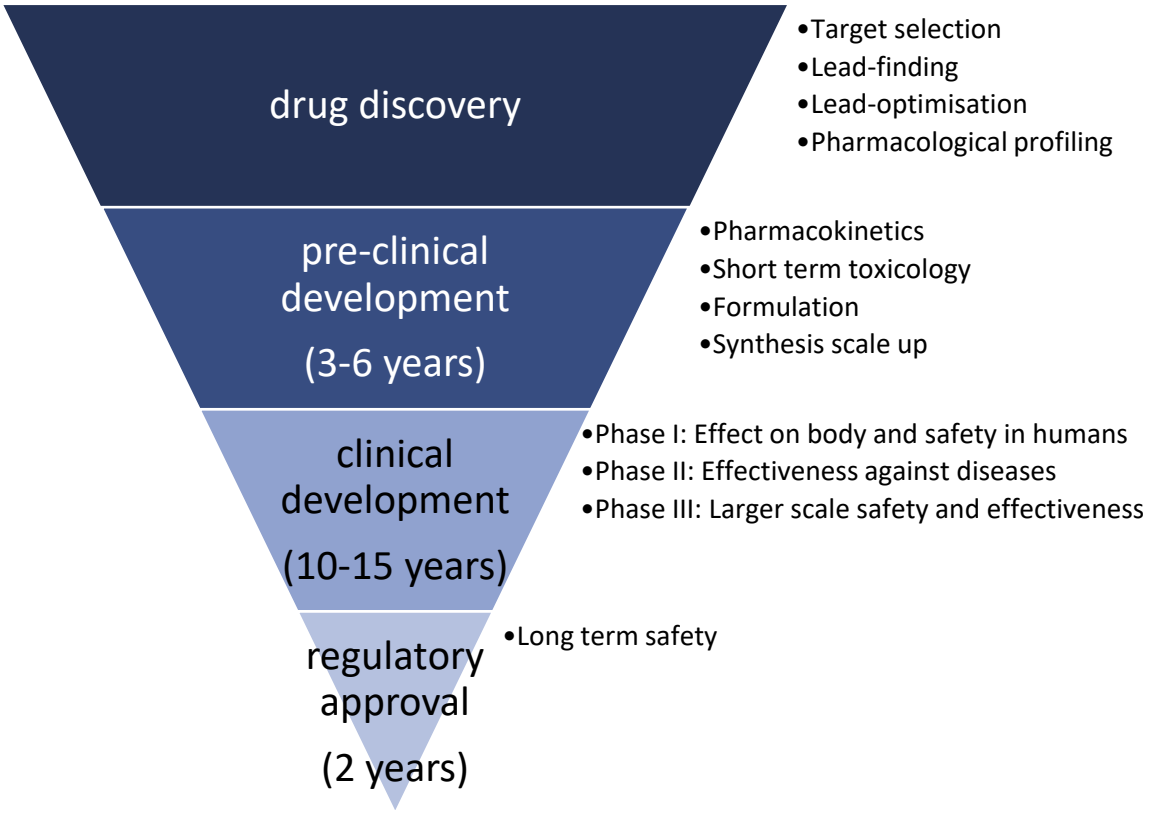

Figure 1. Summary of the different stages during drug development. The inversed pyramid indicates the reduction in the number of compounds in that pass to the next phase of development and safety testing.

1.1.1 Pre-clinical development.

Stage I: in-vitro testing

To optimise the safety of a drug, the compound is tested for carcinogenicity, genotoxicity toxicokinetic and pharmacokinetics, toxicity, reproductive toxicology, photo safety, nonclinical paediatric safety and immunotoxicity among others. Different *in vitro* assays have been developed to test for each one of these, but in many cases, there is still a requirement to test on animals before a drug is allowed onto the market. The first round of preclinical risk assessment incorporates in-vitro assays. At present, AstraZeneca uses five different tests to identify harmful compounds that should be removed from the development pipeline [15]. The panel consists of: 1.) Toxicity to Transformed Human Liver Epithelial (THLE) cells that do not express cytochrome P450 enzymes, 2.) Toxicity to THLE cells that selectively express cytochrome P450 3A4, to estimate drug metabolism-mediated toxicity, 3.) Cytotoxicity in HepG2 cells in glucose and galactose media, which is indicative of drug-induced mitochondrial injury, 4.) Inhibition of human BSEP (hBSEP) in ISOVs, and 5.) Inhibition of the rat multidrug resistance associated protein 2 (MRP2) in ISOVs [16], a protein capable of transporting some bile salts. Additionally, the covalent binding (CVB) burden is estimated by determining the irreversible covalent binding of a radiolabelled compound to human hepatocytes and factoring in both the maximum prescribed daily dose and the fraction of metabolism leading to CVB [15].

Each of these tests individually has a low selectivity to identify potentially harmful compounds but together and combined with the CVB burden, these tests have a sensitivity of 48% and a specificity of 89% [15]. Sensitivity and specificity are terms used in the evaluation of clinical tests. To calculate the sensitivity and specificity, researchers use i.) True positives: the number of compounds the assay correctly identifies to cause DILI. ii.) False positives: the number of compounds where the assay falsely identifies a compound to cause DILI. iii.) True negatives: the assay correctly identifies the compound not to cause DILI and iv.) False negatives: the assay falsely identifies a compound to cause DILI. Accordingly, the sensitivity describes an assay's ability to correctly test which compounds will cause DILI, and the specificity describes an assay's ability to correctly identify which compounds do not cause DILI [17]. Thus, while the described assay panel can identify 84% of the compounds that do not cause DILI, it is only able to identify 48% of compounds that will cause DILI.

There are several limitations in these types of experiments. The selection of human samples causes several issues: 1.) Most established cell lines originate from cancer cell lines that have a completely different protein expression and metabolomic activity compared to normal cells in healthy humans. Studies have shown that primary human hepatocytes (PHH) are the best choice for cell culturing [18], but have the drawback that they are expensive to obtain and that they do not further proliferate. 2.) *In vitro* cultured cells are often monocultures and do not come into contact with other cells that are responsible for mitigating or activating toxic effects of drugs. These cells therefore only provide partial information regarding the human as a whole organism. Yet, alternatives are available such as co-cultures of hepatocytes with nonparenchymal cells or Kupffer cells, but experiments with such co-cultures are often challenging both technically and in terms of interpretation of data [19] 3.) Moreover, cells cultured in *in vitro* layers rather than the *in vivo* 3D structures have significant differences in gene, protein, and P450 enzyme expression [20], all lead to significant deviations from *in vivo* responses.

Stage II: in-vivo testing

The second part of pre-clinical development is the *in vivo* testing of compounds. While EMA supports the implementation of the 3R principle, animal data on drug safety is still a hard requirement before a drug is allowed into clinical trials. The 3R principle describes the Replacement, Reduction and Refinement of animal research, specifically in that order. However, basic animal research findings only translates for about ~10% to the human clinical research [21] and 96% of drugs that pass preclinical tests (including animal research) fail to get market approval [22]. It is, therefore, necessary to carefully asses and draw conclusions from animal data regarding drug safety. There are two types of animal experimentation: a.) Basic, investigating the basic biology of human diseases and b.) Applied: describing drug research and development and, toxicity and safety testing. Irrelevant to the category, the conclusions of these experiments are often used to form conclusions regarding human biology or health sciences. Human hepatocytes have for example a lower capacity than rat hepatocytes to secrete bile acids back into blood. It was suggested that this reduced fractional elimination rate at the sinusoidal membrane contributes to a higher susceptibility towards increased intracellular bile acids concentrations and cholestatic drugs in human hepatocytes [23].

While there are several issues with animal testing, drug safety assessment in animals has been hugely successful considering that the last lethal phase 1 test occurred in 2006 with Theralizumab by PAREXEL [24]. It is, however, vital to develop the preclinical testing to save animal lives and money.

1.2 Bile acid production and the enterohepatic pathway

Bile acids are produced in the liver and then released into the intestines. Bile acids are later recycled back to the liver [12]. This highly efficient process is called enterohepatic circulation (Figure 2) [25] and plays a vital role in liver function, metabolic regulation and liver physiology. Bile contains a complex mixture of endogenous bile salts, bilirubin, phospholipids, cholesterol, amino acids, steroids, enzymes, porphyrins, vitamins and heavy metals as well as exogenous xenobiotics and environmental toxins. Bile functions as a powerful detergent and facilitates lipid and nutrition absorption as well as cholesterol and toxic metabolite excretion [7]. Due to the amphiphilic characteristics of bile salts, their accumulation in the hepatocytes would cause cell membrane damage, impair liver function and lead to cholestasis and cirrhosis. The liver regulates cholesterol homeostasis by balancing *de novo* cholesterol and bile salt synthesis, dietary cholesterol uptake, biliary cholesterol excretion, and reverse cholesterol transport from peripheral tissues.

There are two main pathways in which bile acids can be produced: 1.) the classic (also called the neutral) pathway [26] and 2.) the alternative (also called the acidic) pathway [27]. Most likely, other pathways are also present, but they are considered inconsequential to the bile acid synthesis in humans.

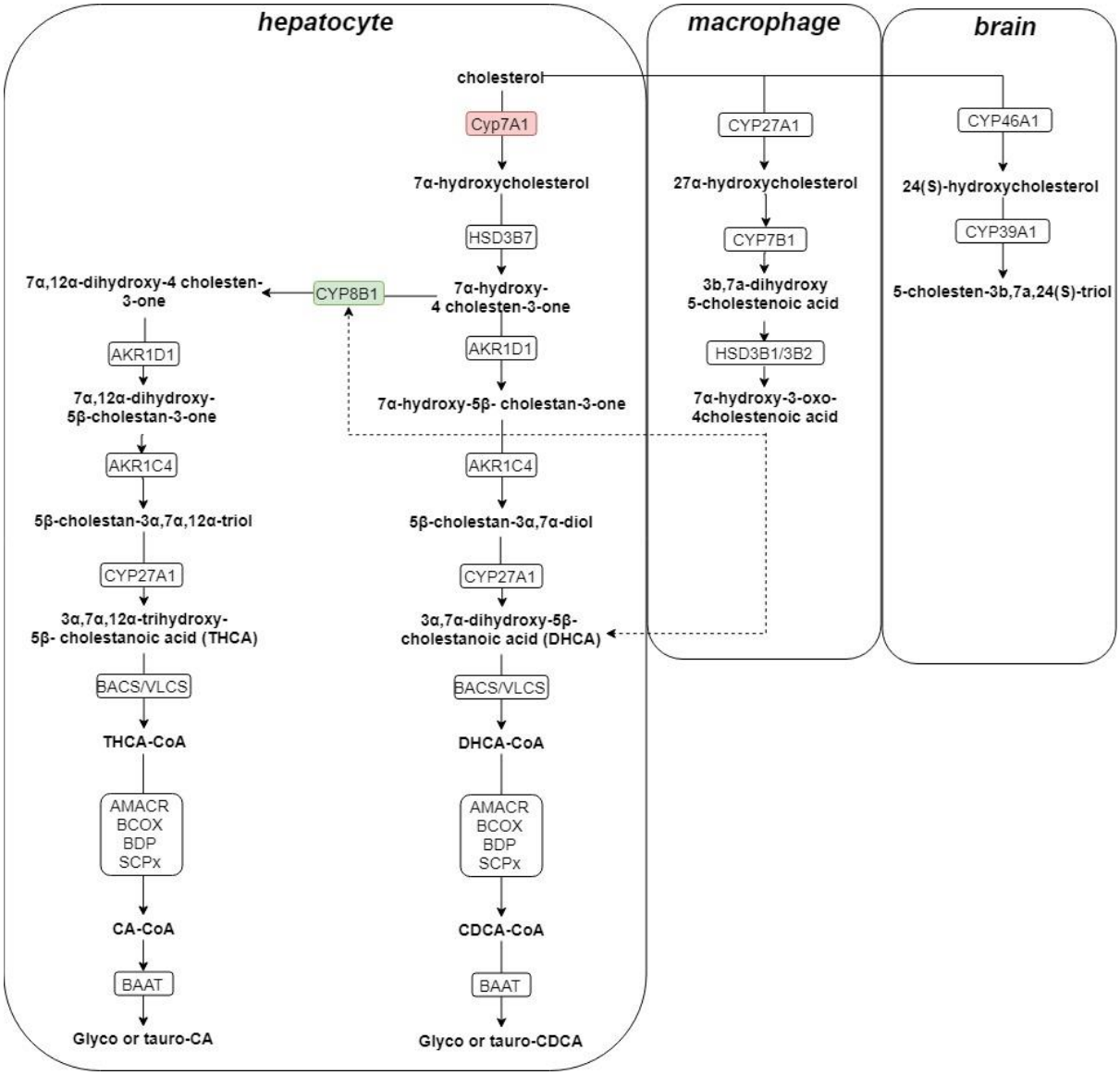

Figure 2. De-novo synthesis of primary bile acids: chenodeoxycholic acid (CDCA) and cholic acid (CA). The classical pathway is displayed on the left and is localised in the hepatocyte. The alternative pathway is displayed on the right and starts in the brain and macrophage. The rate-limiting step in the classical pathway is displayed in red and is catalysed by Cyp7A1, while the green box indicates the enzyme responsible for the composition of the de-novo bile acid pool. While all pathways result in the synthesis of CA and CDCA, the exact steps are not always known and these are indicated as interrupted lines. (Aldo-Keto Reductase Family 1 Member D1 (AKR1D1), Aldo-Keto Reductase Family 1 Member C4 (AKR1C4), Cytochrome P450 Family 27 Subfamily A Member 1 (Cyp27A1), BACS/VLCS, Alpha-Methylacyl-CoA Racemase (AMACR), Acyl-CoA Oxidase 2 (BCOX), BDP, and SCPx and Bile Acid-CoA:Amino Acid N-Acyltransferase (BAAT))

1.2.1 The classical and alternative pathways

De novo synthesis of bile acids occurs in the classical and the alternative pathway at the same time. However, the classical pathway occurs in the hepatocytes and is also known as the neutral pathway because all the intermediates are neutral sterols. *De novo* synthesis of bile acids in the liver in the classical pathway accounts for ~90% of bile acids produced and occurs by converting cholesterol into bile acids by the action of cytochrome P450 enzymes (Figure 2, hepatocyte) [28]. The first conversion is immediately the rate-limiting step. Cyp7A1 converts cholesterol into 7a-hydroxycholesterol which in turn is converted into 7a-hydroxy-4-cholesten-3-one [29]. The pathway then splits into two separate routes, one leading to cholic acid (CA) (Figure 2 left side of the path) and the other to chenodeoxycholic acid (CDCA) (Figure 2, right side of the path). The distinction is caused by Cyp8B1, which is responsible for the composition of the de-novo bile acid pool. Following on from here, the steps are identical again and are catalysed by the enzymes Aldo-Keto Reductase Family 1 Member D1 (AKR1D1), Aldo-Keto Reductase Family 1 Member C4 (AKR1C4), Cytochrome P450 Family 27 Subfamily A Member 1 (Cyp27A1), BACS/VLCS, Alpha-Methylacyl-CoA Racemase (AMACR), Acyl-CoA Oxidase 2 (BCOX), BDP, and SCPx. Following their synthesis, most bile acids are conjugated to taurine and glycine by Bile Acid-CoA:Amino Acid N-Acyltransferase (BAAT) [30].

The alternative pathways start in peripheral tissues, also called the acidic pathway as the intermediates tend to be acids and account for the remaining ~10 % *de novo* produced bile acids. The pathway is initiated by Cyp27A1 inside the macrophage (Figure 2, macrophage)[27]. Following the conversion of cholesterol by Cyp27A1, Cyp7B1 and HSD3B1/3B2 into 7a-hydroxy-3-oxo-4cholestenoic acid, the newly formed acid is transported into the hepatocyte where further conversion via the classical pathway continues into CA and CDCA. The second alternative pathway is initiated by Cyp46A1 in the brain where cholesterol is converted into cholesterol 24(S)-hydrocholesterol. This substrate, in turn, is modified by Cyp39A1 into 5-cholesten-3b,7a,24(S)-triol.

1.2.2 Recycling of the bile acids via the enterohepatic pathway (Figure 3)

The bile salts are then secreted into the canaliculi and subsequently stored into the gallbladder as mixed micelles or immediately released into the duodenum as bile [7]. After each meal, the gallbladder contracts to release bile salts into the duodenum in the form of mixed micelles with phospholipids. In the duodenum, bile salts will act as detergents to solubilise lipids and lipid-soluble vitamins, thus aiding in their absorption by the intestines [31]. A small fraction of the bile acids are further converted by gut microbiota into secondary bile acids such as deoxycholic acid (DCA) and lithocholic acid (LCA) [32,33]. Recycling of bile salts from the gut is initiated by their uptake across the apical membrane of enterocytes by the sodium-dependent bile salt transporter (ASBT). Close to 95% of the bile acids, both primary and secondary bile acids, are reabsorbed through the intestinal wall, enter the enterohepatic circulation, and are transported back to the liver. However, lithocholic acid and sulphate conjugated bile acids are mostly excreted via urine [6]. After the bile acids have been transported back to the liver, hepatocytes reabsorb the bile acids across the basolateral membrane of the hepatocytes by organic anion transport protein 2 (OATP2) and the sodium-taurocholate co-transporting polypeptide (NTCP, $SLC_{10}A_1$) [34]. In this way, bile salts can be secreted and re-adsorbed in more than 20 cycles before being excreted from the body via the faeces or urine.

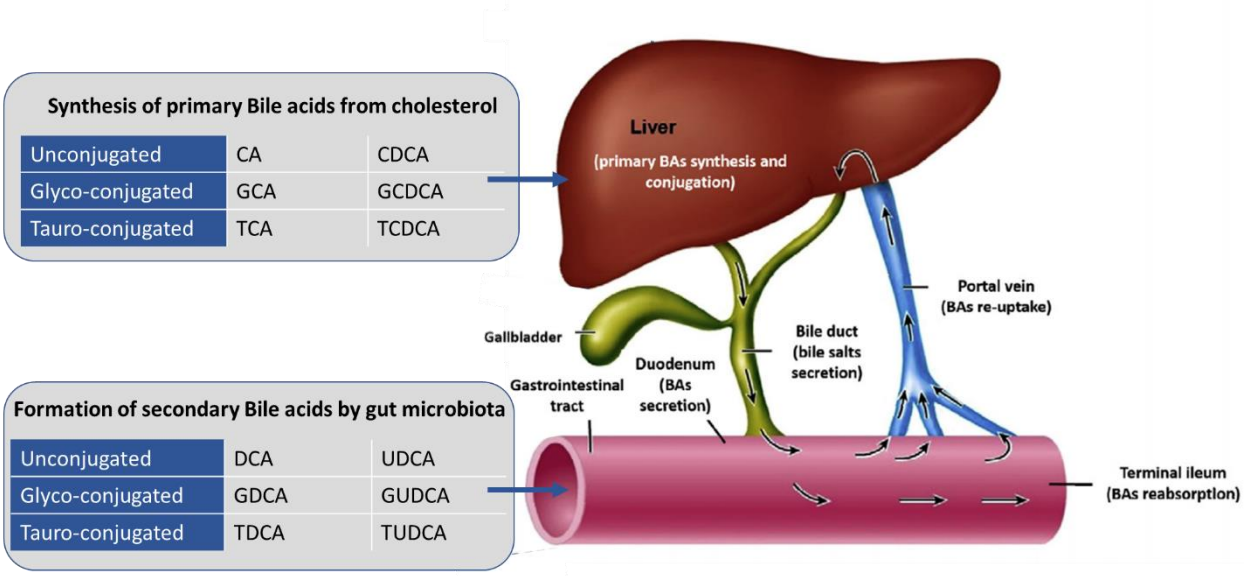

Figure 3. Schematic depicting the enterohepatic pathway. CA = Cholic acid, CDCA = chenodeoxycholic acid, GCA = glycocholic acid, GCDCA = glyco-chenodeoxycholic acid, TCA = taurocholic acid, TCDCA = tauro-chenodeoxycholic acid, DCA = deoxycholic acid, UDCA = Ursodeoxycholic acid, GDCA = glyco-deoxycholic acid, GUDCA = glyco-ursodeoxycholic acid, TDCA = tauro-deoxycholic acid and TUDCA = tauro- Ursodeoxycholic acid. The figure was adapted from [28], the inside of the grey boxes was changed to indicate different bile acids.

1.3 Bile Salt Export pump

The mammalian ABC transporter *ABCB11* known as BSEP was first described by Nishida et al. in 1991 in the canalicular membrane vesicles of the rat liver [35]. Due to BSEP's similarities with ABCB1, BSEP was initially named "Sister of P-glycoprotein" (sPGP). BSEP consists of 1321 amino acids in humans and has a molecular weight of ~160 kDa. While the BSEP's 3D protein structure remains to be determined, it is thought to be similar to that of ABCB1. It is predicted to have two membrane domains (MDs) each containing six transmembrane helices (TMHs), and two cytoplasmic nucleotide-binding domains (NBDs) that contain the Walker A, Walker B and ABC signature sequences for ATP binding and hydrolysis [31]. The two ATP molecules bind at the NBD:NBD interface in two non-equivalent ATP binding pockets of which only one pocket catalyses the hydrolysis of the bound nucleotide. BSEP is specifically expressed in the liver and as its name suggests is responsible for the transport of bile acids as a rate-limiting step in bile acid biogenesis. BSEP is predominantly present in cholesterol-rich rafts in the apical membrane of hepatocytes where it is one of the most abundant canalicular efflux transporters [5].

1.3.1 BSEP: its importance and regulation

Bile acids function as powerful detergents and facilitate lipid and nutrition absorption as well as the absorption of cholesterol and toxic metabolite excretion [36]. Due to these detergent properties of bile salts, their accumulation in the hepatocytes will cause cell membrane damage, impair liver function and lead to cholestasis and cirrhosis. In recent years, interest in canicular BSEP has increased, given its importance in the biliary clearance of numerous bile acids. Focus has shifted to BSEP's roles in several pathogenic phenotypes, including DILI. BSEP expression is tightly controlled, and drugs able to interfere at any level of bile acid synthesis and transport will have a significant effect on the hepatocyte's ability to clear bile acids.

BSEP transcription

BSEP-mediated transport is regulated at three distinct levels, (i) BSEP gene transcription, (ii) protein trafficking and (iii) transport activity. BSEP transcription is regulated by two transcription factors [31,37]. The first is the nuclear hormone receptor FXR and the second its heterodimeric partner, RXR. Both also control the expression of several other liver transporters. Alterations in the expression of either FXF or RXR would be capable of altering the expression of a large number of bile salt synthesis genes and transporter genes. Studies

in human, rat and mouse confirm that bile salts increase BSEP expression in primary human hepatocytes or HEPG2 cells by activating FXR. Several bile acids can directly bind to the FXR and RXR [38]. For example, FXR can be activated by CDCA>DCA>LCA>CA in a reducing order [39], where CDCA selectively activates FXR expression. In another example, LCA inhibits BSEP expression by down-regulating agonist-dependent BSEP expression by directly binding to FXR. Although CDCA is thought to be most potent in activating FXR, LCA was found to exhibit a higher binding affinity. LCA has recently also been identified as an agonist of PXR, which is a second bile acid receptor that plays an essential role in liver detoxification. However, PXR does not regulate BSEP gene expression.

Intracellular trafficking of BSEP

The second level at which BSEP is regulated is the continued recycling of the protein and its trafficking between intracellular endosomes and the canalicular membrane on the apical side of hepatocytes. This regulation is mediated by kinases and ubiquitination, and is based on several mechanisms [40] (see Figure 4). A reduction in the amount of BSEP at the membrane can be achieved by either increasing the recycling away from the apical membrane via hypoxia (through Ca^{2+}-dependents, PKC mediated mechanism [41]) or via the activation IL6, IL1a and TNFα by Lipopolysaccharide (LPS). The transport from Rab 11-positive endosomes to the apical membrane can be disrupted by activation of phosphoinositide 3-kinase (PI3K)/protein kinase B pathway by estradiol-17b glucuronide and oxidative stress, in a Ca^{2+}-dependent manner. This in turn activates the protein kinase C epsilon pathway in a Pi3K dependent manner, which in turn activates AKT pathway and prevents the movement of BSEP towards the membrane [42]. LCA, in turn, can directly activate the PKC pathway in a PI3K dependent way. To increase the amount of BSEP at the membrane, microtubule inhibitors block cyclic AMP dependent insertion BSEP in the membrane. One of the most important reasons for BSEP to move towards the membrane is the need to export bile acids due to high concentrations in the cell. Bile acids can do this either by directly recruiting BSEP to the membrane (in case of TCA) or by recruiting BSEP to the membrane indirectly by activating the p38 and PKC pathway (as is known for TUDCA) [31]. The activity of kinases is intricately tied to levels of oxidative stress in hepatocytes. Thus, any drug affecting oxidative stress can interfere with the presence and activity of BSEP in the canaliculi.

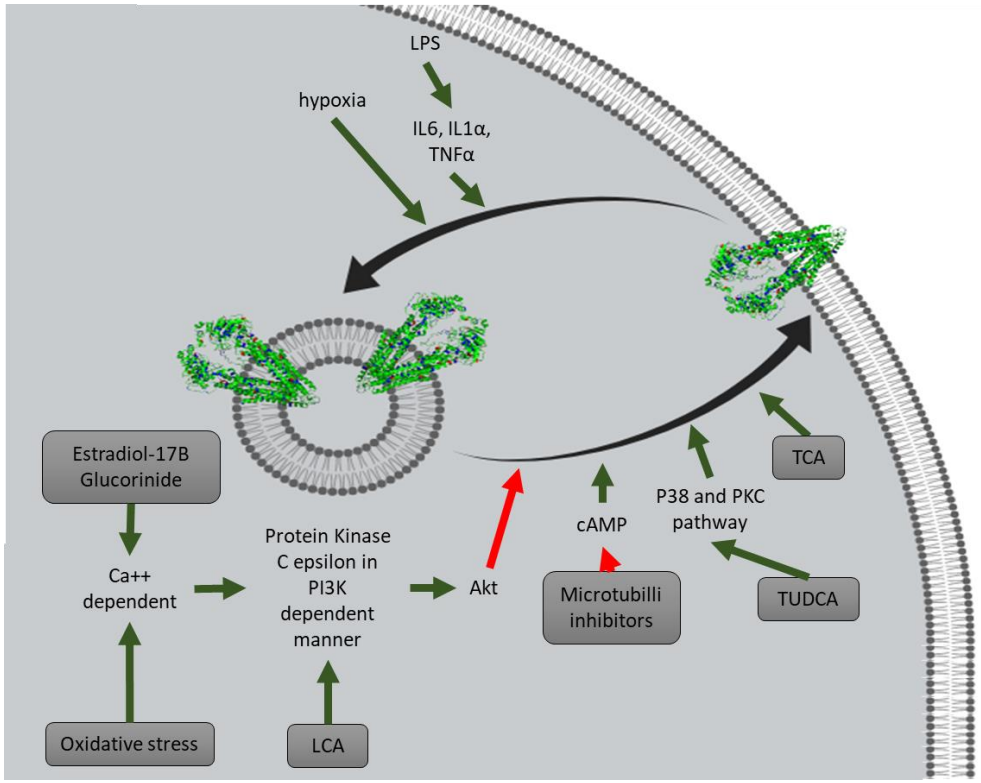

Figure 4. Mechanism of BSEP trafficking within the cell. BSEP is continually recycled between intracellular vesicles and the apical side of the hepatocyte. cAMP, P38/PKC and TCA directly increase BSEP incorporation into the membrane. Estradiol and oxidative stress both inhibit BSEP trafficking to the membrane via a Calcium dependent activation of Akt pathway, LCA inhibits the trafficking by activating he Pi3K pathway directly. While trafficking away is regulated directly by hypoxia and via IL6, Il1α and TNFα via LPS. The green arrows indicate a stimulating effect while the red arrows indicate an inhibitory effect on the trafficking of BSEP protein.

1.3.2 Multiple causes exist for DILI

Due to the recycling of bile acids and BSEP, events causing cholestasis and DILI may be divided in: i) prehepatic events, where the liver is inhibited from taking up unconjugated bilirubin, ii) intrahepatic events, where bile acids are prevented from leaving the liver and iii) post-hepatic events, where an injury of the bile duct prevents clearing of bile acids [43,44]. These effects can be caused by either direct or indirect effects of drugs (Figure 5). Drugs can have an indirect effect by altering the effect of nuclear hormone receptors (responsible for regulating gene transcription), bile acid synthesis or the regulation of BSEP protein expression at the membrane. Direct effects can consist of inhibiting the uptake of bile acids into the hepatocyte, effects on the bile acid pool, and the inhibition of bile acid export from the hepatocyte. It is the latter where BSEP is the rate-limiting step and the designated transporter [31]. Due to BSEPs importance in clearing bile acids from the hepatocyte, it is custom in pharmaceutical companies to investigate the effect of drugs on BSEP inhibition in a transport assay [45]. In this assay, inside-out membrane vesicles are incubated with radiolabelled TCA in the presence and absence of tested drug. After a defined incubation time the excess TCA is washed away, and the TCA accumulated within the membrane vesicles is measured (Figure 6) [35]. Many drugs causing idiosyncratic DILI have been shown to inhibit BSEP at relevant in-vivo steady-state drug concentrations in plasma of humans. However, these assays do not report on the individual effects of drugs on specific bile acid concentrations. The potential indirect effects of bile acids on hepatocytes are also frequently ignored. [46].

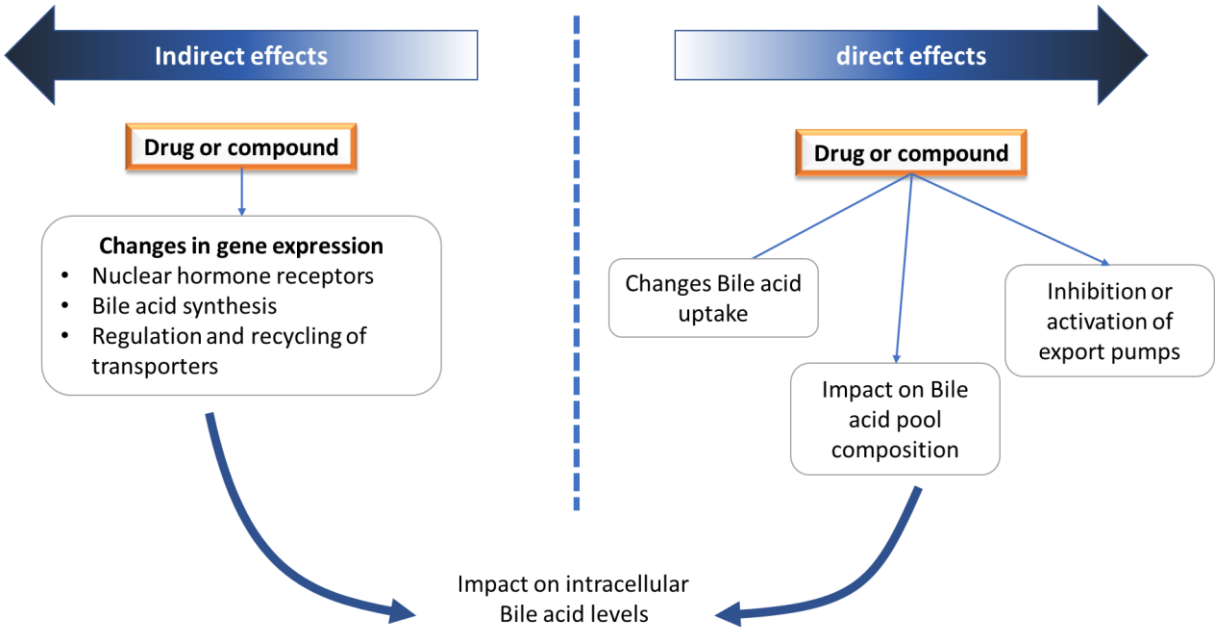

Figure 5. Overview of possible effects of drugs/compounds affecting bile acid concentrations or bile acid compositions within the hepatocyte.

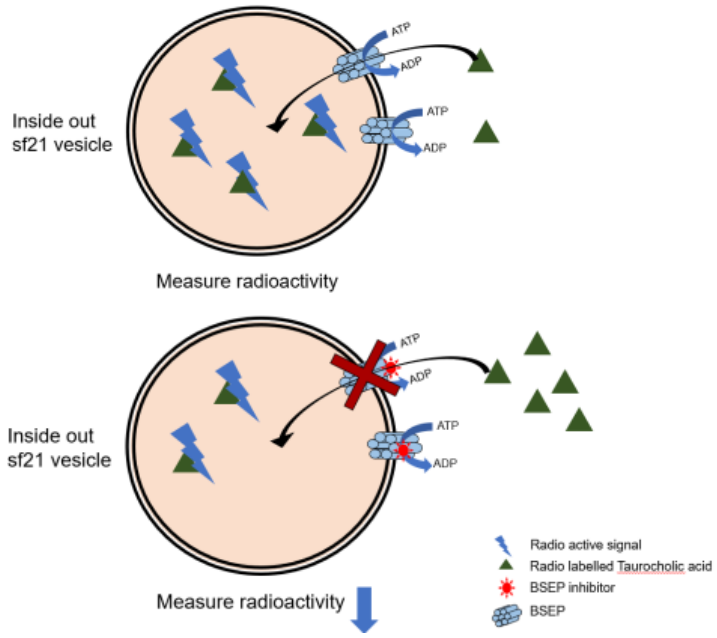

Figure 6. Schematic showing how the direct inhibition of BSEP activity is investigated by pharmaceutical companies. Inside-out Sf21 membrane vesicles are incubated with radiolabelled TCA in the presence of different concentrations of the drug. After a specified incubation time, the excess external radiolabelled TCA is washed away, and the radiolabelled TCA captured in the lumen of the membrane vesicles is measured. If the drug is a weak inhibitor the radioactive signal will be larger than if the drug is a strong inhibitor.

Alternative drug effects on BSEP's efficiency to transport bile acids

Finally, BSEP transport activity can be strongly influenced by drug-protein interactions. BSEP has been shown to interact with many different drugs when it comes to direct inhibition of transport activity. However, drugs can directly inhibit proteins in several other ways. Drugs could irreversible inhibit BSEP by binding covalently to the protein and changing or blocking its binding pockets. Alternatively, BSEP can be inhibited by reversible inhibitors by three different mechanisms: I.) competitive inhibition (Vmax constant, Km increased), where drugs directly compete with the substrate (i.e. bile acids) to be transported for binding in the binding pocket. II.) non-competitive inhibition (Vmax reduced, Km is constant), where drug binding to BSEP is independent of substrate binding, and where drug binding would prevent bile acid transport, and III.) uncompetitive inhibition (Vmax and Km reduced), where drugs would bind to the BSEP-substrate complex, and inhibit further progression of the transport reaction [47]. Type 1 inhibition could be overcome by an increasing the amount of substrate and would be more pronounced for bile acids that bind with reduced affinity to BSEP. This type of inhibition could therefore alter the composition and possibly the toxicity of the bile acid pool in hepatocytes [48]. As BSEP expression and functionality are crucial for liver protection, further studies on these mechanisms are therefore of utmost importance.

1.3.3 BSEP mutations

Due to the crucial role of BSEP in the excretion of bile acids, alterations in BSEP activity have a significant effect on the functioning of hepatocytes [49]. The effects can consist of alteration of liver regeneration, glucose homeostasis, energy expenditure, atherosclerosis or carcinogenesis. The effect may be ascribed to the detergent and hydrophobic aspects of bile acids that activate the apoptotic pathways. There are several liver diseases related to BSEP dysfunction [7]. BSEP mutations are able to cause several detrimental phenotypes in humans, the diseases associated with them are called PFIC2, benign recurrent intrahepatic cholestasis, type 2 (BRIC2), and intrahepatic cholestasis (IHC) of pregnancy.

Many mutations responsible for impaired BSEP function have traditionally been linked to PFIC2 and BRIC2. However recent studies show that BSEP impairment or alteration can explain intrahepatic cholestasis in pregnancy, diabetes type 2, colon cancer, primary biliary cholangitis and primary sclerosing cholangitis.

Missense mutations can influence BSEPs ability to transport bile acids, affect protein stability and degradation and transport and incorporation to the membrane. All of these can influence not only the total bile acid accumulation but could possible cause a shift in internal bile acid composition towards more toxic bile acids.

In a search of the literature, we were able to find 264 known point mutations in BSEP (Figure 9 see Appendix A and B). However, many of them have only been reported in case studies where a patient showing symptoms of cholestasis has been screened for BSEP mutations. The effect of BSEP mutations on protein expression, protein function, or how these point mutations affect protein structure have often been neglected (see Figure 7).

PFIC2

Mutations in ABCB11 causing PFIC2 in the ABCB11 gene, and a typical feature is the absence or reduction of canicular BSEP expression [7,50]. There are many known missense or nonsense mutations associated with PFIC2 [51,52]. Nonsense mutations cause premature termination of translation, thus explaining the absence of BSEP expression. Missense mutations are generally thought to cause a deficiency of BSEP due to interference with splicing efficiency, or by inducing misfolding of BSEP protein and lastly by enhancing BSEP recycling due to changes in ubiquination patterns. Interestingly, almost all missense mutations within the transmembrane helices are associated with severe phenotypes of BSEP disease (PFIC-2, see Figure 8).

BRIC2

BRIC-2 is a milder form of liver cholestasis and can be caused by either heterozygous or homozygous mutations in the *ABCB11* gene [53]. Recently the possibility of a transition between BRIC2 and PFIC2 was proposed in cases of homozygous G374S mutations [54]. Amino acid 374 is part of the sixth transmembrane helix of BSEP and lies in the vicinity of the translocation pore for the substrate, which would explain the reduced transport capacity. A common polymorphism p.V444A has been associated with an increased prevalence of DILI [34]. However, no kinetic difference has been found between WT and P.V44A mutation in TCA transport assays [55].

While both diseases are caused by mutations in BSEP, they differ in their respective phenotypes. PFIC2 is characterized by a continues progression of liver damage and usually

requires a liver transplantation to save the patient. BRIC2 is a more benign disease, characterised by intermittent episodes of cholestasis, which does not show progression. [16] When researching mutations associated with BSEP, D482G and E297G are the most common but there are many inconsistencies in literature dependent on the cell types and assay used to investigate them. Both are known to decrease taurocholic acid transport in Sf21 insect cells expressing BSEP. However, in HEK 293 cells these mutations revealed normal TC transport [53]. One observation is that mutations associated with PFIC2 are more dangerous to BSEP function than BRIC2 associated mutations. Little research has been done into this. Kagawa et al. 2007 showed that six mutations associated with PFIC2 were associated with reduced expression level at the membrane. This is in agreement with Ling et al. [17] who show that expression levels of BSEP at the apical site of the membrane are inversely associated with the severity of cholestasis.

Intrahepatic cholestasis of pregnancy

Another type of cholestasis associated with BSEP is ICP. This is a cholestatic disorder that usually develops in the third trimester of pregnancy and persists until delivery and affects about 1.5% of pregnancies among Caucasians. [18]

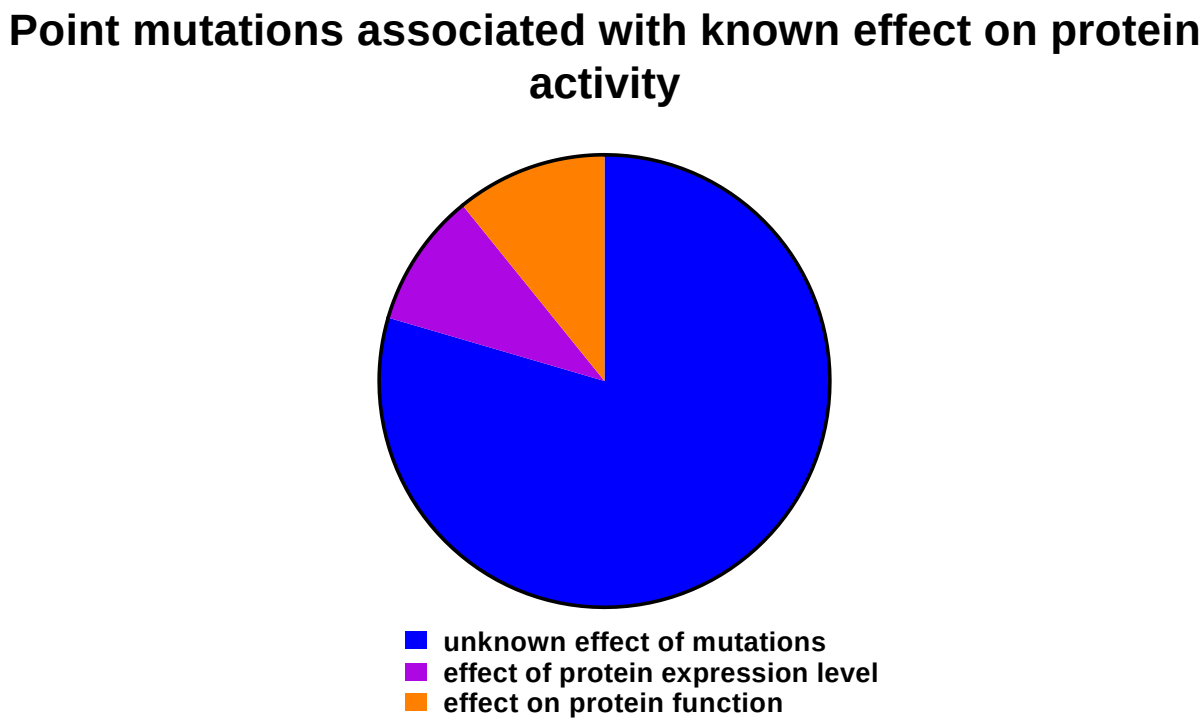

Figure 7. Point mutations and their known influence. 264 total known point mutations, 32 known to affect protein expression and 36 known to influence the activity.

BSEP mutations can have a devastating influence on BSEP functionality. A comprehensive literature review showed that 264 pointmutations are known in BSEP, of which only 32 are known to influence the BSEP expression and 36 affect protein activity. A graphical image regarding the known vs the unknown is presented in Figure 8.

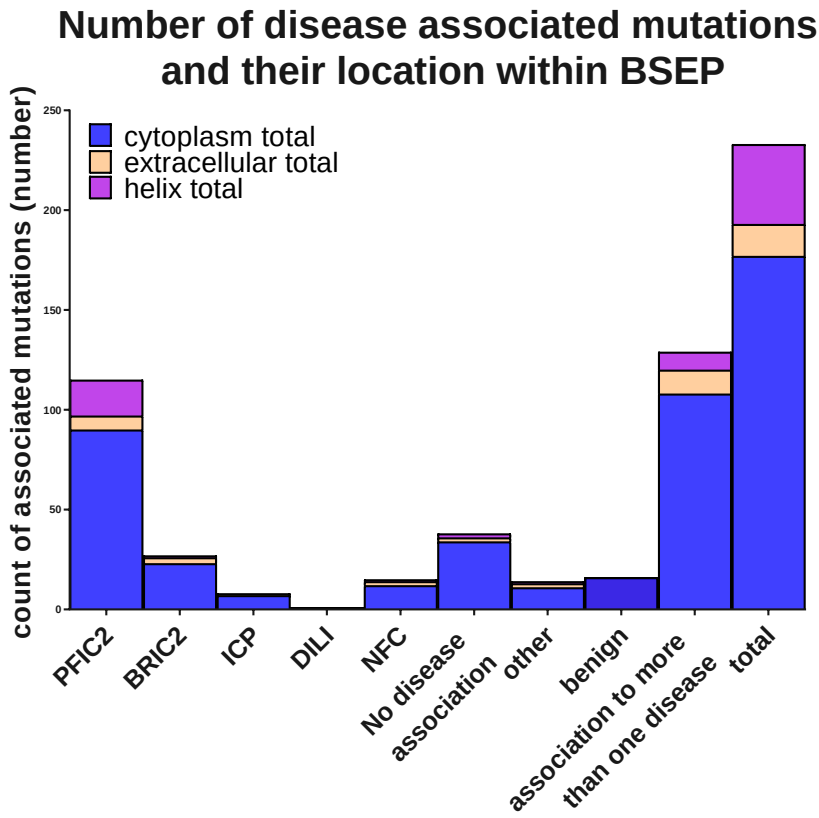

Figure 8. A count of mutations, where they occur compared to the disease they are associated with. The number of mutations associated with progressive familial intrahepatic cholestasis type 2 (PFIC2), benign recurrent intrahepatic cholestasis type 2 (BRIC2), intrahepatic cholestasis of pregnancy (ICP), drug induced liver injury (DILI), non-fibrosing cholestasis (NFC), mutations with no disease association, others, benign association, how many of these mutations are associated with more than one disease, and the total count. (location is based on homology model in figure 9).

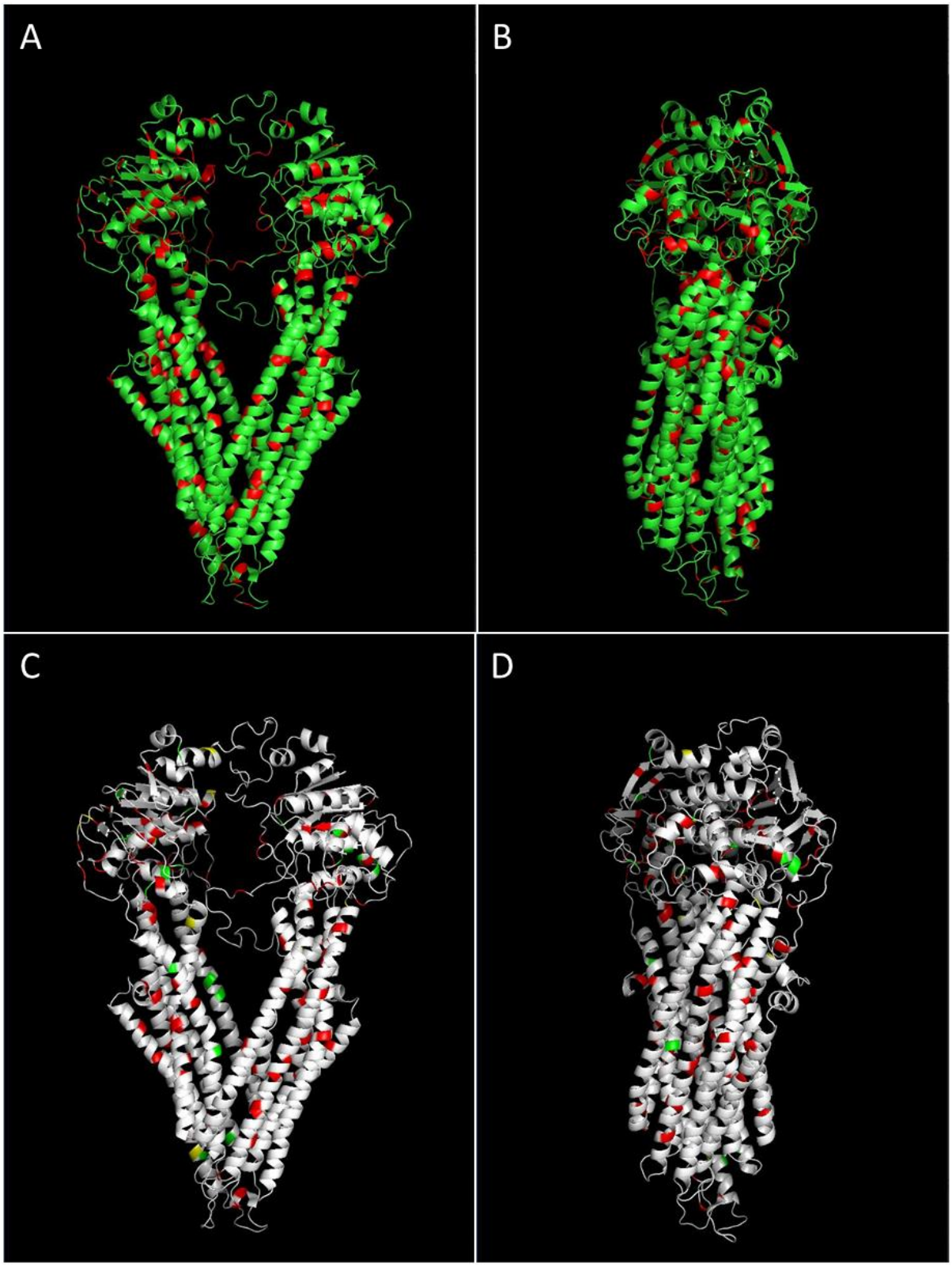

Figure 9. Homology model created based on MDR1 crystal structure. Image A displays all the mutations that have been annotated in literature on top of the proposed structure for BSEP. Image C indicates the location of all mutations that are correlated to the respective diseases PFIC2 (red), BRIC2 (green) and IHC (yellow). Figures B and D are the respective of image A and C turned by 90°. Images were created in PyMol.

1.4 Overview of chapters in this thesis

The aim of this research was to increase our understanding of the bile salt export pump, how it transports bile acid and how dysfunction might cause DILI.

For this we have addressed several hypotheses:

1.) Compounds can inhibit the bile salt export pump in either competitive, non-competitive, uncompetitive or in a mixed competitive manner.

2.) Compounds can affect the bile acid pool composition in addition to the total bile acid concentration.

3.) Compounds can influence BSEP expression at the membrane and thereby affect the bile acid concentration and pool composition.

Chapter 2 will give an overview of methods and procedures that were used in the various experiments.

Chapter 3 will investigate the drug-based mechanisms of direct BSEP inhibition.

Chapter 4 will give a general introduction into metabolomics that is relevant for the results in the next two chapters.

Chapter 5 investigates the effect of drug treatments on the metabolomics of individual bile acids in 2D and 3D cultured primary human hepatocytes.

Chapter 6 investigates the effect of treatments on the metabolomics of signalling lipids that play a role in inflammation or protective measures, and that are responsible for communicating effects to other cells.

In **Chapter 7**, the conclusions and data from this research are discussed in the context of current literature. It also contains recommendations for future experiments in this research area.

2. Material and methods

2.1 Protein expression in Sf21 insect cells

Human BSEP protein was expressed in *Spodoptera frugiperda* (Sf21) insect cells. Similar to human cells, insect cells offer the advantage that expressed proteins undergo post-transcriptional modifications. However, insect cells present several advantages to mammalian cells, such as the ease of culture, the high tolerance to by-products and the generally higher protein expression levels.

The steps involved in the expression of human proteins in insect cells are as follows:

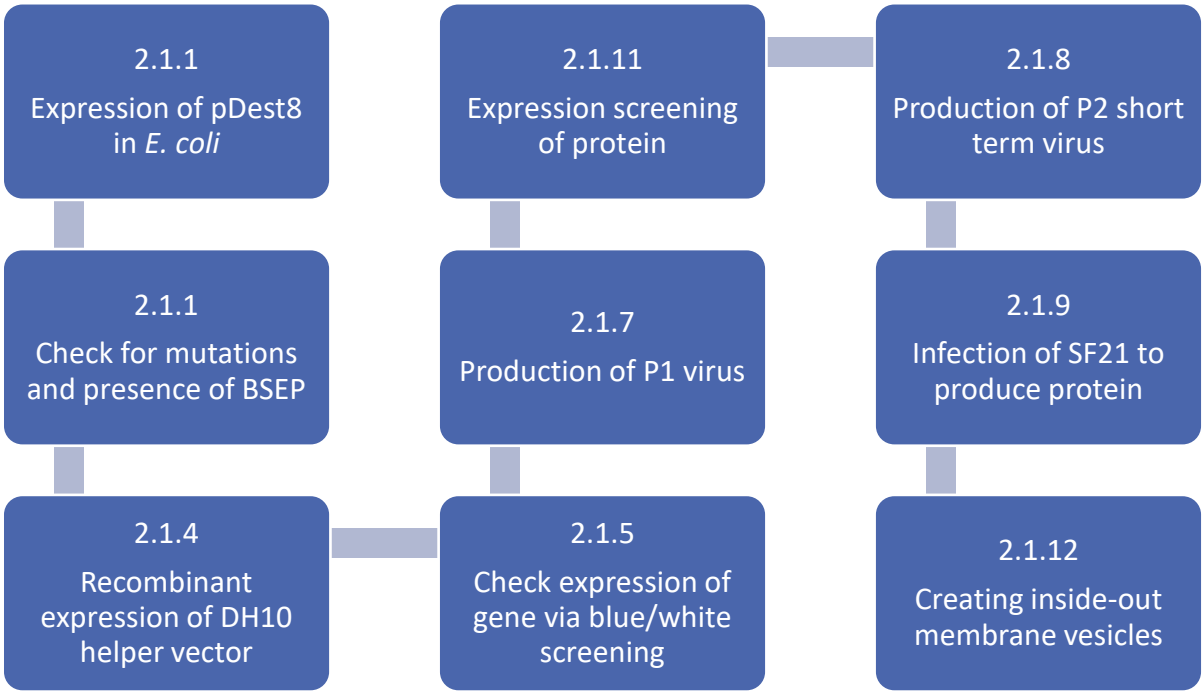

The Bac-to-Bac baculovirus expression system was chosen as the method for protein expression in Sf21 cells. The steps to go from the gene of interest to protein expression are explained in Figure 10. The donor plasmid, providing the gene of interest, used was pDEST8 (Figure 11) which was transformed into competent *E. coli* cells containing a helper plasmid and the Bacmid DNA (Figure 12). The helper plasmids function is to assist in trans-positioning the gene of interest into the Bacmid vector. Following the transposition, the cells were selected with antibiotics, and Bacmid DNA was isolated. The Bacmid was then transfected into Sf21 cells to produce recombinant baculovirus that allowed me to obtain BSEP expression in Sf21 cells.

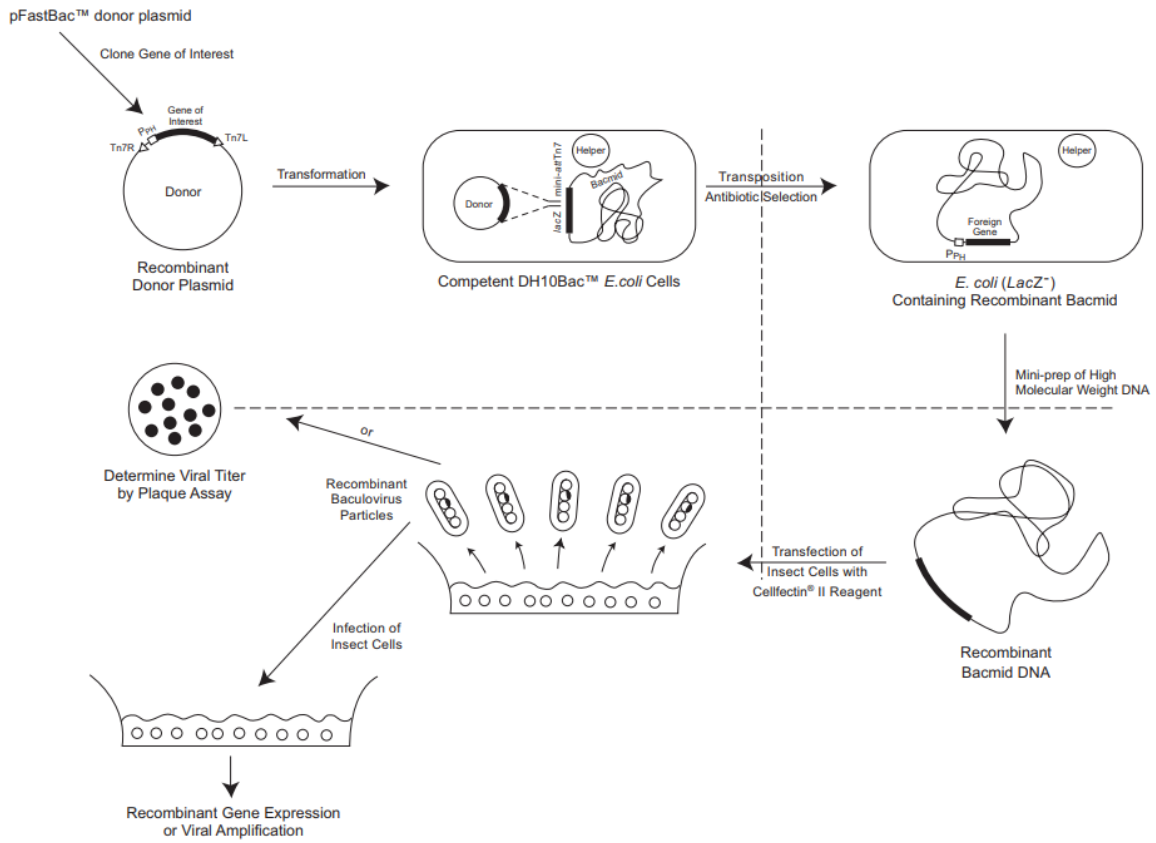

Figure 10. Method of bac to Bac protein expression for Sf21 cells. Image obtained from Invitrogen life technologies [56].

2.1.1 Mutants and gene constructs used in the preparation of inside-out membrane vesicles containing BSEP

To express BSEP in Sf21 cells, the following plasmids and primers were used.

pDest8 construct

pDEST 8 is a Gateway destination vector for expressing proteins in insect cells using the Bac-to-Bac baculovirus system. The plasmid contains a polyhedron promotor and ampicillin and gentamycin resistance genes. The target Gene is inserted between attB1 and attB2 via recombination with attL flanked target gene. AstraZeneca supplied pDest8 vector containing *ABCB11* c.1517T>C causing a P. V444A mutation (Global minor allele frequency: 0.4113(A))

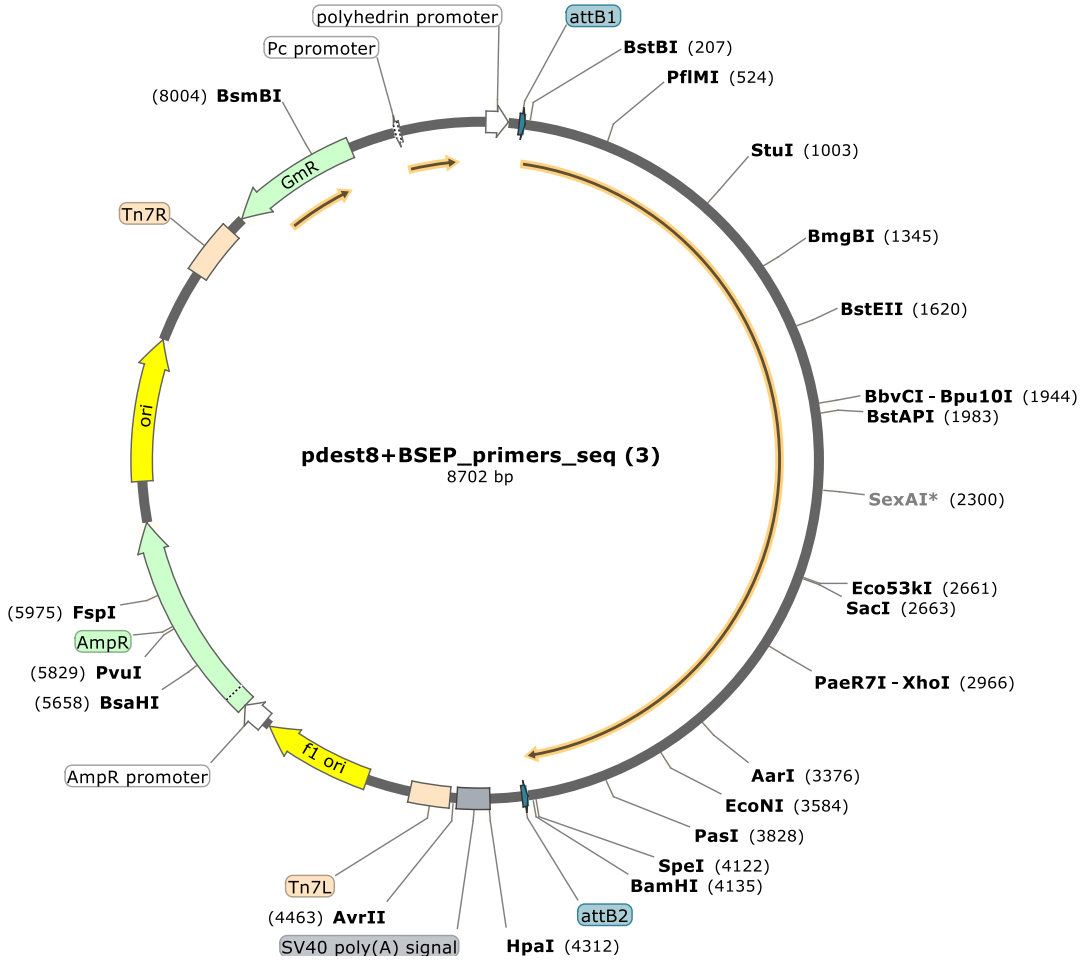

Figure 11. pDEST8 including BSEP sequence. Obtained from Snapgene.

pFastBSEP plasmid map

The pFastBSEP plasmid is provided in competent *E. coli* DH10 cells with the following genotype: F-mcrA Δ (mrr-hsdRMS-mcrBC) Φ80lacZΔM15 Δ lac X74 recA1 endA1 araD139 Δ(ara, leu)7697 galU galK λ - rps L nupG/pMON14272. The plasmid contains a low-copy number mini-F replicon, a kanamycin resistance marker, and a segment coding for LacZa peptide from PUC plasmid into which the attachment site for the bacterial transposin Tn7 (min-attTn7) has been inserted. While the insertion itself does not disrupt LacZα peptide, it can still complement a partial deletion in the bacterial DNA to express LACz peptide. In the presence of blue-gal of X-gal and the inducer IPTG, cells containing this bacmid will produce a blue dye and create blue colonies. The *E. coli* DH10 cells also contain the helper plasmid pMON7124 encoding the transposases which confers resistance to tetracycline. pMON7124 provides the Tn7 transposition function in trans (Barry et al. 1988).

Once the gene of interest has been inserted into the TN77L site, with the use of the helper plasmid pMON7124, the partial LacZ gene on the plasmid has been disrupted, and the colonies (with the correctly inserted gene of interest) are unable to produce blue colonies and will be white instead.

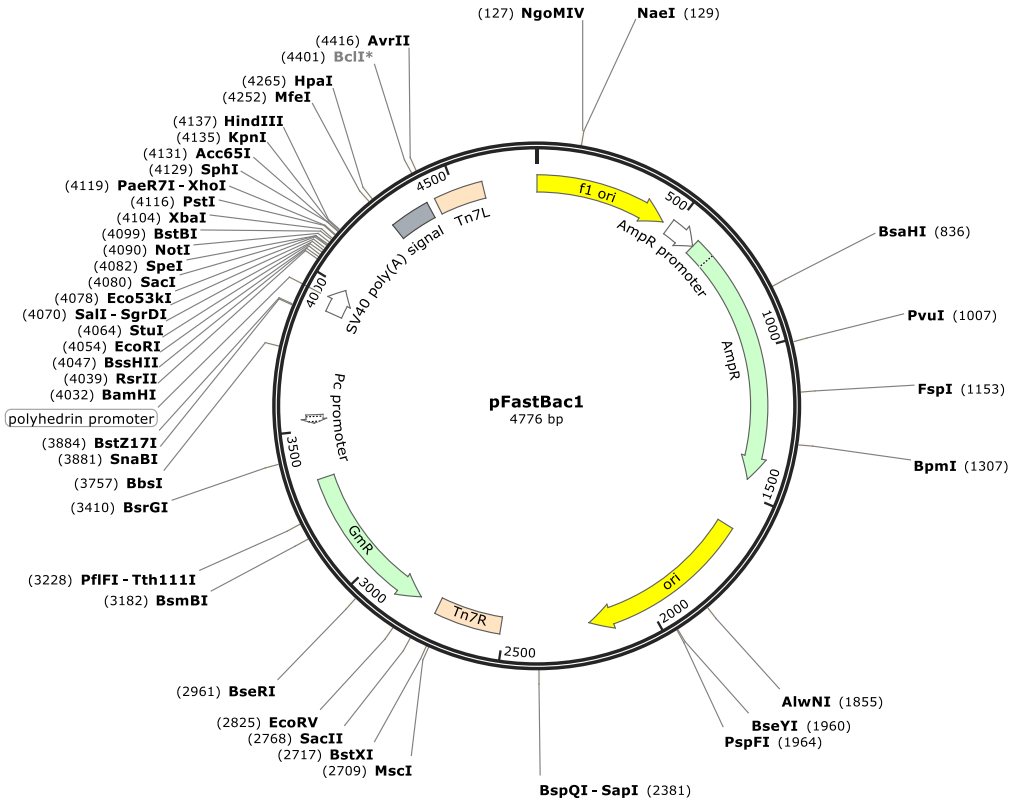

Figure 12. pFastBac1 plasmid map displayed without *ABCB11*. Obtained from Snapgene.

Genes, Sequences and primers

Wild type (WT) of *ABCB11* was achieved via round-the-horn mutation using the primers in Table 1. BSEP mutants indicated with an * in Table 2 were bought from GenScript.

Table 1. Primers used for the creation of WT BSEP.

FW	5'-catttcccctggtttaatgaccatgttgaggtcatttag-3'
RV	5'-ctaaatgacctcaacatggtcattaaaccaggggaaatg-3'

Table 2. Summary of mutants created and acquired via GenScript.

Alternative names	DNA changes	Amino acid change/name
WT	c. 1517C>T	A444V
AZ mutant	c.1517T>C	V444A
*	c.1517C>T, c.1174T>A, c.1175G>C	W330A
*	c.1517C>T, c.1195T>G, c.1196A>C	Y337A
*	c.1517C>T, c.2500T>G, c.2501A>C	Y772A
*	c. 1517C>T, c.3283A>G, c3284G>C	R1033A
*	c. 1517C>T, c.3272A>G	T1092A

To confirm that the amplified DNA sequences only contained the desired mutation, the entire *ABCB11* gene in pDest8 was sequenced using 10 forward and 1 reverse primer (indicated in Table 3)

Table 3. Primers used for sequencing

name	Primer sequence
1	5'-ctccatggaatagcccagcc
2	5'-ctgtcagccctctcattggg
3	5'-gaagcctttgcaactggacg
4	5'-gggatagtggagcaagagcc
5	5'-tgctcatcgcttgtctacgg
6	5'-catgctggtagggtctgtgg
7	5'-tgcttcccAagttcaagggg
8	5'-agaagcccttcaagacagcc
9	5'-cagacactggcgtttgttgg
10	5'-ctccatggaatagcccagcc
11 (RV)	5'-atgcttttgggtcattgccg

2.1.2 Obtaining the *ABCB11* c. 1517C>T gene with round-the-horn site-directed mutagenesis.

To enable ligation of the amplified plasmid DNA after the round-the-horn mutagenesis, primers were first phosphorylated by the addition of 35 µL Milli-Q water, 5 µL polynucleotide kinase (PNK) buffer A (enclosed with PNK), 1µL 50 mM MgCl2, 1 µL 100 mM ATP, 1 µL polynucleotide 5'-hydroxyl-kinase (PNK) and 5 µL 100 µM primer together in sterile Eppendorf tubes. The mixture was then incubated for 30-60 min at 37C, and PNK was inactivated by heating the mixture to 65°C for 20 min. The primers were then mixed and stored at -20°C until use.

The mutagenesis was performed by mixing 10 ng pDest8 containing *ABCB11* c.1517T>C with 35 µL MQ, 10 µL 5x GC buffer, 1 µL (10 mM) dNTP mixture, 5 µL of the combined phosphorylated primers, and 0.5 µL Phusion polymerase. The mutagenesis mix was immediately placed in thermocycler using the settings as specified in Table 4.

Table 4. Thermocycler settings for RTH site-directed mutagenesis

temperature	**time**	**repeats**
Initial denaturation 98°C	60 s	1X
Denaturation 96°C	30-60 s	20-25X
Annealing Tm -5°C	30-60 s	
Extension 72°C	30 s/kb (for Phusion)	
Final extension 72°C	5-10 min	1X
Cooldown and idle 4°C	10 min - O/N	optional

The acquired product was digested with the restriction endonuclease DPN1 overnight at 37°C and subsequently run on an 0.5% agarose gel. After the appropriate band was excised, DNA was extracted using the Gel extraction kit (Thermo Fisher). Equal amounts of binding buffer were added to the gel, and the mixture was heated at 60°C for 10 min. The mixture was then filtered in supplied filter tubes for 1 min at 16000x g. The flow through was discarded and the filter was washed twice. DNA was eluted in sterile MQ and measured for yield and purity.

The linear DNA was then ligated to create a vector with T4 DNA ligase for 1-2 hrs at 22°C and stopped by heat denaturation at 80-85°C for 5-10 min. Plasmids were then stored at -20°C until they were used to transform *E. coli* cells.

2.1.3 Amplification of pDest8 plasmid in *E. coli*

Plasmid isolation

Plasmid pDest8 containing the *ABCB11* gene was extracted from 10 mL overnight *E. coli* cultures using the GeneJET plasmid miniprep kit according to the manufacturer's instructions (Thermo Scientific). The cell pellet was resuspended in 250 µL resuspension buffer. The cells were lysed using the lysis buffer under inversion of the tubes. After the addition of 350 µL neutralisation buffer, the tubes were again carefully inverted. Separation of cell debris from plasmid DNA was achieved by centrifugation at 12800 x g (Eppendorf centrifuge) for 10 min. The supernatant was added to the included spin column and washed twice with wash buffer containing 70% ethanol, after which plasmid was eluted with 30 µL sterile-nuclease free water. Yield and purity of the plasmid preparations were checked using the nucleic acid setting on the NanoDrop 1000 spectrophotometer. The spectrophotometer calculates the absorbance of the sample at different wavelengths (range 220-350 nm) where the DNA concentration is based on absorbance at 260 nm. The purity is determined by two ratios: 260/280 nm and 260/230 nm. The 260/280 nm should be around ~1.8; higher values indicate contamination with RNA and lower values indicate the presence of protein, phenol or other contaminants in the sample. The 230/260 nm ratio is a secondary purity analysis for nucleic acid and is in a good range between 1.8-2.2. Lower values in this ratio indicate the presence of co-purified contaminants.

2.1.4 Transpositioning of DH10 Bacmid

To transpose the *ABCB11* gene from the pDEST8 to the Bacmid vector, 10 ng/µL pDest8 vector was added to DH10 Bacmid cells and incubated on ice for 30 min. The cells and plasmid mixture were heat-shocked at 42 °C for ~45 s. After an incubation on ice for 2 min, 200 µL SOC medium was added to each transformation and incubated at 37°C for 5-6 hours. To perform a blue/white screening the transformed cells were plated on L-agar plates (L-agar: 37 g/L) with kanamycin (50 µg/mL), gentamicin (7 µg/mL), tetracycline (10 µg/mL), IPTG (40 µg/mL) and X-gal (60 µg/mL). Plates were incubated at 37 °C for 48-72 hours. Before picking large white colonies, plates were stored at 2-8 °C for one hour, as this increased the difference between false and true positives. The Bacmid in the *E. coli* DH10 cells encodes LacZα peptide, which is able to produce a blue dye in the presence of X-gal and IPTG. Yet, once the gene of interest has been correctly transposed from pDEST8 to the Bacmid, the lacZα gene has been

replaced after which the DH10 cells are unable to produce blue dye and therefore remain white. White colonies were picked for inoculated in L-broth containing kanamycin (50 µg/ml), gentamicin (7 µg/ml), and tetracycline (10 µg/ml) and placed overnight at 37 °C at 250 rpm.

2.1.5 Plasmid isolation from *E. coli* DH10 cells

Cell pellet obtained from the overnight incubation was frozen and thawed twice before being resuspended in P1 buffer from the Qiagen maxiprep kit and resuspended in P2 buffer. After 4 min incubation P3 was added and carefully mixed. After spinning at 16000x g for 10 min at 4 C. Supernatant was added to 800 µL propan-2-ol and incubated on ice for 10 min. After centrifuging for 16000x g for 15 min at 4°C the pellet was washed in 70% ethanol and centrifuged again at 16000x for 15 min at 4°C. After removing all ethanol, the pellet was dried for 2 min at RT, RNase free MQ was added to the pellet and pellet dissolved by a freeze-thaw cycle. Bacmid DNA was stored at -20°C till use. Extra care was taken to pipet the Bacmid as little as possible due to avoid DNA shearing due to its size.

2.1.6 Sf21 Insect cell culture

Sf21 cells were passaged in Sf900 II medium (Invitrogen) three times per week to ensure cells were maintained within the mid-log phase of growth. Cells were seeded at 3E+05 viable cells/mL (v.c./mL) in new vented shake flasks (corning) or roller bottles (corning) and grown for three days (Friday to Monday) and at 5E+05 v.c/mL for two days (Monday to Weds and Weds to Friday). Cells were incubated at 27°C at 140 rpm in the Innova (25mm orbit) incubator. Cells were checked for viability and diameter size on every passage. Cell cultures that fell below 95% viability were discarded as well as cells that showed defined bloating.

2.1.7 P1 Virus production

The P1 virus stock is used as long-time storage and back-up to produce BSEP-containing membrane vesicles. If the volume falls below 1 ml, a long term P2 virus stock is to be produced. For each construct, 150 µL SF900II media (GIBCO), 20 µL Superfect transfection reagent (Qiagen) and 10 µL Bacmid DNA was added to selected wells and allowed to stand for 30 min at RT. Cells were prepared at 5E+05 v.c./mL in SF900 II SFM +10% accredited fetal calf serum (FCS) and gentamicin (50 µg/ml) and added to the transfection mix. The mixture was then incubated at 27°C for seven days at 140 rpm in the Infors (3mm orbit) incubator. P1 was harvested by centrifugation at 3400 x g at 4°C for 10 min. P1 virus was stored at 4°C in light protected box.

2.1.8 P2 production

Long term virus prep

This stock is necessary if the P1 virus stock would fall below 1 ml and can be used for long term storage. Sf21 cells at 1.5E+6 v.c./ml were seeded in SF900 SFM supplemented with 10% accredited fetal bovine serum (FBS). 1 mL stock virus was added per 500 mL cells in mid-log cells phase, after which the suspension was incubated for 7 days at 27 °C while shaking at 140 rpm. The virus was aseptically harvested using sterile centrifuge tubes and centrifuged at 3400 x g for 15 min at 4°C. Long term virus stock was stored at 4°C in a light-protected box.

Short term virus prep

A short-term virus prep always needs to be done before the infection of Sf21 to produce protein. To achieve a sufficient virus count, 1 mL P1 virus was added to 500 mL 1.5E+6 v.c./mL Sf21 and incubated for 2-3 days at 27 °C while shaking at 140 rpm. A sample was taken to check for infection, if cells were correctly infected with P1 virus the cell growth would be arrested, the cells would be swollen and the viability reduced. 25 ml of this preparation is directly added to 500 ml of prepared mid-log Sf21 cells to infect new cells for large scale protein expression (see section 2.1.9).

2.1.9 Large scale protein expression

The difference between when the Sf21 cells produce virus and when they are optimal for protein expression lies within the time of infection. Sf21 cells express the virus when the cells have not yet reached mid-log phase (2-5E+6 v.c./mL). Protein expression is best while the cells

are still in mid-log (exponential phase) but are about to reach the stationary phase (see Figure 13).

Mid-log cells were grown until they reached a density between 2-5E+6 v.c./mL and directly infected with short term P1 virus (25 mL of the short term virus prep culture in 500 mL mid-log grown cells). After 48 hrs of incubation the cell pellets were harvested by centrifugation at 3400 x g for 15 min at 4°C. Cell pellets were stored at -80 °C until further use.

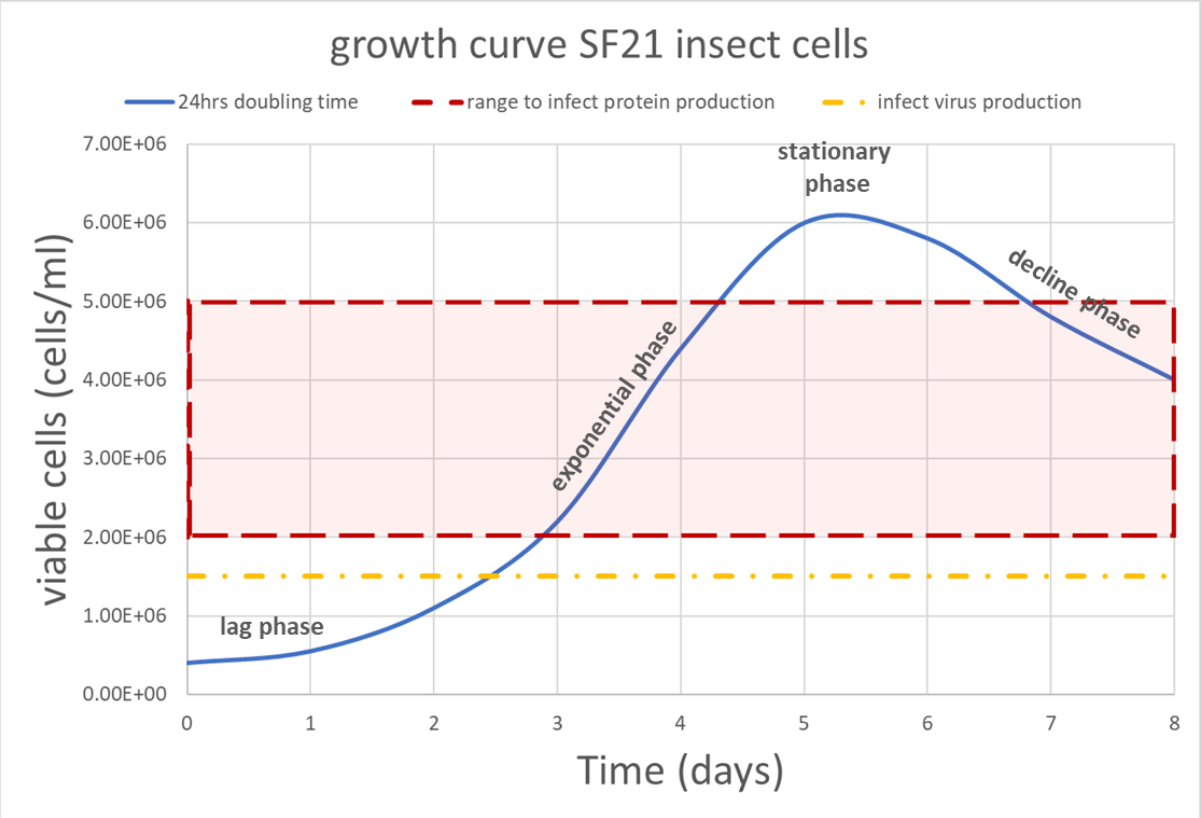

Figure 13. Growth curve of Sf21 cells with infection ranges for protein production and virus production indicated in red and yellow respectively.

2.1.10 Virus titre evaluation

A serial of dilution of 10E-1, 10E-2, 5E-3, 2.5 E-3, 1.25E-3, 0.625E-3, 3E-4 virus stock in SF900 II SFM media was added to 2E+6 v.c./mL Sf21 at a 1:1 ratio. After 24 hrs of incubation, the cells were counted, and cell size was measured in Vi-CELL counter. [57]

Probability that the Sf21 cells were infection was calculated according to the following formulas:

$$probability\ of\ infection\ = \frac{cell\ size[Tx] - cell\ size\ [T0]}{cell\ size[undiluted] - cell\ size\ [T0]}$$

$$Virus\ titer\ \left(\frac{IU}{mL}\right) = Probability\ of\ infection * viable\ cell\ count\ (X1000) * dilution\ factor$$

The virus titer for each dilution was calculated and averaged to estimate the actual virus titer.

2.1.11 Protein expression screening.

A stock of Sf21 insect cells at 3E+6 v.c./mL was prepared in fresh SF900 II SFM media. 180 µL P1 or P2 baculovirus was added to 3 ml cells and incubated at 27°C for 48 hrs. The cell pellet was collected by centrifugation at 3400 x g for 10 minutes at 4 C. SDS-PAGE was used to detect and/or separate the protein using the detergent SDS. Samples containing equal amount of total membrane protein in 1X SDS sample loading dye (5x sample buffer: 2% SDS. 10% glycerol, 1% bromo-phenol blue, 62mM Tris-HCL (pH 6.8), 0.715 mM β-mercaptoethanol) and were separated on 10 % resolving/separating gel (pH 8.8) and 5% stacking gel (pH 6.8) (geneflow). A pre-stained protein marker was also loaded to identify protein size. The gel was run in 1x SDS buffer (25mM Tris base, 150mM glycine and 0.1% SDS, pH 8.3) at 15mA for 15-20 min and then increased to 25 mA until the bromophenol blue reached the end of the gel.

2.1.12 Membrane vesicle production

Cell pellets were thawed on ice. Ultracentrifuge tubes were pre-chilled at 4 °C before use. Pellets were resuspended in hypotonic membrane vesicle buffer (0.5 mM Tris/HEPES, pH 7.4, 0.1 mM EGTA and EDTA free protease inhibitor tablets 1/50 ml). After passing the cell

suspension through the French press twice at 1.0 pounds per square inch (PSI), the solution was centrifuged at 1000xg for 10 min at 4°C. The supernatant was then centrifuged at 72000xg for 60 min at 4°C (Beckman ultracentrifuge). The pellets were combined and resuspended in SMS buffer (10 mM Tris/HEPES, pH 7.4, 50 mM sucrose and protease inhibitor tablets 1/50 ml). Samples were diluted to 5mg/ml and aliquots stored at -80°C.

2.2 Biochemical assays using ISOVs containing BSEP

2.2.1 BSEP-mediated bile acid transport

BSEP mediated transport is measured in inside out membrane vesicles (ISOV) containing functional BSEP. These ISOVs can take up bile acids into the lumen. By using radioactive labelled bile acids, the transported bile acids inside the vesicles can be measured after washing away the excess external bile acids over a filter (see Figure 14). By changing the composition of the external buffer, the effect of drugs and other substrates can be characterized.

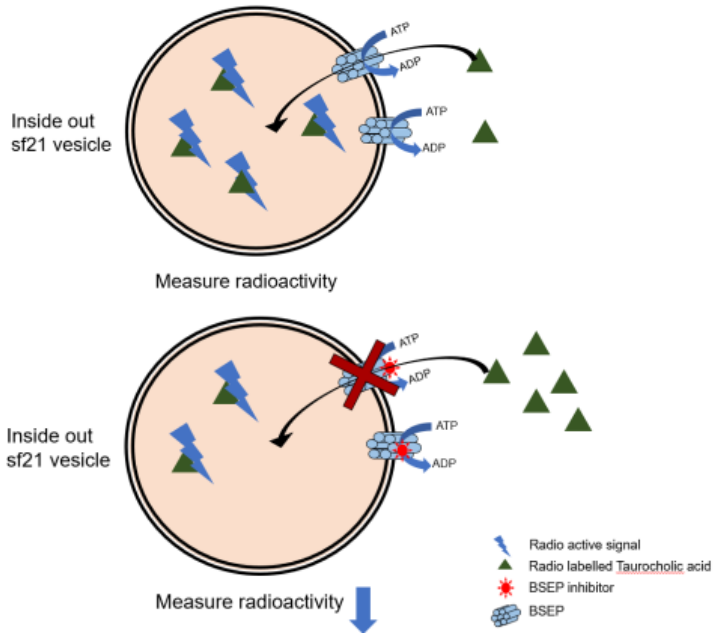

Figure 14. Schematic of BSEP mediated bile acid transport in ISOVs. To detect inhibition of BSEP, bile acid transport is measured in inside out Sf21 membrane vesicles. The membrane vesicles are incubated with radiolabelled TCA in the presence of nucleotides and different concentrations of the tested drug. After a specified incubation time, the excess radiolabelled TCA is washed away, and the radiolabelled TCA captured inside the vesicles measured. If the drug is a weak inhibitor the radioactive signal will be larger than if the drug was a strong inhibitor.

IC_{50} determination for taurocholate transport

Test compounds where serially 1 in 3 diluted from 1000 µM to 4.1 µM in DMSO. Compounds where inbacuted for at least 10 min at 37°C in Uptake buffer (final concentration: 10 mM HEPES/Tris pH7.4, 100 mM KNO3, 50 mM Sucrose and 12.5 mM $Mg(NO_3)_2$, 0.5 µM [3H]-taurocholate + 0.5 µM cold-taurocholate, and 12.5 mM ATP or AMP). Membrane vesicles were then added to a final concentration of 0.5 g/ml. Following incubation for 5 min, samples were added to a filter plate containing Stop buffer (50 mM sucrose, 100 mM KCl, 10 mM HEPES/Tris pH 7.4, 0.1 mM taurocholate, 5 mM EDTA pH7.4), and subsequently filtered and washed twice with Stop buffer. After drying the plate overnight, MicroScint -20 (Perkin Elmer) was added, followed by incubation in the dark for 1 h. The plate was read in MicroBeta2 scintillation counter (Topcount instrument) for 2 min per well.

2.2.2 ATPase assay

The ATPase activity of BSEP was measured in ISOVs in the presence or absence of ortho-vanadate, different bile acid substrates and inhibitors, using the colourimetric malachite green assay. The malachite green assay measures the release of ortho-phosphate (Pi) due to BSEPs ability to hydrolyse ATP into ADP+Pi in the presence of a substrate. Malachite green forms a complex with Pi (Figure 15), the absorbance of which can be measured at 600nm.

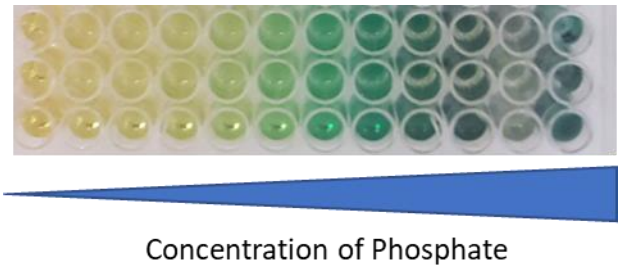

Figure 15. Example of malachite green's colourimetric reaction with increasing concentrations of Pi.

ATPase activity was measured using the malachite green assay to assess the production of Pi over time. Membrane vesicles were diluted to a final concentration of 0.05 mM protein in 30 µL uptake buffer (Section 2.2.1) in the presence or absence of 10 mM ortho-vanadate. After preheating the samples for 10 min at 37°C, the reaction was started by the addition of 2.5 mM Na-ATP (Thermo Fisher Scientific) after which Pi was released. Subsequently, the reaction was stopped at different time points (ranging from 10 s- 20 min) by the addition of 150 µL

freshly prepared malachite green-ammonium molybdate freshly activated by 0.1% Triton X-100. The stopped reaction was then allowed to incubate at RT for 5 min before being stopped by the addition of 30 µL 34% citric acid after which OD600 was determined. The activity of BSEP was calculated by subtracting the ortho-vanadate data from the total ATPase data.

2.3 Primary human hepatocytes

Primary human hepatocytes (PHH) are harvested from donors and therefore considered physiologically more relevant than the easier to acquire cell lines HepG2 and HepaRG cells. Extensive research has been done on the difference between these cell lines and it has been concluded that PHH express Cyp450 enzymes at the same or near physiological levels making them exceptionally valuable to investigate bile acid synthesis and metabolism [58]. However little to no investigation has been done on what effect of 2D and 3D culturing has on toxicity response and metabolism. It was therefore decided to use both culturing methods to describe DILI compound effects on bile acid pools and BSEP function. In the following sections, the 2D sandwich culture and 3D spheroid culture methods are described in more detail (see Figure 16).

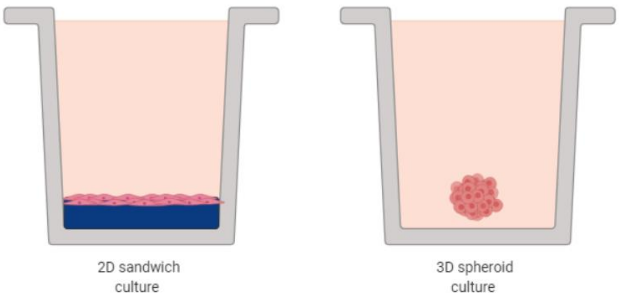

Figure 16. The difference between 2D culture and 3D culture.

2.3.1 Primary human hepatocyte culture

Primary human hepatocytes (AZ bioreclamation) were thawed at 37 °C and poured into 50 mL pre-warmed KLC-TM media (Williams E media (Gibco), 3.3% cocktail A (10000 U/mL, Penicillin, 10000 ug/mL streptomycin, 4 mg/mL human recombinant Insulin, 200 mM GlutaMAX, 1M Hepes PH 7.4), 4.6% FBS, 0.009% dexamethasone). The mixture was then centrifuged at 170x g for 20 min at RT. All but 2-3 ml of supernatant was discarded and resuspended in the supernatant. After gently adding 25 mL pre-warmed thawing media (Williams E media, 3.3% cocktail A, 4.6% FBS, 0.009% Dexamethasone (Sigma)). To increase the viability of the cells, the cells were centrifuged at 100 x g and resuspended in 2-3 mL supernatant while the rest of the supernatant was discarded. The cell count and viability were determined using a 1:1 dilution of trypan blue and counting white (live) cells in a counting chamber. The difference between viable cells and dead cells can be explained because healthy

cells are still able to transport trypan blue out of the cell while dead cells will appear as solid blue dots due to their inability to transport trypan blue. Cell were then plated a density of 7200 v.c./well. The cells were left to adhere for 6 hrs at 37°C, 5% CO_2.

Production of 2D sandwich culture

To produce a 2D sandwich culture, Corning Matrigel was used to separate two different types of media by a layer of PHH (Figure 16). Due to the presence of the different media on each side of the cell, the cells can become as polarised as they would in physiological circumstances. Corning Matrigel (Corning) was diluted to 0.25 mg/mL in ice-cold basement Media (Williams E media containing 3.85% cocktail B and 9.6E-4% dexamethasone). After the cells were checked for adherence, plating media was removed, and 100 µL/well ice-cold Matrigel was added.

Dosing and harvesting of 2D sandwich culture

Dosing occurred 24 hrs after the cells were first plated in 100 µL InSphero tox proprietary media (phenol red was omitted as it interferes in the ultra performance liquid chromotography-MS/MS analysis of the samples). The plates were returned to the incubator till harvest for 6, 24 or 72 hrs. At the point of harvest, media was collected in individual Eppendorf tubes and immediately placed for storage at -80°C.

Cells were washed 3X with cold dulbecco's phosphate-buffered saline (DPBS). After DPBS was removed, 50 µL ice-cold methanol was added to fixate and dehydrate the cells. The samples were immediately stored at -80°C to prevent degradation of samples.

3D cell culture

3D spheroids were either obtained from InSphero or produced in-house by myself.

Inhouse production of Spheroids:

Primary human hepatocytes were obtained as described in 2.3.1 spheroid cells and resuspended in Williams E plating media containing: 10% HyClone FBS (ThermoFisher), 1% L-glutamine-Penicillin-Streptomycin (Sigma), 1% insulin-Transferring- Selenium (life technology), and 0.1% Dexamethasone (Sigma). The cells were plated in a low adhesive 96 well Spheroid plate, at a density of 1500 cells/well. Cells were not seeded in the outer wells instead 200 µL D-PBS was added to these cells to minimise evaporation. The plates were

centrifuged at 125 x g for 2 min and then placed at 37°C. After 5 days a partial media change was performed by removing 50 µL media from the wells and adding 50 µL FBS free media. Seven days after plating the spheroids were ready for dosing.

Dosing and harvesting of Spheroids:

Dosing of InSphero spheroids was done 24 hrs after receiving the spheroids. Spheroids were allowed to settle back to the bottom of the plate for 5 min before the media being removed, after washing three times with InSphero tox proprietary media, 70 µL dosing media was added per well. The plates were returned to the incubator at 37°C for required for 6, 24 or 72 hrs dosing time.

After 6, 24 or 72 hrs of incubation, media was collected in individual Eppendorf tubes and immediately placed for storage at -80°C to prevent degradation of samples.

Cells were washed 3X with cold DPBS, DPBS was removed leaving 10 µL liquid and the spheroid in the base of the well, then 50 µL ice-cold methanol was added. Both methanol and spheroid were transferred to individual Eppendorf tubes and immediately placed on dry ice and stored at -80°C.

2.3.3 Metabolomic analyses

The metabolomic analyses were carried out at the Biomedical Metabolomics Facility in Leiden by Dr A.C. Harms, Dr Alida Kindt-Dunjko and Prof Dr Thomas Hankemeier. Samples obtained from the 2D and 3D experiments were shipped on dry ice to maintain reliability of the measurement and were confirmed to be immediately placed at -80°C after the delivery of the samples at Leiden. For the 3D cells and media samples derived from this, two samples were pooled at Leiden prior to metabolomics analysis. For the 2D cells and media, no samples needed to be pooled. Cell samples and media samples were analysed in a randomised order to prevent any bias and were run in 1 batch, which included calibration lines and blanks.

Bile acids

Table 5. Internal standards used in the bile acids profiling platform. d4 abbreviation indicates the amount of hydrogen isotopes within the different bile acids have been replaced with deuterium to detect the corresponding bile acid.

Internal standards
d4-Cholic Acid
d4-Deoxycholic acid
d4-Glyco-cholic acid
d4-Glyco-deoxycholic acid
d4-Ursodeoxycholic acid
d4-Tauro-ursodeoxycholic acid
d4-Tauro-deoxycholic acid
D4-Glyco-ursodeoxycholic acid

Each sample was spiked with an internal standard solution (Table 5) of 1 mM final concentration. The extraction of bile acids compounds is performed by protein precipitation with methanol, after collection, the supernatant is concentrated by first drying and then reconstituted in a smaller volume, after reconstitution, the extract is transferred into amber auto sample vials for analysis.

Signalling and peroxidised lipids

Table 6. Internal standards used in the signalling and peroxidised lipids profiling platform. the d-number abbreviation indicates the amount of hydrogen isotopes that have been replaced with deuterium to detect the corresponding molecule.

Internal standards
d4-Cortisol
Sphinganine C17_0
Sphingosine C17_1
d4-linoleoyl ethanolamide
d4- dehydroepiandrosterone-2,2,3,4,4,6
d8- anandamide
d4- Palmitoyl Ethanolamide
d8-*N*-arachidonoyldopamine
d4- Oleoyl Ethanolamide
d3- Stearoyl Ethanolamide
d4- thromboxane B2
d5-Tauro-ursodeoxycholic acid
d4-8iso-prostaglandin f2a
d4-prostaglandin f2a
d11-5-iPF2a IV
d11-8,12-iPF2a IV
d4-iPF2a VI
d4-8iso-11-deoxy-13,14-dihydro-15-keto-11β,16.xi.-cycloprostaglandin E2
d4-11-deoxy-13,14-dihydro-15-keto-11β,16.xi.-cycloprostaglandin E2
d4- Prostaglandin D2
d5-Glyco-ursodeoxycholic acid
d4-Tauro-deoxycholic acid
d4-Glyco-cholic acid
d4-Cholic acid
d4-Glyco-deoxycholic acid
d4- Leukotriene B4
d4-(±)12,13-dihydroxy-9Z-octadecenoic acid
d4-(±)9,10-dihydroxy-12Z-octadecenoic acid
d4-Deoxycholic acid
d11-14,15 dihydroxy-5Z,8Z,11Z-eicosatrienoic
d4-15-deoxy-delta12,114-PGJ2
d6- 20-hydroxy Arachidonic Acid
d4-(±)-9-hydroxy-10E,12Z-octadecadienoic acid
d8-12(S)- hydroxy Arachidonic Acid
d4-Lithocholic acid
d8-5(S)- hydroxy Arachidonic Acid
d17-10-Nitrooleate
d4-Ursodeoxycholic acid

Each sample was spiked with antioxidant and internal standard solutions (Table 6). The extraction of the compounds was performed via liquid-liquid extraction. Depending on the preference of the solute, they will either remain in the aqueous phase or move to the organic phase. To extract the signalling lipids from the aqueous phase, butanol and ethyl acetate were used. After collection, the organic phase is concentrated by first drying and then reconstitution in a smaller volume of the organic phase. After reconstitution, the extract is transferred into amber autosampler vials and used for low pH injection.

Equipment

A Shimadzu system formed by three high-pressure pumps (LC-30AD), controller (CBM-20Alite), autosampler (SIL-30AC) and an oven (CTO-30A) from Shimadzu Benelux was coupled online with a LCMS-8050 triple quadrupole mass spectrometer (Shimadzu) operated using LabSolutions data acquisition software (Version 5.89, Shimadzu). The samples were analysed by UPLC-MS/MS using an Acquity UPLC HSS T3 column (Waters). The triple quadrupole mass spectrometer was used in polarity switching mode, and all analytes were monitored in dynamic Multiple Reaction Monitoring. All metabolites were detected in negative mode.

Data Analysis

The acquired peak data was evaluated using LabSolutions software (Version 5.89, Shimadzu), by integration of assigned MRM peaks and normalisation using accordingly selected internal standards. When available, a deuterated version of the target compound was used as internal standard.

2.3.4 The interpretation of data by multivariate analyses

Multivariate analysis is a statistical approach to assess data with more than one variable and thus more than one statistical outcome variable at a time. Multivariate analysis is useful to reduce a large number of variables and identify clusters.

In this case, it was decided to use multivariate analysis for this data due to the high number of y-variables (12 different bile acids) and five different x-variables (2D vs 3D; cell vs media; treatment and time). While several options for modelling are possible, an unbiased PCA-X modelling (see next section) was chosen. The interpretation of multivariate analysis needs to be done with care to exclude the effects of the algorithm, sample handling and data

processing from underlying biological sources. The outline of the workflow is shown in Figure 17.

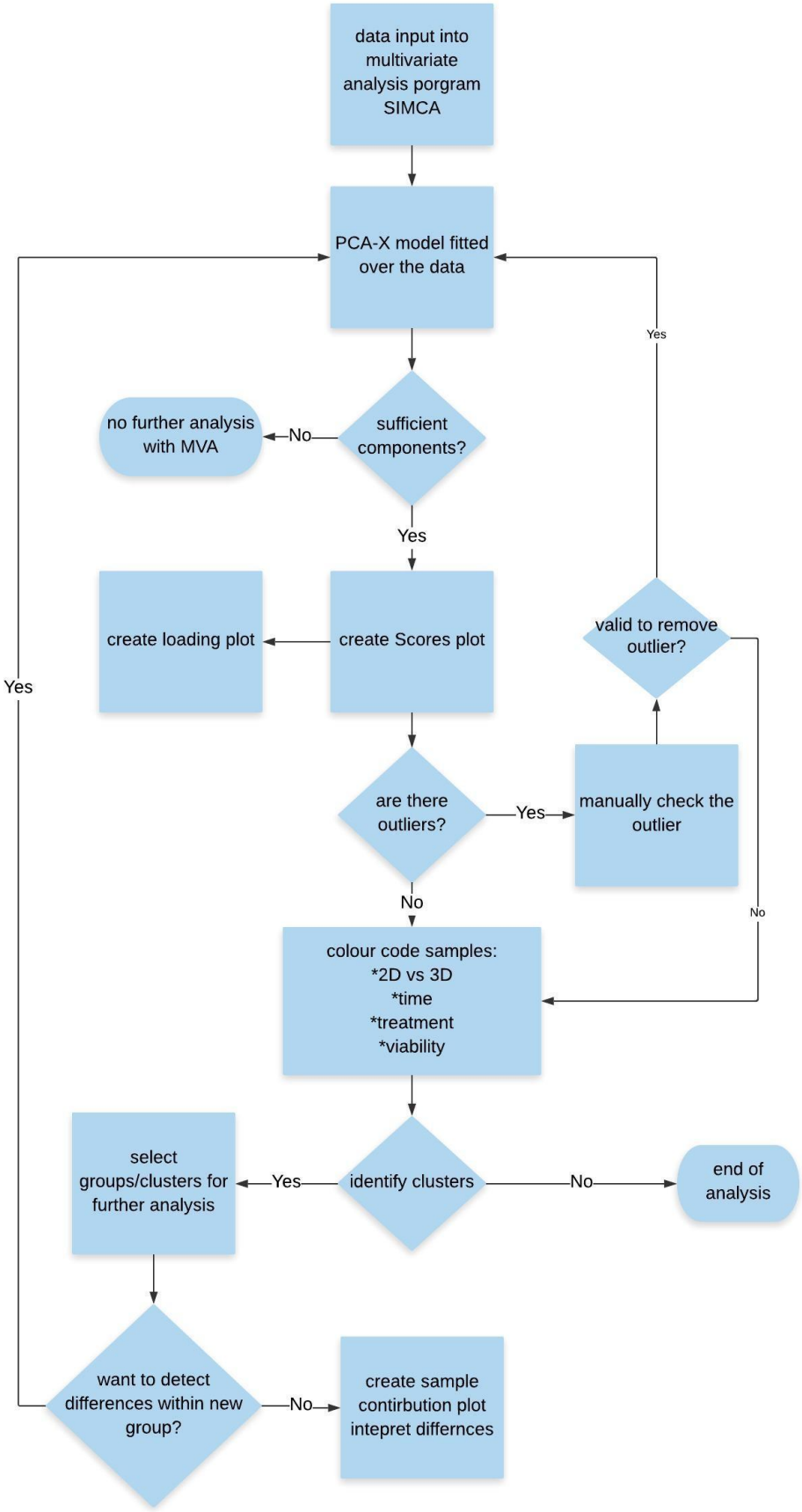

Figure 17. Workflow used to obtain multivariate graphs in SIMCA. (workflow created with: ©2019 Lucid Software Inc.)

PCA-X model fitted over data: To uncover groupings of variables, trends and outliers, the data were fitted to principal component analysis-X (PCA-X) model. PCA-X uses an orthological transformation to reduce the dimensionality of large data sets. It achieves this by changing a large set of variables into a smaller set, without losing information, into new variables called components. Graphs were assessed for their R2, and Q2 values, both of which needed to be above 0 and components were added till neither R2 or Q2 further increased. The R2 values the percent of variation explained by the model and therefore relates to how well the model fits the data. A poor R2 indicates a poor reproducibility in the data set. The Q2 value is the percent of the variation of the data set predicted by the model after cross-validation and therefore indicates how well the model predicts new data. A large Q2 (>0.5) indicates a good predictivity.

Scores plot: A score scatter plot was created if the model was deemed to be adequate and give a sufficient fit. In this new graph, t1 and t2 are newly generated variables summarising all univariate results of the samples at once. Each score is independent of the others, and there are as many scores as there are components in the data. Score t1 explains the largest variation, t2 the second largest and so on. Accordingly, the scatter plot allows us to look at how each sample is situated with respect to each other. Allowing us to see outliers, groups, similarities and other patterns in the data. In Figure 18, an example of a scores scatter plot of t1 and t2 is shown. Four different groups are clearly separated and can therefore easily be identified in the graph. The ellipse indicates the Hotelling's bases T2, indicating the 95% confidence interval. Observations located outside of this ellipse are outliers that cannot be explained by the model. A manual check of outliers was done before exclusion. If no reason for the outlier was found, the outlier was left in the data set. Samples close to the origin of the plot have average properties in this model.

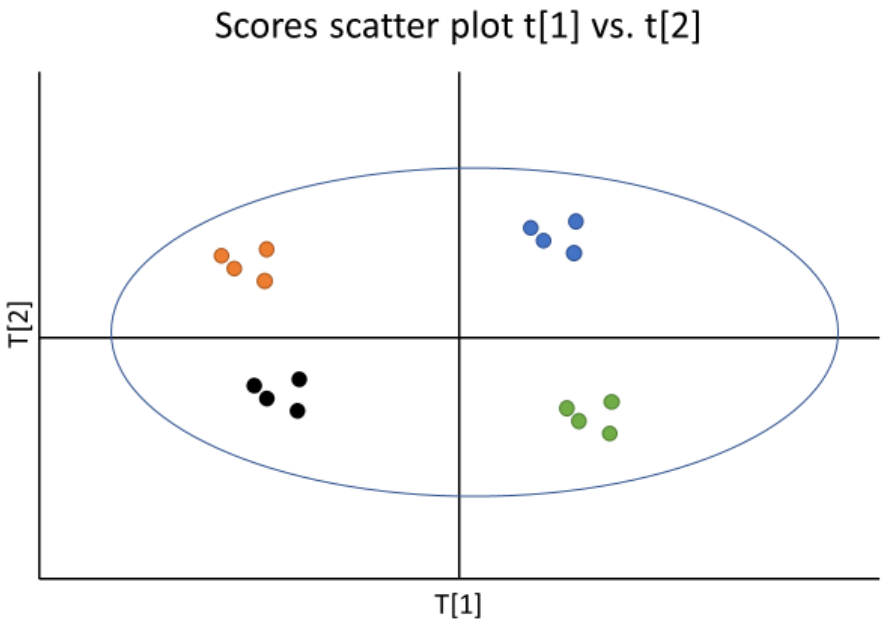

Figure 18. An example of the score scatter plot with four different groups indicated by different colours. T1 explains the largest variation while T2 explains the second largest variation. In this example groups can be identified by clear separation, indicated by different colours. The individual samples within the groups share commonalities among them. The ellipse indicates the Hotelling's bases T2, indicating the 95% confidence interval.

Loading plot: a loading scatter plot was created to evaluate which variables had the most influence on the placement of the individual samples. The scores are weighted averages of the variables with p1 in the first component and p2 in the second component. These values express the correlation structure of the x matrix and show how the X-variables correlate to each other. There are two distinct ways this pot is read and used. I) an imaginary line is drawn through the origin, allowing for the interpretation of the X-variables. Variables near each other are positively correlated see Variable 4 and 2 in Figure 18. Variables opposite to each other are negatively correlated, see Samples 4 and 3 (Figure 18). By drawing a line from the sample through the x-axis we can identify uncorrelated samples. Samples located at a 90-degrees angle from this imaginary line are uncorrelated to each other in these two components, such as the 4 and 1. The further these points lie from the origin, the stronger the impact that variable has on the model. Showing that Variable 4 and 2 are responsible for the separation of the blue group in Figure 19, variable 5 is responsible for the separation of the green group, Variable 1 for orange and Variable 3 for black.

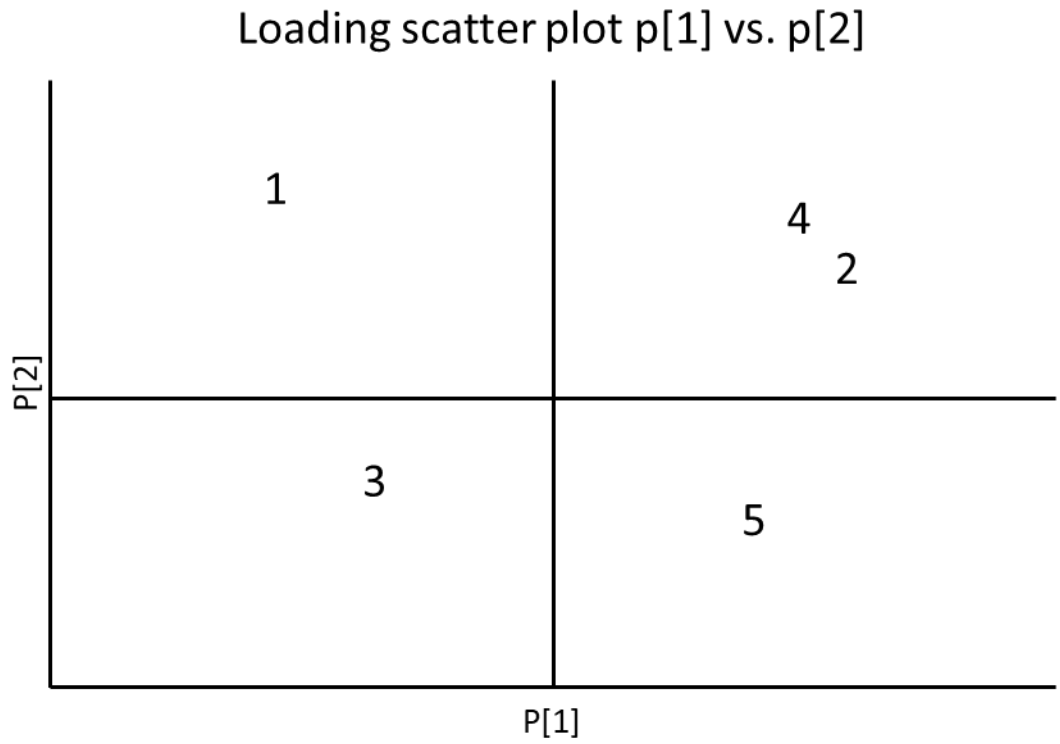

Figure 19. Loading scatter plot in which each number represents a different X-variable. The loading plot correlates and can directly be overlaid with the score scatter plot, indicating which group is associated with which variable. Variables that are located close to each other are positively correlated see examples 4 and 2. Variables that are located at a 90-degree angle are uncorrelated see 4 and 1 as well as 5 and 3. Variables that are opposite each other like variable 4 and 3 are negatively correlated.

2.3.5 ATP (viability) measurement

CellTiter-Glo 3D Reagent (Promega) was thawed overnight at 4°C before use. CellTiter-Glo 3D reagent was equilibrated at RT for approximately 30 min. 100 µL CellTiter-Glo 3D Reagent was added to wells containing 100 µL media and live cells. After thorough mixing, the suspension was transferred into a black 96-well plate and mixed on an orbital well shaker for 5 min to induce cell lysis. Plates were spun at 300 x g for 2 min to remove bubbles. After 25 min incubation at RT, plates were luminescence read on the Envision using an integration time 0.25-1 second/well.

Values were verified against a standard curve prepared with adenosine 5'-triphosphate (ATP) disodium salt hydrate in nuclease-free water.

2.3.6 Total bile acid concentration

Total bile acid concentration within cells was measured with the cell Biolabs "total bile acid kit" (cell Biolabs MET-5005). The principle of the analysis is explained in Figure 20. Bile acids are oxidised with the use of 3α-hydroxysteroid dehydrogenase. In the reaction, the enzyme reduces NAD^+ to NADH. NADH, in turn, is used by the enzyme diaphorase to reduce non-fluorescent resazurin to fluorescent resorufin. After allowing this reaction to take place for an hour the resorufin concentration in the samples is determined spectrophotometrically in a plate reader at excitation and emission wavelengths of 560 and 590 nm, respectively.

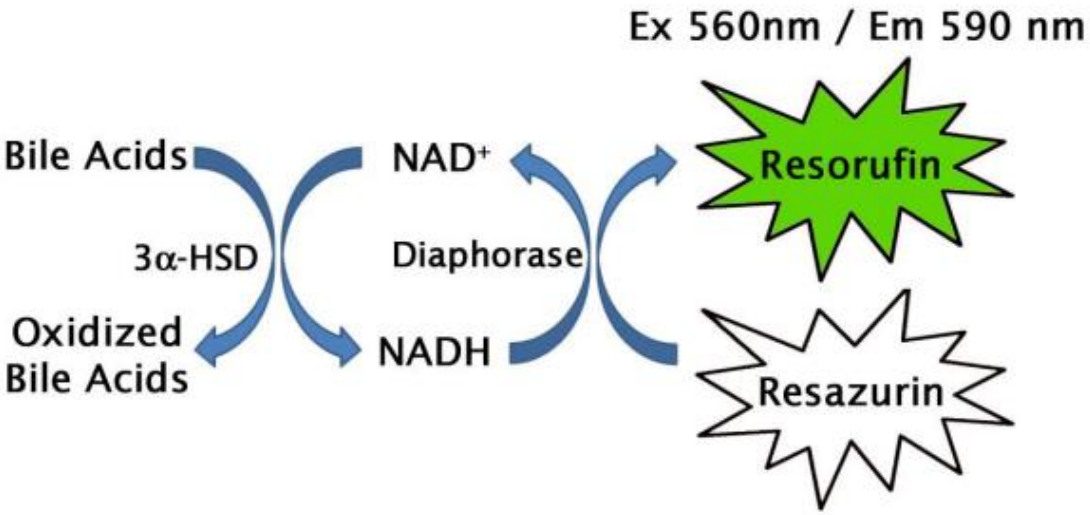

Figure 20. Biochemical mechanisms underlying the total bile acid assay. Bile acids are oxidised via 3α-hydroxysteroid dehydrogenase (HSD) in a step that also reduces NAD + to NADH, this in turn enables diaphorase to change resazurin into a fluorescent resorufin.

Absolute concentrations of all bile acids combined were obtained by generating a standard curve for glycochenodeoxycholic acid with concentrations ranging from 0 to 25 µM. Stock solutions of 250 µM were provided as a standard in MQ water in the kit. Media from both 2D and 3D cell cultures were harvested and stored in Eppendorf tubes, after which the cells were washed three times with cold DPBS. For the 2D cultured cells, 50 µl DPBS was added to the plates and both media and plates were stored at -80°C till further use. The spheroids were washed three times and were transferred to Eppendorf tubes. Before the total bile acids assay, the spheroids were centrifuged at 10.000xg for 10 min and resuspended in 50 µL media to ensure similar dilutions for each of the samples. The media and the cells were stored at -80°C before analysis. On the day of total bile acid concentration analysis, the cells were thawed and refrozen twice before sonication to ensure lysis of the cells. 50 µL of each sample was analysed according to the kit instructions. To prevent interference of fluorescent signal from neighbouring wells the entire assay was performed in black-walled plates.

2.3.7 Staining and imaging

Cells were washed to remove media and fixed at a final concentration of 4% paraformaldehyde in DPBS to retain protein structures, in a final volume of at least 100 µL at RT for 1 h in a biological safety cabinet class 2 and stored at 4 °C until staining.

Antibodies used for imaging of both 2D and 3D cultures:

Primary antibody	Mouse anti-BSEP (F-6) sc 74500 (SantaCruz)
Secondary antibody	Goat anti-mouse IgG (H+L) fluor 488 (thermoFisher A28175)
Nucleus stain	Hoechst 33342 (thermoFisher)
Cell mask	HCS CellMask Deep red stain (ThermoFisher)

2D cells

2D cells were fixed to the plate as stated in 2.3.7 and permeabilised at RT for 15 min with 0.1 % Triton X-100 and 0.2% BSA in PBS to allow the antibodies to enter the cells. After blocking with 2% BSA for 1 h, primary antibody in PBS containing 1% BSA was diluted 1:100 at RT for 1 h. After washing with cold PBS, the secondary antibody was applied with a dilution of 1:500 together with Hoechst (1µgmL), HCS cell mask and 1 % BSA. After 45 min incubation, samples were washed with PBS and imaged with Yokogawa CV8000.

3D cells

Incubation with primary antibody was changed to 18-24 hrs at 37 °C and secondary antibody for 4 hours at 37 °C. Each washing steps was 20 min each to allow for diffusion of antibodies into the microtissue [59].

2.3.8 Image analysis

Images analysis was done on web enabled image analysis platform Columbus (PerkinElmer).

The images were analysed according to the following workflow:

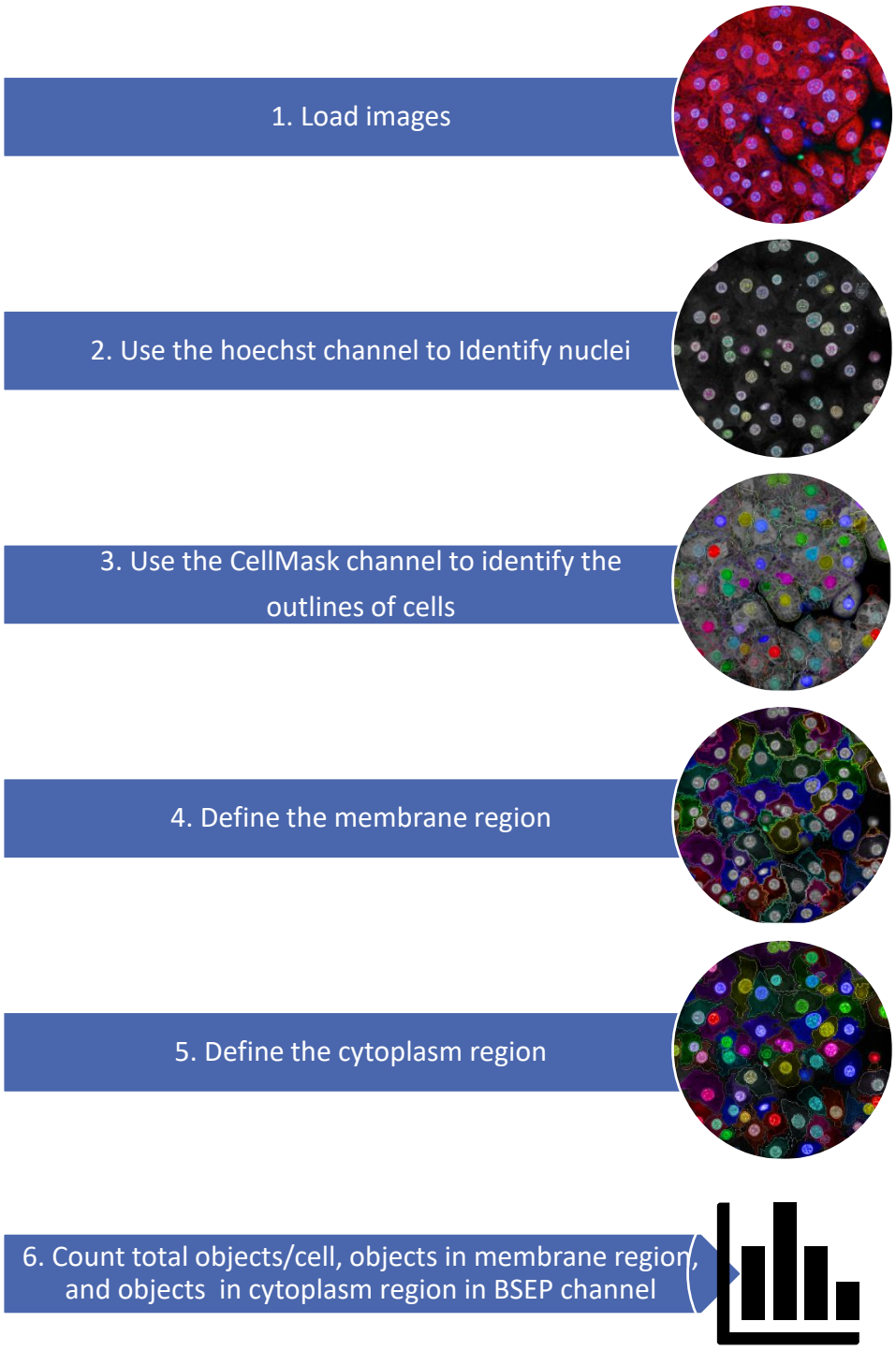

Figure 21. Workflow for analysing the z-stack images in Columbus (PerkinElmer). Z-stacks were loaded into the program where after the Hoechst channel was used to identify and count the number of nuclei. This nuclei count together with the cell mask channel was used to identify the outlines and the correct number of cells within each image. The membrane region was identified by identifying an area of interest 2.5% away from cell outline identified in step 3, the rest was names cytoplasm region. Finally, the objects in the BSEP signal channel were counted and defined by total object count/cell, object in membrane region/ cell and objects in cytoplasm region/cell.

2.4 Statistical analysis

Two-way ANOVA followed by Tukey's multiple comparisons test was performed using GraphPad Prism version 8.0.1 for Windows, GraphPad Software, San Diego, California USA, www.graphpad.com

Significance is displayed as:

Ns	$P > 0.05$
*	$P \leq 0.05$
**	$P \leq 0.01$
***	$P \leq 0.001$
****	$P \leq 0.0001$ (For the last two choices only)

3. Mechanisms of BSEP inhibition

3.1 Introduction

3.1.1 Different bile acids

The current limitations in providing an assay that can predict DILI may be explained by the wide variation in the compounds that can interfere with BSEP expression or transport activity. It might, therefore, be prudent to look at compound interactions beyond the direct inhibition. A few considerations need to be made such as the bile acid pool, which can influence bile salt accumulation in many complex and dynamic ways. While primary bile acids are synthesized in the hepatocytes, they can undergo enzyme-catalysed conjugation with taurine and glycine into amidated bile acids. The mixture is then actively transported out of the hepatocytes by BSEP. Along the small intestines, bile acids may be reabsorbed by the apical sodium-dependent bile salt transporter (ASBT) and the basolateral organic solute transporter (OST) [31,60,61]. In the gut the bile salt may undergo further metabolism by bacteria into secondary bile acids. It is therefore unsurprising that each tissue has its bile salt signature profile, providing different compositions of bile salts in each organ [43,62]. These signatures are dependent on absorption, distribution, metabolism and excretion rates. Each bile salt has an individual uptake rate. For example, there have been confirmed reports of a ~30 fold difference in the uptake rate of specific bile acids by BSEP [43].

3.1.2 Kinetics of transport activity and inhibition.

Membrane transporters are enzymes that mediate the transmembrane movement of their substrates, often without modifying them. Although the traditional Michealis-Menten model was developed to investigate enzyme kinetics, it can also be used to describe the kinetics of drug transporters in terms of Km, Ki, and Vmax [63], which the Km describes the affinity of the drug for the transporter, the Ki defines the affinity for the inhibitor, and the Vmax describes the maximum velocity of substrate transport. Nowadays computer calculations are accurate enough to perform non-linear curve fitting of data to determine the Vmax and Km parameters. However, in the past the hyperbolic Michaelis-Menten graph was transformed into Lineweaver-Burke and/or Eadie-Hofstee plots, which are both linear graphs. In the Lineweaver-Burk plot the x-intersection= -1/Km and y-intersection= 1/Vmax. However due to the transformation process samples with small substrate concentrations, the most prone for variation, has the most influence on intersections. The Eadie-Hofstee plot on the other hand

is less prone to variations and the y intersection=Vmax and the slope=-Km. These linearization methods still provide amazing tools to visualise inhibition types (see Figure 23)

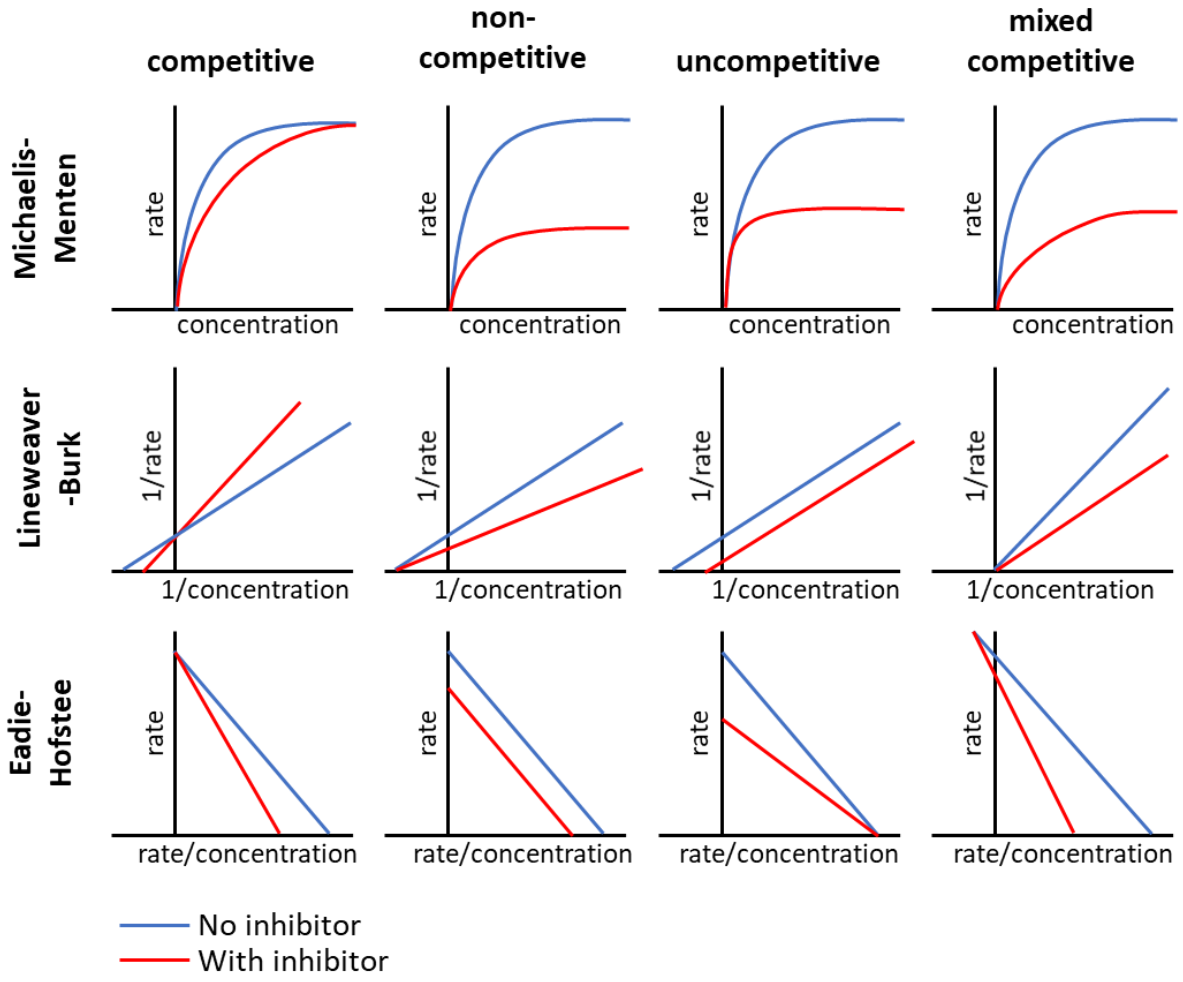

Figure 22. Identification chart for types of inhibition. Includes Michealis-Menten, Lineweaver-Burke and Eadie-Hofstee plots showing competitive, non-competitive, uncompetitive and mixed inhibition.

3.1.3 Types of inhibition

Reversible inhibition can be divided into four groups, competitive, non-competitive, uncompetitive and mixed competitive.

1.) In competitive inhibition the inhibitor competes with the substrate for the same binding at the active site. The Vmax does not change in this instance but the Km increases. The inhibitor can be competed of by increasing the substrate concentration [64].

2.) In non-competitive inhibition the inhibitor binds to a different site than the substrate but in the process alters the shape of the transporter or enzyme, it cannot be overcome with increasing the substrate concentration. In this case the Vmax and the Km decrease with the addition of an inhibitor [64].

3.) In the case of uncompetitive inhibition, the inhibitor binds to the substrate-transporter complex. An uncompetitive inhibitor causes the Vmax to decrease but the Km to remain the same. As the substrate increases so does the complex and thus inhibition, it does therefore not compete off [64].

4.) In mixed inhibition, the inhibitor can bind to the transporters regardless if a substrate is already bound or not although it has a greater affinity for one state or the other. It is in essence a mix between competitive and uncompetitive inhibition. In the case of a mixed inhibitor the substrate affinity may decrease if the inhibitor prefers the free enzyme or the Km may increase if the inhibitor prefers to bind to the substrate-transporter complex. In both cases the Vmax will decrease however [64].

Examples of how these inhibition types would appear in the different graphs is displayed in Figure 22.

3.2 Results

3.2.1 Compounds selection

Before the start of experiments, four compounds were carefully selected to study the consequences of drug interactions in hBSEP. The selection criteria were established before the selection of these four compounds and consisted of: 1. The known inhibitory effect on hBSEP, 2. Have one compound well defined in enzyme kinetics and mechanistic properties 3. Causing different types of DILI injuries. Figure 23 displays the most common hBSEP inhibitors colour coded and then organised according to their physio-chemical properties.

As bosentan has a very low affinity for BSEP but can induce DILI, the inhibition by this positive control was chosen as a cut-off point by AstraZeneca in the analysis of new compounds. Compounds with a weaker affinity than bosentan are not clinically relevant in inducing DILI. All of these properties are used for drug efficiency screening before testing. The ClogP, for example, is a well-established measure of the compound's hydrophilicity. A high hydrophilicity (or low hydrophobicity) and therefore low logP value is associated with poor absorption or permeation. The polar surface area is regularly used to optimise the ability of drugs to permeate cells. It is a common view that a higher polar surface area results in poorer permeation through the cell membrane. The heavy atom count (which refers to the presence of electronegative atoms such as O, N and S) is commonly inversely related to ligand efficiency. The ligand efficiency describes the measurement of the binding energy per atom of a ligand to its binding partners, such as a receptor or enzyme. This is commonly used in drug discovery research programs to assist in narrowing focus to lead compounds with optimal combinations of physicochemical properties and pharmacological properties [65]. Rotatable bonds, h-bond donors and h-bond acceptors are often used to define the compounds solubility and oral bioavailability. By using these properties drug developers are able to discriminate out inactive compounds before further screening.

Before the final selection of the compounds, the physico-chemical properties were plotted against the IC_{50} value for BSEP inhibition. In Figure 23, compounds were sorted from high to low IC_{50}, indicating a low inhibitory effect on BSEP activity to a high inhibitory effect, and were given their unique colour in a colour gradient. Subsequently, the compounds were sorted according to other physico-chemical properties from high to low and colour-marked them with the previously designated colour.

IC50 (uM)	Molecular Weight	CLogP	Polar Surface Area	Heavy Atom Count
pioglitazone	Cyclosporin	Cyclosporin	Cyclosporin	Cyclosporin
Cyclosporin	rifamycin SV	fusidic acid	rifamycin SV	rifamycin SV
troglitazone	Bosentan	acitretin	Bosentan	Bosentan
ketoconazole	ketoconazole	nefazodone	glibenclamide	fusidic acid
nefazodone	fusidic acid	troglitazone	fusidic acid	ketoconazole
glibenclamide	glibenclamide	Alpidem	nifedipine	glibenclamide
rifamycin SV	nefazodone	glibenclamide	troglitazone	nefazodone
rosiglitazone	Clobestasol propionate	Bosentan	Clobestasol propionate	Clobestasol propionate
Clobestasol propionate	troglitazone	rifamycin SV	rosiglitazone	troglitazone
Alpidem	Alpidem	ketoconazole	pioglitazone	Alpidem
fusidic acid	rosiglitazone	pioglitazone	ketoconazole	nifedipine
acitretin	pioglitazone	Clobestasol propionate	acitretin	rosiglitazone
nifedipine	nifedipine	nifedipine	nefazodone	pioglitazone
Bosentan	acitretin	rosiglitazone	Alpidem	acitretin

IC50 (uM)	Rotatable Bonds	H-Bond Donors	H-Bond Acceptors
pioglitazone	Cyclosporin	rifamycin SV	Cyclosporin
Cyclosporin	nefazodone	Cyclosporin	rifamycin SV
troglitazone	rifamycin SV	glibenclamide	Bosentan
ketoconazole	ketoconazole	Bosentan	nefazodone
nefazodone	Bosentan	fusidic acid	ketoconazole
glibenclamide	glibenclamide	troglitazone	glibenclamide
rifamycin SV	pioglitazone	rosiglitazone	fusidic acid
rosiglitazone	rosiglitazone	pioglitazone	troglitazone
Clobestasol propionate	Alpidem	Clobestasol propionate	rosiglitazone
Alpidem	troglitazone	nifedipine	nifedipine
fusidic acid	fusidic acid	nefazodone	pioglitazone
acitretin	acitretin	ketoconazole	Clobestasol propionate
nifedipine	Clobestasol propionate	Alpidem	Alpidem
Bosentan	nifedipine	acitretin	acitretin

Figure 23. Compounds sorted by different chemical properties. Compounds were given a colour to differentiate them from each other and were sorted from low IC_{50} to high IC_{50} . For other criteria (molecular weight, ClogP, polar-surface area, heavy atom count, rotatable bond, h-bond donor, H-bond acceptors), the compounds were sorted from high value to low value. No obvious relationships could be detected between IC_{50} and the other criteria.

Four compounds from the previous list of BSEP inhibitory agents tested by AZ were selected for further studies. As a known BSEP inhibitor, bosentan was included as a positive control. It has a molecular weight of 551.614 and an IC_{50} of 38.1 µM as determined by AZ (see Figure 24 for additional information and chemical structure). The second compound chosen was alpidem with a molecular weight of 404.333 and an IC_{50} of 9.2 µM. The third compound was clobetasol propionate with a molecular weight of 466.97 and an IC_{50} of 8.5 µM. The last compound chosen was cyclosporine A with a molecular weight of 1202.611 and an IC_{50} of 0.5 µM. For both bosentan and cyclosporine it was established previously that they inhibit BSEP-mediated TCA transport in a non-competitive and competitive fashion, respectively [53,66].

Selection of these four compounds enables us to investigate the link between IC_{50}, the mechanisms of inhibition, and the mechanisms underlying different DILI injuries.

As Chapter 4 and 5 will report on the metabolomics and the influence of drugs on the location, two more compounds were included. Cyclohexamide is an inhibitor of protein translation, induced microtubule- and p38(MAP kinase-dependent decrease of Golgi-associated BSEP, accompanied by a more than 2-Fold increase in BSEP-positive pseudocanaliculi [42]. According to previous tests at AZ, cycloheximide is not known to inhibit BSEP directly in ISOVs (see Appendix C for hepatic panel score compounds from AZ). The second compound that was added was estradiol. Estradiol is a naturally occurring steroid hormone responsible for female reproduction, maintenance of body temperature, preserving bone strength, cholesterol production and protection of the heart [67]. Some foods may affect levels of estradiol in the body, and a synthetic form is often prescribed as a birth control measure and in the treatment of menopausal symptoms. Experiments in rats have indicated a reduction of BSEP at the apical membrane of hepatocytes in response to exposure to this compound [68]. AZ has shown that estradiol is a direct weak inhibitor of BSEP with an IC_{50} of 111 µM (data not published) .

3.2.2 Effect of compounds on taurocholate (TCA) transport

hBSEP was expressed in Sf21 insect cells and inside-out membrane vesicles were prepared. The effects of bosentan, clobetasol propionate, cyclosporine A, alpidem and estradiol on the BSEP-mediated TCA uptake in these membrane vesicles is shown in Figure 2. All compounds were found to inhibit TCA transport by BSEP, however the estradiol data did not lend itself to a fitting. The least inhibitory compound was estradiol with an IC_{50} of 437.4 µM and the most inhibitory cyclosporine with an IC_{50} of 0.42 µM. Bosentan, clobetasol and alpidem had IC_{50} of 63.2 µM, 6.44 µM and 3.9 µM, respectively. It is interesting to note that while bosentan exhibits a 150x higher IC_{50} than cyclosporine, both cause cholestatic/mixed DILI. Clobetasol propionate was found to inhibit TCA transport stronger than bosentan but is commonly found not to cause any DILI. These results suggest that the IC_{50} in a TCA transport assay plays a minor role in defining what type of liver damage a compound can cause. It should be noted that TCA is not the most abundant bile salt in human liver and that the possibility exists that the inhibition of BSEP by inhibitors could be bile ion-dependent. The next step was identifying the mechanism of inhibition of BSEP-mediated TCA transport.

IC_{50} evaluation of selected compounds on TCA transport by BSEP

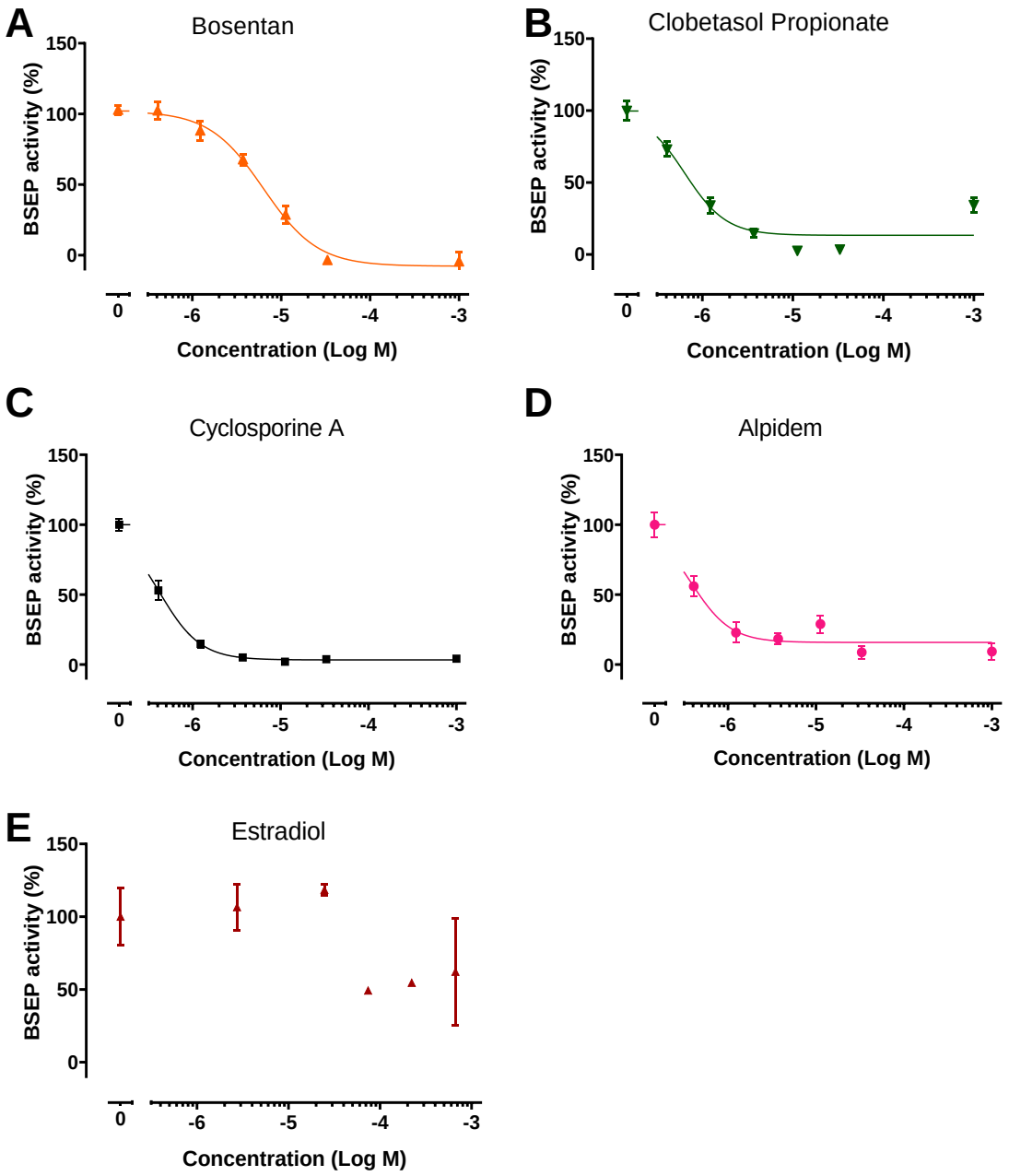

Figure 24. Determination of IC_{50} for inhibition of BSEP-mediated TCA transport by various drugs in the presence of 0.5 µM cold-TCA and 0.5 µM [3H]-TCA, uptake was stopped after 5 min of incubation and samples measure the next day. Graphs were plotted as sigmoidal, 4pl plots were the x is log(concentration) (N=3). Estradiol data did not lend itself to a fitting.

Table 7. Summary of IC_{50} values for inhibition of BSEP-mediated taurocholate transport. * IC50 was determined but the curve did not lend itself to fitting a curve.

Compound	IC_{50} (µM)
Bosentan	63.2
Clobetasol propionate	6.44
Alpidem	3.9
Estradiol	437.4*
Cyclosporine	0.42

The analysis of ATP-dependent TCA uptake in hBSEP-containing membrane vesicles served two purposes: i) To confirm that the BSEP assay was properly performed, and ii) to confirm that IC_{50} values observed for chosen compounds were in the correct range. The findings are within the confidence interval described by Dawson et al [16].

Kinetics of TCA transport

Having identified inhibitors of BSEP, the next aim was to study the biochemical mechanisms (competitive vs non-competitive vs uncompetitive inhibition) by which the inhibitors block BSEP activity. For this purpose, a transport assay was established in which the rate of BSEP-mediated transport was measured as a function of the TCA concentration.

In Figure 25, TCA uptake at increasing TCA concentrations is displayed over 900 seconds. The hyperbolic substrate accumulation curves show that linear uptake occurred between approximately 20 to 180 s. A plot of the initial rate of uptake (Figure 26) versus the TCA concentration revealed a Vmax of 169 pmol/s/mg protein and a Km of 46.45 µM (Table 8, Figure 28). The data were also plotted in linear Lineweaver-Burk and Eadie-Hofstee plots.

To determine the mechanism of inhibition, the TCA transport assays were repeated in the presence of inhibitors at concentrations equal to their IC_{50} and ½ IC_{50} in the uptake assays in Figure 24. As the IC_{50} for estradiol was very high, and its primary influence on BSEP is exerted at the level of expression rather than activity, it was excluded from further kinetic studies. The results are given in Figure 27 and Figure 28.

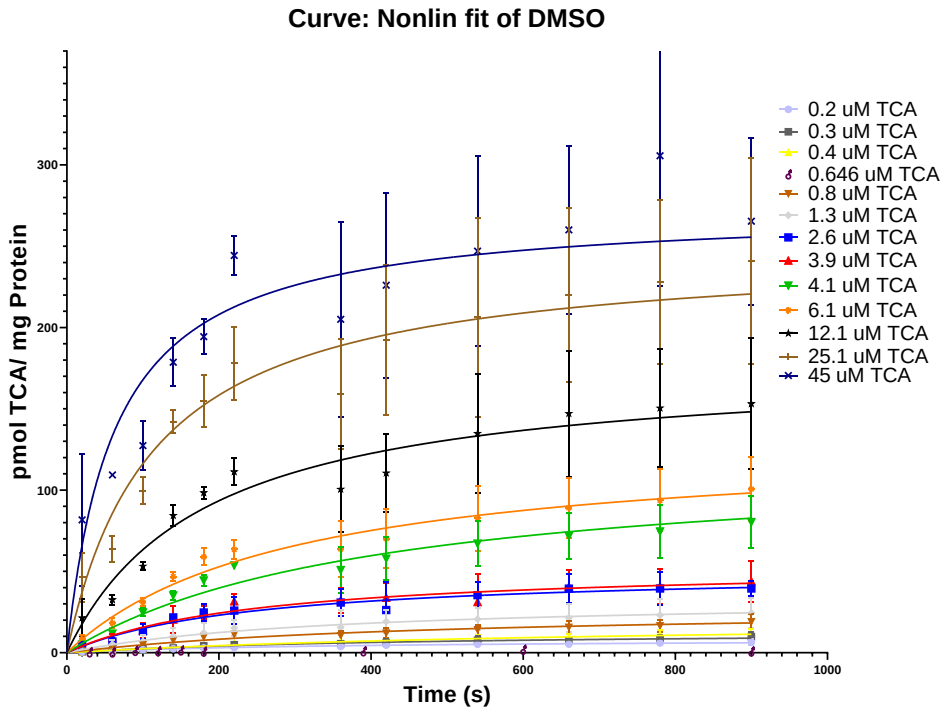

Figure 25. Taurocholate transport over time with different TCA concentrations with DMSO as control. one site binding hyperbolas were fitted onto the data indicating a Ki and Vmax for each concentration of TCA (N=3).

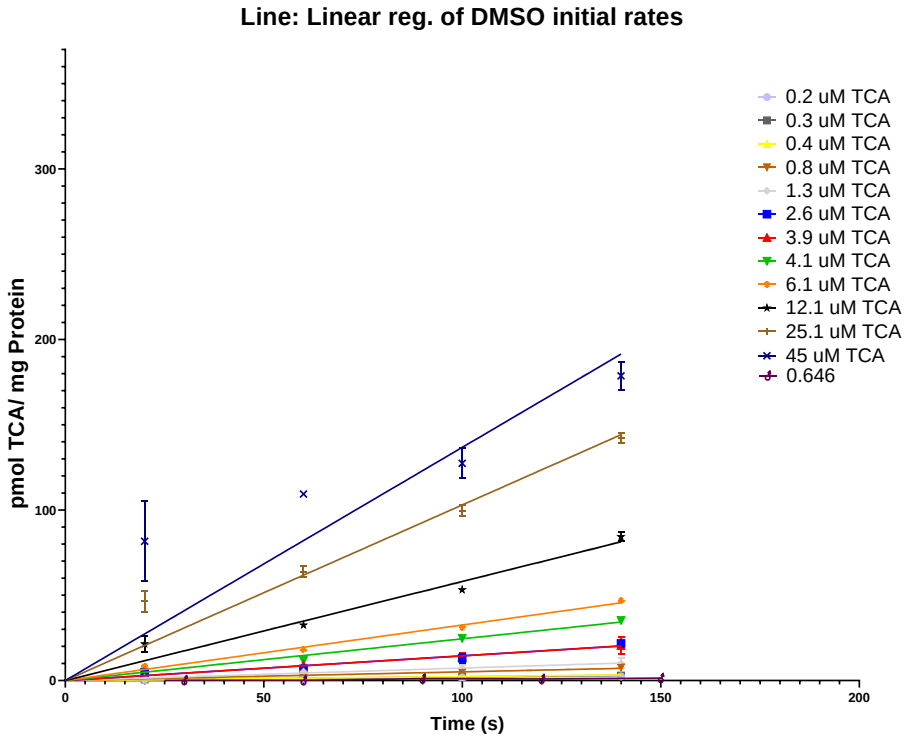

Figure 26. The linear sections in Figure 7 were used to evaluate the initial velocity of TCA uptake at different TCA concentrations. Linear regression were plotted onto the first 140 seconds from figure 25. To determine the individual rates of uptake at different concentrations TCA by BSEP. (N=3)

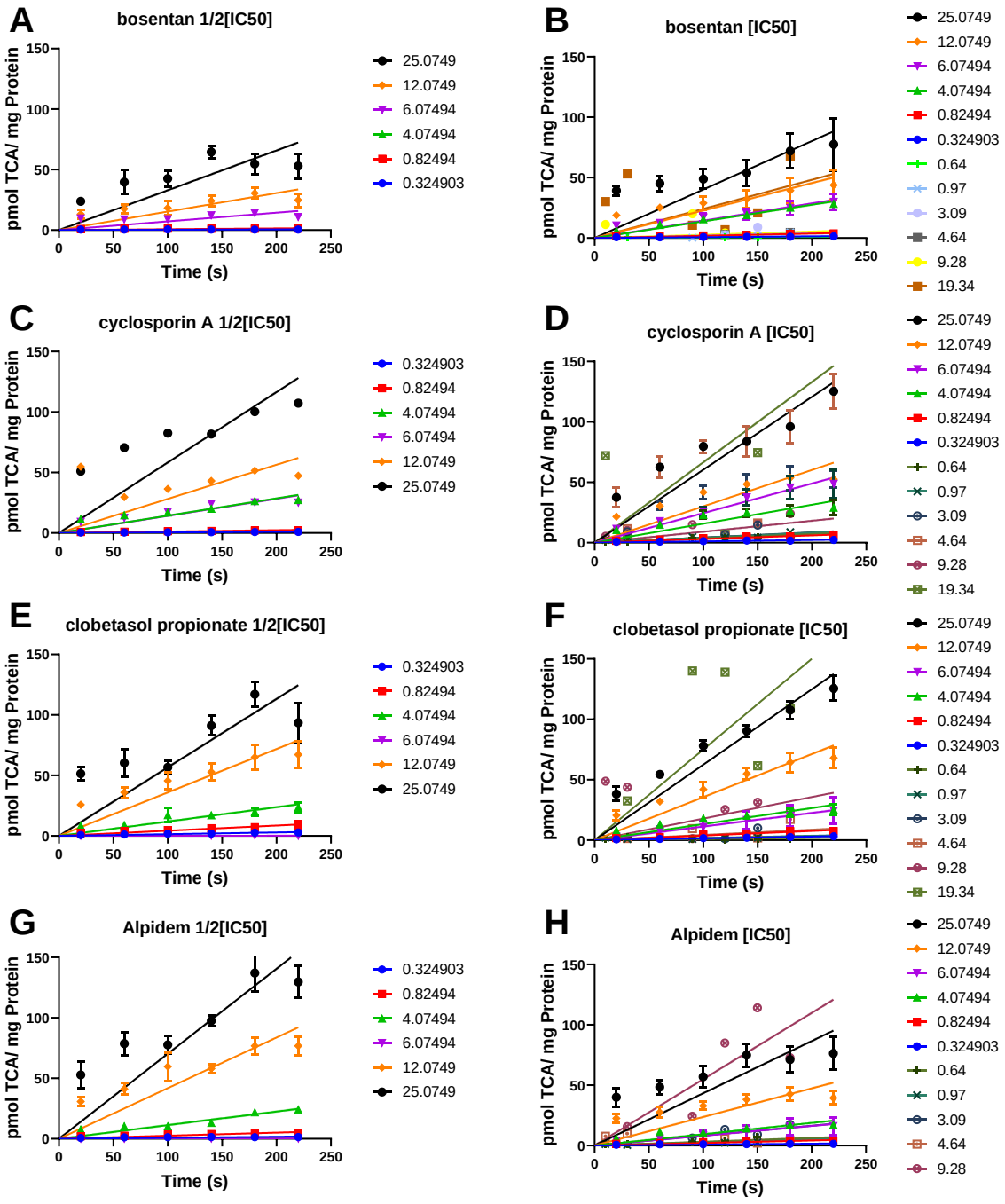

Figure 27. Determination of uptake rates at different concentrations of inhibitor (in µM). Linear regression were plotted onto the first 220 seconds to determine the individual rates of TCA uptake by BSEP. The colour coding of the traces refers to TCA concentrations similar to those in Figure 8. (N=3)

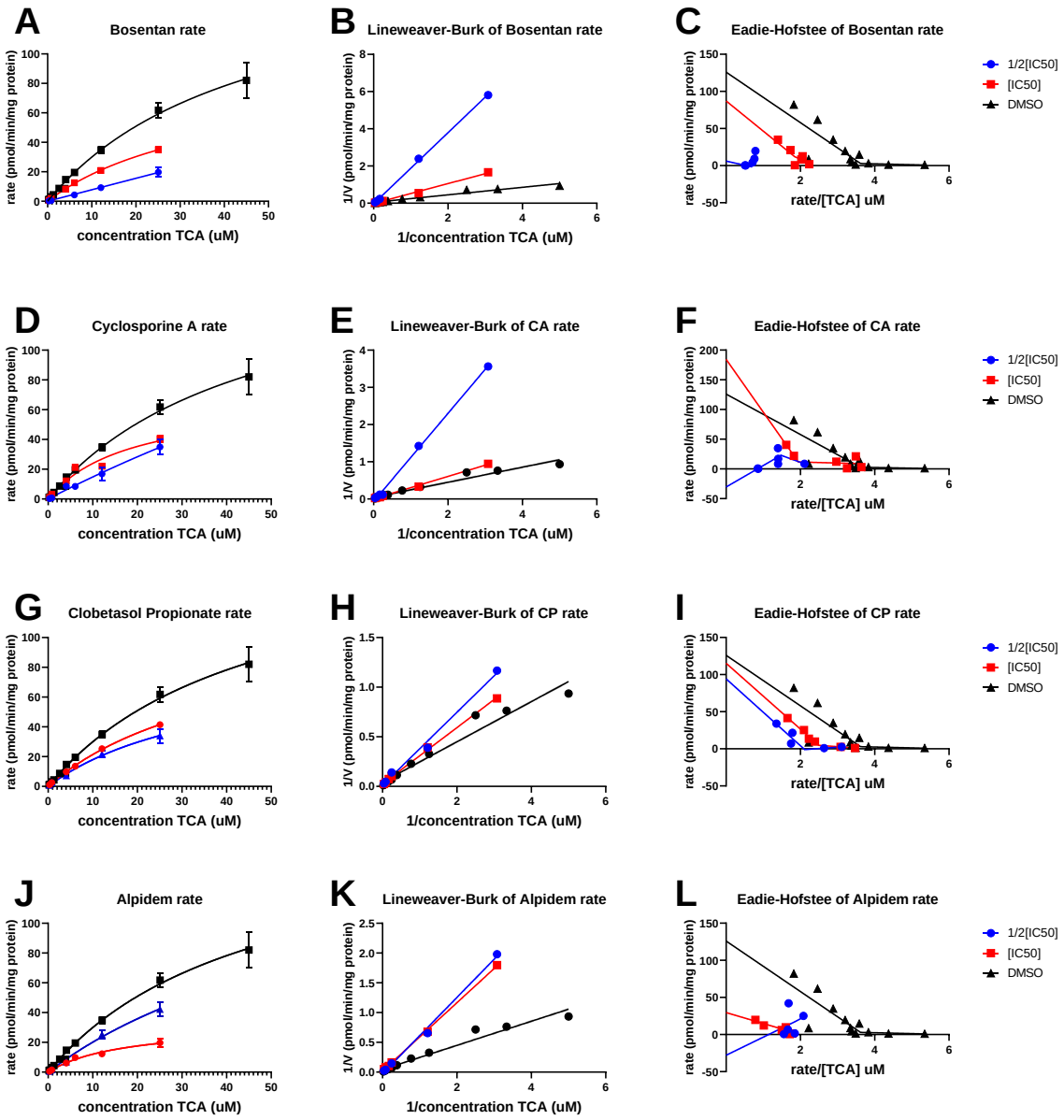

Figure 28 Michaelis-Menten graphs (A, D, G, J), Lineweaver-Burke plots (B, E, H, K) and Eadie-Hofstee plots(C, F, I, L) for TCA transport with 1/2* IC_{50} determined in Figure 6 (blue), IC_{50} (red) and DMSO (black). A non-linear regression was used to identify the Vmax, and Km in the Michaelis-Menten, while a linear regression was used in the Lineweaver-Burke plot, a segmented line was used to identify the initial linear part in the Eadie-Hofstee plot. (N=3)

From the graphs, we can deduce that according to the Lineweaver-Burke plot all compounds cause competitive inhibition of BSEP-mediated TCA uptake. However, it was more difficult to directly fit the data to an Eadie-Hofstee plot as it frequently shows a biphasic relationship between the rate and the rate/[TCA]. The high-affinity component (with significant negative slope) represents BSEP-mediated transport, whereas the low-affinity component (with very shallow slope) represent time-dependent low-capacity binding of TCA to the lipid bilayer in the membrane vesicles. Analysis of the high-affinity component suggests that bosentan, cyclosporin A, and clobetasol propionate act as competitive inhibitors (Vmax is constant, Km increases) or non-competitive inhibitors (Vmax decreases, Km is constant). On the other hand, alpidem appears to act as an uncompetitive inhibitor. However, in most cases, this analysis is based only on the assays containing inhibitors at a concentration that causes 50% inhibition (IC_{50}).

Table 8 Summary of kinetic parameters of TCA transport in Sf21 membrane vesicles. Assays were performed, of which one representative data set is shown in Fig. 1 and 3. ½ IC_{50} dose and IC_{50} dose refer to low dose and high dose, respectively. (No compound n=3 and compounds n=1)

		Michaelis-Menten		*Lineweaver-Burke*		*Eadie-Hofstee*	
		Vmax (pmol/min/mg protein)	Km (µM)	Vmax (pmol/min/mg protein)	Km (µM)	Vmax (pmol/min/mg protein)	Km (µM)
DMSO		169	46.45	22.5	4.6	125.9	34
bosentan	1/2 IC_{50}	~ 3.161E15	~ 4.061E15	-32.6	-62.4	6.1	11.2
	IC_{50}	88.41	38.41	-62.5	-33.4	87.13	40.66
cyclosporine A	1/2 IC_{50}	330	213	-15.0	-17.7	30.42	36.13
	IC_{50}	67.76	18.38	242.2	73.0	184.5	88.91
clobetasol propionate	1/2 IC_{50}	85.39	37.57	82.1	30.2	94.25	45.03
	IC_{50}	110.8	41.79	38.6	10.9	115.2	44.31
alpidem	1/2 IC_{50}	163.6	71.42	-35.9	-23.0	-27.92	29.57
	IC_{50}	32.57	17.08	56.1	32.2	24.4	14.72

The non-linear regression analysis of the Michaelis-Menten appears to be most reliable; it should be noted however that the ½[IC_{50}] showed substantial confidence intervals. In the Lineweaver-Burk plot, the slope of the line is affected the most by the lowest TCA concentration that give high numbers for the reciprocal. Given the low transport rates at low concentrations of TCA, these high data points are the most inaccurate.

3.2.3 Effect of compounds on glycocholate (GCA) transport

There are over 20 bile acids in the human body that are transported continuously by BSEP. However, when it comes to purchasing radiolabelled bile acids, there is only one other bile acid (glycocholic acid, GCA) available in addition to the TCA. GCA is a glyco-conjugated form of CA, which is more abundant in the body than TCA. It was therefore vital to investigate the transport kinetics of BSEP-mediated GCA transport. This endeavour gave us a new challenge as detection of this bile acid from background was difficult. After several experiments, excess amounts of Mg^{2+} in the buffer appeared to be a major issue in this assay.

3.2.4 The effect of magnesium on GCA transport

Mg^{2+} is necessary for the proper hydrolysation of ATP by the nucleotide binding domain of BSEP, however in the BSEP inhibition essay and additional 12.5 mM Mg^{2+} is added in the reaction buffer on top of the 0.1 mM Mg^{2+} in the ATP solution. Figure 29 displays the effects of Mg^{2+} on the transport of TCA and GCA in the presences and absences of ATP. Magnesium is essential to the proper working of ATP hydrolysis by ABC transporters, and in TCA transport excess amounts of Mg^{2+} appeared to be beneficial for the transport reaction in the presence of 5 mM ATP. However, for GCA we see that excess of 12.5 mM Mg^{2+} inhibits the ATP-dependent transport of GCA.

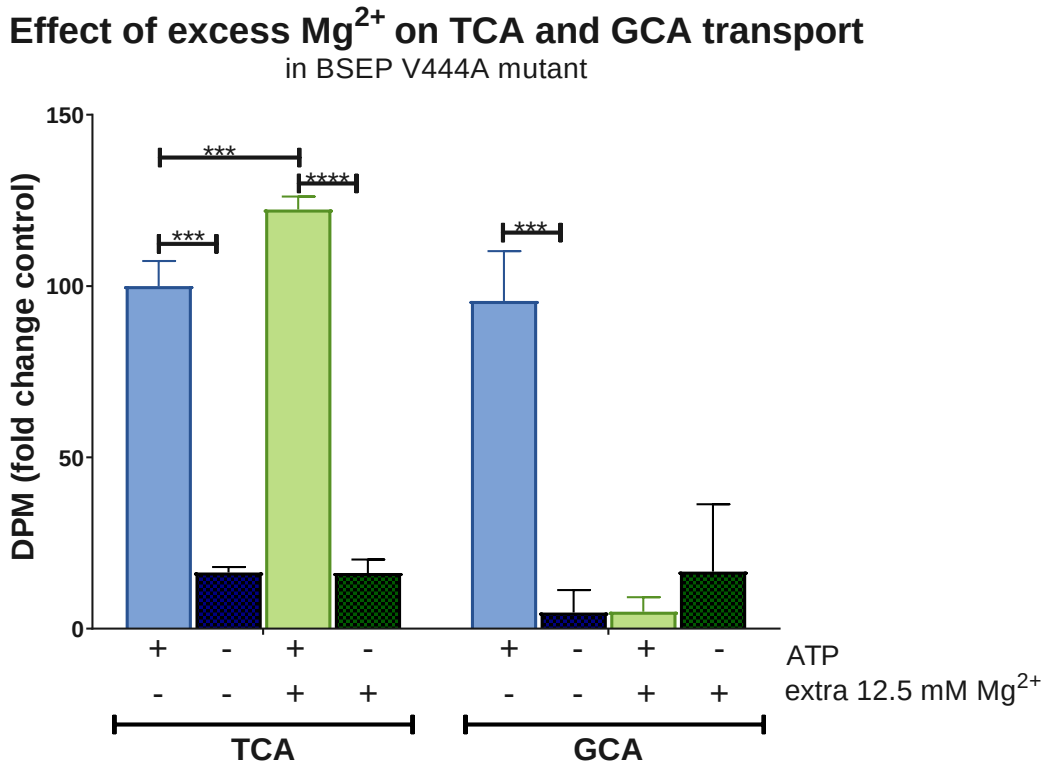

Figure 29 The effect of excess magnesium on BSEPs ability to transport TCA and GCA in the V444A mutant. Disintigrations per minute (DPM) is in direct relation to the accumulation of radio-labelled TCA and GCA. The results indicate that magnesium interferes with BSEP V444A's ability to transport GCA however TCA accumulation is significantly improved by 12.5 mM excess Mg^{2+} (N=3)

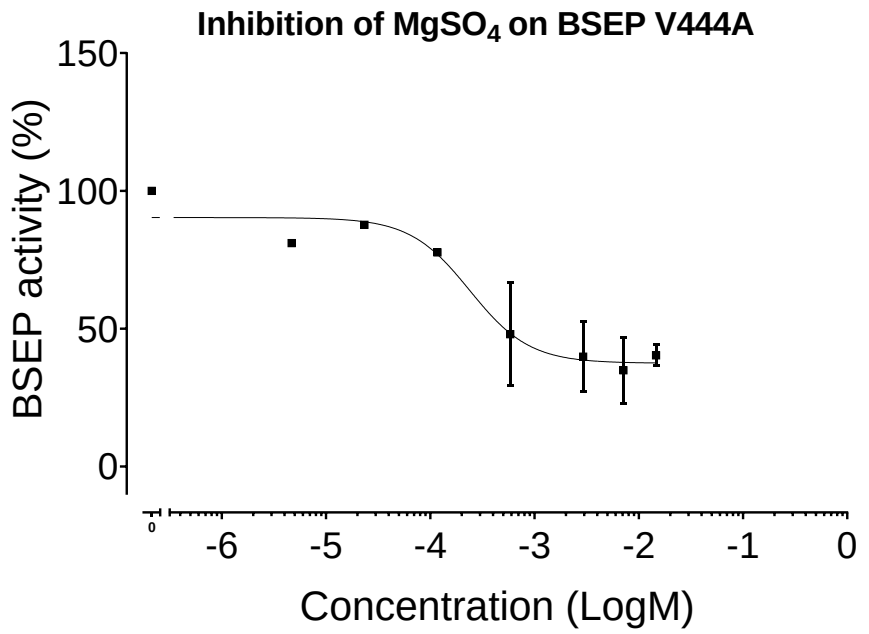

Figure 30. Effect of $MgSO_4$ on BSEP-mediated GCA transport. Increasing concentrations of MgS04 interfere directly with BSEP V444A's ability to transport [^{14}C]- GCA, with an IC_{50} 217.8 µM. interestingly transport was maximally inhibited by 50%. Graphs were plotted as sigmoidal, 4pl plots were the x is log(concentration) (N=3)

To establish the IC_{50} for inhibition of BSEP-mediated GCA transport by Mg^{2+}, MgSO4 was included in the transport assay (see Figure 30). The results indicate an inhibition of the transport reaction with an IC_{50} of 217.8 µM. Interestingly, transport was maximally inhibited by 50%. Hence, part of the transport activity was found to be independent of the excess Mg^{2+}. GCA contains a carboxyl-containing glycine moiety whereas TCA contains a sulfonic acid moiety; these acidic groups might have different interactions with Mg^{2+}. To investigate if Mg^{2+} binds directly to GCA and TCA, Mag-fluo-4 was used to measure the amount of free Mg^{2+} in the presence of increasing amount of bile acids (see Figure 31). Measurements of the Mag-fluo fluorescence emission showed that GCA shows a similar trend as EDTA, and hence, that GCA removes free Mg^{2+} from the solution through binding. In contrast, the Mag-fluo fluorescence emission was relatively unaffected at increasing concentrations of TCA. The complexation of GCA by Mg^{2+} may affect the concentration of free GCA that is available for transport by BSEP; it also possible the GCA and Mg-GCA are both transported by BSEP but with different rates and/or affinities. Furthermore, Mg-GCA formation might cause dissociation of GCA from the membrane in which the free bile acid will partition. In the line of argument, by analogy to ABCB1, BSEP might be able to transport membrane-bound and

cytosolic population of bile acids with different rates and/or affinities. In an attempt to measure the effects of Mg^{2+} on bile acid binding to a membrane surface, the Mag-fluo-4 assay was repeated in the presence of liposomes. However, the results showed that liposomes were incompatible with the probe.

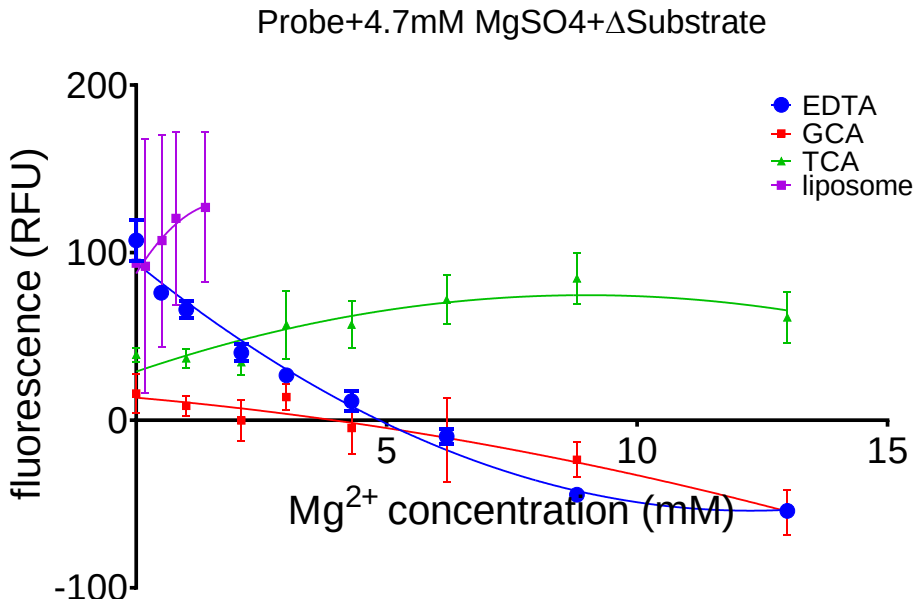

Figure 31. Mag-fluo-4 fluorescence measurements with backgrounds subtracted (only $MgSO_4$ and substrates). Second order polynomial (quadratic) non-linear regressions were fitted on top of the data to indicate the different responses between the individual substrates.

IC_{50} evaluation of selected compounds on GCA transport by BSEP

In further transport assays, the inhibition of BSEP-mediated GCA transport by the selected compounds was measured (Figure 32). The results suggest that only bosentan caused inhibition at a very low concentration, whereas clobetasol propionate, cyclosporin A and alpidem shows no inhibition up to a concentration of 1000 µM. While the SD values for bosentan were acceptable, the standard deviation for the other compounds were very large. Repeats of the measurement did not change this. In spite of this, the data suggest that the inhibition of BSEP by the compounds is bile acid dependent.

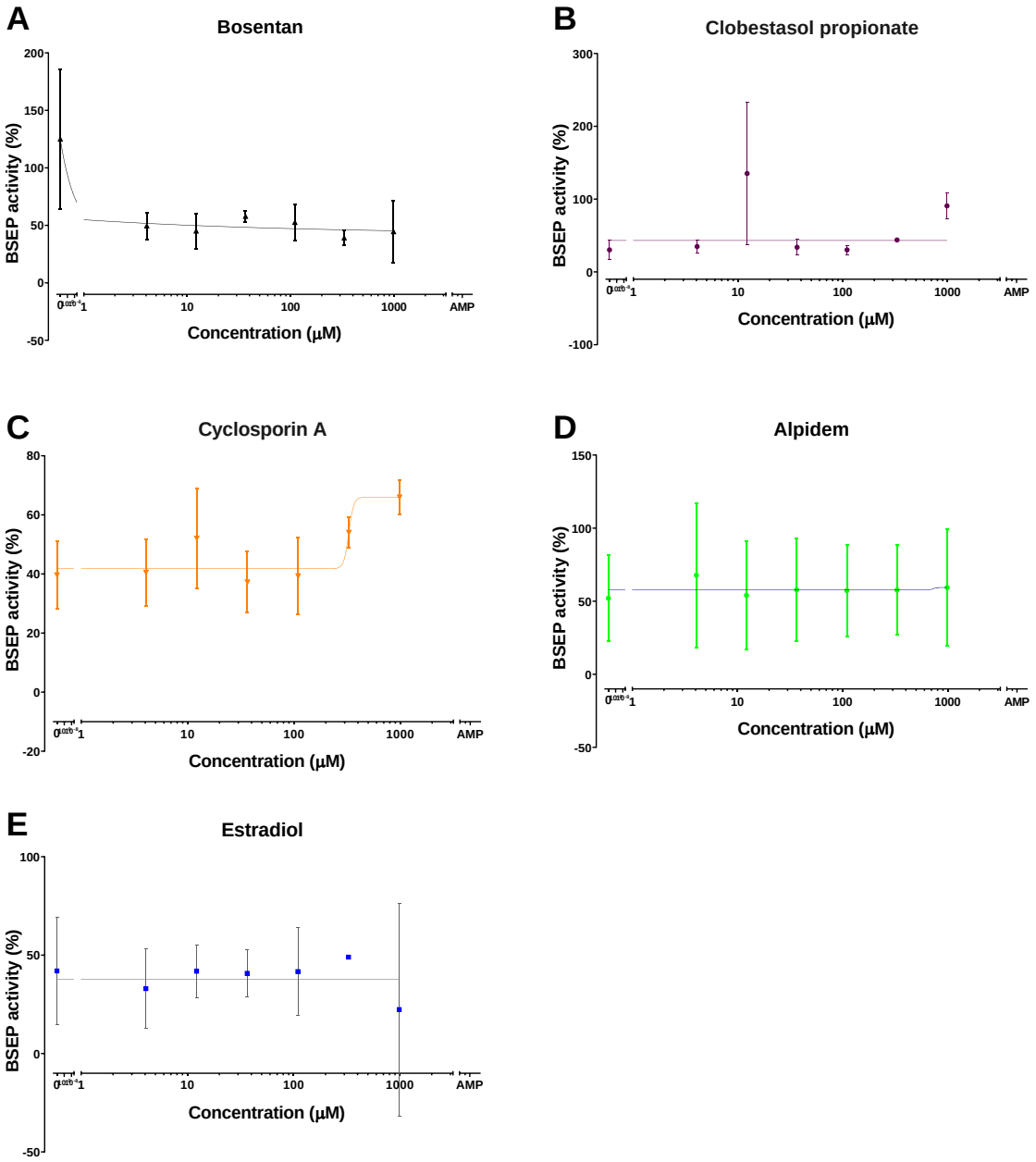

Figure 32 Inhibition of BSEP-mediated GCA transport by selected compounds. Graphs were plotted as sigmoidal, 4pl plots were the x is log(concentration) however no IC_{50} could be detected for GCA uptake inhibition.

3.3 Discussion of the results

The data and analyses in this chapter confirm that there is no clear correlation between the physicochemical or functional properties of compounds and their ability to inhibit BSEP. This finding is in line with the fact that physicochemical are currently unable to predict which compound will cause DILI, and with the conclusion that DILI occurs in an idiosyncratic way. [16].

For TCA transport by BSEP, we found a Vmax of 169 pmol/min/mg protein and a Km of 46.5 µM, with previous literature stating the Vmax around 250 pmol/mg protein/min with a Km of 4.1 µM [69] and another stating the Vmax of 4290 pmol/min/mg protein and a Km of 4.6 µM [70]. Although our measurements yielded a lower affinity for BSEP-mediated TCA transport than reported in the literature, these values are all in the lower µM range. Consistent with this the IC_{50} values were in agreement with those stated in the literature [15,71].

The kinetics of BSEP-mediated TCA transport was determined in the presence of the inhibitors to study the biochemical mechanisms of inhibition. Our Lineweaver-Burk analyses points to a competitive mechanism for the tested compounds. Regarding these compounds, there are conflicting reports in the literature where one study suggests competitive mechanisms [72] whereas another proposes an uncompetitive mechanism for cyclosporine A [73]. The latter study also found that the impact of competitive vs non-competitive BSEP inhibition is of vital importance, as non-competitive inhibitors led to a much more significant bile acid accumulation in the liver and increased potential toxicity. According to the data in this work, the Eadie-Hofstee plots indicate that bosentan, clobetasol propionate and cyclosporin A act as competitive or non-competitive inhibitors. Alpidem on the other hand shows uncompetitive behaviour in the Eadie-Hofstee plot. This difference in inhibition types is very interesting and could explain in part why alpidem, although it has roughly the same IC_{50} as clobetasol propionate, causes liver injury whereas clobetasol propionate does not.

While our kinetic data regarding TCA transport by BSEP shows a possible explanation regarding the toxicity of BSEP beyond simple IC_{50} determination, it is essential to note that kinetic analyses are not generally done within pharmaceutical industries. At present, most pharmaceutical companies rely on a panel of tests that include BSEP IC_{50} determination with TCA, toxicity assays in relevant cell lines and general dosing information to decide what

compounds proceed to the next stage of testing and development. A recent review does not take into account how the type of inhibition can have different outcomes in drug toxicity [74].

Another factor that affects drug toxicity is the prevailing bile acid concentration and composition. In our study, we found significant differences for the inhibition of TCA and GCA transport. This is consistent with published research on the effect of compounds on BSEP-mediated TCA and GCA transport. Although for some compounds little difference was found for the IC_{50} of inhibition, other compounds including acitretin (IC_{50} 29.27 µM for TCA and 100 µM for GCA) and troglitazone (TCA: 1.98 µM, GCA 15.96 µM) yielded significant differences [71]. Hence, it is vital to consider which bile acids are important to investigate. GCA has previously been shown to be a stronger BSEP substrate in humans while TCA is stronger in rats [75]. However, while there is data available, we cannot compare our data with the published date due to the variability in the amount of Mg^{2+} in assay buffers in the published studies. As we have shown in this chapter, excess free Mg^{2+} has a significant inhibitory effect on BSEP-dependent GCA transport. This novel finding requires further investigation. Mg^{2+} is the fourth most abundant cation in the body and plays an essential physiological role in physiology [76]. Some of the primary functions of Mg^{2+} in human biology include the maintenance of ionic gradients (keeping intracellular sodium and calcium low and potassium high), cellular and tissue integrity, mitochondrial oxidative phosphorylation (ATP production and activation), and DNA, RNA and protein synthesis and integrity [76]. Chronic diseases, medications and magnesium decreases in food crops well as the availability of refined and processed foods, causes that the vast majority of people in modern societies are at risk for magnesium deficiencies. Given our finding on the complexation of GCA and Mg^{2+}, the free bile acid concentration might be different in individuals with sufficient or deficient Mg^{2+} levels, and this might relate to the incidence of idiosyncratic Drug induced liver injury (iDILI). In line with this, Mg^{2+} has been shown to have a protective effect on bile duct ligation and liver functions [77,78].

4. The effect of BSEP membrane expression on total bile concentration and cell viability.

4.1 Introduction

Chapter 3 concluded that BSEP has different preferences in the transporting the different bile acids, to investigate this in more detail chapter 5 will look at the influence of compound on bile acid metabolomics. However, in primary human hepatocytes, drugs can have effect on more than just BSEP. Compounds can cause toxicity and influence cell survivability, and they can affect BSEP expression and localisation. However, hepatocytes are also able to take up bile acids in an OATP and NTCP-dependent manner, allowing us to see the effect on bile acid recycling and total bile acid concentration. In this chapter we will introduce the cells prior to looking into the bile acid signalling lipid metabolomics (chapter 5 and 6 respectively).

4.1.1 Donor information

To investigate the effect of DILI inducing drugs on BSEP regulation, BSEP trafficking and bile acid pool composition, experiments were developed in collaboration with AZ and the University of Leiden to explore the effects of iDILI inducing drugs in greater detail. To this end bile acids were measured in two types of cell culture, the first being sandwich cultured (2D) PHH and the second being spheroid cultured (3D) PHH. The donors were close in age, had similar causes of death, and were both Caucasian. However, the donor used for the 2D cell cultures was female while the donor for 3D was male (see Table 9).

Table 9 Summary of primary human hepatocytes donors.

	2D sandwich	3D Spheroids	Donor 3
Gender	female	male	female
Age	78	68	27
Race	Caucasian	Caucasian	African American
Cause of death	cerebrovascular accident	Cerebral anoxia	anoxia
Smoker	yes	no	None reported
Alcohol usage	yes	yes	None reported
Alcohol history	occasional	occasional	None reported
Cytomegalovirus	positive	positive	positive

4.1.2 Selection of test compounds

Chapter 3 looked at the effect of compounds on BSEP directly (Table 10). However, in primary human hepatocytes drugs can have other effects too, the cell cultures were therefore exposed to one of four different compounds chosen for their different effects on BSEP (displayed in Figure 33): i) Bosentan is a dual endothelin receptor antagonist, affecting both endothelin A and B receptors, which prevents the narrowing of blood vessels and is used to treat hypertension. Bosentan was chosen as a test compound because the drug is known to inhibit BSEP and is used by AstraZeneca as a positive control in their BSEP inhibition panel. It can cause severe hepatic side effects in some patients [66]. ii) Clobetasol propionate is a derivative of prednisolone that exhibits a high glucocorticoid activity and is used as a topical treatment for psoriasis. Clobetasol propionate was chosen as a test compounds because while the drug is known to inhibit BSEP no hepatic side effects are known [45]. iii) Cyclohexamide is a naturally occurring fungicide produced by Streptomyces griseus and that is an inhibitor of protein translocation. The precise mechanism of action has yet to be fully understood however it has been shown to inhibit translation elongation through binding to the E-site of the 60S ribosomal unit and interfering with the deacetylated tRNA [79]. However, Kubitz et al. 2004 indicate that cycloheximide increases BSEP expression at the apical membrane of the hepatocyte in a microtubule and p38 map kinase dependent manner, which is why it was chosen as a test compounds for this study. iv) Estradiol is a naturally occurring steroid hormone responsible for female reproduction, maintenance of body temperature, preserving bone strength, cholesterol production and protection of the heart [67]. Some foods may affect levels of estradiol in the body, and a synthetic form is often prescribed as a birth control measure and in the treatment of menopausal symptoms. Estradiol was chosen because experiments in rats have indicated a reduction of BSEP at the apical membrane of hepatocytes in response to exposure to this compound [68]. The effect of estradiol on human liver, however, is age-dependent rather than gender-specific [80].

The cells were harvested at 6 hrs for early assessment, 24 hrs for intermediate and 72 hrs for longer-term effects and DMSO was used as solvent control.

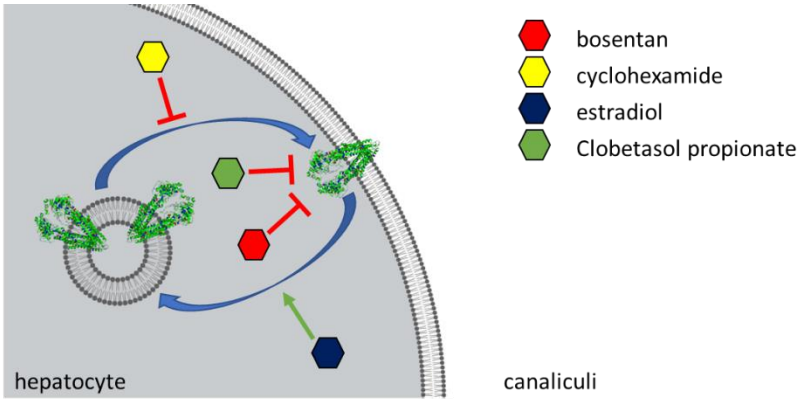

Figure 33. Image depicting the predicted effects of drug exposure. BSEP is recycled continuously within the hepatocyte with a vast amount stored within vesicles in the cytoplasm for fast recruitment to the apical membrane. Bosentan and clobetasol propionate have direct effects on BSEP activity, while cycloheximide is known to increase BSEP expression at the membrane in the first hours. Estradiol is known to cause a decrease of BSEP expression in rats.

A summary of information regarding drugs used so far and is displayed in Table 10.

Table 10. Summary of the drugs used in chapter 4, 5 and 6. Data was obtained from AZ database (not published)

	IC_{50} (µM)	Type of damage	Comments
Cyclosporine A	0.57	cholestatic/mixed	
Bosentan	44.16	cholestatic/mixed	
Alpidem	2.64	hepatocellular	
Clobetasol propionate	7.74	none	
Estradiol	>1000	*unknown in humans	improves liver damage in rats
Cyclohexamide	>1000	hepatocellular	
DMSO	>1000		vehicle control

4.2 Results

4.2.1 Cell survivability in response to treatments is affected by cell donor.

ATP levels were measured as an indication of how cell survivability was affected by the different treatments. In Figure 34A and B the ATP levels of the 2D and 3D cultures are displayed. The effect of treatment on 2D cells indicated significant effects of the different treatments at 72 hrs, while in 3D culture only cycloheximide appeared to be significantly toxic after 72 hrs of incubation. These results might suggest that primary human hepatocytes are better protected against toxicity when cultured in 3D. To exclude the effect of donor variability the experiment was repeated with a third donor, (Figure 35). Figure 35, however, indicates that cells in both 2D and 3D cultures experience significant toxicity in response to dosing. It can therefore not be concluded that 3D cells are better able to cope with the effects of toxicity in response to different treatments. The effect may be donor-specific or gender-specific and further research needs to be done.

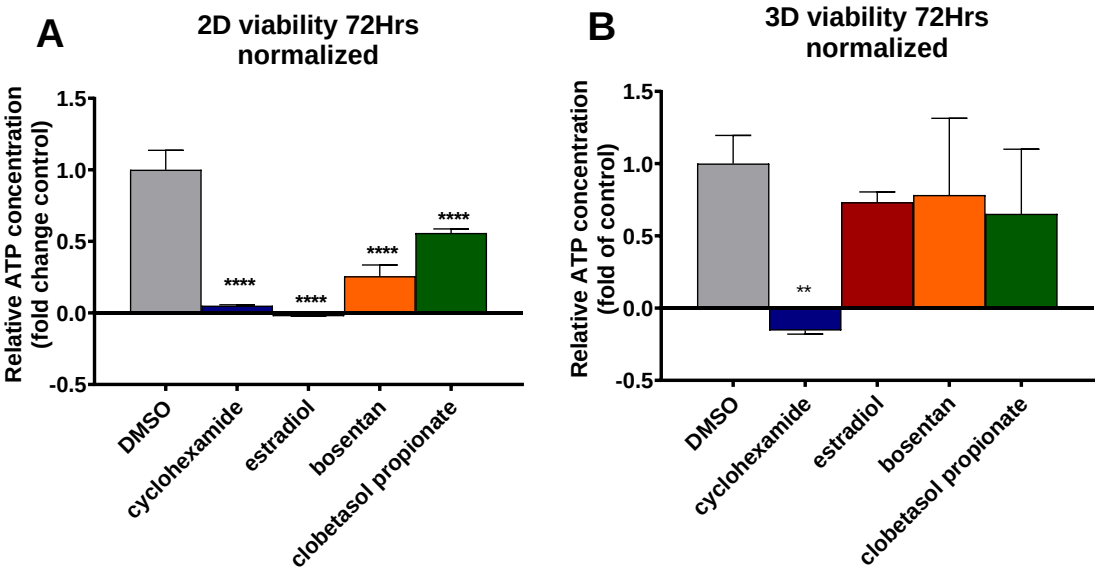

Figure 34. Cell survival of 2D and 3D cultured hepatocytes at 72 hrs. These are the same cells as used and investigated in Chapter 5 and 6. Primary human hepatocytes were obtained from Donor 1 and 2. (N=3)

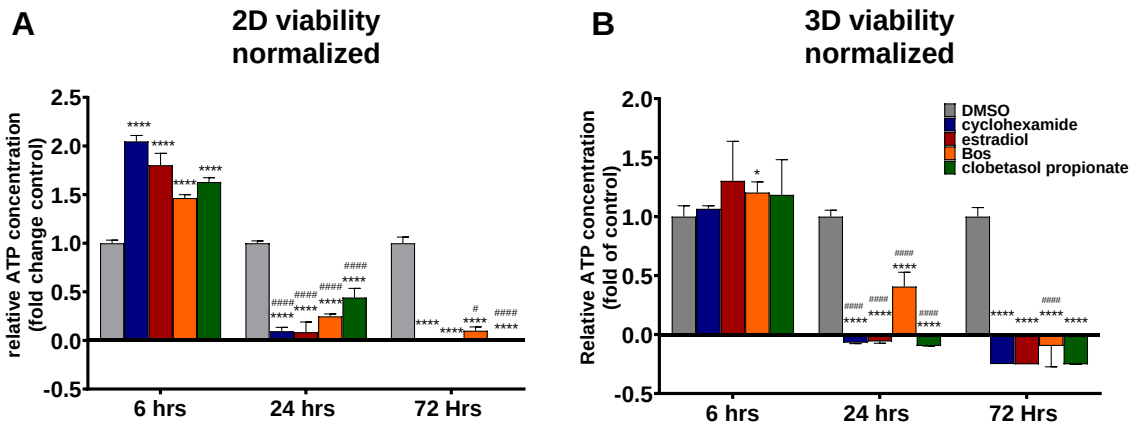

Figure 35. Cell survival of 2D and 3D cultured hepatocytes at 6, 24 and 72 hrs. Primary human hepatocytes were obtained from Donor 3. * indicates comparison with DMSO control, # compares identical treatments with previous time point. (N=3)

4.2.2 The bile acid concentration is not directly related to the position of BSEP in 2D cell cultures.

To investigate the effect of treatments on BSEP distribution in the primary human hepatocytes, the cultures were harvested and stained with anti-ABCB11 for BSEP protein, Hoechst 33342 for nuclei, and CellMask for the cytoplasm (for representative images see Figure 37,Figure 38, and Figure 39). The analysis of staining was done by using Columbus image analysis program, which contains the following steps:

Step 1: Hoechst staining was used to identify the nucleus and identify the number of cells.

Step 2: CellMask staining was used as cytoplasm staining to identify regions of interest, i.e. individual cells.

Step 3: the Columbus program was then able to calculate regions of interests separately, such as cell membranes and cytoplasm.

Step 4: Anti-ABCB11 staining was used to identify the location of BSEP in either the cell membrane or the cytoplasm.

Step 5: Objects, indicating BSEP, were counted per cell, and averages per cells are displayed in the figures.

To investigate the effect of treatments on bile acid displacement and production, the total bile acid concentration was measured in PHH and the media. Figure 36 displays the results obtained from the 2D PHH cultures. After 6 hrs of treatment (Figure 36A), significantly less BSEP in the cell was found in PHH treated with cycloheximide and estradiol. There is also significantly less BSEP in the cytoplasm of PHH treated with cycloheximide and estradiol. However, the cytoplasm of 2D cultured PHH treated with clobetasol propionates showed a significant increase in BSEP expression. In the membrane where BSEP performs its function of effluxing bile acids, only cells treated with estradiol showed a significant decrease in BSEP expression. This decrease, however, does not translate to the incorporation of BSEP into the membrane of cycloheximide treated cells. For cells treated with estradiol however significantly less BSEP was found in the membrane.

Interestingly, the concentrations of total bile acid did not reflect the significant changes in BSEP location. After 6 hrs of treatment a significantly increased concentration of bile acids was only detected in PHH treated with estradiol in the media (Figure 36B). In cycloheximide treated cells, the only change was a significant decrease of total bile acid concentration inside the cell.

At 24 hrs, a significant increase in BSEP expression in the whole cell can be seen in PHH treated with cycloheximide and bosentan (Figure 36C). In the cytoplasm we see a significant increase in BSEP in cycloheximide and bosentan treated cells, but no significant changes were detected in the membrane for any of the treatments. The analysis of the bile acid concentrations showed that no significant changes occurred in the media concentration, but that a significant decrease in bile acid concentration could be detected inside the cell for all treatments. However, this is due to the fact many of the cells probably lysed due to cell death detected in the ATP measurement (Figure 35A).

At 72 hrs (Figure 36E), a significant general decrease of BSEP expression in PHH treated was observed with cycloheximide and estradiol. In the cytoplasm, a significant decrease is seen in cells treated with cycloheximide and estradiol, which in this case is also seen in the expression of BSEP in the membrane. In Figure 36F we see a significant increase in total bile acid concentration in PHH media treated with bosentan. The cell concentrations are once again

significantly different due to the absence of viable cells at the point of harvest. It was, therefore, impossible to detect total bile acid concentrations in these cells.

From these results, we can conclude that BSEP expression in the membrane does not correlate with the concentration of total bile acid in the cell or the media in 2D cultured PHH nor does the expression translate to toxicity.

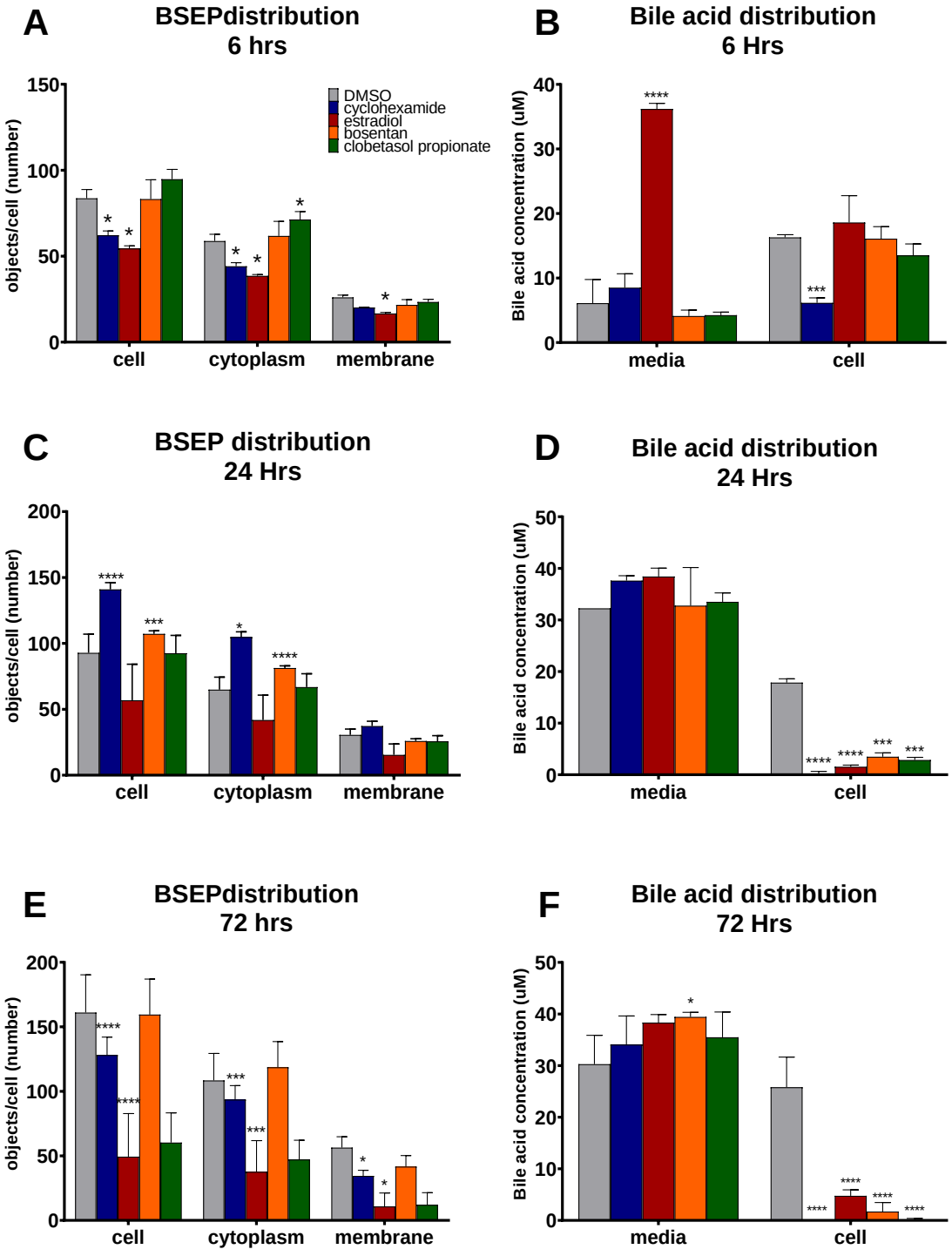

Figure 36. BSEP distribution and bile acid distribution in 2D cultures of primary human hepatocytes obtained from Donor 3. [n=3)

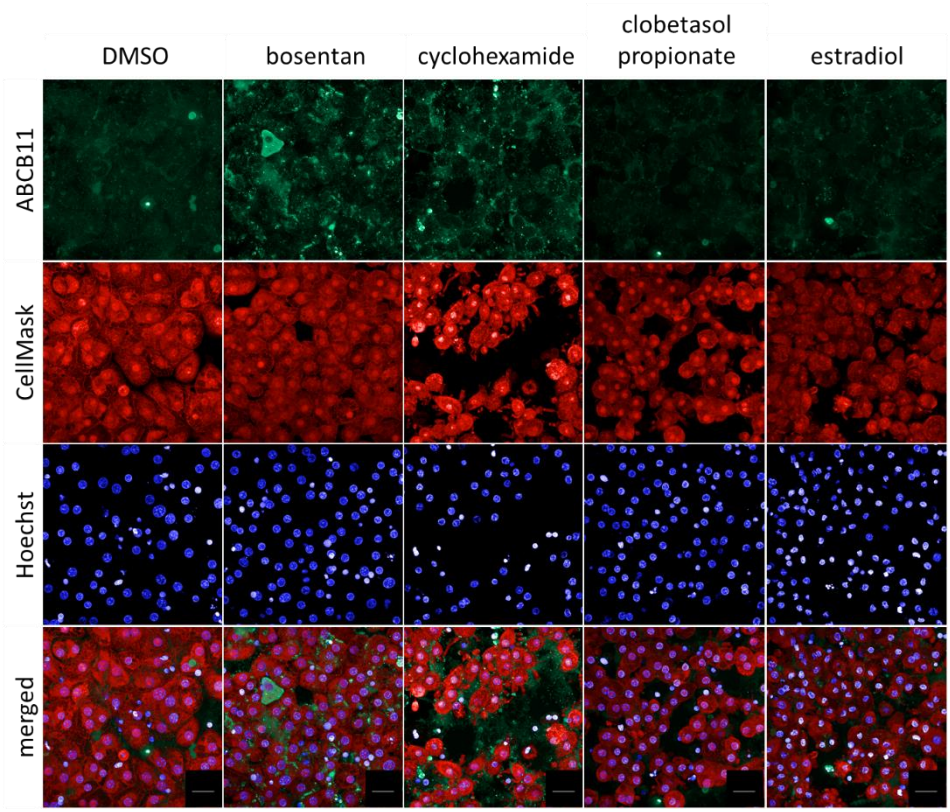

Figure 37 Representative images of 2D cultured PHH harvested at 6 hrs and stained with Anti-ABCB11 (green), CellMask (red), nucleus (Blue). Scale bar: 20 mm

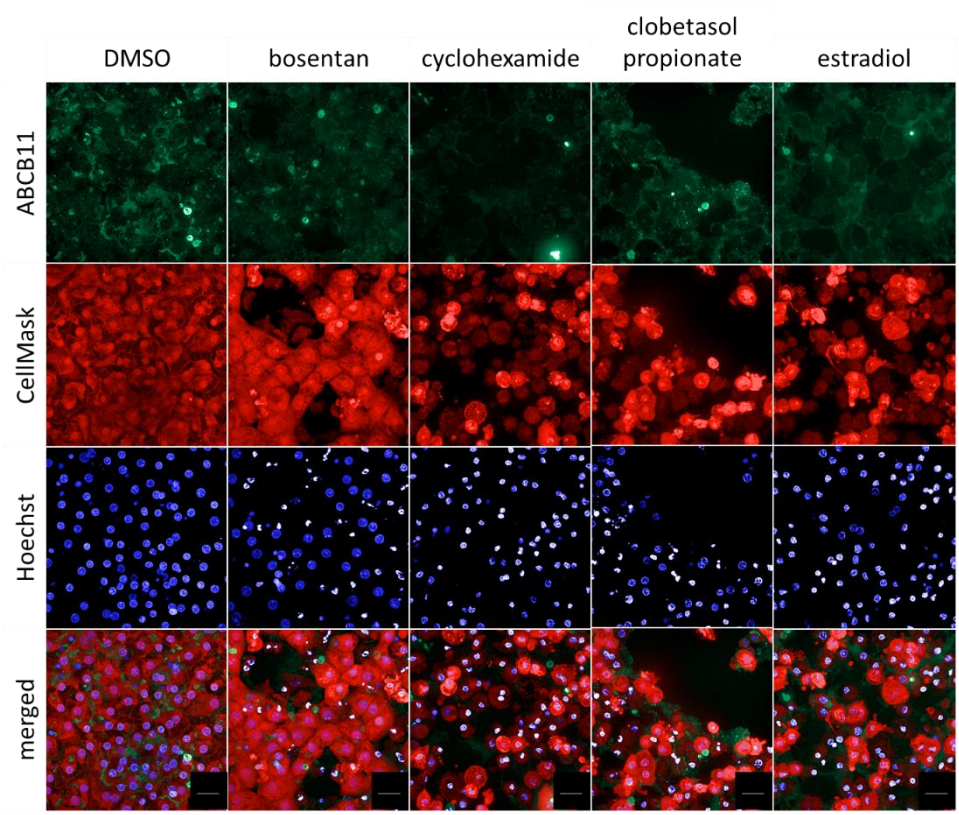

Figure 38. Representative images of 2D cultured PHH harvested at 24 hrs. Scale bar: 20 mm

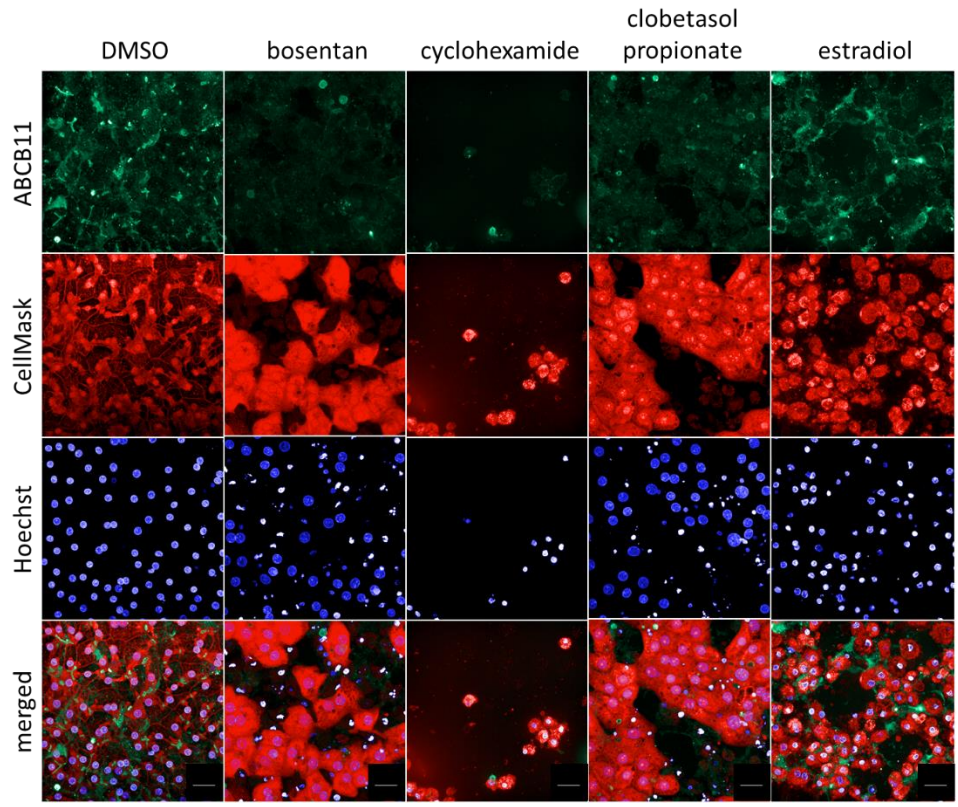

Figure 39 Representative images of 2D cultured PHH harvested at 72 hrs. Scale bar: 20 mm

4.2.3 The effect of treatment on BSEP localisation and bile acid concentration in the 3D cultures

The effect of treatments on BSEP localisation was investigated in the same way for 3D cultured PHH as the 2D cultured cells and results are displayed in Figure 40. However, several problems occurred during the analysis. 3D cultured spheroids appear to be too unstable to transfer to the imaging plate. There was an increasing number of missing samples at 24 hrs and 72 hrs. There were no significant differences detected at 6hrs in the expression of BSEP in the cell, cytoplasm or membrane of treated 3D cultured PHH. The analysis of total bile acid concentration in media and cells indicated a significantly higher concentration of estradiol treated PHH at 6, 24 and 72 hrs, but none of the other samples showed a significant change. It is possible that this result is caused by the low the detection limit could be that the range of detection of total bile acid concentration is caused by the low total bile acid concentration the detection of which is at the limits of what can be achieved in the assay. The experiment should, therefore, be repeated with samples where several spheroids have been pooled together. Pooling, however, does not increase the sensitivity of detection in media samples. Images representing fluorescent staining are displayed in Figure 39 to 41

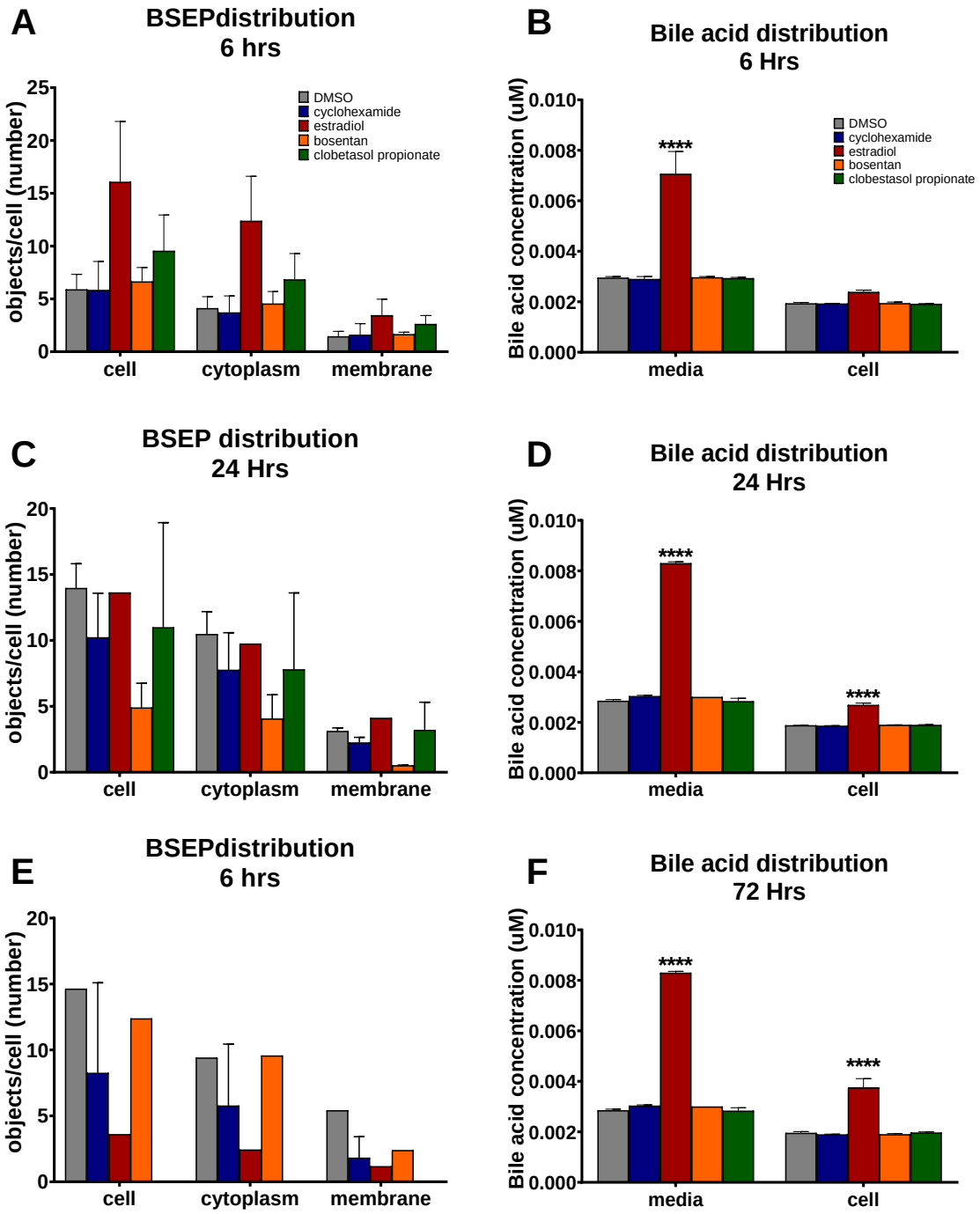

Figure 40. BSEP distribution and total bile acid concentration in 3D cultured PHH obtained from Donor 3. (N=3 for bile acid distribution, for BSEP distribution is N>1)

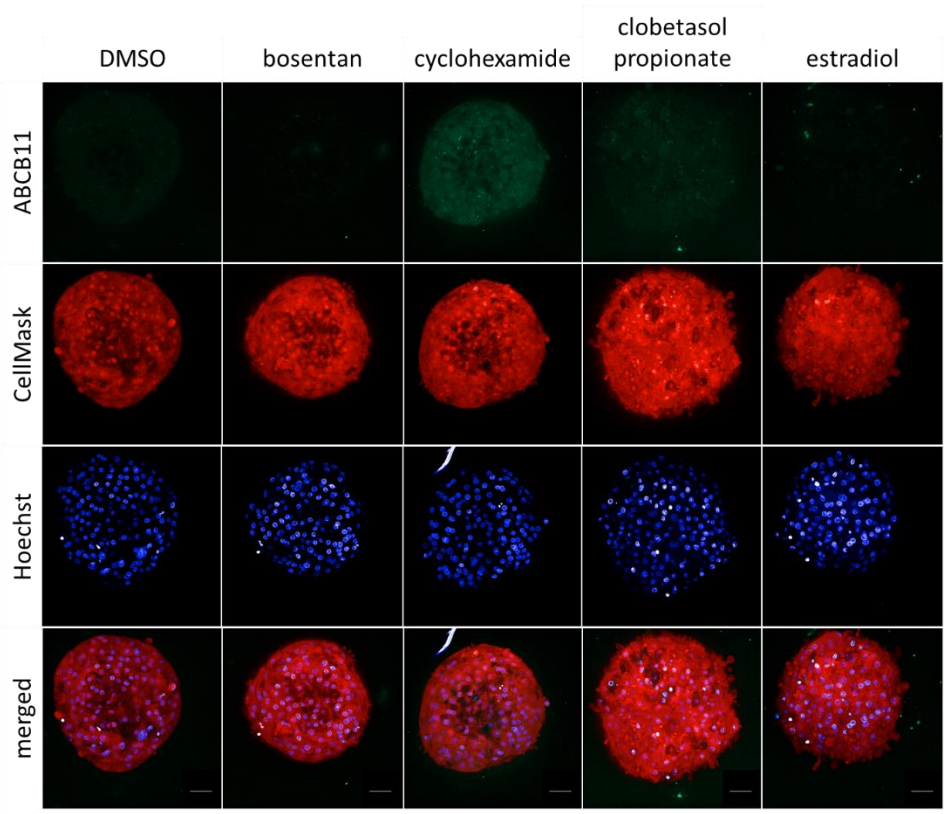

Figure 41. Fluorescently stained images representing 3D cultured PHH at 6 hrs. Scale bar: 50 mm

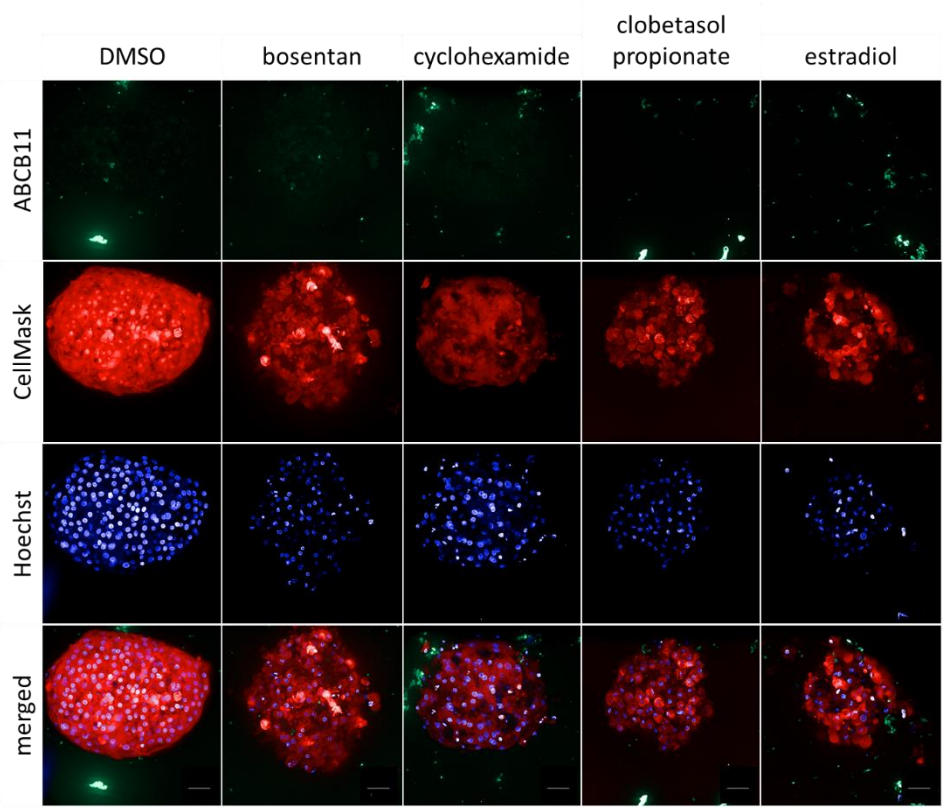

Figure 42. Fluorescently stained images representing 3D cultured PHH at 24 hrs. Scale bar: 50 mm

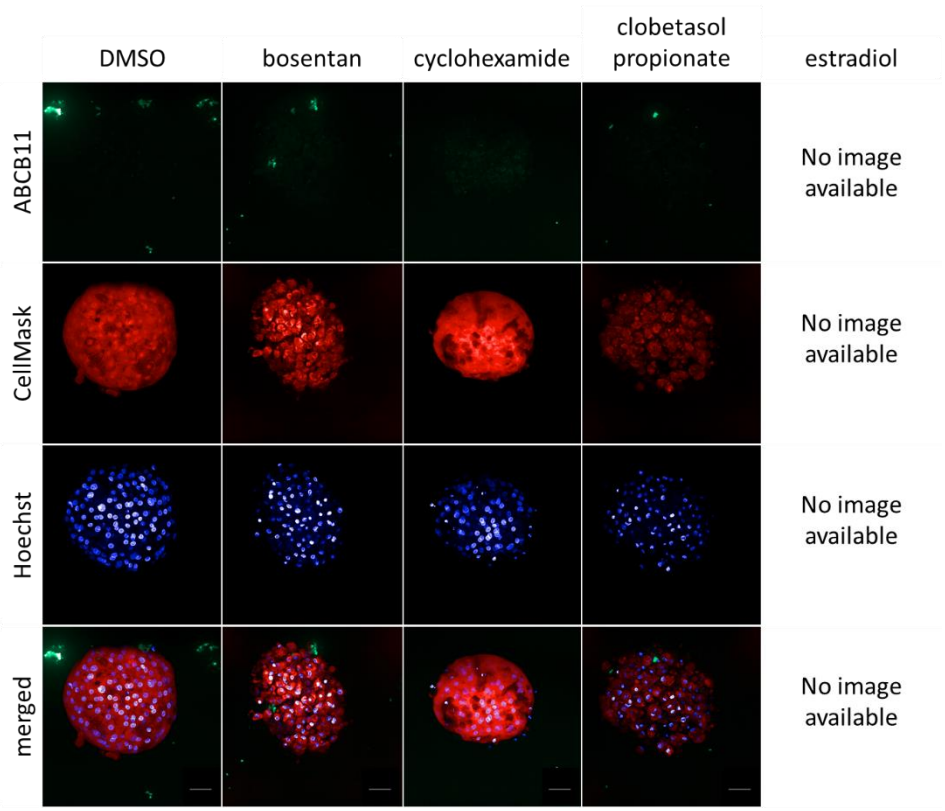

Figure 43. Fluorescently stained images representing 3D cultured PHH at 72 hrs. Images for estradiol were unavailable as no spheroid could be detected after 72 hrs. Scale bar: 50 mm

4.3 Discussion of the results.

3D cultured PHH have previously been shown to have relatively regular Cyp450 enzyme expression compared to human, and it is therefore expected that these cells have a more comparable drug metabolism than 2D cultured cells. This chapter investigated the effects of 2D and 3D cultured PHH in the absence and presence of drugs that are known to either inhibit BSEP directly or change BSEP expression. From the viability assay we can conclude that the effect of treatments on viability is either donor-dependent or gender-dependent. It has previously been stated that there are donor-dependent responses to pharmaceuticals in human hepatocyte cultures. It is, therefore, necessary to analyse cells from multiple donors to obtain reliable results that can be translated to the entire human population [81]. It is, however, essential to note that pharmacokinetics in 3D cultured cells is more reliable than 2D cultured cells due to the near-normal expression of Cyp450 enzymes and critical proteins [18]. Six laboratories have previously shown that 3D cultured spheroids are more sensitive to hepatotoxic compounds and particularly in long term exposures [20]. This study considered inter-donor variability as well as laboratory variability. The 2D systems showed a more predefined differentiated phenotype and lower sensitivity to toxicity. Takayama et al., 2014 showed that differences in hepatic metabolism are mainly due to genetic polymorphisms in its genes and that these polymorphisms have a significant influence on efficacy and adverse reactions to drugs [82]. These findings are all in line with the viability results for the cells. To fully understand the effect of 2D vs 3D on liver toxicity the experiment should be performed with different donors to include the effect of inter donor gene variations. Another way to evaluate the effect to a broader extent is to investigate polymorphisms in genes responsible, such as Cyp450. However, this would not test for genetic polymorphism in genes responsible for transport proteins such as *ABCB11*.

The second part of this chapter looked at the expression of BSEP in PHH cultured in 2D and 3D settings, as well as total bile acid concentration. Very little research has been done to investigate the effect of different treatments on BSEP expression. Often literature infers qPCR levels to an increase in BSEP expression in cells [83]. However, increases in gene expression do not necessarily relate to an increased expression of the functional protein [84]. A second way of looking at BSEP expression is by western blotting [85,86]. Since BSEP is continually recycled from the membrane to vesicles in the cytoplasm [40], quantification of BSEP via

fluorescence, therefore, offers a new and improved method to look at treatment effects on BSEP expression. From the results, we can conclude that BSEP expression if indeed is affected by different treatments does not necessarily correlate to the amount of bile acid being transported.

Previous research using BSEP specific staining and quantification at the membrane has shown that a decreased amount of BSEP at the membrane is related to increased severity of PFIC2 and BRIC2 [87]. The results indicate that while BSEP can significantly change upon different treatments this does not necessarily relate to increased concentrations of BSEP. Estradiol has previously been shown to significantly decrease BSEP expression [88]. This is in line with our findings at 6 and 72 hrs for 2D cultured cells. However, we were unable to replicate the effect in 3D 6 hrs where the effect was not significant. The second compound that affects BSEP expression is cyclohexamide. In previous studies, cycloheximide decreased the amount of BSEP in the Golgi apparatus caused a 2-fold increase of BSEP at pseudo-canaliculi in HepG2 cells after 6 hrs of incubation [40]. After the initial increase of BSEP at the pseudo-canaliculi the number of BSEP positive canaliculi declined again until they reached normal levels at 16 hrs. In the PHH 2D cultured cells we saw a significant decrease at 6 hrs in the whole cells and the cytoplasm, however at 24 hrs cycloheximide treated cells showed a significant increase in BSEP expression in the whole cell and the cytoplasm, but that did not translate to expression of BSEP in the membrane. At 72 hrs we see a significant decrease of BSEP in all compartments of the cell. The differences between the literature and the results in this thesis can be explained by the differences in cell lines as well as different culturing methods. The previous study used simple 2D culturing while this study used 2D sandwich culture.

Several problems were encountered during the staining of the 3D spheroids. The first issue was the difficulty of transferring the spheroids from the culturing plates to the viewing plates. The second was that the loss of spheroids that were severely affected by toxicity and lost their integrity. A third problem was that antibodies required a longer time to sufficiently penetrate the entire spheroid [59]. We were able to get a full set to analyse the 6 hrs treated samples, but we were unable to get enough samples at 24 and 72 hrs. We can therefore not draw any conclusion from the staining data of the spheroids beyond the fact that it needs further optimising. Both the 2D and the 3D cultures, however, indicate a novel way to investigate the effect of DILI inducing compounds on toxicity. While our data is unable to explain the

difference between bosentan and clobetasol propionate-induced toxicity, we were able to conclude that in 2D cultured PHH, BSEP expression does not relate to bile acid concentration. As several samples showed no significant differences in total bile acid concentration relative to control but still experienced toxic effects, we cannot relate the total bile acid concentration to bile acid effects on cell death. It is, therefore, logical to expect that bile acid-mediated toxicity is bile acid-specific rather than dependent on total concentration.

5. The effect of different treatments on bile acid composition inside the cell and the media.

5.1 introduction

This chapter is a continuation of the previous chapter and will look at the bile acid metabolomics inside 2D and 3D cultured primary human hepatocytes. in the previous chapter we have shown that total bile acid accumulation did not account for toxicity, consequently it is important to investigate the individual bile acids and their response to treatments.

Treatment can cause changes in the bile acid pool, by selectively inhibiting export, changing the metabolomics of bile acid formation by interfering with the enzymatic steps or by influencing the uptake of bile acids into the hepatocyte.

5.1.1 primary and secondary Bile acids

As described in chapter 1.2, *de novo* synthesis of bile acids in hepatocytes occurs by converting cholesterol into bile acids by the action of cytochrome P450 enzymes CYP27A1, CYP8B1 and subsequently CYP7A1 [28]. An alternative pathway to produce bile acids occurs in peripheral tissues and is initiated by the CYP27A1 and CYP7B1-dependent conversion of cholesterol into 27- dihydroxycholesterol, a bile salt precursor that is then taken up by the hepatocytes [27]. In both cases only two Bile acids are indicated to be produced by the hepatocyte: CA and CDCA.

After their synthesis, CA and CDCA are either directly transported to the gallbladder and subsequently to the intestines or they undergo glyco- or tauro- conjugation making the Bile acids CA, with its conjugated forms GCA, TCA and CDCA with GCDCA, TCDCA the only bile acids directly produced by the hepatocyte. However, a wider variety of bile acids exist within the human genome, explained by the further conversion by the gut-microbiota able to produce among others Deoxycholic acid [89]. As these are not primarily produced by the hepatocytes they are classified as secondary BAs. The new mixture of primary, conjugated primary and secondary Recycling of Bile salts occurs via Apical sodium-dependent bile salt transporter (ASBT) in the intestines thereafter bile salts enter the enterohepatic circulation and are transported into the hepatocytes by the organic anion transport protein 2 (OATP2) and the sodium-taurocholate co-transporting polypeptide (NTCP) [90,91]. Where the cycle starts of conjugation, release to the gallbladder and intestines starts anew. This cycle takes place around ~20x and permits the liver to only produce ~5% of the primary BA via deNovo synthesis [92].

5.1.2 The toxic and beneficial effect of certain bile acids.

While previously the total accumulation of bile acids in hepatocytes was considered to be toxic, recent investigations show that accumulated bile acids can have different effects within the hepatocyte. The first and foremost is that not all bile acids appear to be equally toxic to the cell. While no publications can be found that state the IC_{50} of different bile acids the general consensus is that the more hydrophobic a bile acid is, the more toxic it is [93,94]. The less hydrophilic bile acids such as UDCA are thought to promote bile acid efflux by stabilising the plasma membrane and increasing BSEP localisation in the membrane [95].

Table 11 hydrophobicity index of Different bile acids obtained from [93,94]. TUDCA = tauro-ursodeoxycholic acid, GUDCA = glyco-ursodeoxycholic acid, UDCA = Ursodeoxycholic acid, THDCA = tauro-hyodeoxycholic acid, GHDCA = glyco0-hyodeoxycholic acid, TCA = taurocholic acid, GCA = glyco-cholic acid, CA = cholic acid, TCDCA = tauro-chenodeoxycholic acid, GCDCA = glyco-chenodeoxycholic acid, CDCA = chenodeoxycholic acid, TDCA = taurodeoxycholic acid, GDCA = glyco-deoxycholic acid, DCA = deoxycholic acid, TLCA = tauro-lithocholic acid, GLCA = glyco-lithocholic acid.

Bile acid	hydrophobicity index
TUDCA	-0.47
GUDCA	-0.43
UDCA	-0.31
THDCA	-0.31
GHDCA	-0.26
TCA	0
GCA	0.07
CA	0.13
TCDCA	0.46
GCDCA	0.51
CDCA	0.59
TDCA	0.59
GDCA	0.65
DCA	0.72
TLCA	1
GLCA	1.05
LCA	NA
HDCA	NA

Increased hydrophobic bile acids in the serum, like CDCA and DCA, have been associated with colon cancer, gallstones and other gastrointestinal diseases [96]. An example is UDCA, which is currently available on the market to treat high cholesterol and gallstones, and to treat cholestatic liver disease [97]. However, bile acids can have further effect on hepatocytes by

interacting with several transcription factors, such as FXR, PXR, LXR, the vitamin D receptor and the G-coupled bile acid receptor [94,98]. As explained previously FXR plays a crucial role in maintaining bile acid homeostasis by influencing the biosynthesis of new bile acids as well as bile acid export by being a transcription factor for BSEP-encoding *ABCB11*. Parks et al. found in 1999 that certain bile salts can activate FXR more effectively than others with the potency order being: CDCA>DCA>LCA>CA. However, the influence of conjugated forms was not investigated [99]. A recent paper found that CDCA can directly bind to FXR and cause activation [38]. However, FXR is not specific to the liver and also occurs in other tissues. In the intestines, the activation of the FXR receptor has been found to increase the incidence of cancer [32]. The wide variety of bile acids and the constant recycling causes major problems in identifying bile acids that are important in toxicity and survival.

This chapter will investigate the effect of different treatments on the concentrations of individual bile acids inside 2D and 3D cultured hepatocytes to elucidate the toxicity effect of treatments and identify relevant bile acids responsible for DILI.

5.2 Results

Primary human hepatocytes were cultured in 2D and 3D conditions with different drugs as described in Section 5.1.4. After their respective incubation times of 6, 24 and 72 hrs, the cells and media were separately harvested and analysed by Leiden (see Figure 44). In a targeted panel of bile acids, several bile acids were detected to be either inside the cell and/or being excreted into the media. By analysing these separately, we were able to investigate the effect of drugs on bile acid pool compositions. The results were returned to us as internal standard ratios of deuterated bile acid compounds described in chapter (2.3.3). The internal standard ratios were also used to create the models in this chapter.

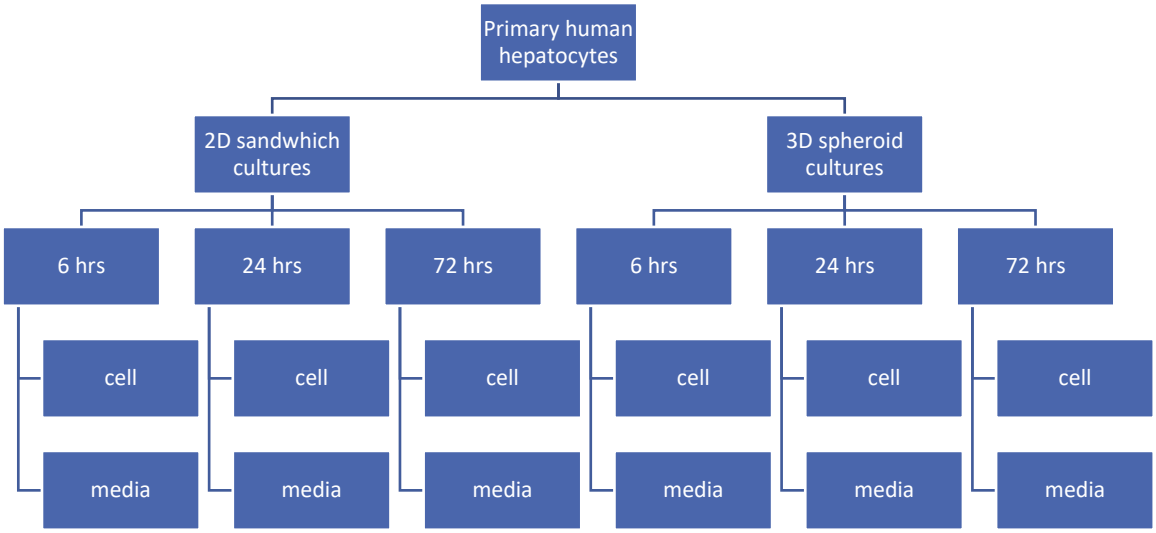

Figure 44. Schematic displaying the way by which samples were generated. This was done for each of the drugs investigated.

5.2.1 2D and 3D samples show apparent different metabolomic fingerprint in both media and cell lysate.

Following the removal of outliers, a score scatter plot was created for all samples (Figure 45). The data were fitted to a four component PCA-X model (R2= 0.946, Q2=0.859). While some outliers can still be observed, no explanation can be found to exclude the samples that are still outside the 95% hoteling's ellipse; they were therefore included in the analysis and regarded as a natural variance. Figure 45A shows that a clear distinction between media and cell samples can be observed on t[1]. A second separation can be observed between 2D media samples and 3D media samples over both the t[1] and t[2]. However, little distinction could

be made between 2D and 3D cell samples. The associated PCA-X loading plot (Figure 45B) shows a separation between the cell and media, and an overall higher association of media samples with bile acids. This shows that the bile acid concentration in the media is higher than in cells (Figure 45B).

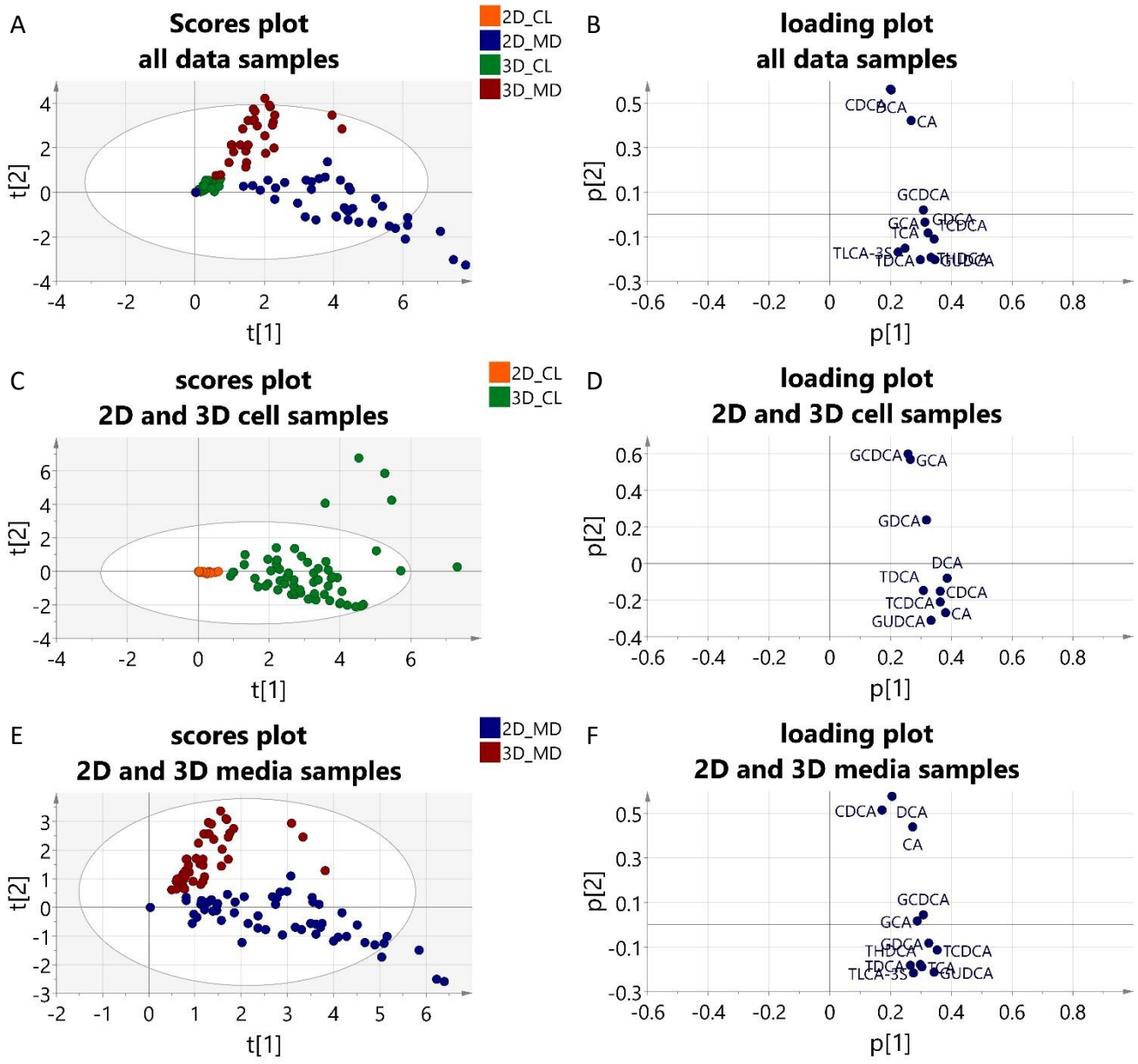

Figure 45. PCA-X scores and loading scatter plots of all samples (A and B), cell samples compared between 2D and 3D (C and D), and media samples compared between 2D and 3D (E and F). Samples were coloured according to primary observations. CL = cell samples, MD = media samples. Ellipse: Hotelling's T2 (95%).

To further analyse the differences between 2D and 3D samples, the data for the cell samples or the media samples were fitted to new models (Figure 45C and D). Individual four component PCA-X models for media (R2= 0.934, Q2 = 0.802) and cell (R2=0.946, Q2=0.742) samples were created. The individual score plot shows a clear distinction between 2D and 3D cell samples on t[1]. The loading plot (Figure 45D), indicates a higher concentration of bile acids in 3D cell samples compared to 2D samples. Overall there is a larger variation within the individual 3D samples compared to the 2D samples, expressed by the wider spread across the t[1]. Within the media samples, a clear separation can be observed between 2D and 3D on both the t[1] and t[2]. The associated loading plot (Figure 45F) indicates that 2D media samples contain more GCDCA, GCA, GDCA, TCDCA, GUDCA, TLCA-3S, THDCA, and TCA while 3D samples have a higher concentration of CDCA, DCA, and CA.

Univariate analysis of 2D and 3D samples

The univariate analysis of 2D and 3D samples (see Figure 46) reveals that the 2D media samples contain significantly higher concentrations of CA, GCA, CDCA, GCDCA, TCDCA, DCA, GDCA, TDCA, GUDCA, and THDCA. However, this conclusion cannot be drawn for TCA and TLCA-3S due to missing samples. This is different from the 3D samples where only CA, GCA, CDCA, GCDCA and DCA have significantly higher concentrations in the media than in cells. The difference between 2D and 3D samples could be due to the near normal expression of proteins in the 3D cultures. The uptake of bile acids and therefore the recycling could be simply be better. Another explanation could be that due to the increased Cyp450 enzyme expression levels in 3D cultures, cells are metabolizing the compound, causing different responses between 2D and 3D samples.

3D cells contain significantly higher concentrations of CA, but none of the other bile acids are significantly higher than in 2D cells. In 3D media, CA, CDCA and DCA are significantly higher than in 2D media. However, in 2D media GCA, TCA, GDCA, TCDCA, GDCA, TDCA, GUDCA, and THDCA are significantly higher in concentration. This is interesting as CA, CDCA are primary bile acids while the others are secondary bile acids. As the formation of secondary bile acids is generally thought to involve bile acid conversions by the gut micro-organisms, and this study was performed under sterile conditions, the results could point to the production of secondary bile acids by 3D cells. Moreover, 3D cells are able to produce primary bile acids more effectively than their 2D sandwich cultured counterpart.

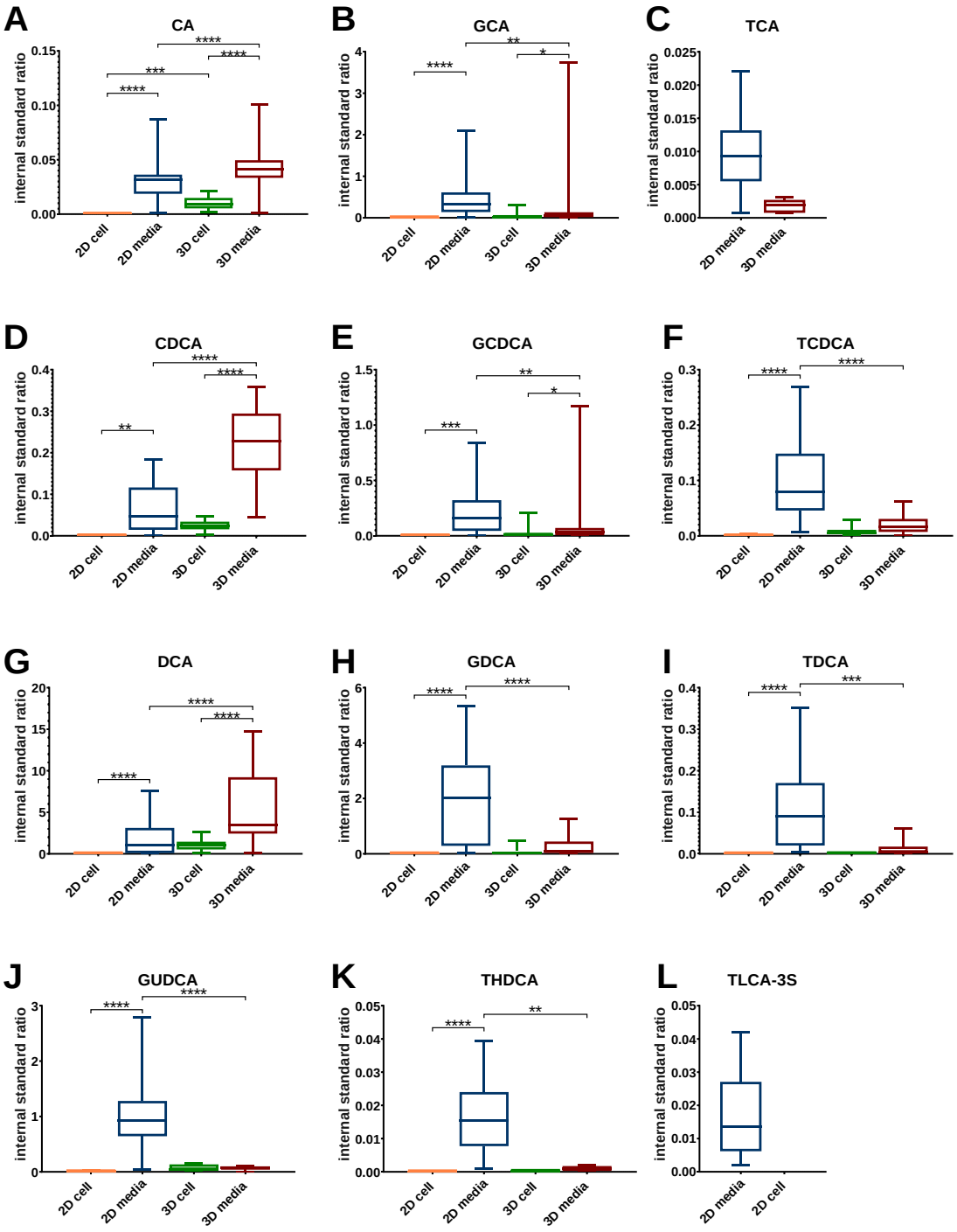

Figure 46. Box and whisker plot (min to max) of univariate analyses of 2D cell and media samples as well as 3D cell and media samples. (N=50) * indicate significant differences as stated in chapter 2.4 by two-way ANOVA

5.2.2 The effect of treatment and time on bile acid compositions within 2D cells and media

To evaluate the effect of treatment and time on samples, individual PCA-X models were created (see Table 3 for R2 and Q2 values). Figure 47 displays the individual score plots of the 2D samples for either cell or media samples with their respective loading plots.

2D cells

In Figure 47A the individually calculate scores for the 2D cell samples are displayed. To indicate the location of the control samples (DMSO treated), a grey ellipse was drawn around them. While no clusters other than the grey-circled cluster can be observed, several samples are located outside the cluster. These samples consist of cells treated for 6 hrs with estradiol, which show a higher concentration for GCDCA. For a single sample treated with estradiol for 24 hrs, the loading plot indicates higher concentrations of CDCA, GDCA, TCDCA and CA. For a single sample treated for 72 hrs with bosentan, the loading plot indicates higher concentrations of TCDCA, GCDCA and CDCA. Finally, the cells treated with cycloheximide for 72 hrs are associated with higher concentrations of GUDCA, THDCA.

The univariate analysis of the 2D cell samples (see Figure 48) shows that different treatments have different effects on bile acid pools within the cells of 2D cultured PHH. Cyclo-hexamide only showed a significant decrease in GCDCA at 72 hrs. This could be due to the death of cells and the subsequent release of the bile acids into the media causing the actual cell concentration to drop. Estradiol showed a significant decrease at 6 hrs for TDCA compared to DMSO control. At 24 hrs estradiol showed no significant differences to DMSO control, nonetheless at 72 hrs a significant decrease in GCA and GCDCA can be observed. However, after 72 hrs of treatment these cells had lost viability (see chapter 4, Figure 35). Bosentan is a strong direct inhibitor of BSEP and it would be expected that the concentrations of all bile acids in the cytoplasm will be increased. But this is not was can be observed in the data. Bosentan only significantly increased TDCA after 6 hrs of treatment. After 24 hrs no significant changes were detected, whereas at 72 hrs a significant decrease in GCA and GCDCA was observed. Clobetasol Propionate is a BSEP inhibitor, but one that does not cause liver injury. A significant increase was obtained at 6 hrs for TCDCA and TDCA. At 24 hrs TDCA was significantly decreased compared to DMSO and at 72 hrs GCDCA was significantly decreased.

Clobetasol propionate was also compared to bosentan to test if any differences in bile acid specificity can be found, possibly explaining why bosentan is toxic while clobetasol propionate is not. What could be observed is a significant difference at 6 hrs for TCDCA between bosentan and clobetasol propionate. However, this observation was not repeated in any other time point or for any other bile acid.

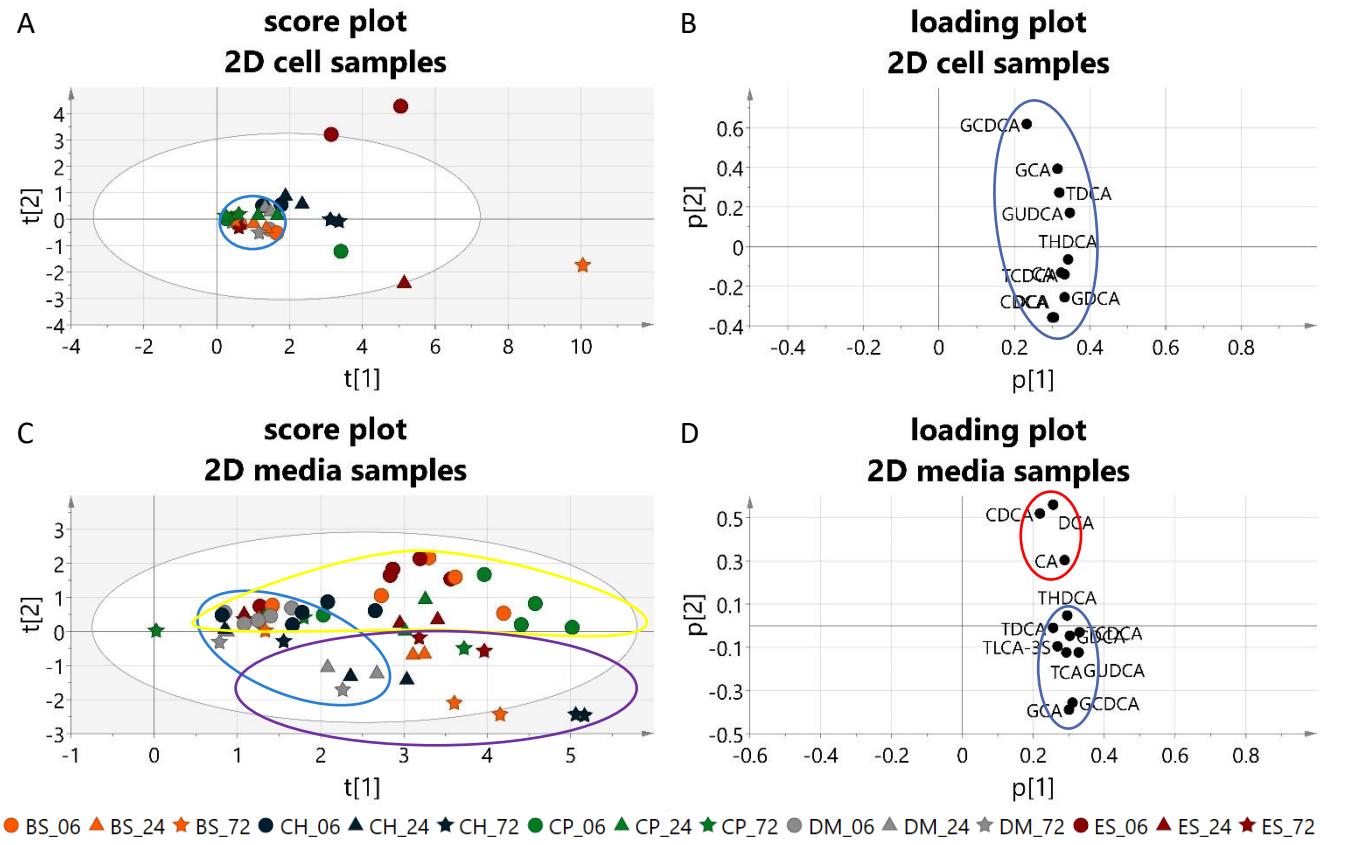

Figure 47. PCA-X scores and loading plots for 2D cell samples (A and B), and media samples (C and D). Treatments are displayed as two letter indicating abbreviations followed by the hours of incubation.: BS= bosentan, CH = cyclo-hexamide, CP = clobetasol propionate, DM = DMSO, ES = estradiol. Times: 06 = 6hrs, 24 = 24hrs, 72 = 72hrs. Grey circle indicates the location of the DMSO samples, yellow circle = location of 6 hrs data, while the purple circle indicates the location of 24 hrs and 72 hrs. red circle identify the primary bile acids, and blue the conjugated forms and secondary bile acids. Ellipse: Hotelling's T2 (95%).

2D media

In the media samples, a more apparent separation between the samples was observed, with the grey circle indicating the location of DMSO vehicle control samples (Figure 47C). Treatment samples show, in general, a higher expression of all the bile acids detected in the panel, compared to DMSO. While a distinct separation was not observed, a shift on the t[2] was obtained as time is increased (yellow circle = 6 hrs, purple circle = 24 and 72 hrs). The associated loading plot (Figure 47C) indicates that the concentrations of THDCA, TDCA, GDCA, TCDCA, GUDCA, TCA, GCDCA, GCA increase over time.

Interestingly this shows that 6 hrs samples have a higher concentration of CDCA, DCA, and CA while 24 hrs and 72 hrs contain more tauro- and glyco-conjugated forms: THDCA, TDCA, GDCA, TCDCA, GUDCA, TCA, GCDCA, GCA.

The univariate analysis of the 2D media samples indicate that the bile acid pool in the media is also affected by the drug.

Cycloheximide showed no significant differences in bile acid concentration after 6 or 24 hrs of treatment, while at 72 hrs a significant increase in TDCA, THDCA and TLCA-3S was observed compared to DMSO control. Estradiol showed significant increases at 6 hrs for CDCA. At 24 hrs CDCA and TDCA were both significantly increased, whereas at 72 hrs these changes were no longer observed. Bosentan caused a significant increase in CDCA at 6 hrs and 24 hrs, whereas clobetasol propionate was not significantly different from DMSO control at any time point for any bile acid. No significant changes were detected between clobetasol propionate and bosentan.

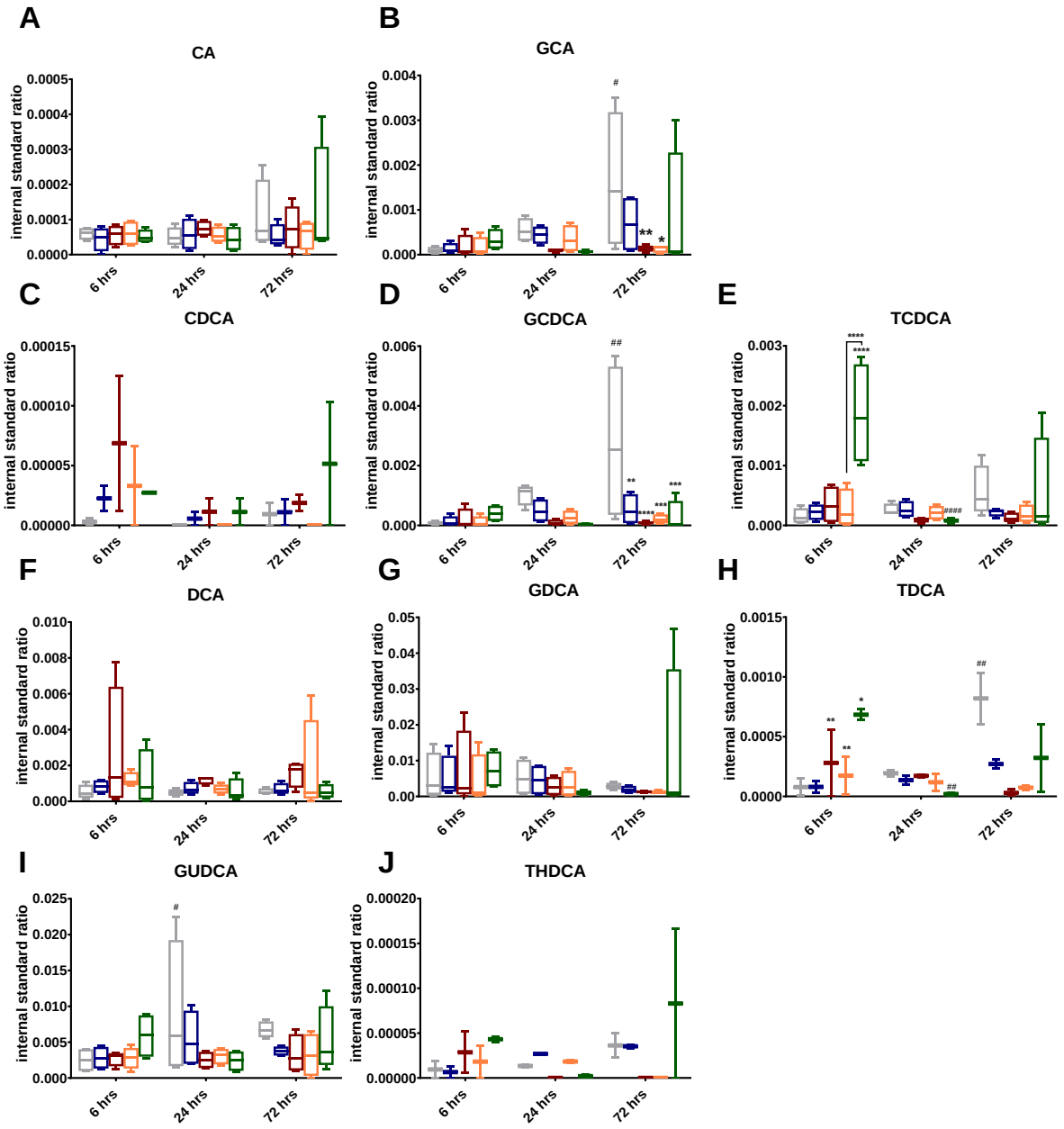

Figure 48. Univariate analyses of bile acids in 2D cell samples displayed as box and whisker plot (min+ max) * indicates comparison to DMSO control or otherwise indicated with a line, # indicates a significant difference from the samples previous time point. (N=4) * and # indicate significant differences as stated in chapter 2.4 by two-way ANOVA. (DMSO = grey, cycloheximide = blue, estradiol = red, bosentan = orange, clobestasol propionate = green)

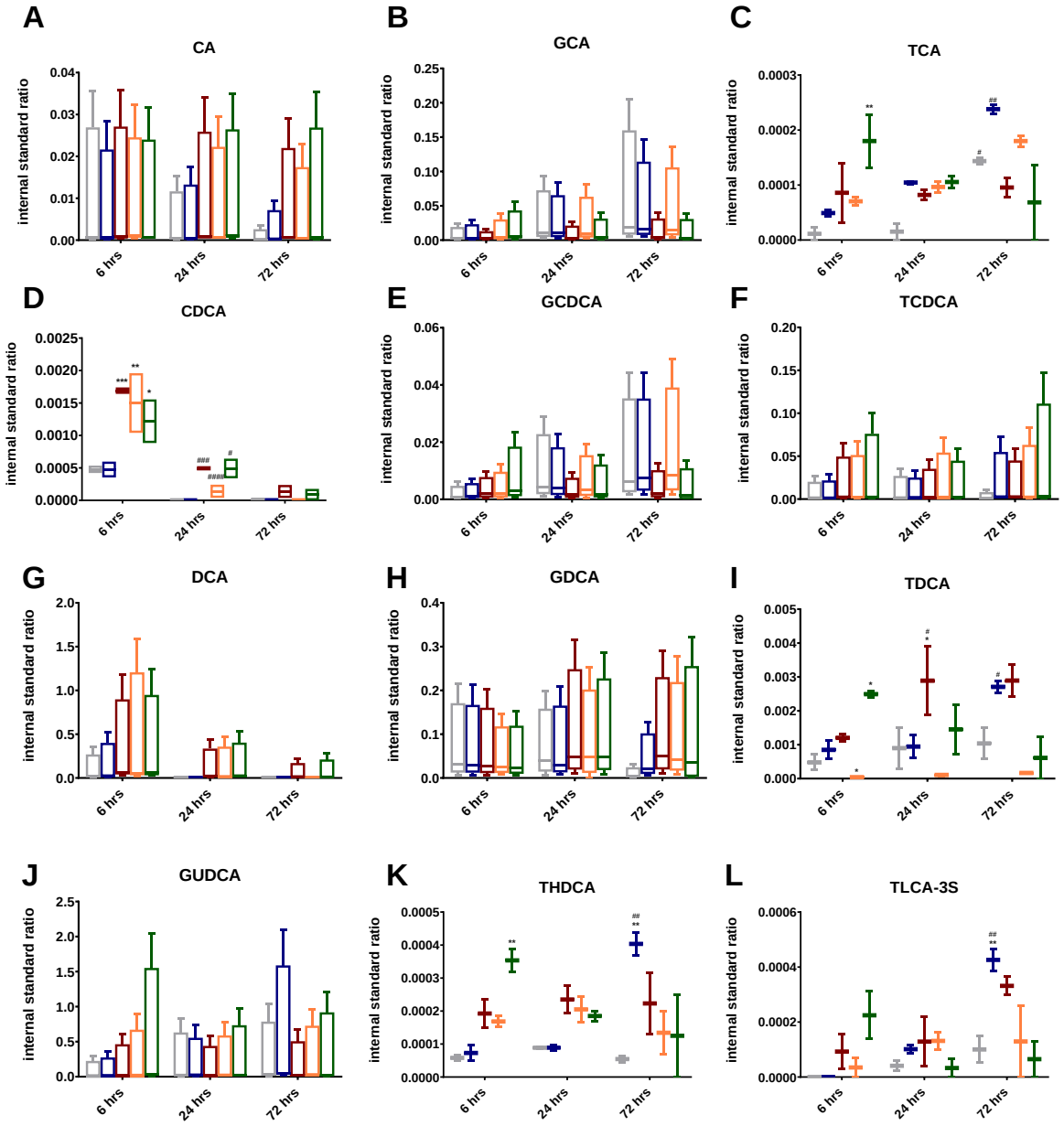

Figure 49 Univariate analyses of bile acids in 2D media samples. displayed as box and whisker plot (min+ max) * indicates comparison to DMSO control or otherwise indicated with a line, # indicates a significant difference from the samples previous time point. (N=4) * and # indicate significant differences as stated in chapter 2.4 by two-way ANOVA. (DMSO = grey, cycloheximide = blue, estradiol = red, bosentan = orange, clobestasol propionate = green)

5.2.3 The effect of treatment and time on bile acid within 3D cell and media

To evaluate the effect of treatment and time on 3D cell and media samples, individual PCA-X models were created (see Table 11 for R2 and Q2 values). Figure 50 displays the individual score plots of the 3D samples for either cell or media samples with their respective loadings.

3D cell

The effect of treatment and time on 3D samples was more defined than the effect on 2D samples. The PCA-X model for 3D cell values indicates a time-dependent shift of samples over the t[1]; 6 hrs samples are indicated by a yellow ellipse while later samples are indicated with a purple circle. The purple circle indicates that 24 and 72 hrs samples have a higher concentration of all the detected bile acids. In the associated loading plot (Figure 50B), Figure 50B, a clear grouping or GCDCA and GCA can be seen, indicating a strong positive correlation between the two. These two variables are associated with the samples in the upper right corner of the score plot. In particular: 24 and 72 hrs for bosentan, and 72 hrs for DMSO suggesting that these samples have higher concentrations of GCDCA and GCA. The grey circle indicates the location of the control samples (DMSO), with a very tight clustering of the 6 and 24 hrs samples and a shift to the right over the t[1] for 72 hrs samples. These data suggest that at 72hrs the cells contain higher concentrations of GCDCA and GCA.

The univariate analyses for 3D cell samples (see Figure 51) treated with cyclo-hexamide showed no significant changes for the first 6 hrs. However, after 24 hrs a significant increase was observed for CDCA and DCA. After 72 hrs a significant increase was observed for CA, CDCA, TCDCA, DCA and TDCA, whereas a significant decrease was seen for GCA. An increase in bile acids at 72 hrs for the cell samples might be interesting as the cells were no longer viable at 72 hrs. Possibly, a few surviving cells must have had very high concentrations of the bile acids. Estrogen significantly increased concentrations of CDCA and DCA after 6 hrs of treatment in 3D cultured cells. After 24 hrs of incubation with estrogen, CA, CDCA and DCA were significantly increased but at 72 hrs only DCA and TCDCA were significantly increased. Bosentan caused CDCA and DCA to accumulate within the cell compared to DMSO at 6hrs. After 24 hrs the effect was lost for CDCA but DCA remained significantly elevated compared to DMSO. At 72 hrs, however, bile acid concentrations were not significantly different from the DMSO control. Clobetasol propionate caused DCA to accumulate within the 3D cultured cells after 6 hrs and 24 hrs of treatment. After 72 hrs DCA was no longer significantly different

but TCDCA had accumulated in the cell. Most notable is the comparison between bosentan and clobetasol propionate after 72 hrs. The GCDCA concentration was significantly higher in cells treated with bosentan but TCDCA was significantly higher in cells treated with clobetasol propionate. It is interesting to note that both GCDCA and TCDCA are conjugated forms of CDCA that are known to activate FXR and enhance BSEP expression.

3D media

In 3D media samples (see Figure 50C), a time-dependent shift can be observed over the t[1], the associated loading plot suggest a general increase of bile acid concentrations. Interestingly the two bosentan samples for 72hrs are the furthest outliers and associate most with GCDCA and GCA.

In the univariate analysis of the 3D media samples (see Figure 52a) cycloheximide only caused an accumulation of DCA at 24 hrs after which levels fell back to normal levels compared to the DMSO control. Estrogen significantly decreased GCA and a significantly increased TCDCA in the media collected after 72 hrs of treatment. Bosentan significantly increased DCA at 6 hrs and 24 hrs and CDCA at 72 hrs when compared with the DMSO control. The exposure to clobetasol propionate significantly decreased the accumulation of GCA, and increased the accumulation of TCDCA at 72 hrs. The comparison of the data for bosentan and clobetasol propionate showed that GCDA was significantly increased in bosentan treated samples whereas TCDCA was significantly increased in the clobetasol propionate treated samples. This is the same change as seen for the cell samples, pointing to increased production and the export of these bile acids from the cells.

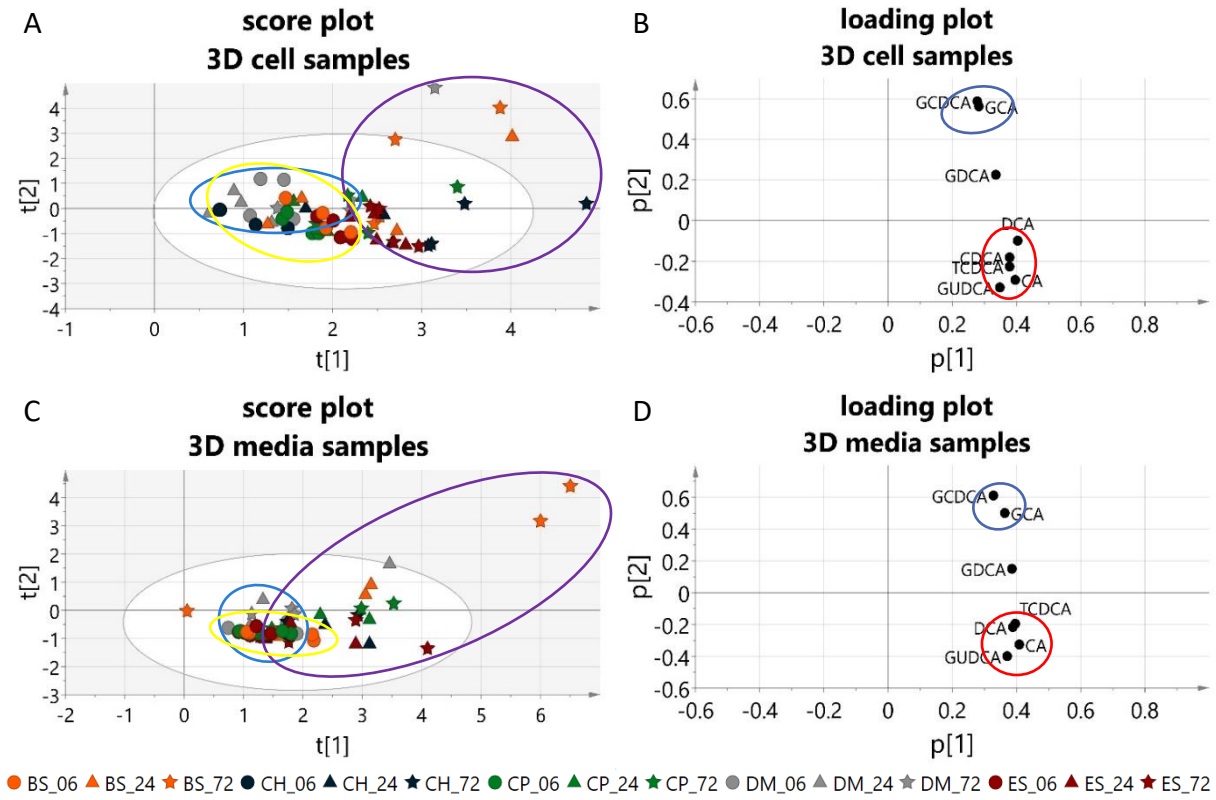

Figure 50 PCA-X score and loading plots for 3D cell samples (A and B), and media samples (C and D). Treatments are displayed by two letter abbreviations followed by the hours of incubation.: BS= bosentan, CH = cyclo-hexamide, CP = clobestasol propionate, DM = DMSO, ES = estradiol. Times: 06 = 6hrs, 24 = 24hrs, 72 = 72hrs. Grey circle indicates the location of the DMSO samples, yellow circle = location of 6 hrs data, while the purple circle indicates the location of 24 hrs and 72 hrs. red circle identify the primary bas, and blue the conjugated forms and secondary bas. Ellipse: Hotelling's T2 (95%).

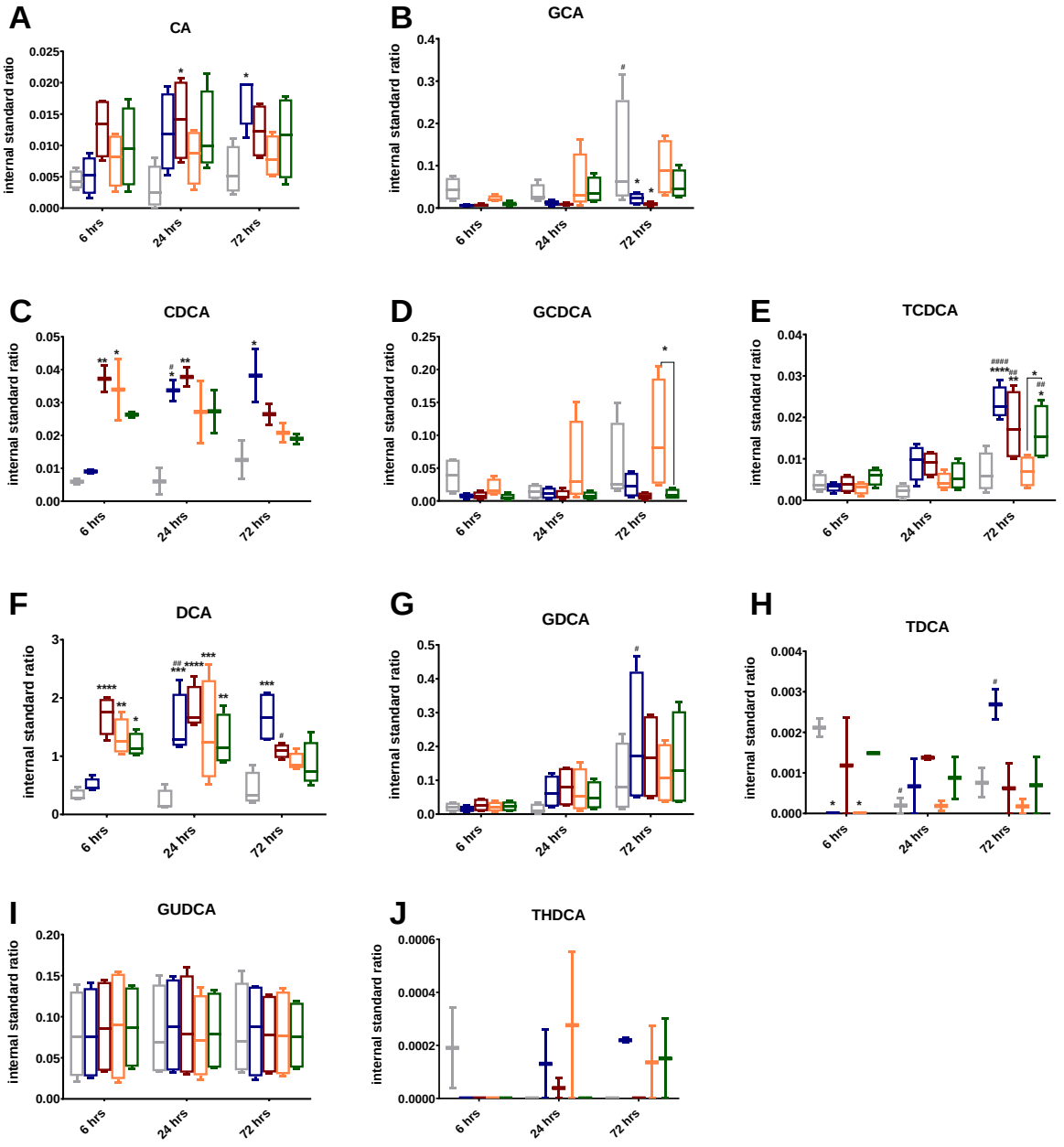

Figure 51 Univariate analyses of bile acids in 3D cell samples displayed as box and whisker plot (min+ max) * indicates comparison to DMSO control or otherwise indicated with a line, # indicates a significant difference from the samples previous time point. (N=4) * and # indicate significant differences as stated in chapter 2.4 by two-way ANOVA. (DMSO = grey, cycloheximide = blue, estradiol = red, bosentan = orange, clobestasol propionate = green)

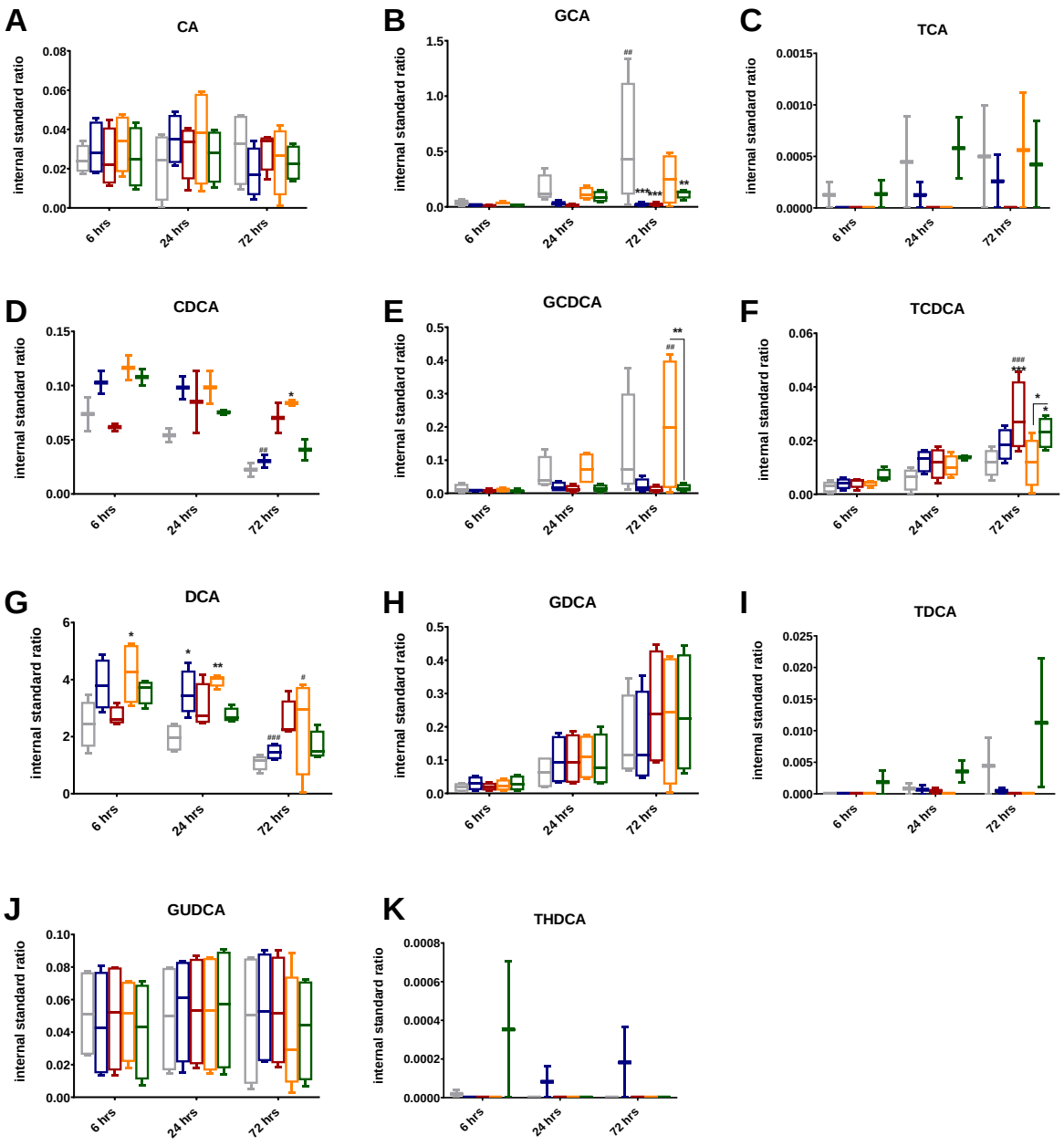

Figure 52 Univariate analyses of bile acids in 3D media samples displayed as box and whisker plot (min+ max). * indicates comparison to DMSO control or otherwise indicated with a line, # indicates a significant difference from the samples previous time point. (N=4) * and # indicate significant differences as stated in chapter 2.4 by two-way ANOVA. (DMSO = grey, cycloheximide = blue, estradiol = red, bosentan = orange, clobestasol propionate = green)

5.2.4 Clustering of bile acids in 2D and 3D cultured samples

The loading plot of the 2D media samples in Figure 47D shows two distinct clusters of variables; this clustering is not, however, observed for the 2D cell samples. It is interesting to note a separation between unconjugated (red circle) and conjugated (blue circle) bile acids was observed in 2D media. As this separation was seen in the same direction as the time-dependent shift, it is very likely that the concentration of unconjugated bile acids lowers over time due to these bile acids being conjugated within the cell, thus increasing the concentration of secondary bile acids. In the 2D cell samples, no separate clusters of bile acids were observed, which can indicate that conjugated forms of bile acids are preferentially transported to the media, or that 2D cells produce CDCA, DCA, and CA. Therefore, even though the conjugated bile acid concentration increases, the concentration of CDCA, DCA and CA is not decreasing over time.

In the 3D samples, two distinct clusters can be observed within the loading plots of either cell and media. Within the cell samples, the first cluster consists of GCDCA and GCA (blue circle) while the second cluster consists of DCA, CDCA, TCDCA, GUDCA and CA (red circle). While a general shift across the t[1] to higher bile acids concentrations can be observed over time, the red cluster is more associated with 24 and 72hrs cycloheximide, 24 and 72 hrs estradiol, 24 and 72 hrs bosentan and 72 hrs clobetasol propionate. The blue cluster is associated with higher concentrations in the 24 and 72 hrs Bosentan as well as a solitary 72 hrs DMSO samples, rather than with a time-dependent element.

In the media samples, a clear distinction between two clusters of variables can be observed, with the first group consisting of GCDCA and GCA (indicated by the blue circle) and the second consisting of TCDCA, CA, DCA, GUDCA) (indicated by the red circle). However as there is no clear separation in the 3D score plot, drawing a conclusion to the meaning of the variable separation is impossible.

5.2.5 Early indications of toxicity

To identify early indications of toxicity during different treatments, new PCS-X models were created for cell and media samples from the 2D and 3D cell cultures (see Table 12 for several components, R2 and Q2 values). In this thesis only the 6hrs data is displayed as cells were assumed to be 100% alive at that time; the viability of each sample was measured at 72hrs.

In the 2D cell samples (Figure 53A) a shift in the estradiol samples towards TDCA, GUDCA, GCDCA and GCA was observed (Figure 53B). None of the other samples shows any change at 6hrs even though bosentan and clobetasol propionate had a significant effect on cell survival compared to DMSO samples at 72 hrs. Normalised ATP expression was only at 26% and 56% respectively for bosentan and clobetasol propionate when compared to DMSO samples, while cycloheximide showed no survival at 72hrs (0%). In the media data (Figure 53C), there is a diagonal shift over t[1] and t[2] with DMSO samples mostly having higher concentrations of CA and GDCA (Figure 53D). Clobetasol propionate, however, had higher concentrations TCA, TLCA-3S, TDCA, GUDCA, THDCA, and TCDCA.

In 3D samples, only cycloheximide treated samples showed signs of toxicity, showing 0% normalised ATP concentration at 72hrs when compared to DMSO. A clear separation between healthy samples and cyclo-hexamide treated samples can be observed on 6hrs 3D cell samples (Figure 53E). The corresponding loading plot indicates that healthy samples have higher expression of all bile acids. 3D media samples did not show any kind of clustering except within two analysis batches (Figure 53G and H).

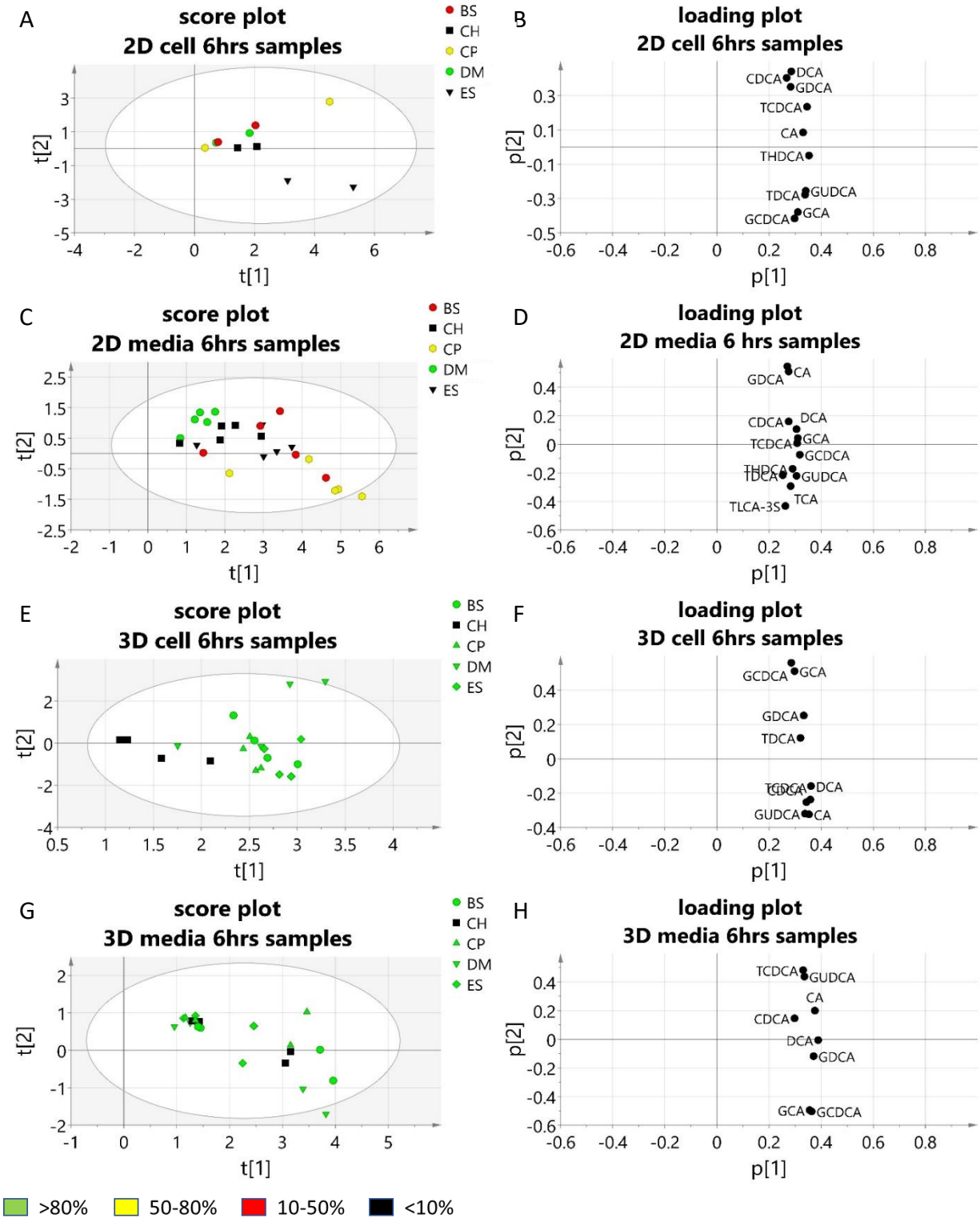

Figure 53. PCA-X score and loading plots for the 6hrs data for 2D cell (A and B) and media (C and D) and 3D cell (E and F), and media samples (G and H). Treatments are displayed as two letters abbreviations followed by hours of incubation: BS= bosentan, CH = cyclo-hexamide, CP = clobetasol propionate, DM = DMSO, ES = estradiol. Grey circle indicates the location of the DMSO samples. Colours indicate viability of the cell samples at 72 hrs (green = >80%, red = 20-50%, black = 0-20%). Red circle identifies the primary bile acids, and blue the conjugated forms and secondary bile acids. Ellipse: Hotelling's T2 (95%).

Table 12 showing the predicted values of components R2 and Q2 in the multivariate analysis.

	Number of components	R2	Q2
All data	4	0.946	0.859
2D vs 3D cell	4	0.946	0.742
2D vs 3D media	4	0.934	0.802
2D cell	4	0.975	0.851
2D media	4	0.949	0.822
3D cell	4	0.969	0.838
3D media	3	0.932	0.765
2D cell 6hrs	2	0.935	0.772
2D media 6hrs	6	0.987	0.801
3D cell 6hrs	4	0.980	0.851
3D media 6hrs	2	0.899	0.701

5.3 Discussion of the results.

Overall very few papers have been published on the metabolism of bile acids in human cell lines, whereas there is a lot of information regarding bile acid pool changes in mice and rats. However, regarding bile salt metabolism, these mammals have three primary bile acids (CA, CDCA, UDCA, and the mouse rodent specific αMCA and βMCA) compared to two in humans (CA and CDCA), and they are therefore very different from humans [100]. They also have several bile salts that are absent in the human (αMCA and βMCA and their conjugated forms) and compared to humans a much larger portion of bile acids originate from the acidic pathway (5% compared to 25%). Furthermore, rats do not have a gallbladder while humans and mice do [101]. Finally rodents have a much lower hydrophobicity index indicating that bile acids are less toxic to them [93]. We therefore need to be especially careful when extrapolating data regarding bile acid formation and the influence of drugs from rodents to human.

My study shows that PHH are a good alternative to rodent studies in order to investigate the changes that occur in bile acid pool and accumulation, they were easy to treat and investigate. There are, however, a few downsides to PHH: due to the lack of gut microbiota there are very few secondary bile acids present in the samples. The secondary bile acids that were found in this study where completely unexpected and are currently under investigation.

The definition of the primary bile acids was first published in 1961 by Bergstrom et al. Bergstrom won the Nobel prize in physiology or medicine in 1982 for his discoveries on prostaglandins. While his experimental set-up is no doubt correct [original experimental paper is not accessible], time has moved on and with the newer equipment we are now able to pick up minute differences. Sama I. Sayin et al. [102] looked at germ free and conventual raised mice, and were able to detect several more bile acid at this point in time. This supports the idea that techniques have become more sensitive. However it is specifically stated that TUDCA is considered a secondary bile acid in humans while in mice TUDCA is recognized as a primary bile acid [26].

My in-depth literature research suggests that no experiments with modern technology has been performed to confirm that humans indeed only synthesize two primary bile acids.

Sharanek et al. 2015 [103] found that FCS and BCS in cell media contains bile acids. However, bile acids in the FCS used in our experiment was tested to be below detection levels.

While we are still investigating the origin of secondary bile acids in this study the presence of DCA in the samples can be explained in several ways:

1. DCA is a primary bile acid and the cells are therefore able to produce DCA. In addition, they are able to produce CA and CDCA. An argument for this is that in 3D cells, where P450 enzymes are considered to be expressed normally, DCA is always clustered together with CA and CDCA.
2. DCA is an artefact and the cells are able to produce this bile acid due to a chemical in the media culture. Within humans this reaction would not be feasible or occurs in very small amounts
3. DCA was present in the media and accumulated in the cells to such an extent that detection was possible. However, none could be found in the media itself.

At this point we cannot conclusively say where DCA originates from, but its presence was an unexpected blessing. DCA is one of the most toxic bile acid in the human body (according to the hydrophobicity index), accordingly it is vital to investigate the effect test compounds have on DCA concentration inside the cell in regards to toxicity studies [104].

Luo et al 2018. [104] assesses the use of bile acids as biomarkers for liver disease. These authors found that in healthy patients, DCA accounted for 12% of the total bile acids serum pool, but in patients with liver disease DCA only accounted for 0.3%. They further observed that the entire bile acid pool shifted within patients with hepatic injury, leading to an increase in TCA, TCDCA, GCA, and a decrease in GDCA, DCA, TDCA, CA, and CDCA compared to healthy individuals. These findings indicate that when looking at bile acid-induced injury we need to look at the bile acid pool composition rather than just one bile acid or total amount of bile acid.

DCA is also able to influence intracellular signalling through membrane perturbations [105]. DCA causes an increase of cholesterol at the plasma membrane which in turn increases BSEPs ability to transport bile acids [106]. Additionally, Jean-Louis et al 2006 found that depending on their physical properties, bile acids are able to influence the membrane activity differently

such as causing membrane capping, disrupting membrane structure (specifically DCA), modulating sphingomyelin and ceramide levels (see chapter 6 for further information), internalization of caveolin-1, activation of tyrosine kinases [105]. The changes in DCA were comparable with changes that occur by apoptosis-inducing agents, they further found that reducing the cholesterol accumulation in the membrane caused by DCA reverted the changes at the membrane back to normal [105]. DCA is further able to activate the EGFR – MAPK - ERK1/2 pathway via non-canonical activation in colon cancer cells after it was shown that DCA is able to activate the same pathway in rat hepatocytes [107]. Overactivation of this pathway leads to uncontrolled proliferation and cell survival in colon cancer cells. This is important because in this chapter we have shown in the univariate analysis of 3D cells that DCA was significantly upregulated in cells treated with estradiol, bosentan and clobetasol propionate at 6 hrs, and cycloheximide, estradiol bosentan, and clobetasol propionate at 24 hrs. However, at 72 hrs DCA was only upregulated in cyclohexamide treated 3D cells. This was the only sample that showed significant toxicity in the 3D samples.

The gut-microbiome and liver axis for bile acids is very important, the gut microbiome has been found to influence liver cancer via natural killer T cells [108]. Primary bile acids increased CXCL16 expression responsible for NKT cell accumulation, whereas secondary bile acids reduced CXCL16 expression. A treatment with vancomycin to remove bacteria responsible for secondary bile acids transformations was enough to increase NKT cell accumulation and decrease liver tumours [108].

Bile fingerprinting via UPLS-MS has shown that TCA secretion was significantly increased in bile samples obtained after liver transplants and that this might be linked to regeneration [109]. TCA was significantly higher in 2D media treated with clobetasol propionate, but not in any of the other samples. This might explain why clobetasol was less toxic in our experiment as well as why it does not cause toxicity in humans.

However, future work should include different cell donors and more samples. In this way, the clustering in the multi variate analysis will be more complete and indicative for toxicity. However, this chapter demonstrates the achievability of MS/MS analyses to explain iDILI and the significant differences between 2D and 3D cultured PHH.

6. Signalling and peroxidised lipid profiling in 2D and 3D cultured primary human hepatocytes.

6.1 The different lipids and the metabolic pathways in this study.

Our understanding of the membrane has evolved from a simple lipid bilayer with embedded proteins to a complex dynamic and heterogenous patchwork of microdomains that contain ion channels, transporters and other proteins, and cholesterol- and sphingolipid-rich lipid rafts. In multicellular organisms, lipids have been recognised as signalling molecules since the early 1930s, when ”slow-reacting substance of anaphylaxis” (SRS-A) was identified. Around the same time, the vasodilating effect of prostaglandins was described [110]. Since then, more and more lipids were identified that are involved in signalling and deemed responsible for the communication between the cells either by cell-cell contact or through soluble factors. The regulation of these lipids is critical and tightly regulated. While lipids are typically thought to be building blocks of membranes and stores of metabolic energy [111], the lipids in this chapter will be described as signalling mediators in cellular responses to drugs.

The metabolic system of a multicellular organism is very complex as the maintenance of homeostasis is crucial. A vast range of metabolic pathways is responsible for carbohydrate and energy metabolism, and the biosynthesis of lipids, lipoproteins, amino acid, nucleic acid and proteins [112]. The Kyoto Encyclopedia of Genes and Genomes (KEGG) provides a large database on investigations of metabolic pathways (https://www.genome.jp/kegg/pathway.html)[113–115] . The next paragraphs describe the pathways where the lipids are located that are found in this study.

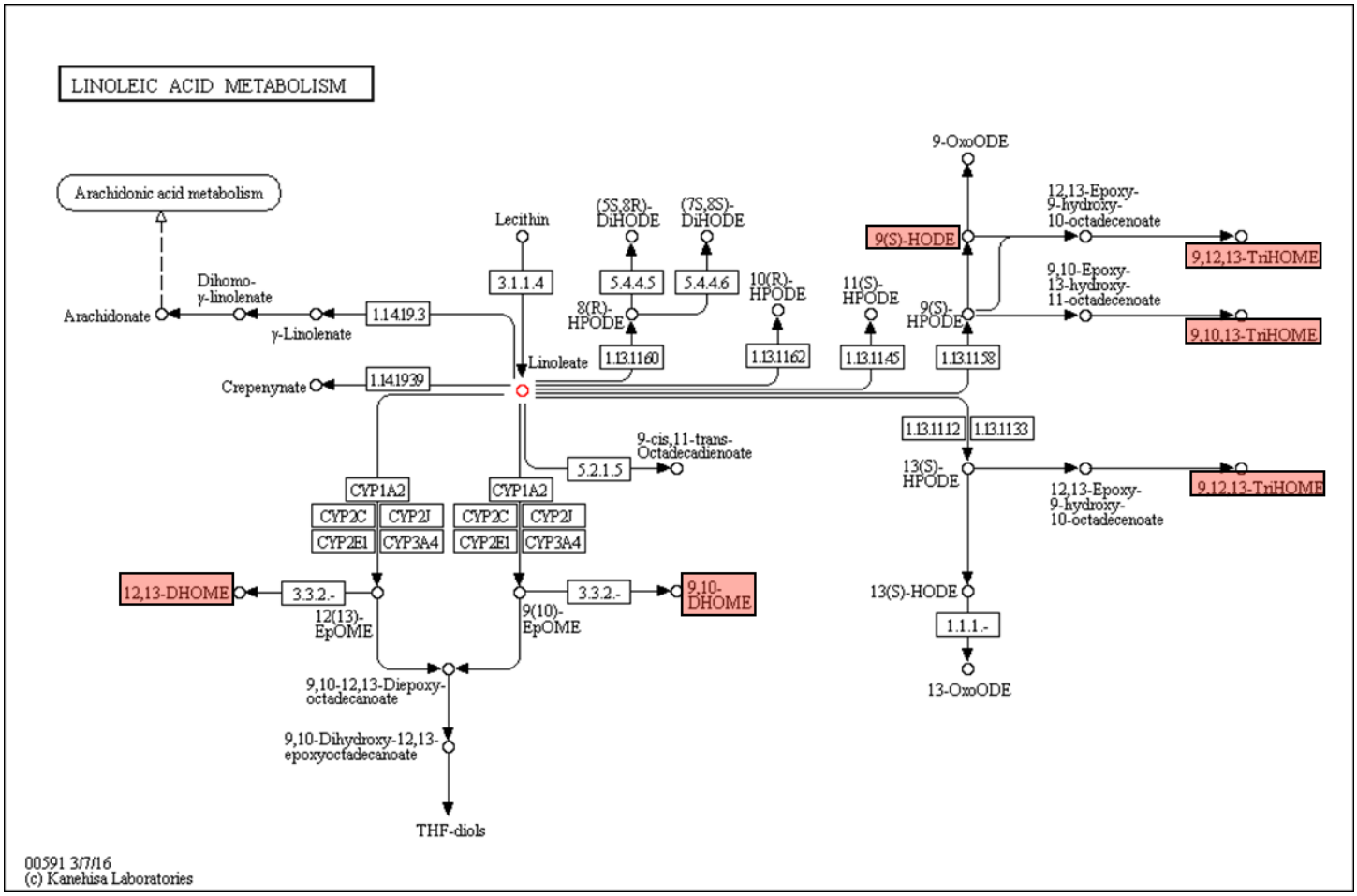

Figure 54. KEGG pathway of linoleic acid metabolism. Displayed in red are metabolites detected and described in this chapter. White rectangles depict genes products, mostly proteins but also RNA. Rounded rectangles depict another map. Circles depict chemical compound, DNA and other molecules. Black arrows: molecular interaction, dashed arrow: indirect or state change. Copied from [113–115]

6.1.1 Metabolites in linoleic acid metabolism

Linoleic acid is an essential omega-6 fatty acid that is obtained from our diet and is vital for maintenance of cell integrity [116]. It is situated in the middle of the metabolic KEGG pathway in Figure 54 (red dot). There are three main pathways by which linoleic acid can be metabolised. In the first pathway, linoleic acid is metabolised to arachidonic acid (AA) via y-linolenate by a desaturase enzyme (top left of Figure 54). This pathway will mostly promote an inflammatory response downstream from AA. The second pathway uses Cyp450 enzymes to transform linoleic acid into 12,13-DHOME; 9,10-DHOME and THF-diols (bottom left of Figure 54). In the third pathway, auto-oxidation converts linoleic acid into 9-sOxoODE; 9,12,13-TriHOME; 9,10,13-TriHOME; 9,12,13-TriHOME and 13-OxoODE. All the products from linoleic acid are known to have effects on living organisms or tissues) and are essential in physiological and pathological circumstances. The metabolites indicated in red in Figure 54 were detected in this chapter. They have the following bioactivities:

- (+/-)-20-hydroxy-4Z,7Z,10Z,13Z,16Z,18E-docosahexaenoic acid ((+/-) 20-HDoHE) is an auto-oxidation product of docosahexaenoic acid (DHA) *in vitro* and is a potential marker for oxidative stress in the brain and retina where DHA is an abundant polyunsaturated fatty acid [117].
- (±)12,13-dihydroxy-9Z-octadecenoic acid (12,13-DiHOME) is the diol form of (±)12(13)-EpOME (isoleukotoxin) and is formed by P450 enzymes from linoleic acid. It is known to increase after spinal cord injury and burn injuries in rats. It was found to increase fatty acid uptake in brown adipose tissue and was elevated in concentration in mice with hepatocellular carcinoma [118,119].
- (±)-9-hydroxy-10E,12Z-octadecadienoic acid (9-HODE) is one of two racemic monohydroxy fatty acids resulting from the non-enzymatic oxidation of linoleic acid. Oxidised LDL contains significant amounts of esterified 9-HODE [120].
- (±)9,10-dihydroxy-12Z-octadecenoic acid (9,10-DiHOME) is a degradation product of leukotoxin, the toxicity of which is associated with mitochondrial dysfunction and apoptosis. In renal proximal tubular cells, 9, 10-DiHOME has been directly implicated as cytotoxic agent responsible for cell death [121–123].
- 9S,10S,13S-trihydroxy-11E-octadecenoic acid (9,10,13-TriHOME) is an oxylipin derived from linoleic acid and may be involved in prostaglandin synthesis.

6.1.2 Metabolites in arachidonic acid metabolism

AA is an omega-6-fatty acid that is obtained via another metabolic pathway from linoleic acid, as described in Chapter 6.1.1. AA is present in the membranes of most cells and is most abundant in the brain, muscles and liver, where it plays an important role as a lipid secondary messenger. It is often considered to be a key player in mediating inflammatory signals. Its metabolism is displayed in Figure 55. In the test panel used for these experiments, we were only able to find three of the metabolites in the arachidonic pathway. However, the evidence for AA involvement in a pro-inflammatory pathway is ambiguous as higher levels of AA may reduce systemic inflammation by reducing pro-inflammatory IL-6 and IL-1 levels and increasing anti-inflammatory tumour necrosis factor-beta (TNFb). In this panel, we were able to detect the following metabolites:

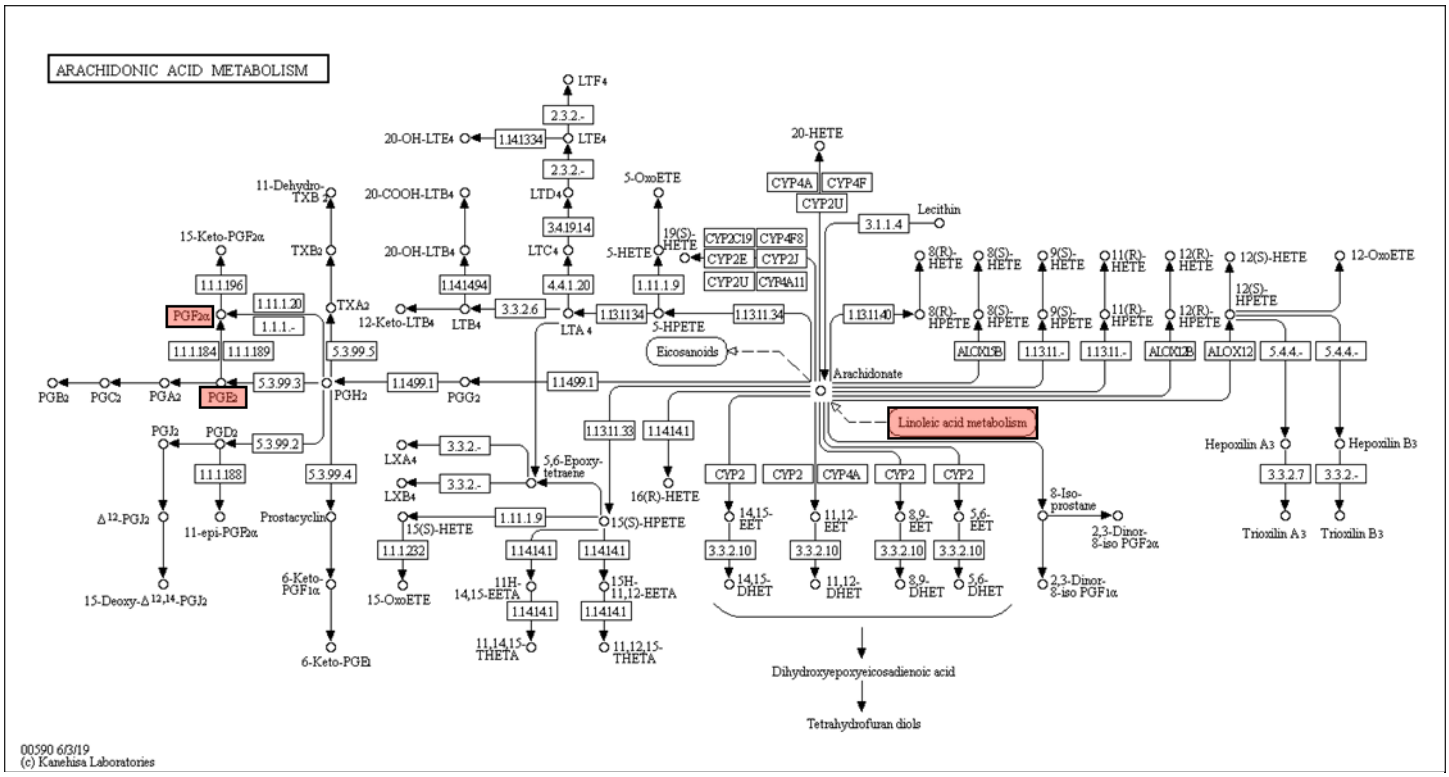

Figure 55. KEGG pathway of arachidonic acid metabolism. Displayed in red are metabolites detected and described in this chapter. White rectangles depict genes products, mostly proteins but also RNA. Rounded rectangle depicts another map. Circles depict chemical compound, DNA and other molecules. Black arrows: molecular interaction, dashed arrow: indirect or state change. Copied from [113–115]

- prostaglandin f2a (PGF2a) is naturally occurring prostaglandin, and through the activation of the Akt/mTOR pathway responsible for muscle growth [123,124].
- 11-deoxy-13,14-dihydro-15-keto-11β,16.xi.-cycloprostaglandin E_2 (bicyclo-PGE2) is a stable breakdown product of prostaglandin E2 (PGE2) and 13,14-dihydro-15-keto PGE2 and is measured instead as a marker for the biosynthesis or metabolism of PGE2. PGE2 is the most biologically active of the mammalian prostaglandins and is known to increase the production of cAMP and enhance the effect of bradykinin and histamine [125].
- linoleoyl ethanolamide (LEA) is the ethanolamide form of linoleic acid, which can inhibit arachidonoylethanolamide amidohydrolase.

6.1.3 N-acylethanolamines (NEAs) (Figure 56)

NAEs are released by N-acylphosphatidylethanolamine (NAPE) in response to a variety of stimuli, and release and accumulation has been attributed to biological activities such as neurotransmission, membrane protection and immunomodulation. The following NEAs were detected in this panel:

- oleoyl ethanolamide (OEA) is a naturally occurring lipid present in both plant and animal membranes and is part of the N-acylethanolamines (NAEs). OEA is known to inhibit sphingolipid signalling pathways by blocking the effect of TNF on intracellular Ca^{2+} concentrations. In adipocytes and hepatocytes, OEA inhibits mitogenic and metabolic signalling by the insulin receptor and produces glucose intolerance. It is also known to reduce visceral and inflammatory responses through a PPAR-alfa activation-independent mechanism [126].
- palmitoyl ethanolamide (PEA) is present in most tissues of mammals. While initially described as a type 2 cannabinoid receptor agonist, this has now been overturned as it was shown that PEA is unable to bind to any cannabinoid receptors. It is currently unknown which physiological stimuli regulate PEA levels. However, many studies show an increase of PEA during cellular stress, particularly tissue injury. While PEA does not have anti-inflammatory abilities, it appears to interact with the LPS-stimulated pathway. Besides its anti-inflammatory effects, it also has analgesic, neuroprotective, and anti-epileptic properties [126].
- stearoyl ethanolamide (SEA) inhibits lipid peroxidation in the membranes of mitochondria in the liver during acute hypoxia and has been found to have a pro-apoptotic activity [126].

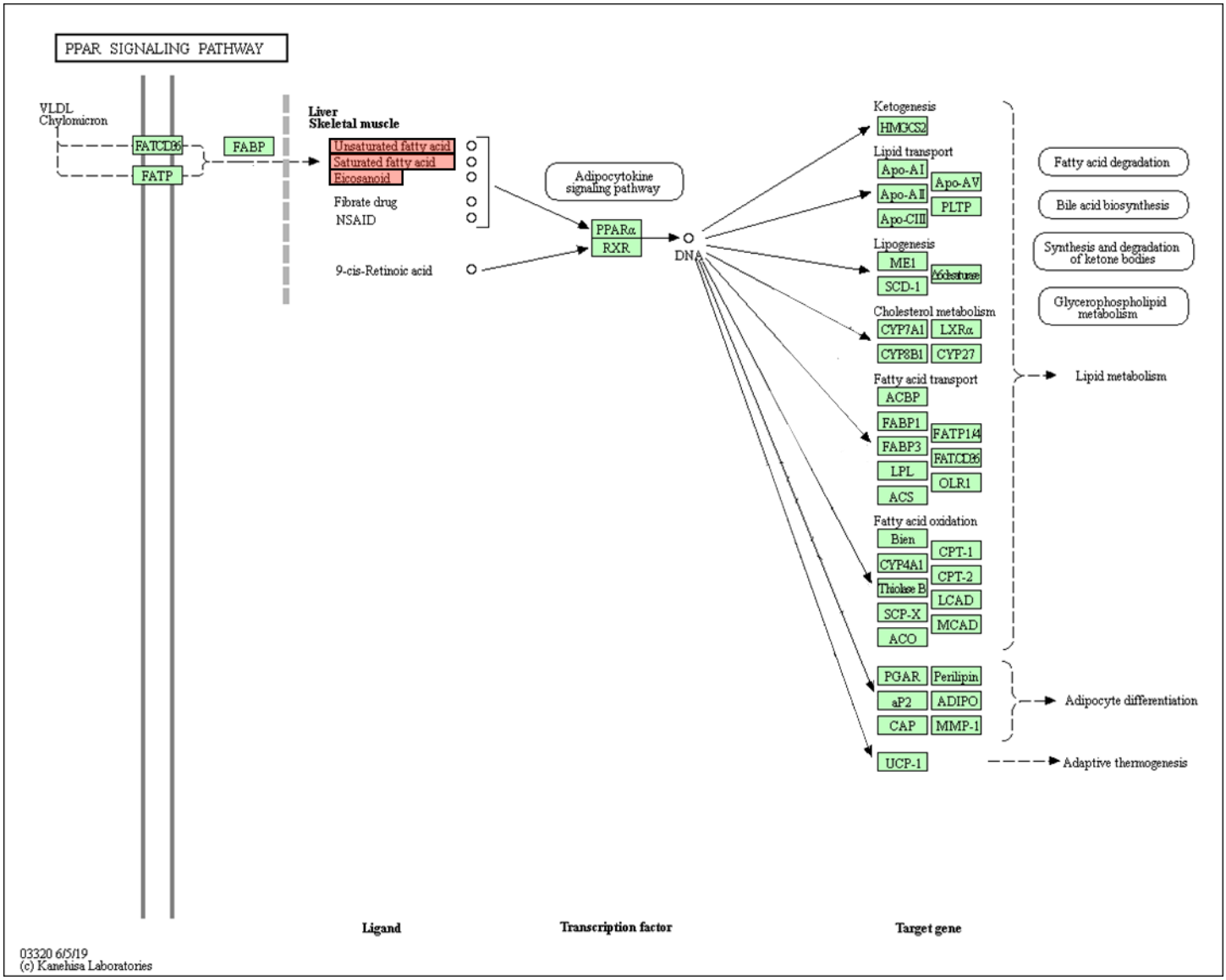

Figure 56. KEGG pathway of PPAR signalling. Displayed in red are metabolites detected and described in this chapter. White rectangles depict genes products, mostly proteins but also RNA. Rounded rectangles depict another map. Circles depict chemical compounds, DNA and other molecules. Black arrows: molecular interaction, dashed arrow: indirect or state change. . Copied from [113–115]

6.1.4 Metabolites in sphingolipid metabolism (Figure 57)

Sphingomyelin (SM) and its metabolic products are now known to have secondary messenger functions in a variety of cellular signalling pathways. Notably, the sphingolipid metabolites ceramide (Cer) and sphingosine-1-phosphate (S1P) have emerged as a new class of potent bioactive molecules. Ceramide can be generated *de novo* or by hydrolysis of membrane sphingomyelin by sphingomyelinase (SMase). Ceramide is subsequently metabolised by ceramidase to generate sphingosine (Sph), which in turn produces S1P through phosphorylation by sphingosine kinases 1 and 2 (SphK1, 2).

- sphinganine (SPHA C18_0) blocks post-lysosomal cholesterol transport by inhibiting LDL-induced esterification of cholesterol and causes unesterified cholesterol to accumulate in the perinucleus vesicles. Is has been suggested that endogenous SPHA inhibits cholesterol transport in Niemann-Pick Type C disease [124,127].
- sphingosine (SPH C18_1) is a derivative of sphinganine and is a major class of sphingolipids in mammals. It can be phosphorylated *in vivo* via two kinases (sphingosine kinase type 1 and type 2) leading the formation of the potent signalling lipid SPHA [127,128].

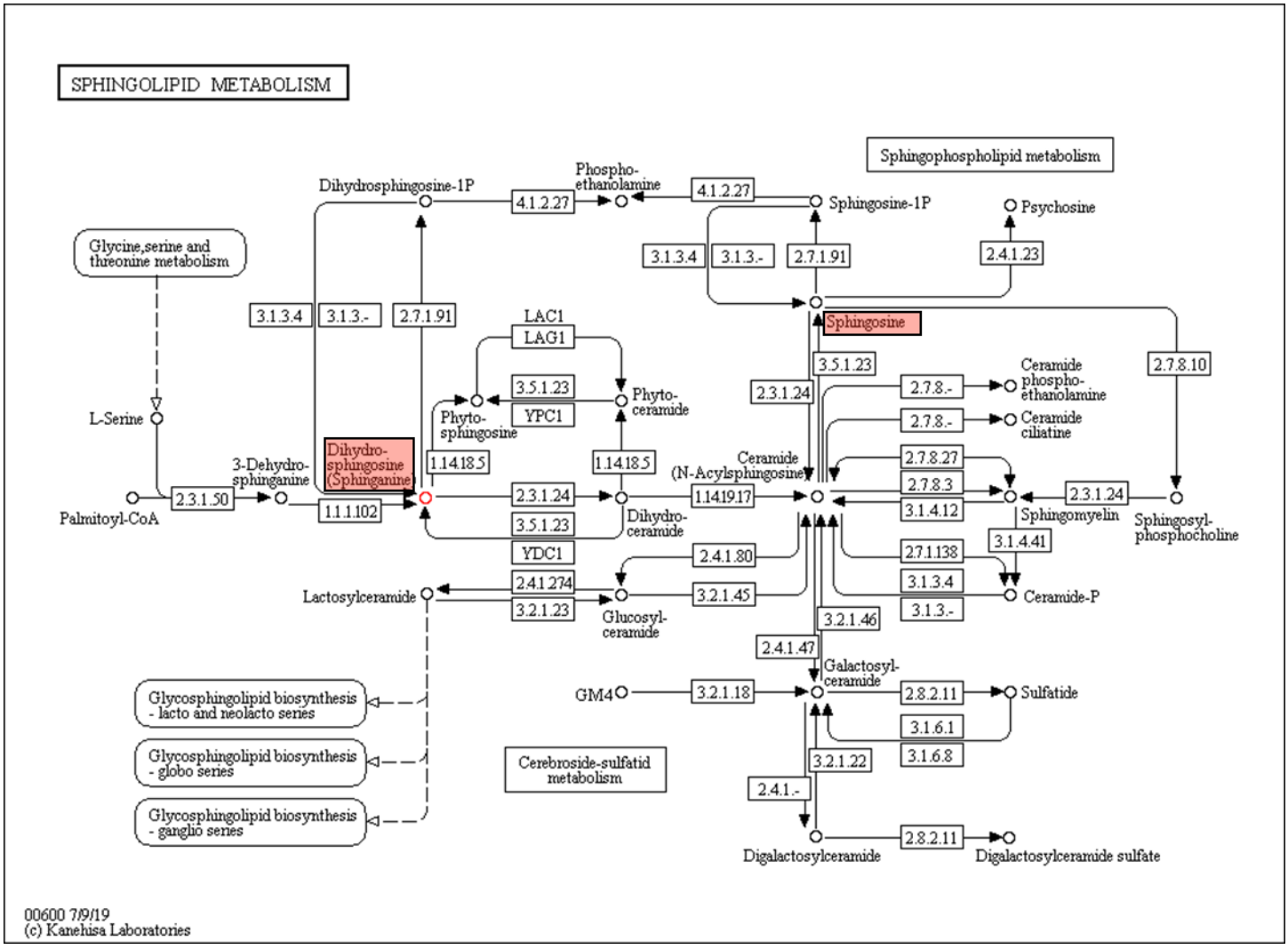

Figure 57. KEGG pathway of sphingolipid metabolism. Displayed in red are metabolites detected and described in this chapter. White rectangles depict genes products, mostly proteins but also RNA. Rounded rectangles depict another map. Circle depicts chemical compounds, DNA and other molecules. Black arrows: molecular interaction, dashed arrow: indirect or state change. . Copied from [113–115]

6.2 Results

6.2.1 2D and 3D samples show apparent different metabolic fingerprint for signalling lipids in both media and cells.

A three-component PCA-X model was fitted over the samples (R2= 0.921 and Q2=0.798) and produced a score plot shown in Figure 58A. Three distinct groups can be identified, 2D cell, 3D cell and the third group consisting of a mixture of both the 2D and the 3D media samples. Consistent with the loading plot, 2D and 3D media contain more of each of the signalling lipids and 3D cell lysates. To investigate the difference within 2D and 3D samples in more detail, two-component PCA-X models were fitted over either the cell samples (Figure 58C, R2=0.939 and Q2=0.9) or the media samples (Figure 58E, Q2=0.63 and Q2=0.189).

Figure 58C shows distinct clustering of 2D samples vs 3D samples. The 3D samples correlate to an increased concentration of all lipid variables. A clustering of SPHA and SPH can be seen in the loading plot compared to the other lipids in the lower right quadrant. The media samples show a less distinct pattern of separation, but a shift over the t[2] can be observed. The 3D samples show a stronger association with PEA, OEA, PGE and SEA expression than 2D samples, indicating that higher concentrations of PEA, OEA and SEA were detected in the 3D samples than in the 2D samples.

To confirm whether these changes are significant, a univariate analysis was performed for each individual signalling lipid (see Figure 60). Compared to 2D cell samples, 3D cells express significantly more 12,13-DiHOME (p= <0.0001), 9-HODE (p= <0.0001), 9,10-DIHOME (p= <0.0001), 9,10,13-TriHOME (p= <0.0001), LEA (p= <0.0001), OEA (p= <0.0001), PEA (p= <0.0001), PGF2a (p= <0.0001), SEA (p= <0.0001), SPHA (p= <0.0001), SPH (p= <0.0001) and Bicyclo-PGE2 (p= <0.0001).

Compared to 2D media samples, the 3D media samples also express significantly more 12,13-DiHOME (p= 0.0283), 9-HODE (p= <0.0017), (+/-) 20-HDoHE (p= <0.0001), LEA (p= <0.0001), OEA (p= <0.0001), PEA (p= <0.0001), PGF2a (p= <0.0065), SEA (p= <0.0002), and Bicyclo-PGE2 (p= <0.0001).

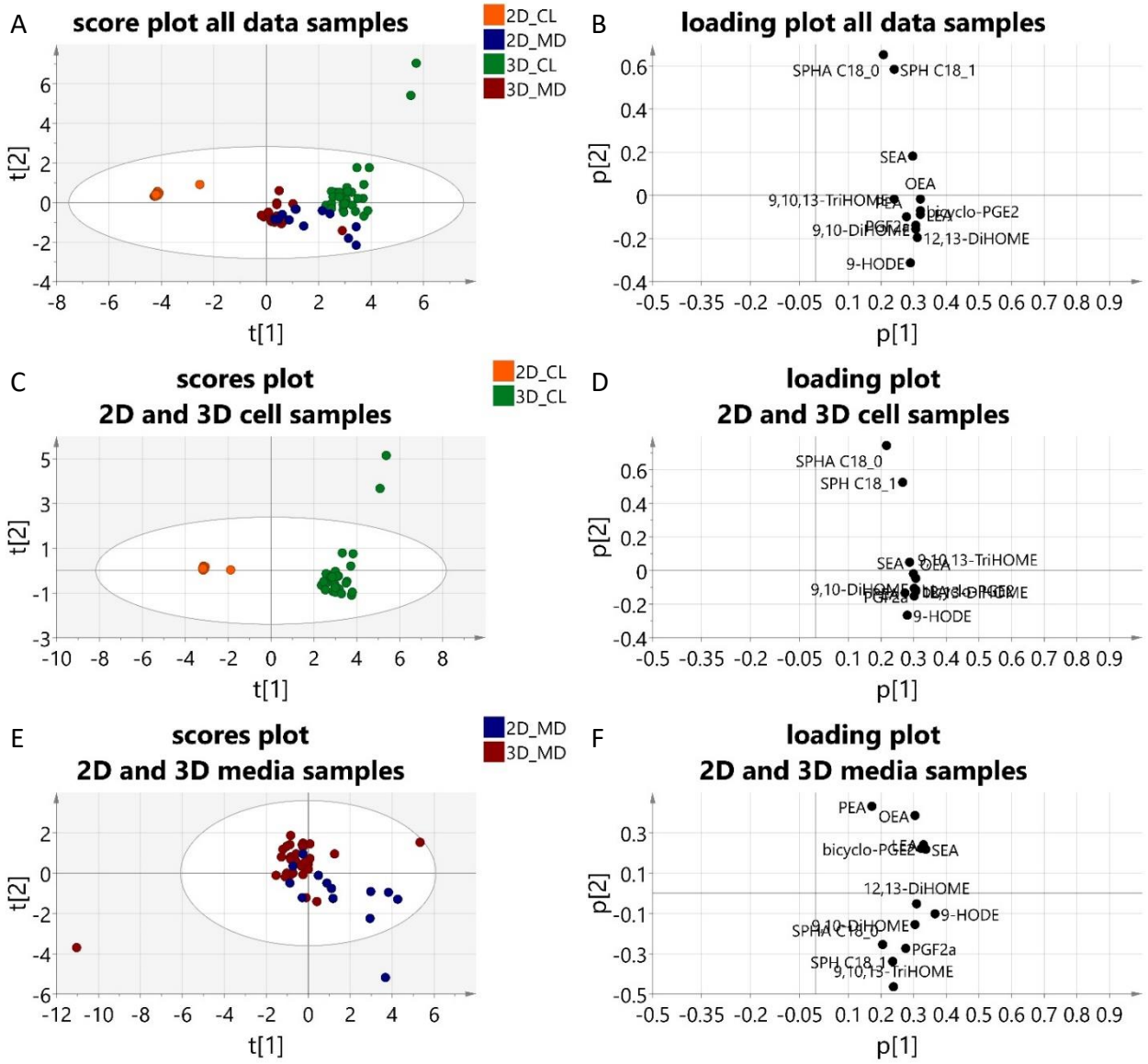

Figure 58. PCA-X scores and loading scatter plots of all samples (A and B), cell samples compared between 2D and 3D (C and D), and media samples compared between 2D and 3D (E and F). Samples were coloured according to primary observations. CL = cell samples, MD = media samples. Ellipse: Hotelling's T2 (95%).

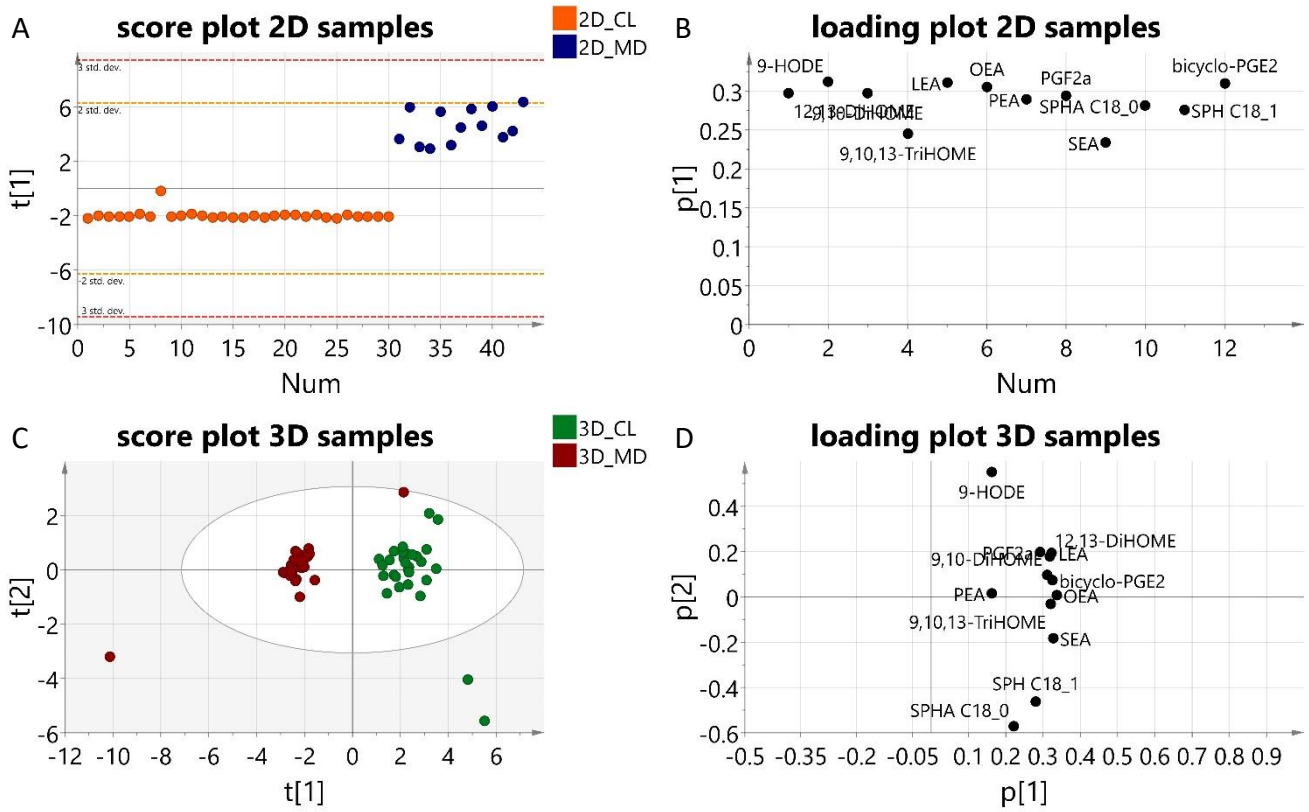

Figure 59. PCA-X scores and loading scatter plots of 2D samples (A), cell and media samples compared for 2D (A) and 3D cell and media samples observed (C) together with their loading plots. Samples were coloured according to primary observations. CL = cell samples, MD = media samples. Ellipse: Hotelling's T2 (95%).

6.2.2 Separation between media and cell samples in both 2D and 3D.

To test whether there was a difference between excreted lipids and those retained within the cells, the samples were divided into 2D and 3D, and a one and two-component PCA-X was fitted over the data. The samples were then coloured according to their primary observation ID into cell and media. In the 2D model in Figure 59A, (R2= 0.82, Q2=0.71), a clear separation of t[1] can be seen between media and cell samples. Though only one component is present in the model, Figure 59B shows that media samples contain more lipids than the cell lysate. These results indicate that most lipids are exported out of the cell or released from the cell membrane.

The PCA-X model fitted over the 3D samples (R2=0.781 and Q2=0.579) is shown in Figure 59C. The model shows once again a clear separation between media and cells. This separation is explained by t[1]. Figure 59D indicates that in the 3D samples the lipids remain within the cell or bound to the membrane. Interestingly this observation is the opposite to that for 2D samples.

The univariate analysis of the individual signalling lipids showed significant differences, where 2D media samples express significantly more 12,13-DiHOME (p= <0.0001), 9-HODE (p= <0.0001), 9,10-DIHOME (p= <0.0001), 9,10,13-TriHOME (p= 0.0002), LEA (p= <0.0001), OEA (p= <0.0001), PEA (p= <0.0001), PGF2a (p= <0.0001), SEA (p= 0.0002), and Bicyclo-PGE2 (p= <0.0001) than 2D cell samples.

Interestingly, within 3D samples, the media contain significantly less 12,13-DiHOME (p= 0.0283), 9-HODE (p= 0.0017),(+/-) 20-HDoHE (p= <0.0001), LEA (p= <0.0001), OEA (p= <0.0001), PEA (p= <0.0001), PGF2a (p= 0.0065), SEA (p= 0.0002), and Bicyclo-PGE2 (p= <0.0001) than observed for 3D cell samples. This is the exact opposite reaction compared to 2D samples.

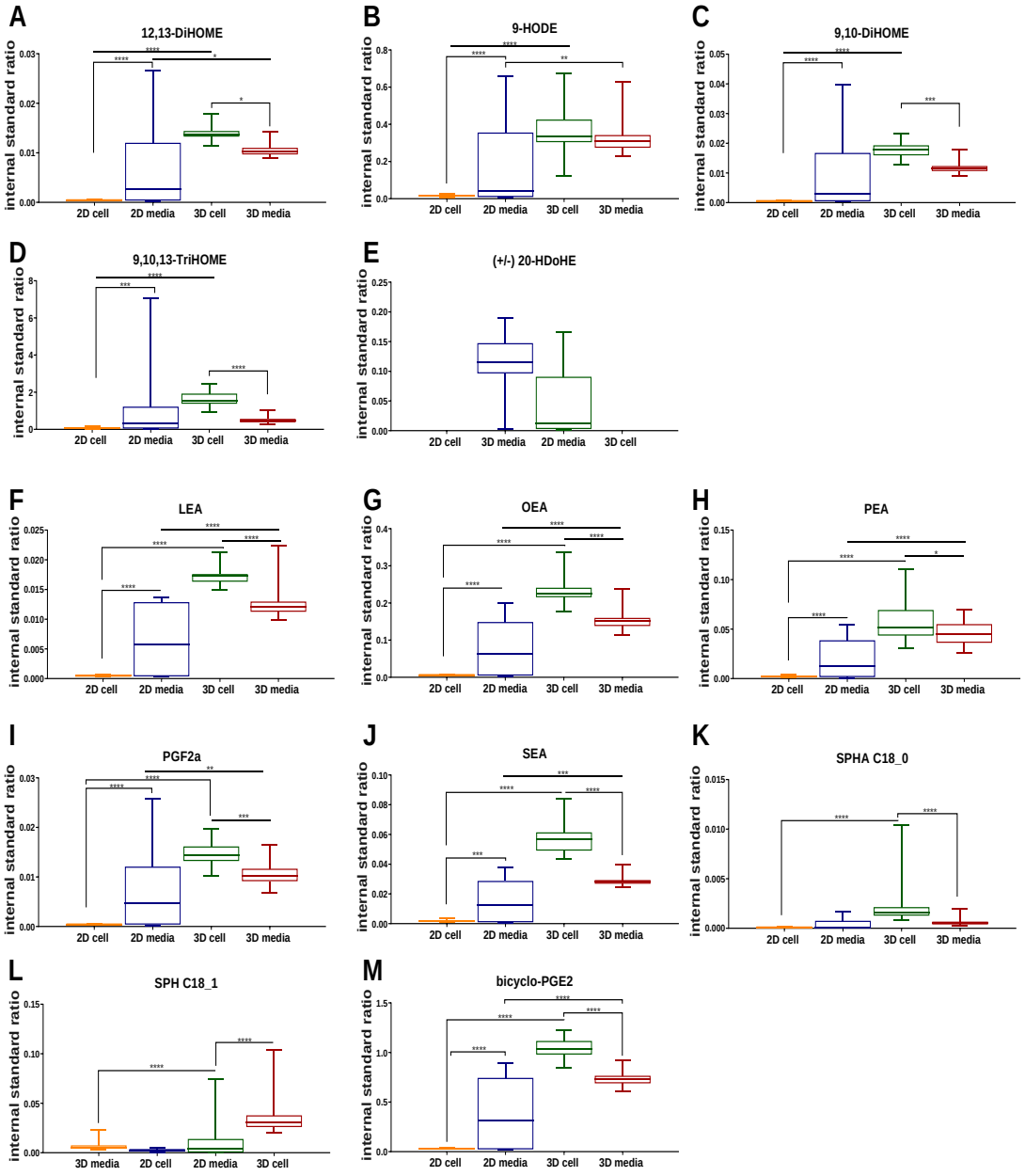

Figure 60 Univariate analyses of signalling lipids in 2D cell and media samples as well as 3D cell and media samples displayed as box and whisker plot (min+ max). (N=50) * indicate significant differences as stated in chapter 2.4 by two-way ANOVA. (DMSO = grey, cycloheximide = blue, estradiol = red, bosentan = orange, clobestasol propionate = green)

6.2.3 The effect of treatments and time on signalling lipid fingerprints.

To investigate the effect of treatments on signalling lipid metabolism, PCA-X models were fitted over 2D cell data, 2D media samples as well as the 3D cell samples and 3D media samples. However, none but the 3D media sample models had a positive R2 and Q2 value for the first component.

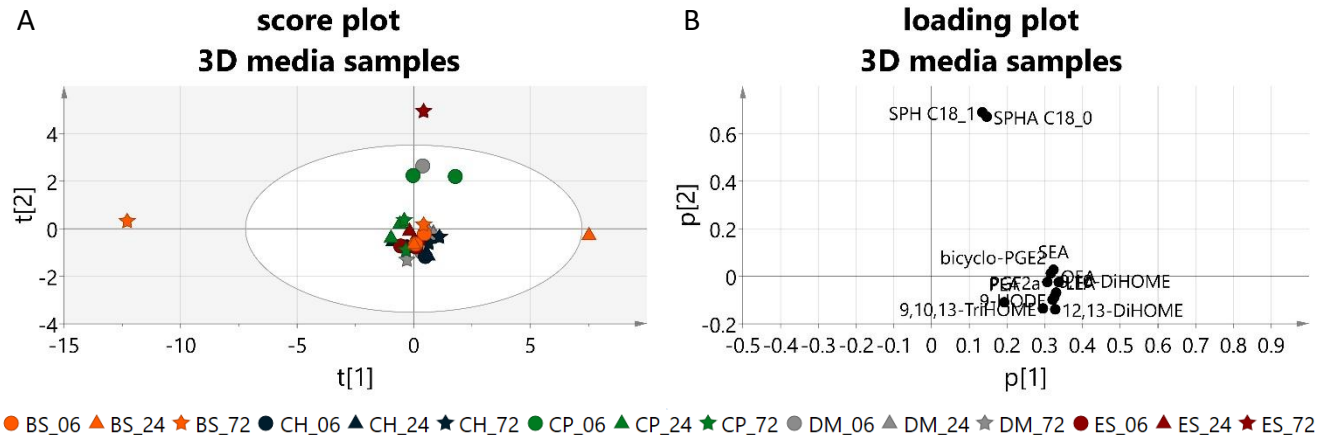

Figure 61. PCA-X scores and loading scatter plots of 3D media samples (A and B). Samples were coloured according to primary observations. BS= bosentan, CH = cyclo-hexamide, CP = clobetasol propionate, DM = DMSO, ES = estradiol. Times: 06 = 6hrs, 24 = 24hrs, 72 = 72hrs. Grey circle indicates the location of the DMSO samples, yellow circle = location of 6 hrs data, while the purple circle indicates the location of 24 hrs and 72 hrs. Ellipse: Hotelling's T2 (95%).

The univariate analysis of 2D cell, 2D media and the 3D cell samples are displayed in Figure 62, Figure 63 and Figure 64, respectively. A two-way ANOVA test was performed to identify any significant changes, but none were recognised. A possible explanation of why no model could be fitted over the data is that no variance is detected between the samples. The 3D media samples, however, showed a far larger variance and a model could, therefore, be fitted over the data. The univariate analysis of the 3D media samples showed significant changes at 24 hrs 9,10-DiHOME compared to 72 hrs for cells treated with bosentan (Figure 65C p= 0.0380).

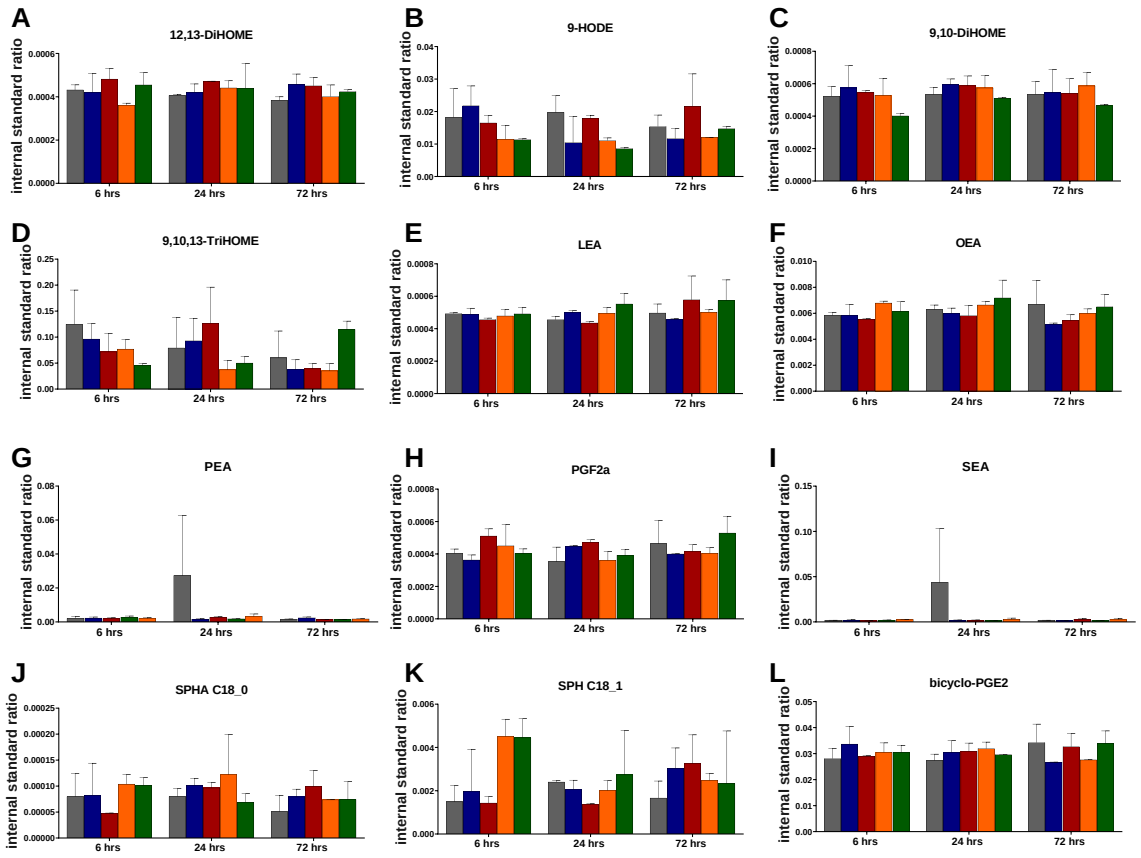

Figure 62. Univariate analysis of signalling lipids in 2D cell samples. Colours indicate same treatment as indicated in Chapter 4 and 5. No significant differences by two-way ANOVA between DMSO and individual treatments or for time dependency within treatments found (n=2). (DMSO = grey, cycloheximide = blue, estradiol = red, bosentan = orange, clobestasol propionate = green)

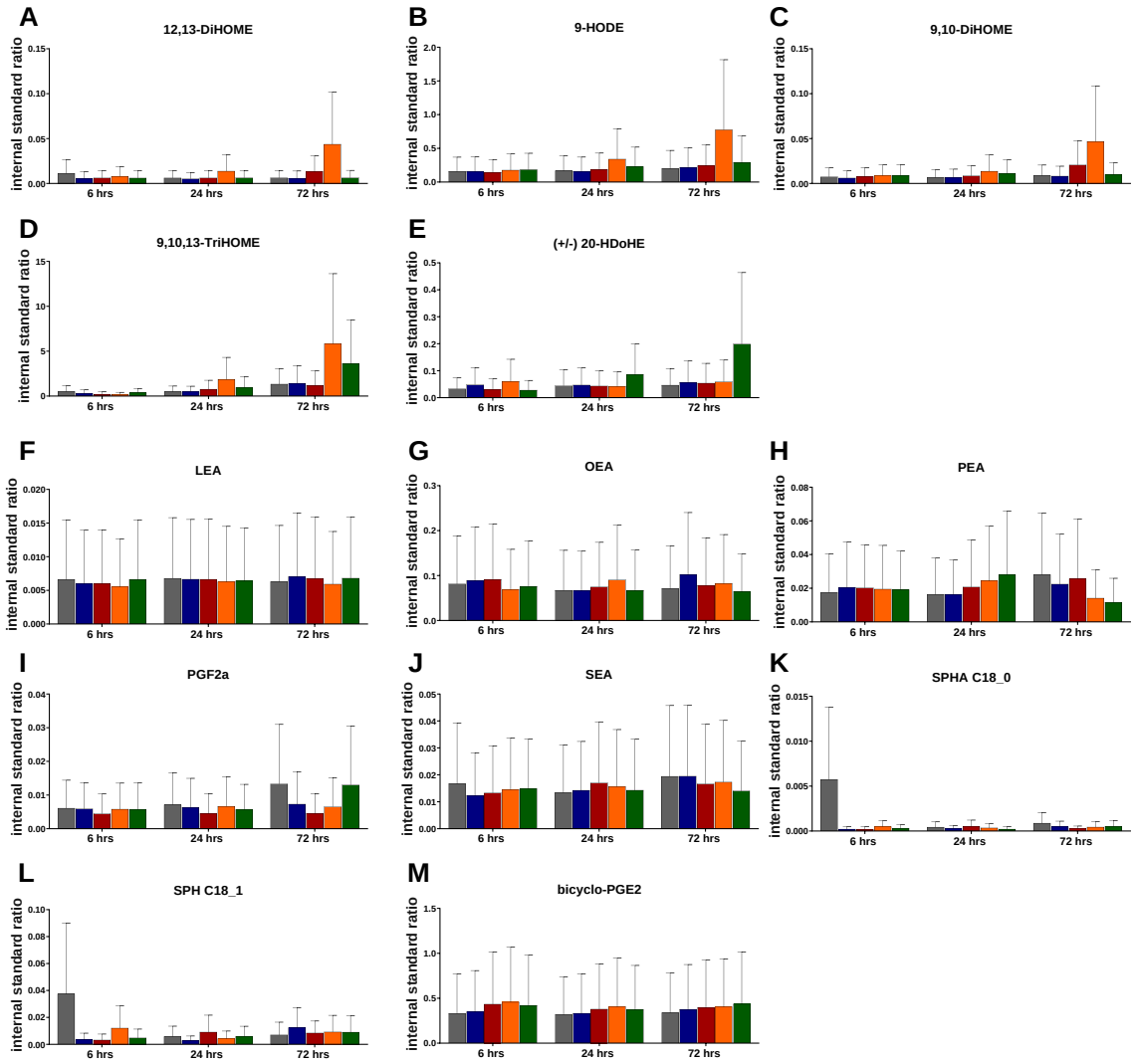

Figure 63. univariate analysis of signalling lipids in 2D media. Colours indicate same treatment as indicated in chapter 4 and 5. No significant differences by two-way ANOVA between DMSO and individual treatments or for time dependency within treatments found n=2). (DMSO = grey, cycloheximide = blue, estradiol = red, bosentan = orange, clobestasol propionate = green)

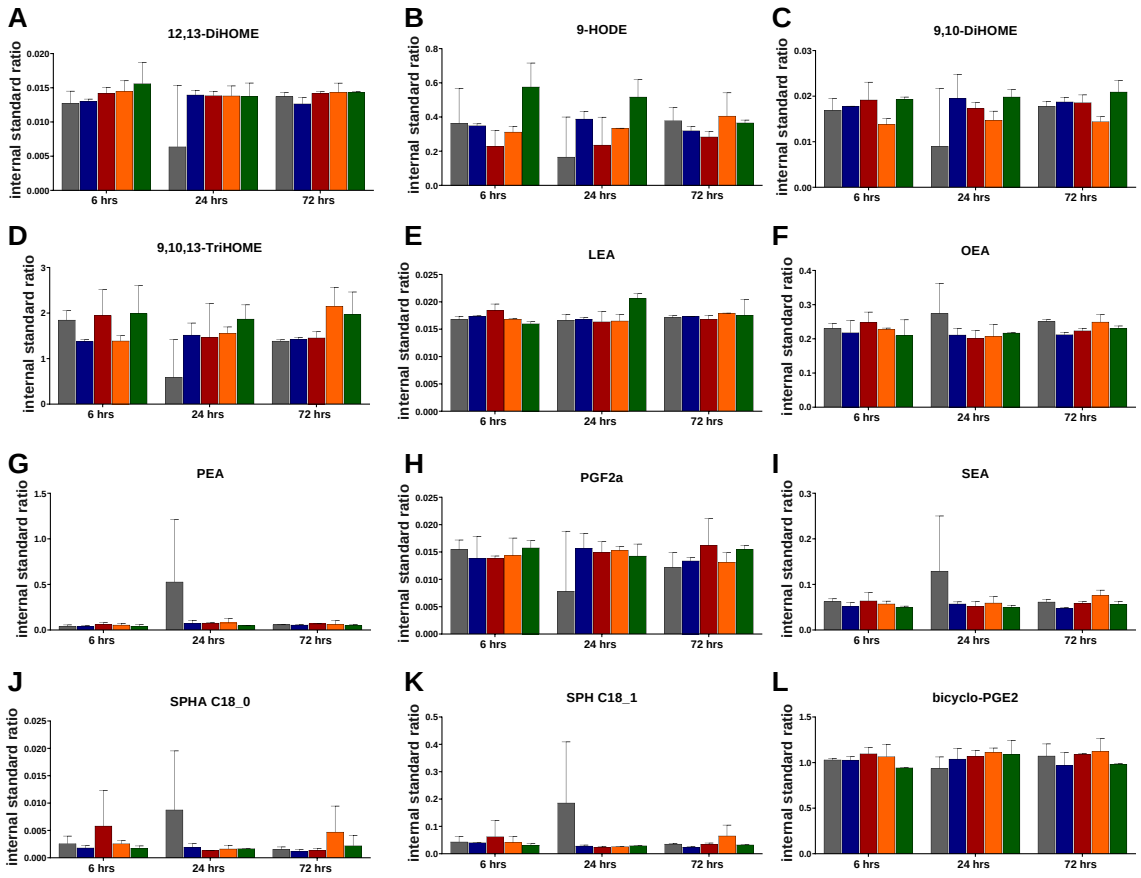

Figure 64. Univariate analysis of signalling lipids in 3D cells. Colours indicate same treatment as indicated in chapter 4 and 5. No significant differences by two-way ANOVA between DMSO and individual treatments or for time dependency within treatments found (n=2). (DMSO = grey, cycloheximide = blue, estradiol = red, bosentan = orange, clobestasol propionate = green)

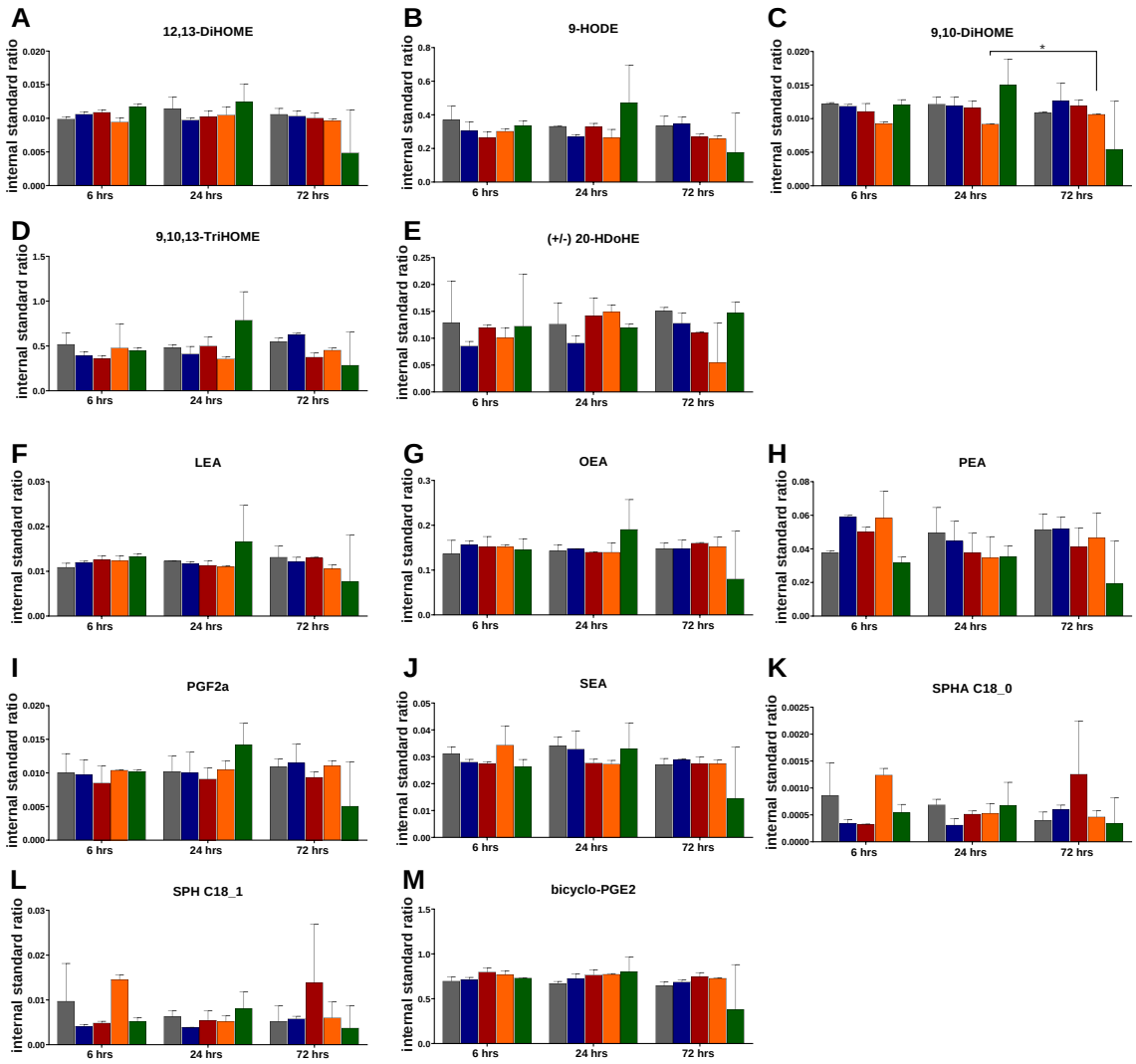

Figure 65. Univariate analysis of signalling lipids in 3D media. Colours indicate same treatment as indicated in chapter 4 and 5. (n=2). Significance indicated with *: p > 0.05. (DMSO = grey, cycloheximide = blue, estradiol = red, bosentan = orange, clobestasol propionate = green)

6.3 Discussion of the results.

These analyses with cultured hepatocytes provided novel insights into the response of hepatocytes to stress factors such as the exposure to drugs, but unfortunately large portions of signalling pathways that are only present in other cells such as the liver specific macrophages, known as Kupffer cells were left out due to the absence of these cells. Kupffer cells are responsible for defence and liver disease [129]. We should, therefore, be careful with the assessment of conclusions made in this chapter.

Multivariate analysis revealed a different metabolic fingerprints between 2D and 3D cell data in signalling lipids with a strong indication that 3D cells contain higher concentrations of signalling lipids; this finding was confirmed in the univariate analysis. The elevation in signalling lipids in the 3D cells could be due to the differences in enzyme and protein expression in the 3D cultured cells. The latter might be able to imitate normal physiological behaviour while the 2D cultured cells are less able to do so [20,130]. While PHH are undoubtedly the best choice for investigating liver toxicity, the absence of other cell types, especially Kupffer cells, is a major limitation. Kupffer cells do not only have the task of mediating inflammation but also have a protective role [131]. We expected the cells treated with compounds to show significant effects in the activation of inflammatory and anti-inflammatory pathways of the signalling lipids and hint at bile acid background processes in cell toxicity. However, our treatments of the cells do not show any significant effect, due to the possible absence of Kupffer cells described above. It could however also be that there is a direct effect of the bile acids to toxicity, but it is unlikely as bile acids such as DCA have been shown to have effect on signalling lipids such as sphingomyelin, and ceramide [105].

The only a significant increase occurred in 9,10-DiHOME after 72 hrs following the incubation with bosentan. 9,10-DiHOME can be synthesized as a result of inflammation and oxidative stress and has been proposed as diagnostic marker for intra cholestatic diseases in humans [132,133]. Surprisingly this could be an early indicator of oxidative stress and identify which BSEP inhibitors will cause oxidative stress. Hence, the production of 9,10-DiHOME could be used as a criterium to exclude compounds from further drug development. Elisa kits for 9, 10-DiHOME detection already exist for the detection in plasma, serum and bronchoalveolar lavage fluid to investigate chronic obstructive pulmonary disease (COPD) and other inflammatory diseases.

This is a novel approach into looking into toxicity of compounds, which will require further research before a good conclusion can be made. It would be beneficial to consider co-cultures of PHH and Kupffer cells for further investigating lipid signalling and, where possible, to increase the number of technical replicates to at least three.

7. General discussion

7.1 Summary and conclusions for each chapter

Chapter 3 the details of BSEPs ability to transport TCA and GCA were described in the presence and absence of compounds. We used radio-labelled TCA and GCA to measure the accumulation in ISOVs containing BSEP. By changing the conditions of the assay used by pharmaceutical companies, we were able to investigate the mechanism of inhibition by which the compounds influence bile acid transport. From the experiments we were able to draw the following conclusions:

1.) The IC_{50} *by which compounds inhibit BSEP-mediated TCA transport does not directly relate to the toxicity of the compound.*

2.) The compounds tested, have different mechanisms of inhibition. This could explain why some might be non-toxic despite being strong BSEP inhibitors.

3.) Transport of GCA is negatively influenced by the presence of Mg^{2+}.

4.) In the absence of Mg^{2+} *compounds do not interfere with BSEP's ability to transport GCA.*

Chapter 4 describes the use of 2D and 3D cultured cells in accessing toxicity of Bosentan, cycloheximide, clobetasol propionate and estradiol. Since cycloheximide and estradiol were reported to not inhibit BSEP directly but to influence the expression and localisation of BSEP in hepatocytes, we also investigated the localisation of BSEP in the cells via fluorescent staining. Lastly, we used a total bile acid kit to investigate the effect of our treatments on the total bile acid concentration within the hepatocyte cultures and the media. The conclusions we drew from this chapter were:

1.) Toxicity of compounds appeared to be donor dependent rather than dependent on culture.

2.) Staining of BSEP and analysing its localisation is a viable method to investigate the effect of compounds on BSEP expression.

3.) The ability of compounds to increase or decrease BSEP expression in the membrane did not correlate with total bile acid accumulation within the cell, indicating that other transporters might also contribute to the transport of bile acids.

4.) Total bile acid concentration did not correlate with toxicity in hepatocytes, demonstrating that the bile acid pool composition might be more important than the total bile acid concentration.

Chapter 5 investigates the effect of the drug treatments on the individual bile acid levels within the PHH cultures. With the use of multivariate analysis and univariate analysis we were able to see the effects of bosentan, cycloheximide, clobetasol propionate and estradiol on individual bile acids. We were further able to study the effect of time on the conjugation of bile acids. The conclusions from this chapter were:

1.) 2D cell, 2D media, 3D cell and 3D media samples each have a unique metabolic bile acid fingerprint, indicating that type of culture influences the fingerprint.

2.) 2D cells and 3D cells are both able to conjugate bile acids in a time dependent manner.

3.) Drug treatments can significantly change the bile acid pool composition.

4.) Several secondary bile acids were detected within the samples, the most prominent one being DCA.

Chapter 6 examines the influence of the selected drug treatments on different signalling lipids. 2D and 3D hepatocyte cultures were compared and the conclusions from this chapter were as follows:

1.) 2D cell, 2D media, 3D cell and 3D media each had a unique metabolic signalling lipid fingerprint, showing that metabolic profiling can identify the origin of the sample and culturing type.

2.) Signalling pathways are activated by the different treatments, but whether this is due to bile acids and/or to other molecules is unknown.

3.) Multivariate analysis of individual treatments in 2D cell, 2D media and 3D cells was not possible due to the lack in variation, indicating that these samples do not have an individual metabolic fingerprint.

4.) Multivariate analysis of 3D media was possible due to increased variation.

7.2 Discussion

My research aims to improve the understanding of how the inhibition of BSEP activity contributes to DILI and improves the prediction of compounds that will cause liver injury as well as identify compounds that will not.

The current standard includes a panel which takes into account the IC_{50} of BSEP inhibition as well as toxicity of cell cultures and the total compound that would be available in the patient [15]. Several in silico methods are already able to predict the likeliness of drugs inhibiting BSEP [134]. However as this is only one step up from *in vitro* testing of BSEP inhibition, these methods alone are unlikely to predict DILI in humans [135]. To improve the prediction of DILI-inducing compounds, we need to consider that the cell is a complex system and that drugs can influence cells at a multitude of levels. With regards to BSEP and bile acids, drugs can: 1.) affect BSEP's ability to transport bile acids, 2.) affect total BSEP expression, 3.) affect the localisation of BSEP at the membrane or in the endosomes inside the cell, or 4.) induce changes in the bile acid pool composition [43,44]. In whole organisms we also need to consider that other cells can have an ameliorating effect on hepatocytes, either by stimulating inflammatory processes or by preventing toxicity through exerting a rescuing effect [129,131].

One way by which pharmaceutical companies have worked on improving the prediction of DILI, is by combining all the gathered information and use machine learning to predict drug effects. Using machine learning methods to predict in-silico toxicity has previously been stated to be the future [136]. Machine learning describes the scientific study that computer systems use to perform a specific task without using explicit instructions. Instead it relies on large quantities of information to set up its own set of rules. So, with this, there is already a limitation. For machine learning to work there is a large quantity of training data necessary, this data is then used to set-up the rules applied by the computer to differentiate between possible toxic effects of compounds [136]. The success rate of these approaches have been shown to improve over time. Recently AstraZeneca showed an improvement of Dili predictions with Bayesian machine learning [137]. The model they use is based on physicochemical properties, IC_{50} of drug-induced BSEP inhibition in ISOVs, toxicity assays from different cell systems, and the maximum plasma concentration of the drug that is reached following its administration. For a binary DILI prediction, there is a 86% accuracy, 87%

sensitivity, and 85% specificity. The model was also able to predict 92% of compounds that will cause DILI and 78 % that will not [137].

My data could prove invaluable to training machine learning algorithms by adding mechanisms of drug-induced inhibition of BSEP. The results from chapter 1 indicates that BSEP inhibition occurs in different ways, which could explain why toxicity happens regardless of BSEP inhibition in the case of clobetasol propionate. Clobetasol propionate was proven to be more inhibitory than bosentan when looking at TCA transport. However, with regards to toxicity, bosentan causes liver injury while clobetasol propionate does not [15].

Non-competitive inhibition is more dangerous than competitive inhibition because it cannot be overcome by increasing the substrate concentration. With competitive inhibition the increase of bile acid would at some point compete away the inhibitory compound. However, non-competitive inhibition is independent of bile acid concentration or composition [138]. However, either due to the amount of work involved or the difficulty in establishing accurate Km and Vmax values in the presence of drug candidates, this type of analysis is not commonly done [74]. A novel biochemical assay to analyse the type of inhibition was established, and it showed that bosentan, cyclosporin A, and clobetasol propionate act as competitive or non-competitive inhibitors, and that alpidem might act as an uncompetitive inhibitor. This data is based on concentrations where drugs cause 50% of total inhibition. However, this result does completely explain the severity of the effects of the drugs in inducing liver injury. Bosentan alpidem and cyclosporine A are considered dangerous and cause liver injury while clobetasol propionate does not cause any injury. Due to its propensity to not cause liver damage clobetasol propionate was expected to be either a competitive or mixed competitive inhibitor, while the other drugs were expected to be non or mixed competitive inhibitors. There is however an argument against the use of TCA in these kinetic experiments. TCA, while used the most in analyses of BSEP-mediated transport, is not the most abundant bile acid or the most appropriate bile acid to investigate [75]. GCA is more appropriate, as the conjugation rate between glyco and tauro is approximately 3 glyco- to 1 tauro-conjugation within the hepatocyte. Previous investigations suggested that no difference exists between TCA and GCA transport [71,139,140]. However, anecdotally, several experts and sources stated the difficulty of using radiolabelled GCA in transport studies but it was attempted anyway. During the optimisation of the assay we found that GCA is negatively affected by Mg^{2+}. Magnesium

ions are present in all the buffers used to analyse BSEP mediated transport at both AZ as well in the literature. Mg^{2+} is the fourth most common ion in human and is influenced in concentration by drugs such as antibiotics or simple dietary uptake [141,142] Drugs can negatively influence the uptake of magnesium from food by utilizing the same uptake systems [141]. Another source besides food is the availability of over-the-counter magnesium supplements, these supplements currently do not come with many warnings and a literature search on PubMed revealed no studies into the health effects of long-term exposure to these supplements or how many people are taking term regularly. “webmd.com” only states mild warnings for previously established conditions (https://www.webmd.com/vitamins/ai/ingredientmono-998/magnesium), but these warnings do not relate to liver injury. The influence of Mg^{2+} on bile acids as well as the influence of other physiologically relevant ions on bile acid transport (such as K^{+} and Ca^{2+}) needs further investigation. Both of these ions have already been shown to influence the free pools of bile acids in hepatocytes. DCA is a secondary bile acid that can induce calcium signalling [105]. On the other hand, TCA, UDCA [96] and other bile acids have been reported to influence the excretion is sodium and potassium ions. Thus, a secretory link exists and this is also consistent with the Mg^{2+}-GCA effects that is described in this thesis [143]. It is interesting to note that previous research in 1994 found that intracellular increases in magnesium promoted GDCA induced apoptosis in rat [144], but little to no further investigation has been undertaken in Mg^{2+}’s influence on bile acid transport. Considering both the previous finding in rats and the data in this thesis show an effect on a glyco-conjugated bile acids, it should be investigated if the effect is dependent due to the glyco-group. Currently only radiolabelled GCA and TCA are commercially available, so in order to investigate the effect of inorganic ions on the transport of other bile acids by BSEP, a new assay needs to be developed. Whereas radiolabelled bile acids other than TCA and GCA could possibly be synthesized, a non-radiolabelled assay would be preferred. One possibility is to use fluorescent-labelled bile acids or use assay kits that can change bile acids into a fluorescent signal, such an assay is currently being optimised in the hope to use the information gathered from Chapter 5 to prioritise bile acids that are relevant to this investigation.

In the introduction to Chapter 1.1.1, the current standard in pre-clinal development of compounds was described. The passing of a compound to the next stage is dependent on it

passing a panel of tests. However, in the same chapter the limitations in these studies were described. One of these limitations is the use of immortalised cell lines rather than primary cells. The main important difference that was considered previously, was that immortalised cell lines can proliferate (giving you a near endless supply of cells) whereas primary human hepatocytes are unable to do so. However, in recent literature [96,145–148] profound differences were observed between the two cell types in gene expression, enzyme expression and protein expression [146], Primary cells therefore are more comparable to humans, but in traditional mono-layers cultures of PHH the cells rapidly dedifferentiate and lose their hepatic functions [145]. To prevent this dedifferentiation, the cells can either be cultured as 2D sandwich cultures with a matrix gel overlay (that causes cell polarisation), or as 3D spheroid models (microtissues) or microfluidic systems (liver on a chip) [149,150]. In this PhD work 2D sandwich and 3D cultured PHH were compared to establish the effect of selected compounds on toxicity, BSEP expression, total bile acid concentration, bile acid metabolomics and signalling lipids. A large study in which long term toxicity in 2D cultures was compared with 3D cultures found that 3D cultures are more sensitive to toxicity in the long term (14 days culture) [145]. However, in this study donor specific effects were found to be more important, which could be in agreement with previous literature stating the importance of polymorphisms in Cyp450 enzymes [82]. With regards to bile acid metabolomics, 3D cells were found to have a closer resemblance to the actual physiological bile acid pool in humans than 2D cultured PHH. As our system does not contain gut microbiota responsible for transforming primary bile acids into secondary bile acids, the entire bile acid pool could not be investigated. Bile acid profiling receives more attention at present time because bile acids have been shown to be involved in liver and colon cancer [108,151], cardio-protection in the form of UDCA [96], and regulation of inflammation [152]. Furthermore, bile acids show significant changes in the brain of Alzheimer patients [153]. Although this work able to identify several significant changes in bile acids, no specific conclusion regarding toxicity could be drawn.

A second major finding was the presence of secondary bile acids in the experimental samples. Previous literature states that the occurrence of secondary bile acids in hepatocyte cultures was due to their presence in FCS used to preincubate the cells. During this time the cells are able to take up secondary bile acids from the FCS-supplemented medium and concentrate

them to a level in the cell at which they are detectable [103]. Either way DCA is known as one of the most toxic bile acid and its presence in PHH cultures was an unexpected advantage in this study when investigating toxicity [105,154,155].

Compared to ISOVs, in cells you are not only looking at the transport activity of BSEP but also take into account that several other transporters are influenced by the change in bile acid pool concentrations. Uptake of bile acids at the basolateral side of hepatocytes is facilitated by OATP2, mEH and NTCP whereas, in addition to BSEP, MRP2 is able to export bile acids at the apical side of the hepatocytes [156]. Currently, many studies investigate the effect of compounds and mutations by looking at mRNA levels and quantitative western blots of BSEP, this is not completely accurate. BSEP is continuously recycled from the apical membrane to Rab 11-positive vesicles in the cytoplasm. When the need arises the hepatocyte is able to recruit a large amount of BSEP from these vesicles to the membrane [157]. Our staining revealed that compounds can influence the localisation of BSEP within the cell. This manner of investigating transporter expression is a more accurate way of looking at BSEP expression because only BSEP within the plasma membrane is involved in bile acid efflux from the cell. However, for 3D spheroids some optimisation is still required. Firstly, due to the size of the spheroids, more diffusion of the antibodies through the microtissues is required than in 2D cultured cells. Secondly, even confocal microscopes have a limitation in depth; it is therefore necessary to clarify the cells prior to imaging [59] (cells are made transparent), which enables the confocal microscope to look through larger structures [158]. While this is regularly done for tissues, the application of these methods are more difficult for spheroids which are not attached and can be lost in any steps that remove liquid. BSEP staining and quantification via confocal microscopy can easily be adapted for large scale investigation and should be considered to be included in any future toxicity study, as well as in any machine learning panel.

Finally, lipid signalling was investigated. Lipids are important in the communication of the stress signals not only within the cell but also to other cells, such as macrophages, that are responsible for immune responses and protection. In the liver, macrophages are Kupffer cells that have been proven to have protective effects in acetaminophen-induced liver injury [131]. Because we looked at monocultures we now know how hepatocytes react to bosentan, estradiol, cycloheximide and clobetasol propionate. However, large parts of the lipid

signalling pathways happen within the Kupffer cells. Since signalling lipids go from cell to cell and our culture only contained hepatocytes, the signalling lipids show little to no significant difference in response to the different compounds. To make a proper comparison between *in vitro* and physiological process, the metabolomics of signalling lipid should be studied within co-cultures of hepatocytes and Kupffer cells [159]. These co-cultures have been proven to be more robust and relevant to investigate inflammatory and toxic effects of compounds [159]. The FDA also encourages to investigate such cocultures and the frequency of such studies will therefore most likely increase in the future. The FDA's model for a co-culture showed a continued metabolic capacity characteristic of PHH, an ability to secrete pro-inflammatory cytokines in response to LPS, and responses to interleukin species for 2 weeks. Although the co-culture is currently not well established enough to be a valid toxicity assay, the FDA encourages to investigate such co-cultures and the frequency of such studies will therefore most likely increase in the future. The continued interest into these cultures is also evident from the advances that are currently being made towards organ investigations instead of simple cell systems. Current spheroid systems are the golden standard for investigating toxicity. Liver on a chip is already under development [160]; these chips use microfluidic systems to imitate the flow of body liquids. The next step is to combine several cell types to create an organ on a chip , which when linked together would create a human on a chip [160,161].

7.3 Future experiments:

Considering the discussion of this work, the following experiments are proposed that will increase our understanding of BSEP and bile acid-mediated toxicity in hepatocytes:

1.) Use the A444V, W330A, Y337A, Y772A, R1033A and T1029A BSEP mutants generated in this PhD research to investigate their effects on the kinetics of TCA and GCA transport.

2.) Develop a high-throughput non-radioactive assay to investigate the effect of mutations and compounds on BSEP's efficiency to transport different bile acids.

3.) Investigate the effect of physiologically relevant ions such as calcium, potassium and chloride on BSEPs ability to transport bile acids.

4.) Investigate the effect of co-cultures of hepatocytes and Kupffer cells on cell toxicity, BSEP localisation, bile acid metabolism and lipid signalling.

5.) Establish the origin of the secondary bile acid DCA in hepatocytes. Is it possible that human cells have a direct pathway for DCA synthesis?

6.) Combine the information obtained under point 1, 2, and 3 with literature data on BSEP to carry out a non-linear regression analysis that investigates the correlation between mutation position, disease association, and effects on transport activity.

Bibliography

1. Wilkens S. **Structure and mechanism of ABC transporters**. F1000Prime Rep. 2015;7(February):1–9.

2. Theodoulou FL, Kerr ID. **ABC transporter research: going strong 40 years on**. Biochem Soc Trans. 2015;43(5):1033–40.

3. Berger EA, Heppel LA. **Different Mechanisms of Energy Coupling for the Shock-sensitive and Shock-resistant Amino Acid Permeases of Escherichia coli**. J Biol Chem. 1974;249(24):7747–55.

4. Dean M, Rzhetsky A, Allikmets R. **The human ATP-binding cassette (ABC) transporter superfamily.** Genome Res. 2001;11(7):1156–66.

5. Burt HJ, Riedmaier AE, Harwood MD, Crewe HK, Gill KL, Neuhoff S. **Abundance of hepatic transporters in Caucasians: A meta-analysis**. Drug Metab Dispos. 2016;44(10):1550–61.

6. Chiang JYL. **III. Bile acids and nuclear receptors**. Am J Physiol Liver Physiol. 2015;284(3):G349–56.

7. Nicolaou M, Andress EJ, Zolnerciks JK, Dixon PH, Williamson C, Linton KJ. **Canalicular ABC transporters and liver disease.** J Pathol. 2012;226(2):300–15.

8. Zimmerman HJ. **Drug-induced liver disease.** Clin Liver Dis. 2000 Feb;4(1):73–96, vi.

9. Williams CD, Stengel J, Asike MI, Torres DM, Shaw J, Contreras M, et al. **Prevalence of nonalcoholic fatty liver disease and nonalcoholic steatohepatitis among a largely middle-aged population utilizing ultrasound and liver biopsy: A prospective study**. Gastroenterology. 2011;140(1):124–31.

10. Hayashi H. **Development of new therapeutic strategy for transporter-related diseases**. YAKUGAKU ZASSHI. 2014;134(10):1007–11.

11. Xu JJ, Diaz D, O'Brien PJ. **Applications of cytotoxicity assays and pre-lethal mechanistic assays for assessment of human hepatotoxicity potential.** Chem Biol Interact. 2004 Nov;150(1):115–28.

12. Chiang JYL. **Bile acid metabolism and signaling**. Compr Physiol. 2013;3(3).

13. Pedersen JM, Matsson P, Bergström CAS, Hoogstraate J, Norén A, LeCluyse EL, et al. **Early identification of clinically relevant drug interactions with the human bile salt export pump (BSEP/ABCB11)**. Toxicol Sci. 2013;136(2):328–43.

14. Hughes J, Rees S, Kalindjian S, Philpott K. **Principles of early drug discovery**. Br J Pharmacol. 2011;162(6):1239–49.

15. Thompson RA, Isin EM, Li Y, Weidolf L, Page K, Wilson I, et al. **In vitro approach to assess the potential for risk of idiosyncratic adverse reactions caused by candidate drugs**. Chem Res Toxicol. 2012 Aug;25(8):1616–32.

16. Dawson S, Stahl S, Paul N, Barber J, Kenna JG. **In vitro inhibition of the bile salt export pump correlates with risk of cholestatic drug-induced liver injury in humans**. Drug Metab Dispos. 2012;40(1):130–8.

17. Lalkhen AG, McCluskey A. **Clinical tests: Sensitivity and specificity**. Contin Educ Anaesthesia, Crit Care Pain. 2008;8(6):221–3.

18. Sison-Young RLC, Mitsa D, Jenkins RE, Mottram D, Alexandre E, Richert L, et al. **Comparative Proteomic Characterization of 4 Human Liver-Derived Single Cell Culture Models Reveals Significant Variation in the Capacity for Drug Disposition, Bioactivation, and Detoxication**. Toxicol Sci. 2015;147(2).

19. Underhill GH, Khetani SR. **Bioengineered Liver Models for Drug Testing and Cell Differentiation Studies**. Cmgh. 2018;5(3):426–439.e1.

20. Bell CC, Dankers ACA, Lauschke VM, Sison-Young R, Jenkins R, Rowe C, et al. **Comparison of Hepatic 2D Sandwich Cultures and 3D Spheroids for Long-term Toxicity Applications: A Multicenter Study**. Toxicol Sci. 2018 Apr 1;162(2):655–66.

21. Pound P, Bracken MB. **Is animal research sufficiently evidence based to be a cornerstone of biomedical research?** BMJ. 2014;348(May):1–4.

22. Akhtar A. **The Flaws and Human Harms of Animal Experimentation**. Cambridge Q Healthc Ethics. 2015;24(4):407–19.

23. Kubitz R, Dröge C, Kluge S, Stindt J, Häussinger D. **Genetic variations of bile salt transporters.** Drug Discov Today Technol. 2014;12:e55-67.

24. FDA, Union B, Trust SM, Society H. **Nine out of ten statistics are taken out of context**. 2006;1–3.

25. F. HA. **Enterohepatic Circulation of Bile Acids**. In: Comprehensive Physiology. American Cancer Society; 2011. p. 567–96.

26. Russell DW. **The Enzymes, Regulation, and Genetics of Bile Acid Synthesis**. Annu Rev Biochem. 2003;72(1):137–74.

27. Pandak WM, Kakiyama G. **The acidic pathway of bile acid synthesis: Not just an alternative pathway**. Liver Res. 2019;3(2):88–98.

28. Mostarda S, Passeri D, Carotti A, Cerra B, Colliva C, Benicchi T, et al. **Synthesis, physicochemical properties, and biological activity of bile acids 3-glucuronides: Novel insights into bile acid signalling and detoxification**. Eur J Med Chem. 2018;144(December):349–58.

29. Chiang JYL. **Bile acids: regulation of synthesis**. J Lipid Res. 2009;50(10):1955–66.

30. Monte MJ, Marin JJG, Antelo A, Vazquez-Tato J. **Bile acids: Chemistry, physiology, and pathophysiology**. World J Gastroenterol. 2009;15(7):804–16.

31. Soroka CJ, Boyer JL. **Biosynthesis and trafficking of the bile salt export pump, BSEP: Therapeutic implications of BSEP mutations**. Mol Aspects Med. 2014;37(October

2015):3–14.

32. Ridlon JM, Harris SC, Bhowmik S, Kang DJ, Hylemon PB. **Consequences of bile salt biotransformations by intestinal bacteria**. Gut Microbes. 2016;7(1):22–39.

33. Devlin AS, Fischbach MA. **A biosynthetic pathway for a prominent class of microbiota-derived bile acids**. Nat Chem Biol. 2015;11(9):685–90.

34. Kubitz R, Dröge C, Stindt J, Weissenberger K, Häussinger D. **The bile salt export pump (BSEP) in health and disease.** Clin Res Hepatol Gastroenterol. 2012;36(6):536–53.

35. Nishida T, Gatmaitan Z, Che M, Arias IM. **Rat liver canalicular membrane vesicles contain an ATP-dependent bile acid transport system**. Med Sci. 1991;88:6590–4.

36. Hofmann AF, Hagey LR. **Bile acids: Chemistry, pathochemistry, biology, pathobiology, and therapeutics**. Cell Mol Life Sci. 2008;65(16):2461–83.

37. Scotto KW. **Transcriptional regulation of ABC drug transporters**. Oncogene. 2003;22:7496–511.

38. Mi L-Z, Devarakonda S, Harp JM, Han Q, Pellicciari R, Willson TM, et al. **Short Article Structural Basis for Bile Acid Binding and Activation of the Nuclear Receptor FXR**. Mol Cell. 2003;11:1093–100.

39. Peet DJ, Janowski BA, Mangelsdorf DJ, Dev OG, Mangelsdorf DJ, Peet DJ, et al. **Bile Acids: Natural Ligands for an Orphan Nuclear Receptor**. Science (80-). 1999;284(5418):1365–8.

40. Wakabayashi Y, Lippincott-schwartz J, Arias IM. **Intracellular Trafficking of Bile Salt Export Pump (ABCB11) in Polarized Hepatic Cells: Constitutive Cycling between the Canalicular Membrane and rab11-positive Endosomes □ V**. Mol Biol Cell. 2004;15(July):3485–96.

41. Pérez LM, Milkiewicz P, Elias E, Coleman R, Sánchez Pozzi EJ, Roma MG. **Oxidative stress induces internalization of the bile salt export pump, Bsep, and bile salt secretory failure in isolated rat hepatocyte couplets: A role for protein kinase C and prevention by protein kinase A**. Toxicol Sci. 2006;91(1):150–8.

42. Kubitz R, Tfels GS, Hlkamp TK, Lling RK, Ussinger DH. **Trafficking of the Bile Salt Export Pump From the Golgi to the Canalicular Membrane Is Regulated by the p38 MAP Kinase**. Gastroenterology. 2004;126(2):541–53.

43. Rodrigues AD, Lai Y, Cvijic ME, Elkin LL, Zvyaga T, Soars MG. **Drug-induced perturbations of the bile acid pool, cholestasis, and hepatotoxicity: Mechanistic considerations beyond the direct inhibition of the bile salt export pump**. Drug Metab Dispos. 2014;42(4):566–74.

44. Beckingham IJ, Ryder SD. **Investigation of liver and biliary disease**. Bmj. 2001;322(7277):33.

45. Dawson SE, Stahl S, Paul N, Barber J, Kenna JGG. **In Vitro Inhibition of the Bile Salt Export Pump Correlates with Risk of Cholestatic Drug Induced Liver Injury in Man.**

Drug Metab Dispos. 2011;40(1):130–8.

46. Kenna JG, Taskar KS, Battista C, Bourdet DL, Brouwer KLR, Brouwer KR, et al. **Can BSEP Inhibition Testing In Drug Discovery And Development Reduce Liver Injury Risk? - An International Transporter Consortium Perspective**. Clin Pharmacol Ther. 2018;

47. Aldred EM, Buck C, Vall K. **Chapter 14 - Pharmacokinetics and pharmacodynamics: Introduction**. In: Aldred EM, Buck C, Vall K, editors. Pharmacology. Edinburgh: Churchill Livingstone; 2009. p. 113–4.

48. Aldred EM, Buck C, Vall K. **Chapter 40 - Toxicology**. In: Aldred EM, Buck C, Vall K, editors. Pharmacology. Edinburgh: Churchill Livingstone; 2009. p. 317–27.

49. Doshi R, Ali A, Shi W, Freeman E V., Fagg LA, Van Veen HW. **Molecular disruption of the power stroke in the ATP-binding cassette transport protein MsbA**. J Biol Chem. 2013 Mar;288(10):6801–13.

50. Giovannoni I, Callea F, Bellacchio E, Torre G, De Ville De Goyet J, Francalanci P, et al. **Genetics and Molecular Modeling of New Mutations of Familial Intrahepatic Cholestasis in a Single Italian Center**. PLoS One. 2015;1–13.

51. Davit-Spraul A, Fabre M, Branchereau S, Baussan C, Gonzales E, Stieger B, et al. **ATP8B1 and ABCB11 Analysis in 62 children with normal gamma-glutamyl transferase Progressive Familial Intrahepatic Cholestasis (PFIC): Phenotypic differences between PFIC1 and PFIC2 and natural history**. Hepatology. 2010;51:1645–55.

52. Roustit M, Fonrose X, Montani D, Girerd B, Stanke-Labesque F, Gonnet N, et al. **CYP2C9, SLCO1B1, SLCO1B3, and ABCB11 Polymorphisms in Patients With Bosentan-Induced Liver Toxicity.** Clin Pharmacol Ther. 2014;95(6):583–5.

53. Lam P, Pearson CL, Soroka CJ, Xu S, Mennone A, Boyer JL. **Levels of plasma membrane expression in progressive and benign mutations of the bile salt export pump (Bsep/Abcb11) correlate with severity of cholestatic diseases**. Am J Physiol Physiol. 2007;293(5):C1709–16.

54. Lam CW, Cheung KM, Tsui MS, Yan MSC, Lee CY, Tong SF. **A patient with novel ABCB11 gene mutations with phenotypic transition between BRIC2 and PFIC2**. J Hepatol. 2006;44(1):240–2.

55. Lang C, Meier Y, Stieger B, Beuers U, Lang T, Kerb R, et al. **Mutations and polymorphisms in the bile salt export pump and the multidrug resistance protein 3 associated with drug-induced liver injury**. Pharmacogenet Genomics. 2007;17(1):47–60.

56. Manual I. **Guide to Baculovirus Expression Vector Systems (BEVS) and Insect Cell Culture Techniques**. none.

57. Janakiraman V, Forrest WF, Seshagiri S. **Estimation of baculovirus titer based on viable cell size**. Nat Protoc. 2006;1(5):2271–6.

58. Sison-Young RLC, Mitsa D, Jenkins RE, Mottram D, Alexandre E, Richert L, et al.

Comparative Proteomic Characterization of 4 Human Liver-Derived Single Cell Culture Models Reveals Significant Variation in the Capacity for Drug Disposition, Bioactivation, and Detoxication. Toxicol Sci. 2015;147(2):412–24.

59. Smyrek I, Stelzer EHK. **Quantitative three-dimensional evaluation of immunofluorescence staining for large whole mount spheroids with light sheet microscopy**. Biomed Opt Express. 2017;8(2):484.

60. Wolf SJ, Bachtiar M, Wang J, Sim TS, Chong SS, Lee CGL. **An update on ABCB1 pharmacogenetics: insights from a 3D model into the location and evolutionary conservation of residues corresponding to SNPs associated with drug pharmacokinetics.** Pharmacogenomics J. 2011;11(5):315–25.

61. Le Goff W, Peng D-QQ, Settle M, Brubaker G, Morton RE, Smith JD. **Cyclosporin A Traps ABCA1 at the Plasma Membrane and Inhibits ABCA1-Mediated Lipid Efflux to Apolipoprotein A-I**. Arterioscler Thromb Vasc Biol. 2004;

62. Kis E, Ioja E, Rajnai Z, Jani M, Méhn D, Herédi-Szabó K, et al. **BSEP inhibition - In vitro screens to assess cholestatic potential of drugs**. Toxicol Vitr. 2012;26:1294–9.

63. Vivian D, Polli JE. **Mechanistic interpretation of conventional Michaelis–Menten parameters in a transporter system**. Eur J Pharm Sci. 2014 Nov;64:44–52.

64. **Types of Inhibition** [Internet]. 2010. p. New chemical Genomics Center.

65. Raha K, Peters MB, Wang B, Yu N, Wollacott AM, Westerhoff LM, et al. **The role of quantum mechanics in structure-based drug design**. Drug Discov Today. 2007;12(17–18):725–31.

66. Mano Y, Usui T, Kamimura H. **Effects of Bosentan, an Endothelin Receptor Antagonist, on Bile Salt Export Pump and Multidrug Resistance–Associated Protein 2**. Biopharm DRUG Dispos Biopharm Drug Dispos. 2007;28(April 2006):13–8.

67. Paranjape SG, Turankar A V., Wakode SL, Dakhale GN. **Estrogen protection against coronary heart disease: Are the relevant effects of estrogen mediated through its effects on uterus - Such as the induction of menstruation, increased bleeding, and the facilitation of pregnancy?** Med Hypotheses. 2005;65(4):725–7.

68. Wu T, Zhang Q, Li J, Chen H, Wu J, Song H. **Up-regulation of BSEP and MRP2 by Calculus Bovis administration in 17??-ethynylestradiol-induced cholestasis: Involvement of PI3K/Akt signaling pathway**. J Ethnopharmacol. 2016;

69. van Beusekom CD, van den Heuvel JJMW, Koenderink JB, Schrickx JA, Russel FGM. **The feline bile salt export pump: A structural and functional comparison with canine and human Bsep/BSEP**. BMC Vet Res. 2013;9(January 2015).

70. Hirano M, Maeda K, Hayashi H, Kusuhara H. **Bile Salt Export Pump (BSEP / ABCB11) Can Transport a Nonbile Acid Substrate , Pravastatin**. J Pharmacol Exp Ther. 2005;314(2):876–82.

71. Yucha RW, He K, Shi Q, Cai L, Nakashita Y, Xia CQ, et al. **In Vitro Drug-Induced Liver**

Injury Prediction: Criteria Optimization of Efflux Transporter IC50 and Physicochemical Properties. Toxicol Sci. 2017 Jun;157(2):487–99.

72. Stieger B. **Role of the bile salt export pump, BSEP, in acquired forms of cholestasis**. Drug Metab Rev. 2010;42(3):437–45.

73. Woodhead JL, Yan K, Siler SQ, Watkins PB, Brouwer KLR, Barton HA, et al. **Exploring BSEP inhibition-mediated toxicity with a mechanistic model of drug-induced liver injury**. Front Pharmacol. 2014;5(NOV).

74. Kenna JG, Taskar KS, Battista C, Bourdet DL, Brouwer KRKLRKR, Brouwer KRKLRKR, et al. **Can Bile Salt Export Pump Inhibition Testing in Drug Discovery and Development Reduce Liver Injury Risk? An International Transporter Consortium Perspective**. Clin Pharmacol Ther. 2018;104(5):916–32.

75. Deibert E, Jackson J, Mitchell J, Amaral K, Witek R, Ferguson S, et al. **Taurocholate or Glycocholate – which is the more appropriate Substrate for Assessing Hepatic Bile Salt Transport ?** Sci life. 2010;2010.

76. DiNicolantonio JJ, O'Keefe JH, Wilson W. **Subclinical magnesium deficiency: a principal driver of cardiovascular disease and a public health crisis**. Open Hear. 2018 Jan 13;5(1):e000668.

77. Eidi A, Mortazavi P, Moradi F, Rohani AH, Safi S. **Magnesium attenuates carbon tetrachloride-induced hepatic injury in rats**. Magnes Res. 2014;26(4):165–75.

78. Eshraghi T, Eidi A, Mortazavi P, Asghari A, Tavangar SM. **Magnesium protects against bile duct ligation-induced liver injury in male Wistar rats**. Magnes Res. 2015;28(1):32–45.

79. Schneider-Poetsch T, Ju J, Eyler DE, Dang Y, Bhat S, Merrick WC, et al. **Inhibition of eukaryotic translation elongation by cycloheximide and lactimidomycin**. Nat Chem Biol. 2010 Mar 31;6(3):209–17.

80. Porter LE, Elm MS, Van Thiel DH, Eagon PK. **Hepatic estrogen receptor in human liver disease**. Gastroenterology. 1987;92(3):735–45.

81. Sahu SC. **Hepatotoxicity : from genomics to in vitro and in vivo models** [Internet]. Chichester, England; Hoboken, NJ: John Wiley & Sons; 2007.

82. Takayama K, Morisaki Y, Kuno S, Nagamoto Y, Harada K, Furukawa N, et al. **Prediction of interindividual differences in hepatic functions and drug sensitivity by using human iPS-derived hepatocytes**. Proc Natl Acad Sci U S A. 2014;111(47):16772–7.

83. Verhaag EM, Buist-Homan M, Koehorst M, Groen AK, Moshage H, Faber KN. **Hormesis in cholestatic liver disease; Preconditioning with low bile acid concentrations protects against bile acid- induced toxicity**. PLoS One. 2016;11(3).

84. Kuang J, Yan X, Genders AJ, Granata C, Bishop DJ. **An overview of technical considerations when using quantitative real-time PCR analysis of gene expression in human exercise research**. Kalendar R, editor. PLoS One. 2018 May 10;13(5):1–27.

85. Ou QQ, Qian XH, Li DY, Zhang YX, Pei XN, Chen JW, et al. **Yinzhihuang attenuates ANIT-induced intrahepatic cholestasis in rats through upregulation of Mrp2 and Bsep expressions**. Pediatr Res. 2016;79(4):589–95.

86. Afroz F, Jonkman E, Hua J, Kist A, Zhou Y, Sokoya EM, et al. **Evidence that decreased expression of sinusoidal bile acid transporters accounts for the inhibition by rapamycin of bile flow recovery following liver ischemia**. Eur J Pharmacol. 2018;838(May):91–106.

87. Kagawa T, Watanabe N, Mochizuki K, Numari A, Ikeno Y, Itoh J, et al. **Phenotypic differences in PFIC2 and BRIC2 correlate with protein stability of mutant Bsep and impaired taurocholate secretion in MDCK II cells**. Am J Physiol Liver Physiol. 2007;294(1):G58–67.

88. Yu L, Liu X, Li X, Yuan Z, Yang H, Zhang L, et al. **Protective effects of SRT1720 via the HNF1α/FXR signalling pathway and anti-inflammatory mechanisms in mice with estrogen-induced cholestatic liver injury**. Toxicol Lett. 2016;

89. Martinot E, Sèdes L, Baptissart M, Lobaccaro JM, Caira F, Beaudoin C, et al. **Bile acids and their receptors**. Mol Aspects Med. 2017;56:2–9.

90. Crocenzi FAFA, Zucchetti AE, Boaglio AC, Barosso IR, Sanchez Pozzi EJ, Mottino AD, et al. **Localization status of hepatocellular transporters in cholestasis**. Front Biosci. 2012;17(1):1201.

91. Jones H, Alpini G, Francis H. **Bile acid signaling and biliary functions**. Vol. 5, Acta Pharmaceutica Sinica B. 2015.

92. Hofmann AF. **Enterohepatic circulation of bile acids**. Handb Physiol - Gastrointest Syst. 1978;19(7):567–96.

93. Heuman DM. **Quantitative estimation of the hydrophilic-hydrophobic balance of mixed bile salt solutions**. J Lipid Res. 1989;30(5):719–30.

94. Thomas C, Pellicciari R, Pruzanski M, Auwerx J, Schoonjans K. **Targeting bile-acid signalling for metabolic diseases.** Nat Rev Drug Discov. 2008;7(8):678–93.

95. Roma MG, Toledo FD, Boaglio AC, Basiglio CL, Crocenzi FA, Sánchez Pozzi EJ. **Ursodeoxycholic acid in cholestasis: Linking action mechanisms to therapeutic applications**. Clin Sci. 2011;121(12):523–44.

96. Hanafi NI, Mohamed AS, Kadir SHSA, Othman MHD. **Overview of bile acids signaling and perspective on the signal of ursodeoxycholic acid, the most hydrophilic bile acid, in the heart**. Biomolecules. 2018;8(4):1–19.

97. Paumgartner G, Beuers U. **Ursodeoxycholic acid in cholestatic liver disease: Mechanisms of action and therapeutic use revisited**. Hepatology. 2002;36(3):525–31.

98. Parks DJ. **Bile Acids: Natural Ligands for an Orphan Nuclear Receptor**. Science (80-). 1999;284(5418):1365–8.

99. Ellis E, Axelson M, Abrahamsson A, Eggertsen G, Thörne A, Nowak G, et al. **Feedback**

regulation of bile acid synthesis in primary human hepatocytes: Evidence that CDCA is the strongest inhibitor. Hepatology. 2003;38(4):930–8.

100. Glossmann Ha. **The Bile Acid Metabolome in Humans and Rodents Hartmut**. biocrates life Sci. 2015;

101. Higashiyama H, Uemura M, Igarashi H, Kurohmaru M, Kanai-Azuma M, Kanai Y. **Anatomy and development of the extrahepatic biliary system in mouse and rat: a perspective on the evolutionary loss of the gallbladder**. J Anat. 2018 Jan;232(1):134–45.

102. Sayin SI, Wahlström A, Felin J, Jäntti S, Marschall HU, Bamberg K, et al. **Gut microbiota regulates bile acid metabolism by reducing the levels of tauro-beta-muricholic acid, a naturally occurring FXR antagonist**. Cell Metab. 2013;17(2):225–35.

103. Sharanek A, Burban A, Humbert L, Bachour-El Azzi P, Felix-Gomes N, Rainteau D, et al. **Cellular accumulation and toxic effects of bile acids in cyclosporine a-treated hepaRG hepatocytes**. Toxicol Sci. 2015;147(2):573–87.

104. Luo L, Aubrecht J, Li D, Warner RL, Johnson KJ, Kenny J, et al. **Assessment of serum bile acid profiles as biomarkers of liver injury and liver disease in humans**. PLoS One. 2018;13(3):1–17.

105. Jean-Louis S, Akare S, Ali MA, Mash EA, Meuillet E, Martinez JD. **Deoxycholic acid induces intracellular signaling through membrane perturbations**. J Biol Chem. 2006;281(21):14948–60.

106. Kis E, Nagy T, Szente L, Here K, Ioja E, Nagy T, et al. **Effect of Membrane Cholesterol on BSEP / Bsep Activity : Species Specificity Studies for Substrates and Inhibitors ABSTRACT :** Drug Metab Dispos. 2009;37(9):1878–86.

107. Centuori SM, Gomes CJ, Trujillo J, Borg J, Brownlee J, Putnam CW, et al. **Deoxycholic acid mediates non-canonical EGFR-MAPK activation through the induction of calcium signaling in colon cancer cells**. Biochim Biophys Acta - Mol Cell Biol Lipids. 2016;1861(7):663–70.

108. Ma C, Han M, Heinrich B, Fu Q, Zhang Q, Sandhu M, et al. **Gut microbiome–mediated bile acid metabolism regulates liver cancer via NKT cells**. Science (80-). 2018 May 25;360(6391):eaan5931.

109. Legido-Quigley C, Mcdermott L, Vilca-Melendez H, Murphy GM, Heaton N, Lindon JC, et al. **Bile UPLC-MS fingerprinting and bile acid fluxes during human liver transplantation**. Electrophoresis. 2011;32(15):2063–70.

110. Wymann MP, Schneiter R. **Lipid signalling in disease**. Nat Rev Mol Cell Biol. 2008;9(2):162–76.

111. Van Meer G, Voelker DR, Feigenson GW. **Membrane lipids: where they are**. Nat Rev Mol Cell Biol. 2009;101(1):1–4.

112. Komoda T, Matsunaga T, Komoda T, Matsunaga T. **Metabolic Pathways in the Human**

Body. Biochem Med Prof. 2015 Jan 1 [cited 2019 Sep 11];25–63.

113. Kanehisa M. **Toward understanding the origin and evolution of cellular organisms**. Protein Sci. 2019;

114. Kanehisa M, Sato Y, Furumichi M, Morishima K, Tanabe M. **New approach for understanding genome variations in KEGG**. Nucleic Acids Res. 2019;47(D1):D590–5.

115. Kanehisa M. **KEGG: Kyoto Encyclopedia of Genes and Genomes**. Nucleic Acids Res. 2000 Jan 1;28(1):27–30.

116. Stark AH, Reifen R, Crawford MA. **Past and Present Insights on Alpha-linolenic Acid and the Omega-3 Fatty Acid Family**. Crit Rev Food Sci Nutr. 2016;56(14):2261–7.

117. VanRollins M, Baker RC, Sprecher HW, Murphy RC. **Oxidation of docosahexaenoic acid by rat liver microsomes**. J Biol Chem. 1984;259(9):5776–83.

118. Li Y, Lin N, Xu J, Lu Y, Chen S, Pan C, et al. **Measurement of Serum and Hepatic Eicosanoids by Liquid Chromatography Tandem-Mass Spectrometry (LC-MS/MS) in a Mouse Model of Hepatocellular Carcinoma (HCC) with Delivery of c-Met and Activated β-Catenin by Hepatocyte Hydrodynamic Injection**. Med Sci Monit. 2018 Mar 21;24:1670–9.

119. Stanford KI, Lynes MD, Takahashi H, Baer LA, Arts PJ, May FJ, et al. **12,13-diHOME: An Exercise-Induced Lipokine that Increases Skeletal Muscle Fatty Acid Uptake**. Cell Metab. 2018;27(5):1111–1120.e3.

120. Hampel JKA, Brownrigg LM, Vignarajah D, Croft KD, Dharmarajan AM, Bentel JM, et al. **Differential modulation of cell cycle, apoptosis and PPARγ2 gene expression by PPARγ agonists ciglitazone and 9-hydroxyoctadecadienoic acid in monocytic cells**. Prostaglandins Leukot Essent Fat Acids. 2006;74(5):283–93.

121. Thompson DA, Hammock BD. **Dihydroxyoctadecamonoenoate esters inhibit the neutrophil respiratory burst**. J Biosci. 2007;32(2):279–91.

122. Lecka-czernik B, Moerman EJ, Grant DF, Manolagas SC, Jilka RL. **Divergent Effects of Selective Peroxisome Proliferator-**. Endocrinology. 2002;143(13):2376–84.

123. Ha J, Dobretsov M, Kurten RC, Grant DF, Stimers JR. **Effect of linoleic acid metabolites on Na+/K+ pump current in N20.1 oligodendrocytes: Role of membrane fluidity**. Toxicol Appl Pharmacol. 2002;182(1):76–83.

124. Lecour S, Smith RM, Woodward B, Opie LH, Rochette L, Sack MN. **Identification of a novel role for sphingolipid signaling in TNFα and ischemic preconditioning mediated cardioprotection**. J Mol Cell Cardiol. 2002;34(5):509–18.

125. Ansari KM, Sung YM, He G, Fischer SM. **Prostaglandin receptor EP2 is responsible for cyclooxygenase-2 induction by prostaglandin E2 in mouse skin**. Carcinogenesis. 2007;28(10):2063–8.

126. Kiezel-Tsugunova M, Kendall AC, Nicolaou A. **Fatty acids and related lipid mediators in the regulation of cutaneous inflammation**. Biochem Soc Trans. 2018;46(1):119–29.

127. Kwong E, Li Y, Hylemon PB, Zhou H. **Bile acids and sphingosine-1-phosphate receptor 2 in hepatic lipid metabolism**. Acta Pharm Sin B. 2015;5(2):151–7.

128. Vance DE, Vance JE, Merrill AH. **Biochemistry of Lipids, Lipoproteins and Membranes (5th Edn.) Sphingolipids**. Biochem Lipids, Lipoproteins Membr. 2008;363–97.

129. Bilzer M, Roggel F, Gerbes AL. **Role of Kupffer cells in host defense and liver disease**. Liver Int. 2006;26(10):1175–86.

130. Hendriks DFG, Fredriksson Puigvert L, Messner S, Mortiz W, Ingelman-Sundberg M, Stevens JL, et al. **Hepatic 3D spheroid models for the detection and study of compounds with cholestatic liability**. Sci Rep. 2016;6(July).

131. Ju C, Reilly TP, Bourdi M, Radonovich MF, Brady JN, George JW, et al. **Protective role of kupffer cells in acetaminophen-induced hepatic injury in mice**. Chem Res Toxicol. 2002;15(12):1504–13.

132. Zhang Y, Guallar E, Blasco-Colmenares E, Harms AC, Vreeken RJ, Hankemeier T, et al. **Serum-based oxylipins are associated with outcomes in primary prevention implantable cardioverter defibrillator patients**. PLoS One. 2016;11(6):1–12.

133. Gouveia-Figueira S, Späth J, Zivkovic AM, Nording ML. **Profiling the oxylipin and endocannabinoid metabolome by UPLC-ESI-MS/MS in human plasma to monitor postprandial inflammation**. PLoS One. 2015;10(7):1–29.

134. Montanari F, Pinto M, Khunweeraphong N, Wlcek K, Sohail MI, Noeske T, et al. **Flagging Drugs That Inhibit the Bile Salt Export Pump**. Mol Pharm. 2016;13(1):163–71.

135. Chan R, Benet LZ. **Measures of BSEP inhibition in vitro are not useful predictors of DILI**. Toxicol Sci. 2018;162(2):499–508.

136. Idakwo G, Luttrell J, Chen M, Hong H, Zhou Z, Gong P, et al. **A review on machine learning methods for in silico toxicity prediction**. J Environ Sci Heal - Part C Environ Carcinog Ecotoxicol Rev. 2018;36(4):169–91.

137. Williams DP, Lazic S, Foster AJ, Semenova E, Morgan P. **Predicting Drug-Induced Liver Injury with Bayesian Machine Learning**. Chem Res Toxicol. 2019 Sep 19;acs.chemrestox.9b00264.

138. Mazzei L, Ciurli S, Zambelli B. **Hot biological catalysis: Isothermal titration calorimetry to characterize enzymatic reactions**. J Vis Exp. 2014;(86):1–8.

139. Nagana Gowda GA, Shanaiah N, Cooper A, Maluccio M, Raftery D. **Bile acids conjugation in human bile is not random: New insights from 1H-NMR spectroscopy at 800 MHz**. Lipids. 2009;44(6):527–35.

140. Ali I, Khalid S, Stieger B, Brouwer KLR. **Effect of a Common Genetic Variant (p.V444A) in the Bile Salt Export Pump on the Inhibition of Bile Acid Transport by Cholestatic Medications**. Mol Pharm. 2019 Mar 4;16(3):1406–11.

141. Gröber U. **Magnesium and Drugs**. Int J Mol Sci. 2019 Apr 28;20(9):2094.

142. Romani AMP. **Intracellular magnesium homeostasis**. Magnes Cent Nerv Syst. 2011;512(1):13–58.

143. Loria P, Carulli N, Medici G, Tripodi A, Iori R, Rovesti S, et al. **Determinants of bile secretion: Effect of bile salt structure on bile flow and biliary cation secretion**. Gastroenterology. 1989 Apr;96(4):1142–50.

144. Patel T, Bronk SF, Gores GJ. **Increases of intracellular magnesium promote glycodeoxycholate-induced apoptosis in rat hepatocytes**. J Clin Invest. 1994;94(6):2183–92.

145. Bell CC, Dankers ACA, Lauschke VM, Sison-Young R, Jenkins R, Rowe C, et al. **Comparison of Hepatic 2D Sandwich Cultures and 3D Spheroids for Long-term Toxicity Applications: A Multicenter Study**. Toxicol Sci. 2018 Apr 1;162(2):655–66.

146. Pan C, Kumar C, Bohl S, Klingmueller U, Mann M. **Comparative proteomic phenotyping of cell lines and primary cells to assess preservation of cell type-specific functions**. Mol Cell Proteomics. 2009;8(3):443–50.

147. Proctor WR, Foster AJ, Vogt J, Summers C, Middleton B, Pilling MA, et al. **Utility of spherical human liver microtissues for prediction of clinical drug-induced liver injury**. Arch Toxicol. 2017;91(8).

148. Letzsch S, Böttcher K. **Imaging Bile Canaliculi in 3D Liver Microtissues using the Opera Phenix High Content Screening System**. PerkinElmer Appl Note. 2015;

149. Andersson TB. **Evolution of Novel 3D Culture Systems for Studies of Human Liver Function and Assessments of the Hepatotoxicity of Drugs and Drug Candidates**. Vol. 121, Basic and Clinical Pharmacology and Toxicology. 2017.

150. Lauschke VM, Hendriks DFG, Bell CC, Andersson TB, Ingelman-Sundberg M. **Novel 3D Culture Systems for Studies of Human Liver Function and Assessments of the Hepatotoxicity of Drugs and Drug Candidates**. Chem Res Toxicol. 2016 Dec 19;29(12):1936–55.

151. Nguyen TT, Ung TT, Kim NH, Jung Y Do. **Role of bile acids in colon carcinogenesis**. World J Clin Cases. 2018;6(13):577–88.

152. Popper H, Zhu C, Fuchs CD, Halilbasic E, Trauner M. **Bile acids in regulation of inflammation and immunity: friend or foe?** Clin Exp Rheumatol. 2016;34(20):25–31.

153. Pan X, Elliott CT, McGuinness B, Passmore P, Kehoe PG, Hölscher C, et al. **Metabolomic profiling of bile acids in clinical and experimental samples of Alzheimer's disease**. Metabolites. 2017;7(2):1–12.

154. Oizumi K, Sekine S, Fukagai M, Susukida T, Ito K. **Identification of Bile Acids Responsible for Inhibiting the Bile Salt Export Pump, Leading to Bile Acid Accumulation and Cell Toxicity in Rat Hepatocytes**. J Pharm Sci. 2017 Sep;106(9):2412–9.

155. Song P, Zhang Y, Klaassen CD. **Dose-response of five bile acids on serum and liver bile**

acid concentrations and hepatotoxicty in mice. Toxicol Sci. 2011;123(2):359–67.

156. Alrefai WA, Gill RK. **Bile acid transporters: Structure, function, regulation and pathophysiological implications**. Pharm Res. 2007;24(10):1803–23.

157. Kipp H, Pichetshote N, Arias IM. **Transporters on demand. Intrahepatic pools of canalicular ATP binding cassette transporters in rat liver**. J Biol Chem. 2001;276(10):7218–24.

158. Azaripour A, Lagerweij T, Scharfbillig C, Jadczak AE, Willershausen B, Van Noorden CJF. **A survey of clearing techniques for 3D imaging of tissues with special reference to connective tissue**. Prog Histochem Cytochem. 2016;51(2):9–23.

159. Nguyen T V., Ukairo O, Khetani SR, McVay M, Kanchagar C, Seghezzi W, et al. **Establishment of a Hepatocyte-Kupffer Cell Coculture Model for Assessment of Proinflammatory Cytokine Effects on Metabolizing Enzymes and Drug Transporters**. Drug Metab Dispos. 2015 May;43(5):774–85.

160. Khetani SR, Berger DR, Ballinger KR, Davidson MD, Lin C, Ware BR. **Microengineered Liver Tissues for Drug Testing**. J Lab Autom. 2015;20(3):216–50.

161. Sosa-Hernández JE, Villalba-Rodríguez AM, Romero-Castillo KD, Aguilar-Aguila-Isaías MA, García-Reyes IE, Hernández-Antonio A, et al. **Organs-on-a-chip module: A review from the development and applications perspective**. Micromachines. 2018;9(10).

162. Byrne JA, Strautnieks SS, Ihrke G, Pagani F, Knisely AS, Linton KJ, et al. **Missense mutations and single nucleotide polymorphisms in ABCB11 impair bile salt export pump processing and function or disrupt pre-messenger RNA splicing**. Hepatology. 2009;49(2):553–67.

163. Liu T, Wang R, Han J, Hao C, Qiu Y, Yan Y, et al. **Comprehensive bile acid profiling in hereditary intrahepatic cholestasis: Genetic and clinical correlations**. Liver Int. 2018 Sep 12;38(9):1676–85.

164. Vitale G, Gitto S, Raimondi F, Mattiaccio A, Mantovani V, Vukotic R, et al. **Cryptogenic cholestasis in young and adults: ATP8B1, ABCB11, ABCB4, and TJP2 gene variants analysis by high-throughput sequencing**. J Gastroenterol. 2018;53(8):945–58.

165. Li L, Deheragoda M, Lu Y, Gong J, Wang J. **Hypothyroidism Associated with ATP8B1 Deficiency**. J Pediatr. 2015;167(6):1334–1339.e1.

166. Chen HL, Liu YJ, Su YN, Wang NY, Wu SH, Ni YH, et al. **Diagnosis of BSEP/ABCB11 Mutations in Asian Patients with Cholestasis Using Denaturing High Performance Liquid Chromatography**. J Pediatr. 2008;153(6).

167. Lang T, Haberl M, Jung D, Drescher A, Schlagenhaufer R, Keil A, et al. **Genetic variability, haplotype structures, and ethnic diversity of hepatic transporters MDR3 (ABCB4) and bile salt export pump (ABCB11)**. Drug Metab Dispos. 2006;34(9):1582–99.

168. Telbisz Á, Homolya L. **Recent advances in the exploration of the bile salt export pump**

(BSEP/ABCB11) function. Expert Opin Ther Targets. 2015;20(4):1–14.

169. Tanaka Y, Wake N, Kato K. **Letters to the Editor: Clinical variability of mutations in the ABCB11 gene: A case report**. Menopause. 2009 Mar;16(2):424.

170. Mosesson Y, Yarden Y. **Monoubiquitylation: a recurrent theme in membrane protein transport.** Isr Med Assoc J. 2006 Apr;8(4):233–7.

171. Hayashi H, Sugiyama Y. **Short-Chain Ubiquitination Is Associated with the Degradation Rate of a Cell-Surface-Resident Bile Salt Export Pump (BSEP/ABCB11)**. Mol Pharmacol. 2009;75(1):143–50.

172. Wang L, Soroka CJ, Boyer JL. **The role of bile salt export pump mutations in progressive familial intrahepatic cholestasis type II**. J Clin Invest. 2002;110(7):965–72.

173. Trauner M, Boyer JL. **Bile Salt Transporters : Molecular Characterization , Function , and Regulation TRANSPORT**. Physiol Rev. 2003;83:633–71.

174. Ito K, Suzuki H, Horie T, Sugiyama Y. **Apical/basolateral surface expression of drug transporters and its role in vectorial drug transport**. Pharm Res. 2005;22(10):1559–77.

175. Noe J, Kullak-Ublick GA, Jochum W, Stieger B, Kerb R, Haberl M, et al. **Impaired expression and function of the bile salt export pump due to three novel ABCB11 mutations in intrahepatic cholestasis**. J Hepatol. 2005;

176. Hu G, He P, Liu Z, Chen Q, Zheng B, Zhang Q. **Diagnosis of ABCB11 gene mutations in children with intrahepatic cholestasis using high resolution melting analysis and direct sequencing**. Mol Med Rep. 2014;10(3):1264–74.

177. Stindt J, Ellinger P, Weissenberger K, Dröge C, Herebian D, Mayatepek E, et al. **A novel mutation within a transmembrane helix of the bile salt export pump (BSEP, ABCB11) with delayed development of cirrhosis**. Liver Int. 2013;33(10):1527–35.

178. Keitel V, Vogt C, Häussinger D, Kubitz R. **Combined Mutations of Canalicular Transporter Proteins Cause Severe Intrahepatic Cholestasis of Pregnancy**. Gastroenterology. 2006;

179. Liu LY, Wang XH, Lu Y, Zhu QR, Wang JS. **Association of variants of ABCB11 with transient neonatal cholestasis**. Pediatr Int. 2013;55(2):138–44.

180. Aamann L, Ørntoft N, Vogel I, Grønbaek H, Becher N, Vilstrup H, et al. **Unexplained cholestasis in adults and adolescents: diagnostic benefit of genetic examination**. Scand J Gastroenterol. 2018;53(3):305–11.

181. Noé J, Stieger B, Meier PJ. **Functional Expression of the Canalicular Bile Salt Export Pump of Human Liver**. Gastroenterology. 2002;1213:1659–66.

182. Gomez-Ospina N, Potter CJ, Xiao R, Manickam K, Kim MS, Kim KH, et al. **Mutations in the nuclear bile acid receptor FXR cause progressive familial intrahepatic cholestasis**. Nat Commun. 2016;7:1–8.

183. Wang N-L, Qiu Y-L, Guan W-C, Li G, Lu Y, Zhang M-H, et al. **Splicing analysis of rare/novel synonymous or intronic variants identified in *ABCB11* heterozygotes presenting as progressive intrahepatic cholestasis with low γ-glutamyltransferase**. Hepatol Res. 2018;48(7):574–84.

184. Hillgren KM, Keppler D, Zur AA, Giacomini KM, Stieger B, Cass CE, et al. **Emerging transporters of clinical importance: An update from the international transporter consortium**. Clin Pharmacol Ther. 2013;94(1):52–63.

185. Pauli-magnus C, Lang T, Meier Y, Zodan-marin T, Jung D, Breymann C, et al. **Sequence analysis of bile salt export pump (ABCB11) and patients with intrahepatic cholestasis of pregnancy**. Pharmacogenetics. 2003;3.

186. Piątek K, Kurzawińska G, Magiełda J, Drews K, Barlik M, Malewski Z, et al. **The role of ABC transporters' gene polymorphism in the etiology of intrahepatic cholestasis of pregnancy**. Ginekol Pol. 2018;89(7):393–7.

187. Boyer JL. **Bile formation and secretion.** In: Comprehensive Physiology. Hoboken, NJ, USA: John Wiley & Sons, Inc.; 2013. p. 1035–78.

188. Wadsworth CA, Dixon PH, Wong JH, Chapman MH, McKay SC, Sharif A, et al. **Genetic factors in the pathogenesis of cholangiocarcinoma**. Dig Dis. 2011;29(1):93–7.

189. Keitel V, Burdelski M, Vojnisek Z, Schmitt L, Häussinger D, Kubitz R. **De novo bile salt transporter antibodies as a possible cause of recurrent graft failure after liver transplantation: A novel mechanism of cholestasis**. Hepatology. 2009;50(2):510–7.

190. Strautnieks SS, Bull LN, Knisely a S, Kocoshis S a, Dahl N, Arnell H, et al. **A gene encoding a liver-specific ABC transporter is mutated in progressive familial intrahepatic cholestasis.** Nat Genet. 1998;20(3):233–8.

191. Strautnieks SS, Byrne JA, Pawlikowska L, Cebecauerová D, Rayner A, Dutton L, et al. **Severe Bile Salt Export Pump Deficiency: 82 Different ABCB11 Mutations in 109 Families**. Gastroenterology. 2008;

192. Sohail MI, Schmid D, Wlcek K, Spork M, Szakács G, Trauner M, et al. **Molecular Mechanism of Taurocholate Transport by the Bile Salt Export Pump, an ABC Transporter Associated with Intrahepatic Cholestasis**. Mol Pharmacol. 2017;92(4):401–13.

193. Imagawa K, Hayashi H, Sabu Y, Tanikawa K, Fujishiro J, Kajikawa D, et al. **Clinical phenotype and molecular analysis of a homozygous ABCB11 mutation responsible for progressive infantile cholestasis**. J Hum Genet. 2018;569–77.

194. Qiu X, Zhang Y, Liu T, Shen H, Xiao Y, Bourner MJ, et al. **Disruption of BSEP Function in HepaRG Cells Alters Bile Acid Disposition and Is a Susceptive Factor to Drug-Induced Cholestatic Injury**. Mol Pharm. 2016;

List of Tables

List of Figures

List of Figures

List of Figures

List of Appendices

Appendix A. Summary of mutations

*Mutations without a literature refence were mined from

https://www.ncbi.nlm.nih.gov/variation/view/

** missense mutations without description are only mention in article but not investigated further.

mutation	description
M1V	Heterozygous for M1V and R387H without other mutations, no information about biliary BA concentration or staining. [51]
G19R	[34]
V43I	[34]
L50S	[162]
R52W	Heterozygous for R52W with a second mutation at H615R had reduced staining for IHC anti-BSEP at canaliculi [50]
S56L	[34]
M62K	[51]
C68Y	[34]
L71H	no information about symptoms of the patient. L71H was present in combination with S226L [163] immunostaining of BSEP revealed an absence
V79E	
L80P	
T87R	[34]
Y93S	Y93S together with V597L and R1128C in patients presenting with history of neonatal jaundice, DIC, ICP, juvenile cholelithiasis, itching [164]
C107R	[34]
I112T	[51]
I112V	[165]
W114R	[34][51] heterozygous for this mutation no second mutation was found, biliary BA concentration was reduced (0.5) and staining for BSEP at canaliculi was negative.
Q121K	[34]
M123T	[34]
R128H	[34]
E135K	[23,34,50,164] has been reported to produce mature BSEP protein but with some reduction in the protein levels. [50] while it should not produce structural changes the E135K mutation might cause changes in N-glycosylation of the nearby asparagines 109, 116, 122, 125 that have been reported to undergo the post-translational modification.
E137K	present in a patient with recurrent cholestasis 6Y, together with a P740Qfs*6 [34,163] Immunostaining of BSEP was not present
Y157C	[34]
A167V	[34,162]

A167T	Biliare BA 0.5, BSEP not present in immunohistochemistry staining [51] was identified in patient together with G1058HfsX38 on the second allele and together was also determined to be heterozygous for V444A and heterozygous for M677V
A168D	
R181I	[165]
I182K	[34,51]
M183T	[34,51]
M183V	[34,51,166] patient positive heterozygous with second mutation G455E, harbouring the homozygous ABCB11 mutation p.V444A and harboured, the homozygous ATP8B1 mutation p.R952Q. no further information available.
W186G	
G188W	only mentioned/no further information in this article[34]
S194P	[34]
L198P	[34]
I206V	[23,34,167,168]
A212T	Patient died at the age of 1.5Y. immunostaining was not done and A212T was present in combination with Q546H and E238D [163]
M217R	[34]
R223C	[34]
S226L	Homozygous for this mutations as well as homozygous for V444A, no information about biliary flow or staining at canalicular site [51], no canalicular staining present. Biliary BA reduced. no information about symptoms of the patient. L71H was present in combination with S226L [163] immunostaining of BSEP revealed an absence
L233S	[169]
C236S	
G238V	Homozygous for this mutation, [51] Led to a reduced expression at the apical membrane, when expressed in MDCK cells [23].
T242I	
G253R	
A257G	
A257V	[31] patient that was heterozygous for this mutation and G982R mutation and a homozygous mutations for V444A, no further information was available [51].
G260D	[34]
Y267M	
A277E	
E283D	Patient died at the age of 1.5Y. immunostaining was not done and A212T was present in combination with Q546H and E238D [163]
V284A	[34,55,167]
V284L	
I285T	
T290R	
V291A	
G295C	[34]

G295R	[34]
G295S	[34]
E297G	a decrease in half-life may shorten residency of BSEP at the canalicular membrane[34], [170] A higher proportion of short-chain ubiquitination was observed in $BSEP^{E297G}$ and $BSEP^{D482G}$ as compared to wild type BSEP suggesting that ubiquitin dependent degradation is involved in the reduction of transporter half live [171] patient that was homozygous for this mutation and V444A showed reduced (0.80) biliary BA concentration, BSEP staining at canaliculi was negative. A second patient heterozygous for E297G and S699P with the homozygous V444A mutation was identified, no information about biliary BA concentration or BSEP staining. [51] BSEP genotype could also have a predictive value because the PFIC2 patient with BD success had a homozygous p.E297G mutation and two other PFIC2 patients with BD partial failure harboured on one allele the p.E297G mutation. [51] This mutant is known to be associated with impaired membrane trafficking but to retain some transport activity when correctly targeted. The with impaired membrane trafficking but to retain some transport activity when correctly targeted [51]. Led to a reduced expression at the apical membrane, when expressed in MDCK cells [23]. Homozygosity is linked to PFIC-2, heterozygosity was detected in 1.4% of 491 patients with ICP [23].
E297K	
R299K	[34,167]
R303K	
R303G	[34]
Q312H	[34]
R313S	[34]
G327E	
W330R	[34]
C336S	[34,168,172–175]
Y337H	[176]
L339V	[34]
W342G	[34]
G374S	Siblings with the homozygous mutation, development of liver cirrhosis was delayed and occurred after childhood. Amino acid 374 is part of the putative sixth transmembrane helix and lies in vicinity to the channel pore, which may explain the severely reduced transport capacity of BSEP [23,34,177] showed an increased membrane expression of BSEP (as compared to wild type BSEP) despite the severity of the phenotype [23,34]
N375S	
A382G	

R387H	Heterozygous for M1V and R387H without other mutations, no information about biliary BA concentration or staining[51]
A389P	[34]
A390P	
G410D	
L413W	
R415Q	
I420T	
H423R	[34]variant of uncertain significance found in patient with high GGT without fibrosis [164]
R432T	
P433A	[34,164]
D440E	
V444A	The frequent BSEP polymorphism p.V444A represents the mildest form of BSEP deficiency[23]. The allele frequency of c.1331T>C (p. V444A) was 76% in patients with DILI as compared to 59% in controls with an odds ratio of 4.0 [23]. Has been linked to ICP. The C-allele is more frequent in ICP-patients as compared to healthy pregnant women [34] and also predisposes for the development of drug-induced liver injury (DILI). common explanation for the relation between p.V444A and ICP or DILI is a decreased expression of BSEP in the presence of the polymorphism as shown in a small cohort. BSEP expression may be severely reduced in MDR3- dependent ICP when p.V444A is present and p.V444A may influence development of liver fibrosis in patients with chronic hepatitis C infection. In a recent study a higher prevalence of p.V444A was observed in Cholangiocarcinoma-patients. Patients with ICP or CIC have higher prevalence of V444A [23]. If V444A was present in combination with G982R and Y818F, complete degradation of triple-mutated BSEP via ERAD was observed [23]. Further-more, hepatitis C infected patients, who are homozygous for valine of p.V444A have less severe liver fibrosis and some but not all HCV-cohorts show better treatment responses towards interferon/ribavirin treatment [23].
V444D	[23,31,34,51,53,55,72,164,166–168,177–187] A role of BSEP for the development of CC was also suggested on the basis of an association to the BSEP polymorphism V444A in a study of 172 CC patients. [188] frequency ~50%, which may occur iso allelic to mutations, strongly increases ERAD, as shown in expression studies of cloned BSEP [189]
V444G	[34]
V454L	[34]
G455E	patient positive heterozygous with second mutation G455E, harboring the homozygous ABCB11 mutation p.V444A and harboured, the homozygous ATP8B1 mutation p.R952Q. no further information available [51]
A459V	
K461E	[34]
Q463I	

Q466K	[34,87,190]
I469I	[34,191]
R470Q	Two patients with homozygous expression of R470Q, no further information [50]
Y472C	
V481E	
D481Q	
D482G	A decrease in half-life may shorten residency of BSEP at the canalicular membrane [34] [170]A higher proportion of short-chain ubiquitination was observed in $BSEP^{E297G}$ and $BSEP^{D482G}$ as compared to wild type BSEP suggesting that ubiquitin dependent degradation is involved in the reduction of transporter half live [171] patient homozygous for D482G showed negative staining for IHC anti-BSEP at canaliculi [50] Homozygosity was linked to PFIC-2 and heterozygosity detected in 1.4% of 491 patients with ICP [23] splicing and exon skipping was reported for this typical PFIC-2 mutation [23]
R487P	
R487H	[34]
R487L	[34]
N490D	[34]
I498T	[34,191]
G499E	[34,54,163]
G499E	[34]
T510T	[34]
I512T	
N515T	[34]
R517H	
A523G	two sisters with likely pathogenic homozygous mutation: both had a history of neonatal jaundice, itching and DIC [164]
M525V	[34,191]
I528T	
F540L	
I541T	[34]
I541L	Two patients both homozygous for I541L, was negative for IHC staining at canaliculi [50]
Q546H	Patient died at the age of 1.5Y. immunostaining was not done and A212T was present in combination with Q546H and E238D [34,163,191]
Q546K	
F548Y	
D549V	
G556R	[34]
G557D	[34]
G557G	
Q558H	only mentioned/no further information in this article[34]
G562D	

V567I	[23,34,168,186]
A570T	Heterozygous for I669V with a second mutation at A570T, was negative for IHC BSEP staining. [50] A patient homozygous for this mutation was negative for IHC staining for BSEP[50] This mutation introduces a steric hindrance that interferes with the packing of three helices formed by residues 512-519, 525-534 and 561-575 in the first ABC transporter domain The two 'BRIC-2 mutations' p.A570T and p.R1050C had lower expression levels than the 'ICP mutation' p.N591S, but higher expression levels as compared to the PFIC-2 mutations p.D482G and p.E297G [23]
A570V	
N576S	
L581F	
M584E	[34]
M584I	[192]
T586I	
A588V	
D590G	[23,34]
N591S	Canalicular expression of BSEP with the ''typical'' ICP mutation p.N591S was higher than that of the BRIC-2 (p.A570T, p.R1050 C) or PFIC-2 mutations (p.D482G, p.E297G) [34],6] Recently, a neonate has been described with homozygosity for p.N591S and, in addition, a homozygous mutation (p.H338Y) in the SLC27A5 gene. SLC27A5. This child presented with liver fibrosis within the first year of life, while a sibling was free of symptoms although it had the same homozygous SLC27A5 mutation, while it was heterozygous for p.N591S [151], demonstrating a ''dose effect'' of N591S. [34]
E592Q	[192]
S593R	[34]
V597L	[34], Y93S together with V597L and R1128C in patients presenting with history of neonatal jaundice, DIC, ICP, juvenile choleithiasis, itching [164]
V597V	[164]
V597M	[51]
L601P	[34]
H615R	Heterozygous for R52W with a second mutation at H615R had reduced staining for IHC anti-BSEP at canaliculi [50] H615R was inherited from the mother (look up for negative effects, while R52W was a *de novo* mutation.
R616G	In particular, ABCB11 p.R616G is suspicious for changing the physicochemical properties of the resulting protein (highest Grantham score of 125) is probably deleterious according to the low SIFT value (0.01), is supposed to affect protein function because of its high PSIC score, and is evolutionarily less favourable considering the negative BLOSUM62 value, although sequence alignments indicated that p.R616G is located in a probably less deleterious, evolutionarily unconserved region [167]
T619A	[34,167]

I627T	[34,167]
A634T	[34]
E636G	
G648V	[34,193]
T655I	[34]
I669V	Heterozygous for I669V with a second mutation at A570T, was negative for IHC BSEP staining. [50]
D676Y	[34]
M677L	[34,55,168,194]
M677V	[34]
R696W	[31,34,51,55,72,164,167,168,185,187]
R696Q	[176]
R698H	[34] heterozygous for R698H and the heterozygous ABCB11 mutation p.V444A, no information about biliary BA concentration but focal positive and negative canalicular staining [51] A second patient heterozygous for R698H, but with homozygous ABCB11 mutation p.V444A and heterozygous ABCB11 mutation p.M677V, there was no information about biliary BA concentration but patient was focal positive and negative canalicular staining [51]
R698C	[34,51,55,167,179]
S699P	A patient heterozygous for E297G and S699P with the homozygous V444A mutation was identified, no information about biliary BA concentration or BSEP staining [51]
S701P	[34]
S704P	[34]
E709K	
P710P	[34]
L712L	[34]
P731S	[34], [167]
G758R	
G766R	
Y818F	[30] caused intracellular retention of BSEP, shown *in vitro* [6] If V444A was present in combination with G982R and Y818F, complete degradation of triple-mutated BSEP via ERAD was observed [23]
L827I	[34], [23]
R832C	Homozygous for R382 mutations showed negative results for IHC anti-BSEP staining at canaliculi. [50]
R832H	
G855R	[34,166]
T859R	
A865V	
A865D	[34,55,168]
Q869P	[34]
S874P	[34]
G877R	[34]
M839V	[34]

S901R	
T923P	[34,193]
A926P	[34]
R928Q	[34] , [23]
Q931P	[179]
E934K	[176]
I939M	
S945N	[34]
R948C	Two patients Heterozygous for R948C with a second mutation at S1027R, not further information. [50]
R958Q	
F959V	[34], [167]
T965S	[34]
K969E	[34]
K969K	
F971L	[178]
Q976R	[34]
Q979D	
G982R	A patient that was heterozygous for this mutation and G982R mutation and a homozygous mutations for V444A, no further information was available [51]. Second patient was heterozygous for this mutation additionally to the silent mutation R1001R, and the heterozygous ABCB11 mutation p.V444A, no information about biliary BA concentrations but canaliculi staining for BSEP was negative. Led to a reduced expression at the apical membrane, when expressed in MDCK cells [23]. Caused intracellular retention of BSEP shown *in vitro* [23]. If V444A was present in combination with G982R and Y818F, complete degradation of triple-mutated BSEP via ERAD was observed [23]
G1003E	
G1004D	
L1006F	
N1009H	[34]
S1027R	Two patients Heterozygous for R948C with a second mutation at S1027R, not further information. [50] p.S1027R replaces a serine with an arginine residue in a transmembrane helix, influencing electrostatic properties and the packing of this helix with adjacent transmembrane helices. [50]
G1032R	[34]
A1044P	[34]
R1050C	Analysis of the effects of p.R1050C mutation revealed an important reduction in BSEP levels and activity [50] research showed the protein expression is reduced by 30 to 50% compared to WT and reduces activity by up to 50% [50] but does not significantly impair the processing.

	It can be seen in article [50] that R1050 (site of the R1050C mutation) is engaged in a salt bridge with Glu734, which helps to anchor the short helix formed by residues 731–735 to the remainder of the protein structure. [50] The two 'BRIC-2 mutations' p.A570T and p.R1050C had lower expression levels than the 'ICP mutation' p.N591S, but higher expression levels as compared to the PFIC-2 mutations p.D482G and p.E297G [23]
L1055P	[34]
R1057C	[34]
Y1064H	[34]
I1078T	
C1083Y	
R1090X	
S1102W	[34,193]
A1110E	
V1112F	
S1114R	
G1116E	[34]
G1116R	[34]
G1116F	[23,34] patient heterozygous for G1116F and R387H, homozygous ABCB11 mutation p.V444A and harbouring compound heterozygous status for ATP8B1 mutations p.R952Q and p.E429A. there was no information about biliary BA concentration or BSEP staining.
C1117Y	[51]
S1120N	
R1128C	
R1128H	Only mentioned [34]. Patient was homozygous for this mutations, showed reduced biliary concentration (0.10), canaliculi staining for BSEP was negative. [51] second patient was also homozygous for this mutation and showed reduced biliary BA concentrations (0.58) and was also negative for BSEP staining at canaliculi. A third patient who was homozygous for this mutations and homozygous mutation for V444A. (due to drop out no information about biliary BA concentration of staining)[51], Y93S together with V597L and R1128C in patients presenting with history of neonatal jaundice, DIC, ICP, juvenile cholelithiasis, itching [164]
D1131V	[34], [23]
S1144R	[176] By the use of an *in vitro* minigene approach, interference with splicing was shown [34]
K1145N	[34], [23]
R1153H	By the use of an *in vitro* minigene approach, interference with splicing was shown [34] Patient with heterozygous for R1153H and R1050C, positive for IHC anti-BSEP staining at canaliculi. [50] p.R1153H mutation of ABCB11 produces severe splicing alteration resulting in only 3% of wild-type-like splicing product. In a patient carrying the homozygous p.R1153H mutation BSEP protein was not detected. [50]

	The p.R1153H produces severe splicing alteration leading to only 3% of WT like splicing product [50] The eventual tiny residual fraction of correctly spliced BSEP protein is not expected to be capable of proper transport activity, since the p.R1153H mutation affects residues interacting with and determining the structure of the Walker motif in the second ABC transporter domain of BSEP. [50] Led to a reduced expression at the apical membrane, when expressed in MDCK cells [23].
R1153C	
R1153G	
S1154P	
M1171T	
N1173D	
I1183T	[34]
E1186K	[34]
L1197G	[23,34,168]
H1198R	[34]
Y1208C	[176]
T1210P	Homozygous for this mutation and V444A, showed reduced biliary concentration and was negative for BSEP canaliculi staining. [51]
N1211D	
V1212F	[34]
G1216A	[34]
E1223D	
E1223Q	[60]
R1226H	[192]
R1226P	
A1228V	
R1231Q	By the use of an *in vitro* minigene approach, interference with splicing was shown [34]
R1231W	By the use of an *in vitro* minigene approach, interference with splicing was shown [34]
L1242I	
D1243G	
E1244Q	[34]
T1256R	[192]
R1268Q	Led to a reduced expression at the apical membrane, when expressed in MDCK cells [23]
A1283A	[4,23,31,34,87,168,172–174,177,190]
A1283V	[167]
G1292V	[34]
G1298R	
Y1311A	[34]
D482G	By the use of an *in vitro* minigene approach, interference with splicing was shown [34]

S1154P	By the use of an *in vitro* minigene approach, interference with splicing was shown [34]

Appendix B. Accompanying table to figure 8

Table 13 Mutation counts according to disease and if the mutations are either located in the cytoplasm, extracellular matrix side or in the helixes. Locations are based on homology models and information on https://www.uniprot.org/uniprot/O95342

	cytoplasm total	extracellular total	helix total	total
PFIC2	90	7	18	102
BRIC2	23	3	1	27
ICP	7	1		8
DILI	1	0	0	1
NFC	12	2	1	15
No disease association	34	2	2	38
other	11	2	1	14
benign	16	0	0	16
association to more than one disease	108	12	9	132
total	177	16	40	264

Appendix C. Information regarding compound sorting

	Cyclosporin	Clobestasol propionate	Alpidem	Bosentan
AZFilters	U	U	C	B
Molecular Weight	1202.611	466.97	404.333	551.614
CLogP	14.36	3.49	5.581	4.167
CLogP error	Very high LogP unrealistic in nature	All fragments measured	Adjusted (1) from measured value	All fragments measured
Polar Surface Area	290.066	86.166	29.96	142.956
Heavy Atom Count	85	32	27	39
Rotatable Bonds	33	4	7	10
H-Bond Donors	5	1	0	2
H-Bond Acceptors	12	4	3	10
Positive charges	0	0	0	0
Basic charges	0	0	0	0
Acid centers	0	0	0	1
	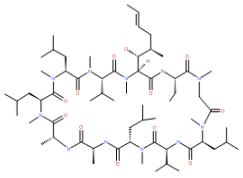	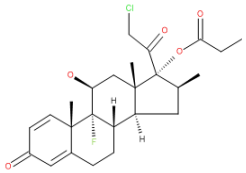	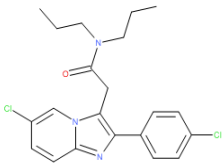	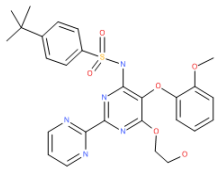
IC50 (uM)	0.5	8.5	9.2	38.1
Ki values	9.5 mol/L			0.000012 mol/L
DILI category	Cholestatic mixed	None	Hepatocellular	Cholestatic mixed

	pioglitazone	troglitazone	ketoconazole	nefazodone
AZFilters	C	C	C	C
Molecular Weight	356.439	441.54	531.431	470.007
CLogP	3.533	5.585	3.635	5.725
CLogP error	All fragments measured	All fragments measured	Derived from measured fragment value	Calculated fragment value
Polar Surface Area	70.464	92.197	57.825	43.716
Heavy Atom Count	25	31	36	33
Rotatable Bonds	7	6	10	12
H-Bond Donors	1	2	0	0
H-Bond Acceptors	4	5	7	7
Positive charges	0	0	0	0
Basic charges	0	0	1	1
Acid centers	0	0	0	0
	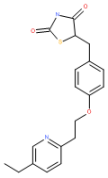	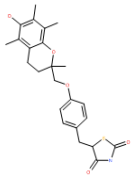	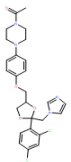	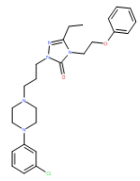
IC50 (uM)	0.3	2.7	2.9	4.2
Ki values				
DILI category	cholestatic mixed	cholestatic mixed	cholestatic mixed	cholestatic mixed

	glibenclamide	rifamycin SV	rosiglitazone	fusidic acid
AZFilters	C	U	C	U
Molecular Weight	494.004	697.768	357.427	516.709
CLogP	4.239	3.861	3.02	7.284
CLogP error	All fragments measured	All fragments measured	All fragments measured	All fragments measured
Polar Surface Area	126.894	218.3	71.338	113.013
Heavy Atom Count	33	50	25	37
Rotatable Bonds	9	12	7	6
H-Bond Donors	3	6	1	2
H-Bond Acceptors	5	11	5	5
Positive charges	0	0	0	0
Basic charges	0	0	0	0
Acid centers	1	2	0	1
	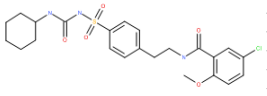	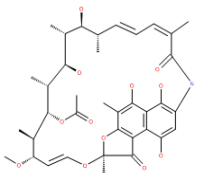	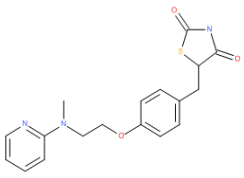	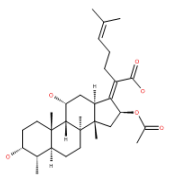
IC50 (uM)	5.3	6.3	6.4	11.5
Ki values	27.5 mol/L	31 mol/L		
DILI category	cholestatic mixed	cholestatic mixed	cholestatic mixed	cholestatic mixed

	acitretin	nifedipine
AZFilters	U	C
Molecular Weight	326.429	346.335
CLogP	6.065	3.125
CLogP error	All fragments measured	Derived from measured fragment value
Polar Surface Area	49.935	112.851
Heavy Atom Count	24	25
Rotatable Bonds	6	4
H-Bond Donors	0	1
H-Bond Acceptors	3	5
Positive charges	0	0
Basic charges	0	0
Acid centers	1	0
	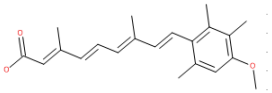	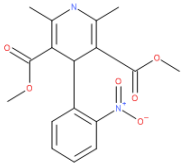
IC50 (uM)	18.2	30.7
Ki values		
DILI category	cholestatic mixed	cholestatic mixed